Probing Structures of Membrane Proteins and Their Inhibitors

Chang Gyeom Kim

Submitted in partial fulfilment
of the requirements for the
degree of Doctor of Philosophy

St. Hugh's College, Oxford

Michaelmas, 2005

Contents

Abbreviation and symbols

^	denotes operator
↔	denotes tensor variable or operator
→	denotes vector variable or operator
~	denotes interaction frame of Hamiltonian
2D	two dimensions
3D	three dimensions
ACh	acetylcholine
AChE	acetylcholinesterase
AChR	acetylcholine receptor
ADP, ATP	adenosine diphosphate, adenosine triphosphate
AM	amiloride (3,5-diamino-6-chloro-N-(diaminomethylidene)pyrazine-2-carboxamide)
B_0	static magnetic field
CNS	central nerve system
CSA	chemical shift anisotropy
CD	circular dichroism
CP	cross polarization
CW	continuous wave
DMPIP	N,N-dimethyl-8-(phenylmethoxy)imidazo[1,2- α]pyridinium iodide
DQ	double quantum
DQF	double quantum filter
E_1, E_2	conformation of the P-type ATPases sensitive to cytoplasmic and extracytoplasmic ions, respectively

EeAChE	Electrophorus electricus AChE
FT-IR	fourier transform infrared spectroscopy
GI	sealed, H^+/K^+-ATPase-enriched microsomes
GPCRs	GTP-binding protein-coupled receptors
GTP	guanosine triphosphate
HMA	5-(N,N-hexamethylene) amiloride
HMB	hexamethylbenzene
IC_{50}	concentration of inhibitor which inhibits 50% of H^+/K^+-ATPase K^+-stimulated activity
IST	irreducible spherical tensor
$K_{i(app)}$	apparent inhibition constant
MAS	magic angle spinning
MD	molecular dynamics
NMR	nuclear magnetic resonance
PDB	protein data bank
REDOR	rotational echo double resonance
RMSD	root mean square deviation
rf	radiofrequency
rpm	revolutions per minute
SCH28080	2-methyl-3-cyanomethyl-8-(phenylmethoxy)imidazo[1,2-α]pyridine
SDM	site-directed mutagenesis
SQ	single quantum
TcAChE	Torpedo californica AChE
TFE	2,2,2-trifluoroethanol

TM	transmembrane
TM2FPIP	N,N,N-trimethyl-8-(2-fluorophenylmethoxy)imidazo[1,2-α]pyridinium iodide
TM4FPIP	N,N,N -trimethyl-8-(4-fluorophenylmethoxy)imidazo[1,2-α]pyridinium iodide
TMCHIP	N,N,N -trimethyl-8-(cyclohexylmethoxy)imidazo[1,2-α]pyridinium iodide
TMPFPIP	N,N,N -trimethyl-8-(pentafluorophenylmethoxy)imidazo[1,2-α]pyridinium iodide
TMPIP	N,N,N -trimethyl-8-(phenylmethoxy)imidazo[1,2-α]pyridinium iodide
TMTFA	m-(n,n,n-trimethylammonio)trifluoroacetophenone
TMTFBIP	N,N,N -trimethyl-8-(trifluorobuthylmethoxy)imidazo[1,2-α]pyridinium iodide
TPPI	time proportional phase incrementation
T_R	magic angle spinning rotor period
TRIS	tris-[hydroxymethyl]-aminomethane

Acknowledgements

There are so many people who have supported and helped me to come to this point. I could not have finished my D.Phil without their continuous encouragements and supports. First of all, I would like to thank Dr Jung Sungho who convinced me that I could finish D.Phil course successfully when I had been doubt about it.

I would like to thank Professor Tony Watts. Tony gave me the opportunity to start my D.Phil course in his lab. His seamless strong supports allowed me to endure all of the difficulties during the course and made me to complete the work successfully. Thank you very much for your encouragements and a lot of advices again.

I still remember how much Jude showed me his patience against my poor English. His helps, suggestions and advices during the project were remarkably helpful for me. I really appreciate his helps.

Stephan and Scott introduced me to solid-state NMR, and answered to many stupid questions in patience. Scott provided his valuable labelled samples to me. I really appreciate it. Xin led me to a more theoretical world of solid-state NMR. I could not have completed my last NMR experiments without his helps. Discussions with him were invaluable. It was a very pleasant time for me to discuss with Tracy about NMR and also about wine.

Wolfgang introduced me to a world of molecular modelling. The discussion with him was excellent but his German joke was a bit tricky for me to understand.

I should say 'thank you' to Liz who sorted out a lot of things for me for whole my D.Phil period.

I would like to thank Lubica who gave me a chance to see a small cow with a big bell.

Also I couldn't forget about all the trips I made with lab members, Tracy, Miya, Lubica, and Vincent. It will be a long lasting memory to me.

I would like to thank Krisztina and Satita who encouraged me to stand on the ice rink again.

I also would like to thank the other members of Watts' group, Tim, Peter F., Peter H., Peter J., Boyan, Jonny, Susanna, Paul, Simon and Helen. I wish you all the best.

Finally I would like to thank my parents and family. My parents have always been supporting, encouraging, and providing me with their love. I really thank to my parents.

Abstract

Probing Structures of Membrane Proteins and Their Inhibitors

Chang Gyeom Kim, DPhil Thesis

Michaelmas, 2005

Using solid-state NMR and computational approaches, this study examines the binding-site conformations of inhibitors of membrane proteins such as the gastric H^+/K^+-ATPase, an integral membrane protein that represents the major target in the treatment of gastric ulcer disease, oesophageal acid reflux, and duodenal ulcer disease, an acetylcholinesterase (AChE) that has an important role in signal transduction in a nerve cell, and a Vpu which is a HIV-1 viral protein.

Solid-state NMR techniques are applied to the study of these compounds, which are derivatives of the substituted imidazopyridine SCH28080, to refine the ligand binding site and to develop more accurate protein models. ^{2}H-^{19}F and ^{19}F-^{13}C REDOR NMR experiments are employed to measure the distance between site-specific substitutions in the inhibitors. Using symmetry-based R sequence, a new DQF pulse sequence ($R16_6^5$) which can be applied to a high spinning MAS experiment is developed and applied to the complex of *Electrophorus electricus* acetylcholinesterase (EeAChE) and its inhibitor, to probe the chemical environments of the bound inhibitor.

Protein 3D structure models are created using MODELLER for two conformers of the gastric H^+/K^+-ATPase, in order to confirm the experimental data, to study its three-dimensional structure, and to provide details about inhibitor bound to the protein. The Ca^{2+}-ATPase is chosen as a template for the gastric H^+/K^+-ATPase.

For probing the protein-ligand interaction, docking simulations are performed using AutoDock3. The simulations revealed different results according to the catalytic (E_1 or E_2) state of the H^+/K^+-ATPase. In the E_1 state, inhibitors bound lumenally at the TM5-TM6 interhelical loop and proximal to TM6. In the E_2 conformation, the inhibitor bound consistently in the interhelical space which is proposed to be the site of ion translocation.

For the Vpu, the binding site for two ion channel blockers, amiloride (AM) and cyclohexamethyleneamiloride (HMA), are examined by using a protein-ligand docking approach. The three different protonation states of both inhibitors are tested for the docking simulations and the simulations show that the inhibitor binds to the Ser23 through the hydrogen bond interaction.

Published Papers

Work in this thesis has appeared in:

Kim, C.G., Watts, J.A. & Watts, A. (2005) Ligand docking in the gastric H^+/K^+-ATPase - homology modeling of reversible inhibitor binding sites. *J. Med. Chem.,* **48** (23), 7145-7152.

Lemaitre, V., Ali, R., **Kim, C.G.**, Watts, A**.** & Fischer, W.B. (2004) Interaction of amiloride and one of its derivates with Vpu from HIV-I: A molecular dynamics simulation. *FEBS Letts.*, **563**, 75-81.

1. Introduction to Membrane Protein Structure and Solid-State NMR

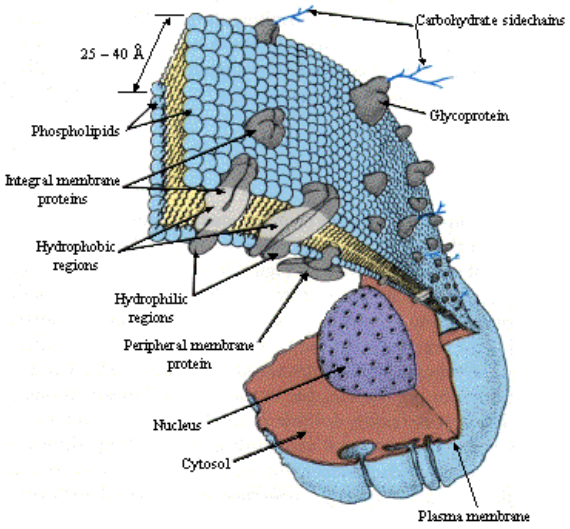

Fig 1.1. Diagram describing the organisation of a typical cell membrane and its relationship to the cell (Matthews & van Holde, 1990).

1.1 Structural studies on biological membranes

Biological membranes exist as a dynamic structure that acts as a barrier between the cell and its external environment whilst also being a platform for a range of energetic processes crucial to the function of the cell. Membranes are highly selective permeability barriers because they contain specific channels and pumps, they may respond to and generate signals or be used to create vital energy for the cell. The various functions of a biological membrane are dependent on its structure, which is defined by its composition.

Biological membranes have two essential components; lipids and proteins (Fig 1.1) and the nature of these components define the membrane's function. The fluid mosaic model of the organisation of biological membranes (Singer & Nicolson, 1972) describes membranes as two-dimensional solutions of oriented lipids and globular proteins. The membrane lipids are amphipathic molecules containing hydrophilic and hydrophobic moieties that form bimolecular sheets in aqueous media. The hydrophobic tails of the lipids are sequestered from the aqueous environment whilst the polar headgroups can enjoy electrostatic and hydrogen bonding attractions with water molecules. The resulting asymmetric environment, which is highly impermeable to ions and most polar molecules, supports integral membrane proteins. Integral membrane proteins have domains that pass through the membrane one or more times and are made up of both hydrophobic and hydrophilic amino acids that interact either with the hydrophobic interior of the membrane of the aqueous exterior. These interactions serve to anchor the protein in the membrane and prevent protein "flip-flop" such that membrane proteins can generally be thought of having a single orientation in the membrane. The very properties that make membrane proteins stable in a membrane environment make them insoluble in most solutions and inactive in organic solvents and hence almost impossible to crystallise by conventional methodology. Despite progress made using detergents and novel crystallisation methods such as co-crystallisation with antibodies (Kovari *et al*, 1995) or use of lipidic cubic phases (Landau & Rosenbuch, 1996), crystallisation successes are rare and hence biological membranes represent one of the last frontiers of structural biology where structural information cannot be expected to be obtained as a matter of course. In comparison with soluble proteins or membrane attached proteins the numbers

of membrane protein structures known at high resolution is minute. Only a handful of structures of polytopic membrane proteins have been described so far and this lack of knowledge hampers our understanding of one of the most important and interesting areas of molecular cell biology. For this reason, alternative methods of structure determination have been applied to membrane proteins. One of the more successful methods is electron diffraction of two-dimensional crystals. As mentioned above, a biological membrane has two-dimensional asymmetry and when protein is densely packed, either naturally as in the case of purple membrane (Fig 1.2) or in reconstituted samples as in the case of rhodopsin, a 2D crystal or array can be formed.

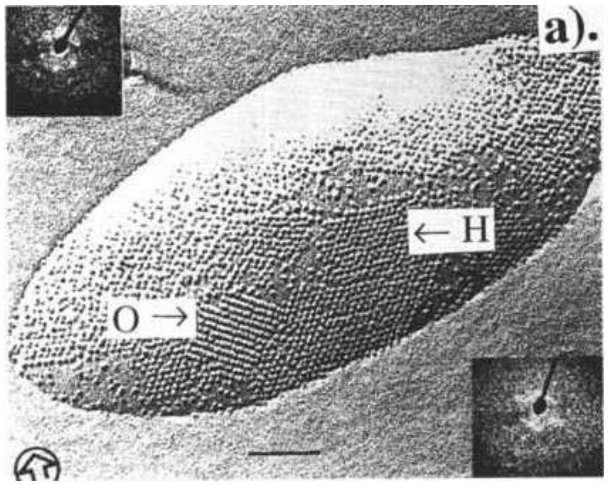

Fig 1.2. Freeze-fracture electron micrograph of purple membrane patch showing orthogonal (O) and hexagonal (H) arrays (Watts, 1995).

Electron diffraction of such 2D arrays can produce structures at relatively low resolution, which are shown as areas of high electron density to which a polypeptide chain is fitted. Some notable successes have been made using this technique particularly with bacteriorhodopsin (Grigorieff *et al*, 1996), rhodopsin (Schertler *et al*, 1993; Unger &

Schertler, 1995; Unger *et al*, 1995; Schertler, 1998; Krebs *et al*, 1998 (Fig 1.3)) the sarcoplasmic ATPase (Stokes & Green, 1990; Toyoshima *et al*, 1993; Ogawa *et al*, 1998; Zhang *et al*, 1998[a]), although largely superseded by successes with 3D x-ray crystallography (Palczewski *et al*, 2000; Toyoshima *et al*, 2000), and the nicotinic acetylcholine receptor (Miyazawa *et al*, 1999 (Fig 1.4)) in both open and closed states (Unwin, 1993; 1995).

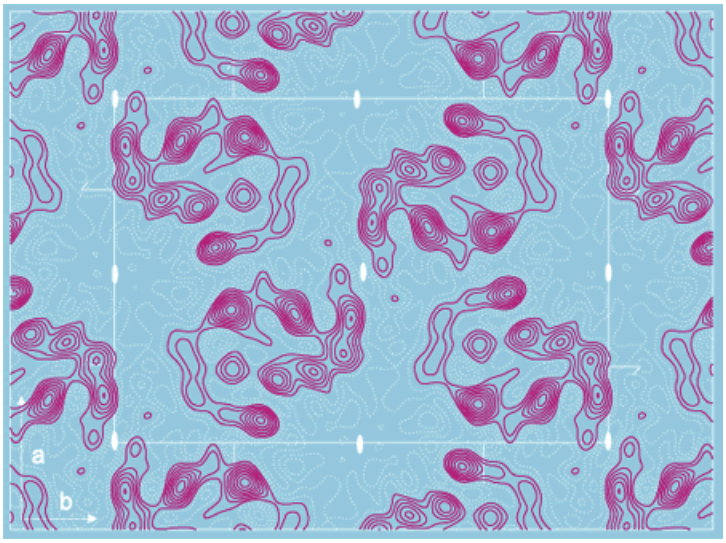

Fig 1.3. Projection density map of bovine rhodopsin p22121 crystals to 5 Å (Krebs *et al*, 1998).

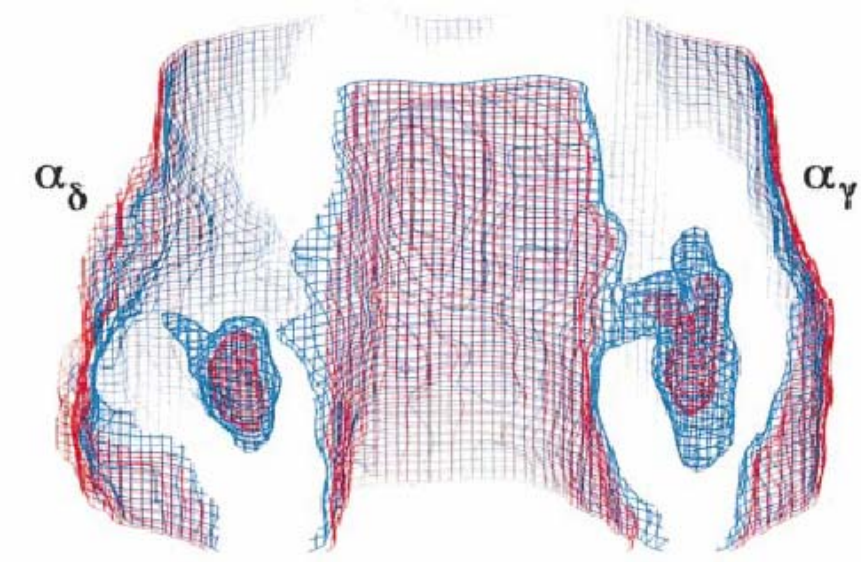

Fig 1.4. Demonstration of resolution obtainable using electron diffraction. This image of the nicotinic acetylcholine receptor from *Torpedo* postsynaptic membranes shows a cut through the extracellular portion of the receptor showing the putative ACh-binding pockets in the two α subunits, which connect by tunnels to the central vestibule (Miyazawa *et al*, 1999).

Electron diffraction can be seen above to be a very useful technique for describing gross structure and improvements have been made to the technology such that resolution and detail as shown in Fig 1.4 is achievable. However, resolution is still not comparable with that of x-ray techniques and is not sufficient to describe subtle but important structural details and/or conformational changes in membrane proteins. 2D crystals are generally difficult to prepare if not present in nature and, although progress has been made including attempts to link non-native proteins with proteins such as bacteriorhodopsin in native 2D crystals (Turner *et al*, 1999), this remains a considerable limitation of the technique. Conventional solution NMR has not been extensively applied to membrane proteins or indeed even large soluble proteins however recently a number of technical improvements have extended the range of proteins that can be studied. A range of samples employing a variety of residue specific labelling and protein deuteration strategies has led to the determination of the structure of a 47kDa enzyme complex (Kelly *et al*, 2001) whilst the advent of transverse relaxation optimised spectroscopy (TROSY) (Pervushin *et al*, 1997) has increased significantly the size limit restriction on NMR experiments performed in the liquid state. NMR can also be performed on proteins and peptides in biological membranes by applying solid-state NMR methods. The amount of information available in a solid-state experiment is much less than can be expected from

a solution NMR experiment but valuable structural and functional insights can still be obtained.

Solid-state NMR, as applied to biological samples, is a rapidly expanding field that has developed into one of the major biophysical techniques for the study of structure in biological membranes (Watts, 1998). This chapter will provide a selective overview of the history of solid-state NMR as applied to biological samples and will show the proliferation of the experiments and their applications.

Solid-state NMR has long been the poor cousin of liquid state NMR in structural biology so it is important to know why one might be interested in using such a technically difficult method. Considerable advances have meant that solid state NMR is now readily applicable to biological systems and a wide variety of information can be elucidated with solid-state NMR. How far the technique can be pushed, its limitations and how they might be removed is an area of intense discussion and has seen rapid progress in recent years. This introduction seeks to illustrate these points and will, at the same time, justify our approach and show what might be achieved through an extension of the solid-state NMR approach to biological structural studies.

1.2 Why solid-state?

As stated previously, high-resolution structures of membrane and structural proteins as well as high molecular weight complexes are rare. Both membrane and structural proteins are difficult to crystallise, membrane proteins are surrounded by lipids and may aggregate when removed from their normal environment whilst structural

proteins may have long filaments and may also aggregate. These same characteristics also hinder solution spectroscopy which is also not suitable for very large complexes due to the lack of fast isotropic tumbling needed for good spectral resolution.

Solid-state NMR is not hindered by these problems and, in principal, can be readily applied to most systems to yield a variety of structural information. The molecular weight limit that can be studied by solid state NMR is almost unreachable and the field has seen a number of publications on high molecular weight proteins (e.g. Demura *et al*, 1998; Shon *et al*, 1991; Kim *et al*, 1998; Williamson *et al*, 1998; 2000; 2001 (Fig 1.5); Spooner *et al*, 1999; Appleyard *et al*, 2000; Middleton *et al*, 1997).

Solid-state NMR can be used to provide three main classes of structural information: orientational, distance and torsion constraints. This chapter will describe the physical basis for experiments that yield such information and will present some key examples.

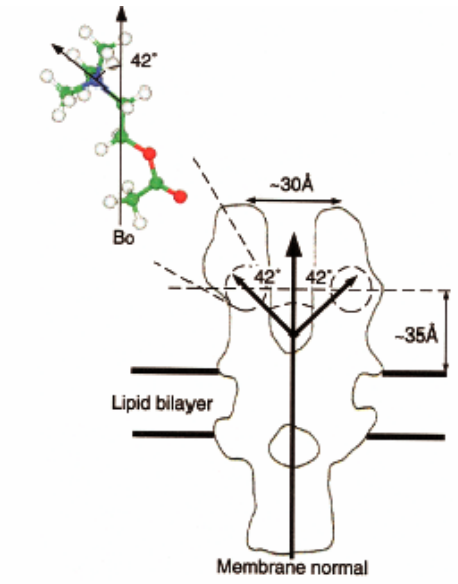

Fig 1.5. Diagram showing the relative position and orientation of the agonist acetylcholine while bound to the nicotinic acetylcholine receptor based on electron diffraction data, fluorescence energy transfer

measurements, and solid state NMR data (Williamson *et al*, 2001). This receptor consists of five glycosylated subunits with a total molecular mass of around 280kDa.

Despite recent successes in crystallising such proteins as bacteriorhodopsin and a potassium channel, solid state NMR may emerge as the most valuable tool for determining structural information at high resolution for membrane, structural and high molecular weight proteins. The potential of the technique has now begun to be realised with the determination of the first three-dimensional structure for the Protein Data Bank (1mag.pdb; Ketchem *et al*, 1996).

Commonly, biological solid-state NMR experiments can be divided into two methodologies; experiments performed under static conditions harnessing the anisotropy associated with biological membranes, and experiments performed under Magic Angle Spinning (MAS) conditions which attempt to emulate experiments developed in solution state spectroscopy.

1.3 Magic Angle Spinning

Nuclear magnetic resonance spectra for solids are very much broader than for liquids. This presents a problem in that chemically distinct species cannot be resolved because their resulting lines are so broad that they merge in the NMR spectrum. The broadening effect can be most dramatically demonstrated for the case of water where a proton NMR linewidth at room temperature is about 0.1Hz, while for ice at low temperatures it is 10^5Hz, six orders of magnitude broader. The static anisotropic interactions that cause this broadening are averaged out by the rapid isotropic motions in

the liquid state but remain in the solid state. It might be thought therefore that NMR would be a redundant technique for studying specimens in a solid state or any condition where full isotropic motion is not possible. This would be a serious limitation considering the number and importance of solid materials about which no information can be obtained. Improving the resolution obtainable in a solids experiment has therefore been a goal that arouses much interest.

It is possible to manipulate the experimental conditions to improve the resolving power of a solid sate NMR experiment. A quick glance at a series of solid-state NMR spectra will show that some lineshapes are sharper than others, which reflects varying levels of motion within "solid" samples. Hence it was noted that increased motion could lead to narrower lineshapes. The first attempts at imposing motion on a solid specimen involved rapidly spinning the sample (Andrew *et al,* 1958; Lowe, 1959). By varying the angle of rotation of the sample with respect to the magnetic field varying degrees of line narrowing were observed. Rotating the specimen about $\boldsymbol{B}_0$ has no effect; rotation about an axis perpendicular to $\boldsymbol{B}_0$ halves the spectral width and rotation about an angle of 54.73°, for example, reduces the dipolar broadening to zero. This reduction occurs because dipolar interactions (D), indirect electron coupled interactions, chemical shift anisotropy (σ) and quadrupolar interactions are all affected in a similar way by sample spinning about the magic angle. Take for example the dipolar interaction for which the Hamiltonian, in the homonuclear case, can be written thus:

$$\mathrm{H_d} = \sum_{i<j} \tfrac{1}{2}\gamma_i\gamma_i\eta^2 r_{ii}^{-3}\left(I_i \cdot I_i - 3I_{iz}I_{iz}\right)\left(3\cos^2\theta_{ii} - 1\right) \qquad (1)$$

where γ_i is the nuclear gyromagnetic ratio, $\boldsymbol{r}_{ii}$ is the internuclear displacement and θ_{ii} is the angle between $\boldsymbol{r}_{ii}$ and the Zeeman magnetic field $\boldsymbol{B}_0$ which is defined as being along the z-axis in the laboratory frame. If a sample is rotated about an axis inclined to $\boldsymbol{B}_0$ at angle β then the resulting spectrum will retain its shape but be reduced in width by the scale factor:

$$F(\beta) = \left|\tfrac{1}{2}\left(3\cos^2\beta - 1\right)\right| \qquad (2)$$

such that when β = 0, ½π and 54.73° then $F(\beta)$ = 1, ½ and 0 explaining the above observations of the effects of spinning samples at these angles with respect to the magnetic field. The beneficial properties of spinning a sample at 54.73° led to the angle being referred to as the "magic angle".

As all the above anisotropic interactions behave in a similar fashion under MAS conditions they can, in theory, be removed under fast rotation. Under these conditions the isotropic shift interactions and the isotropic J couplings remain so that high resolution NMR spectra may be recorded from solid specimens just as in liquids.

Unfortunately, however, this is an ideal situation and is rarely achieved with biological samples for a number of reasons. Firstly, whilst rapid isotropic motions within a solid may help to reduce linewidths which can then be subsequently further reduced by MAS, slow or moderate isotropic motion may still leave broadened lines. To narrow further lines that have already been narrowed by internal motions may require magic angle spinning at a rate exceeding that of the internal motion (perhaps as fast as 10^6Hz) which is technically impossible to achieve. In this instance molecular motion is a hindrance to achieving liquid state like resolution (Andrew, 1996).

Instrumental factors, such as magnetic field inhomogeneities, deviations in spinning from the magic angle and insufficiently fast spinning, can also compromise spectra. Anisotropic interactions that cause broadening can often not be removed by fast spinning as they are too large, this is often the case for dipolar couplings involving protons and quadrupolar couplings.

Today, many standard biological solid-state NMR experiments employ MAS and cross polarisation (CP). The biologically interesting NMR active nuclei ^{13}C and ^{15}N give weak signals and so coupled with isotopically enriching samples a cross polarisation double resonance method is employed. This procedure decouples the strong proton heteronuclear dipolar interactions and, by using the Hartmann-Hahn condition enhances the weak signal from either ^{13}C or ^{15}N by proton polarisation transfer. MAS removes the residual $^{13}C/^{15}N$ CSA and dipolar interactions. CP MAS can also be applied to ^{31}P and ^{2}H nuclei in biological systems although it is not always desired or necessary.

1.4 Orientations

Orientational constraints have been historically determined on static samples that have a unique orientation with respect to the magnetic field of the NMR spectrometer. Orientational constraints are different from distance measurements or torsion angles in that they define structure in an absolute manner and as such any errors inherent in the experiment do not sum when a model is built up from multiple constraints.

Orientational constraints are determined by observing a wide range of anisotropic interactions such as chemical shift anisotropies (CSAs), dipolar and quadrupolar

interactions. These anisotropic interactions have an orientational dependence and, once the interactions have been characterised, usually in a powder sample, a comparison of spectra from aligned samples with simulated spectra allows determination of molecular orientation. It is important that the relative orientation of the interaction of interest is known with respect to the molecular frame and some knowledge of the degree of orientation of the sample is available. The alignment of the sample can be determined indirectly, for example by studying the ^{31}P lineshape for phospholipids in a membrane when the sample is a membrane protein, or directly from a comparison of the oriented lineshape with that of the powder pattern. Variations can, however, have only a slight impact on the accuracy of the measurement and hence the accuracy of these measurements is typically very high.

The orientation of the amide ^{15}N CSA tensor, for example, has been well studied and has shown that although the tensor element magnitudes may vary by up to 20%, the orientation of the tensor with respect to the molecular frame is invariant excepting the case of glycine. Tensor orientations have been determined using single crystals of model compounds and also in more complicated systems such as peptides (Teng & Cross, 1989; Teng *et al*, 1992).

Variations in sample alignment can be a serious experimental problem and may eventually be a limiting factor on what sort and what size of protein can be studied in this way. Samples can be aligned in one of two ways, either macroscopically by drying or spinning samples onto glass plates or by taking advantage of diamagnetic or indeed paramagnetic (e.g. Assfalg *et al*, 1998; Prosser *et al*, 1999) susceptibilities of the samples which will cause them to assume a preferred orientation in a magnetic field.

Magnetically oriented samples can be divided into two categories: firstly there are soluble proteins in solution that are mixed with either a bicellar (Ottiger & Bax, 1999), purple membrane (Fig 1.6) or phage suspension. The suspension components are susceptible to the magnetic field and will assume a definite orientation. The soluble component may have transient interactions with the lipids of a membrane or even the protein component of that membrane (Koenig *et al*, 2000) and so possesses a transient orientation. This orientation and restricted motion allows dipolar couplings to be measured in solution (Tjandra & Bax, 1997; Tjandra, 1999; Zweckstetter & Bax, 2000). These dipolar couplings provide an additional source of constraints for the model building procedure in liquid state NMR (Prestegard, 1998) and leads to more precise structures with far lower RMSD's (Delaglio *et al*, 2000;). A number of examples have been shown where these anisotropic interactions help the refinement of structure in a liquid state experiment. Despite the use of anisotropic interactions, this is not, however, solid state NMR.

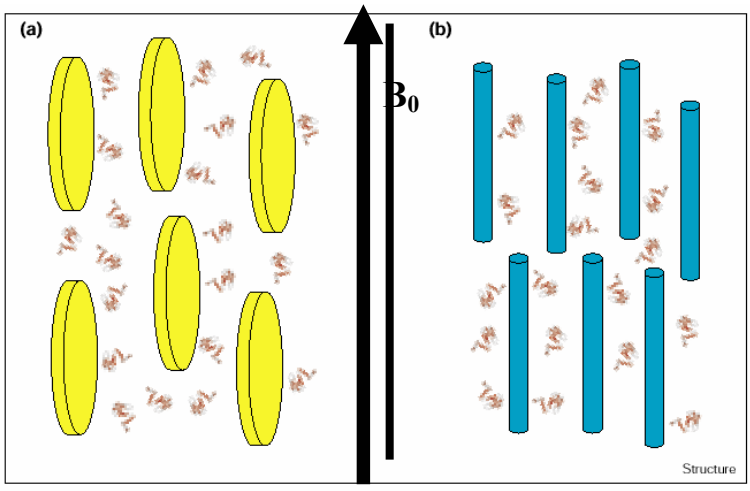

Fig 1.6. Cartoon illustrations of the two different classes of magnetically orienting media. (a) The large disc particles represent lipid bicelles or the purple membrane. (b) The long rods represent viral particles. The

bicelles orient with their normal perpendicular to the magnetic field whilst the phage particles align with their long axis parallel to the field (Tjandra, 1999).

The second category includes magnetically oriented samples in the solid state. In these cases proteins that are incorporated into bicellar or other magnetically susceptible membranes assume a definite orientation as the suspensions respond to the magnetic field (Opella, 1997; Struppe & Vold, 1998). The proteins are oriented but are also motionally restricted so can be considered to be in the solid state. This is a newly developing technique where the best conditions for orienting bicelles are still being refined (Vold & Prosser, 1996). There are a number of examples of structural details that have been found in this way, including a myristoylated PKA peptide (Hauer *et al*, 1997) and mastoparan X (Whiles *et al*, 1998), however the applicability of this technique depends heavily on the ability of the protein of interest to be incorporated into bilayers which then remain susceptible to orientation in the magnetic field.

1.4.1 NMR on Static Oriented Samples

A more practised technique uses macroscopically oriented samples, usually membrane films dried onto glass plates. Macroscopic orientation of small peptides and proteins (particularly bacteriorhodopsin) can be readily achieved by pipetting a small volume of a membrane suspension on to a glass disk and, in a controlled atmosphere, allowing evaporation. Larger proteins such as rhodopsin (Gröbner *et al*, 2000) or the nicotinic acetylcholine receptor (Williamson *et al*, 2001) or at least those with larger extra-membraneous domains are harder to orientate in this manner and so the technique

of Isopotential Spin Dry Ultracentrifugation (ISDU) is used to simultaneously centrifuge and dry membrane films onto glass discs (Gröbner *et al*, 1997). It must be stressed that under these circumstances the membrane films remain hydrated and the proteins functional.

One of the problems that affects these orientational studies, usually performed on static oriented samples, is that the linewidths in these spectra are large which means that signals for multiply labelled samples would be impossible to resolve. One way of improving resolution is to apply MAS to oriented samples, a subject that will play a major part in this thesis. However another possibility exists, without having to introduce spinning, as further dimensions can be used to help distinguish between labelled sites with similar characteristics in an NMR experiment. One example of this has been particularly successful. Polarisation inversion spin exchange at the magic angle (PISEMA) experiments introduce a further, heteronuclear dipolar coupling dimension, to the initial ^{15}N or ^{13}C CP spectrum. The high resolution, based on the orientational dependence of the ^{1}H-^{15}N dipolar coupling makes it an ideal way to resolve individual resonances from multiply labelled samples (see Fig 1.7). PISEMA experiments have been used to determine structural constraints for the M2 channel lining segments from nicotinic and NMDA receptors (Opella *et al*, 1999).

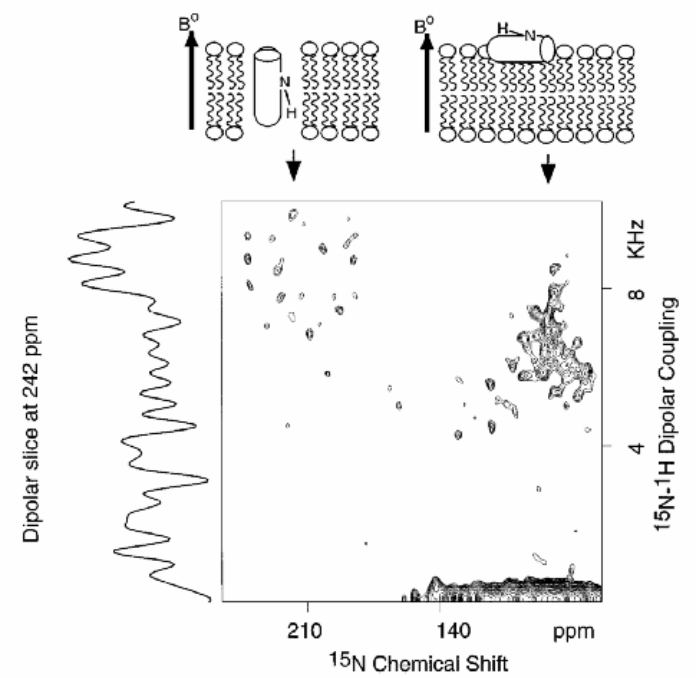

Fig 1.7. Two- dimensional PISEMA spectrum of uniformly ^{15}N-labelled colicin E1 P190 in oriented, hydrated lipid bilayers of DMPC and DMPG. The spectral region for alpha helices aligned parallel and perpendicular to the bilayer surface are indicated. Figure taken from Fu & Cross, 1999 (originally from Kim *et al*, 1998).

1.4.2 Magic Angle Oriented Sample Spinning (MAOSS)

A perfectly oriented single crystal would give rise to a spectrum containing sharp lines. However biological samples are not perfectly ordered and thus the multiple orientations present produce anisotropically broadened spectra. These broad spectra do, however, contain all the angular components of the nuclear interactions, which have been exploited, for example in the case of bacteriorhodopsin, by studying deuterons placed at specific positions along the retinal chromophore (Ulrich *et al*, 1994). For deuterium, the dominant quadrupolar interaction gives an angular dependence of the quadrupole splitting

measured as the frequency separation between the two resonances. The angular dependence of the quadrupolar splitting simplifies to:

$$\Delta\upsilon_Q(\beta_{PM}) = \frac{3}{2}\left(\frac{e^2qQ}{h}\right)\left(\frac{3\cos^2\theta - 1}{2}\right) \qquad (3)$$

An evaluation of this angular dependence of the deuterium spectral line-shape has led to a determination of the orientations of the individual C-CD_3 bond vectors with respect to the membrane normal.

The problems of broad spectra under static conditions and the unlikely availability of single crystals can be solved by the process of rotating solids in an NMR experiment. This technique was initially demonstrated when a sample was rotated about an axis that is tilted by an angle θ with respect to the magnetic field $\mathbf{B}_0$ a far greater resolution was achieved (Andrew *et al*, 1958). As discussed above the $3\cos^2\theta$-1 expression can collapse when θ = 54.73° such that rapid spinning of the sample at this "Magic Angle" causes anisotropic interactions to be averaged out, leaving only the isotropic chemical shift. If, however, spinning is performed at speeds less than the chemical shift anisotropy then the anisotropic information is refocused into the spinning side bands (Maricq & Waugh, 1979). The sharp lines observed in the MAS spectrum allow for identification of chemically inequivalent sites which will then allow information about bio-molecules, with many differing resonances, to be obtained. In a MAS experiment, however, there is no orientational information available so a combination of MAS and oriented sample preparation comprises the technique of Magic Angle Oriented Sample Spinning (MAOSS).

The application of magic angle spinning (MAS) NMR to uniformly aligned biomembrane samples has recently been demonstrated in our laboratory as a new general approach toward structural studies of membrane proteins, peptides and lipids (Glaubitz & Watts, 1998; Glaubitz *et al*, 1999; Middleton *et al*, 2000; Glaubitz *et al*, 2000) (Glaubitz, D.Phil thesis, 1998).

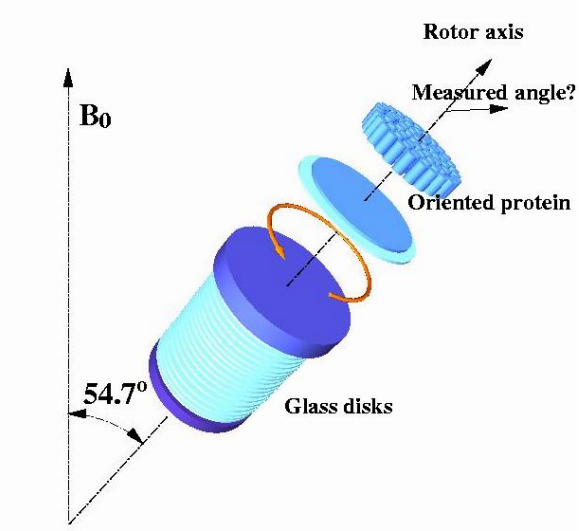

Fig 1.8. Diagram describing the MAOSS experiment where membrane films are dried under controlled humidity onto glass disks and placed in a rotor. The rotor is then spun at the magic angle (54.7˚) at speeds less than a frequency required to average the anisotropic spectral features of the anisotropy being studied (Figure, C Glaubitz).

MAS applied to uniformly aligned membranes consists of aligning membranes macroscopically on thin, round, glass plates which are then stacked in an NMR rotor (Fig 1.8) and spun at modest spinning frequencies at the magic angle. In this set-up the membrane normal is parallel to the rotor axis such that lipids rotate about the magic angle which to a large extent averages the strong ^{1}H-^{1}H dipolar couplings whilst sample rotation averages orientation defects. These two effects contribute significantly towards

high ^{1}H resolution for lipids in a membrane as shown in Fig 1.9. The reduction in linewidth shown in Fig 1.9 is from about 2400Hz for samples oriented at the magic angle to between 9 and 29Hz when the samples are additionally rotated around the magic angle.

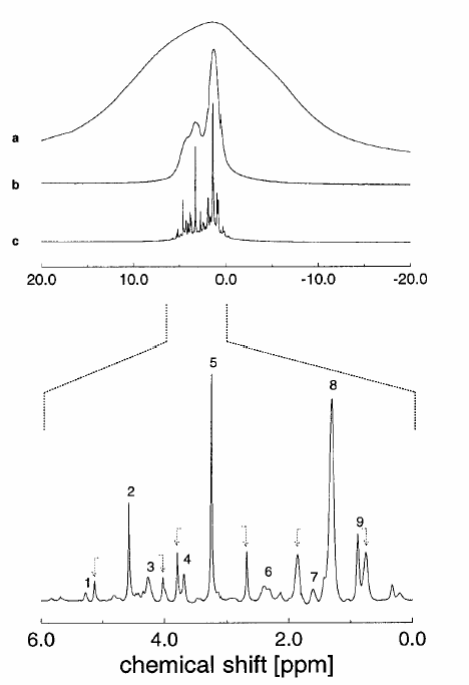

Fig 1.9. 400.13-MHz proton spectra of uniformly aligned (b, c) and randomly distributed (a) DMPC in D_2O at the magic angle and at T = 318 K. All resonances are already resolved at a spinning speed of 220 Hz. (a) Static, random distribution; (b) static, sample macroscopically oriented; (c) same as (b) but at 220 Hz spinning speed. Spectrum (c) is shown below on an expanded horizontal scale. Sidebands are labelled by arrows (Glaubitz & Watts, 1998).

Whilst a sideband pattern is produced for many of the resonances in Fig 1.9 their intensities are reduced by the averaging of the chemical shift anisotropy through rotation about the lipid long axis. In other cases larger anisotropies and slower correlation times lead to significant sideband patterns when the sample is spun at spinning frequencies which do not exceed the size of the chemical shift anisotropy. The orientational

dependence of the relative sideband intensities can be analysed for a determination of the orientation of the principal axis of the chemical shift anisotropy with respect to the magnetic field. An example of the application of this technique is shown in Fig 1.10 where tilt angles have been determined for lipid acyl chains in dimyristoyl-phosphatidylcholine (DMPC) bilayers in the gel phase from a ^{13}C MAOSS sideband pattern (Glaubitz & Watts, 1998). A comparison of ^{13}C MAOSS spectra for lipid acyl chains in two phases is shown. The sideband pattern is radically different for the two cases where the acyl chains become tilted through the phase transition. In fact little or no sideband intensity is observed for the Lα phase since, when the lipids are aligned parallel to the rotor long axis, in this case the angle between the principal axis of the chemical shift anisotropy and the rotor axis becomes zero and only the isotropic line is observed.

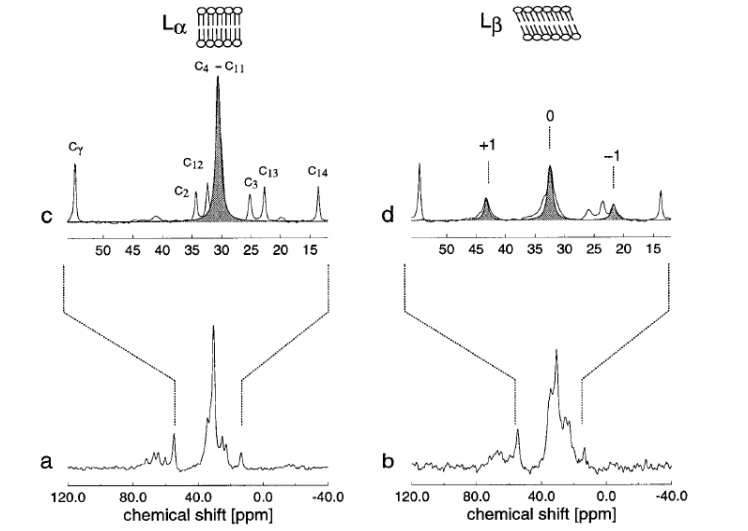

Fig 1.10. ^{13}C spectra of uniformly aligned DMPC with the membrane normal parallel to the rotor axis in both static and MAOSS experiments. The acyl chains in DMPC are tilted from 0° to 30° while undergoing a phase transition from the Lα to the Lβ phase which is reflected in a change of the sideband pattern of the methylene group (C4–C11 in spectrum (c)). (a) Static spectrum at T = 318 K (Lα), (b) static spectrum at T

= 280 K (Lβ), (c) same as (a) but at ω_r = 1080 Hz, and (d) same as (b) but at ω_r = 1080 Hz. The shaded peaks are computer simulations for the two different orientations (Glaubitz & Watts, 1998).

Prior to the first crystal structure of the G-protein coupled receptor (GPCR) rhodopsin being determined (Palczewski *et al*, 2000), understanding of its function was hampered by a lack of high-resolution structural information. Although rhodopsin structural models do exist, based on low resolution electron crystallographic data (Schertler *et al*, 1993), a structural understanding of the mechanism of light activation was lacking. A combination of static and MAOSS methods (Fig 1.11) (as developed for bacteriorhodopsin in this thesis) was used to determine the precise orientation of three deuterated methyl groups of the retinal chromophore in both the ground state and light activated states to give the first insights into how rhodopsin's conformational change is triggered (Gröbner *et al*, 1998; 2000). The conjugated polyene chain of retinal and its five methyl groups and cyclohexene ring all interact with various amino acids of the retinal pocket and so may also induce conformational changes within the protein upon light induced isomerisation. To study the conformational change of retinal in rhodopsin during the photocycle, three separate retinals were synthesised, deuterated ($C(^2H)_3$) on the C_{18}, C_{19} and C_{20} methyl groups, and incorporated in bovine rhodopsin, prepared from bovine retina, and reconstituted in DMPC. The reconstituted membranes were aligned on glass plates using the technique of Isopotential Spin Dry Ultracentrifugation (Gröbner *et al*, 1997). The solid state NMR spectra obtained from these samples contained direct information about the orientation of the methyl bond vector for each labelled site and hence provided orientational constraints for each of the three labelled segments of the chromophore within the protein.

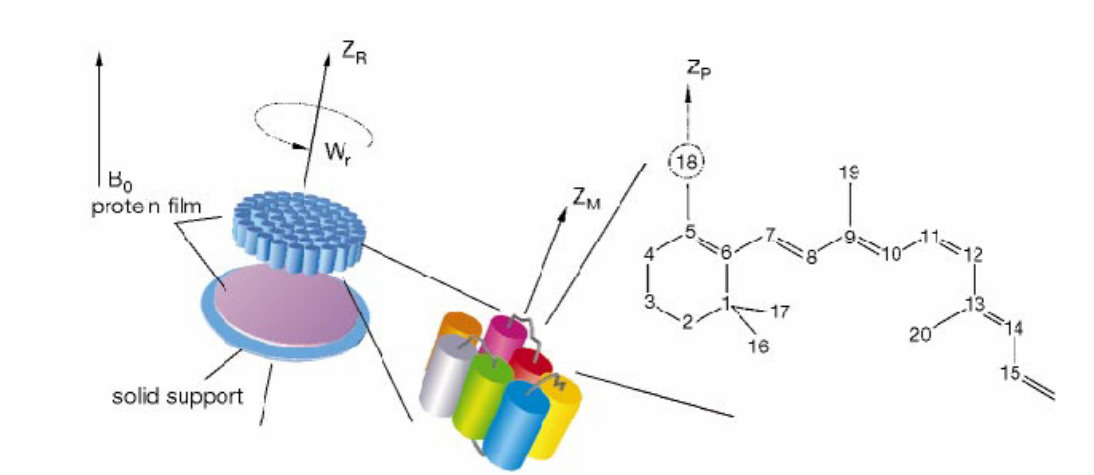

Fig 1.11. A description of an NMR technique used to determine bond angles in the retinal chromophore of rhodopsin (Gröbner *et al*, 2000). In the magic angle oriented sample spinning (MAOSS) NMR approach used here, uni-axially oriented phospholipid membranes containing bovine rhodopsin were stacked on glass plates in a MAS rotor, with rotor axis Z_R parallel to the sample director. The chromophore retinal (shown as 11-*cis* retinal in its 6-s-*trans* form) carried a deuterated methyl group at position 18 for which the orientation could be determined.

A combination of these direct orientational constraints and a number of distance and torsion constraints also measured by solid-state NMR (Feng *et al*, 1997; 2000 Verdegem *et al*, 1999) allowed the construction of a three dimensional model of 11-*cis* retinal in the binding pocket of rhodopsin. The orientation of the labelled methyl bond vectors was followed in the M_I-state of the protein by irradiating the protein samples at low temperatures prior to performing NMR measurements. Upon photo-excitation of rhodopsin the deuterium spectra exhibit significant changes (Fig 1.12) which reflect the

structural and orientational changes taking place in the chromophore on conversion to the M_I photostate from the initial ground state.

The three methyl bond vectors determined for the relaxed all-*trans* conformation of the retinal are roughly collinear such that incorporating the determined torsion angle (Feng *et al*, 2000) leads to the production of a retinal structure with a tilt of 30° to 35° away from the horizontal plane.

These results and those determined for bacteriorhodopsin (Ulrich *et al*, 1994) using static methods found good agreement with results from later crystal structures and showed how accurate structural information can be determined using solid state NMR methods when crystals are unavailable. The MAOSS methods applied to rhodopsin were, in part, developed in this thesis and will be built upon to improve the amount and range of orientational information obtainable from membrane proteins.

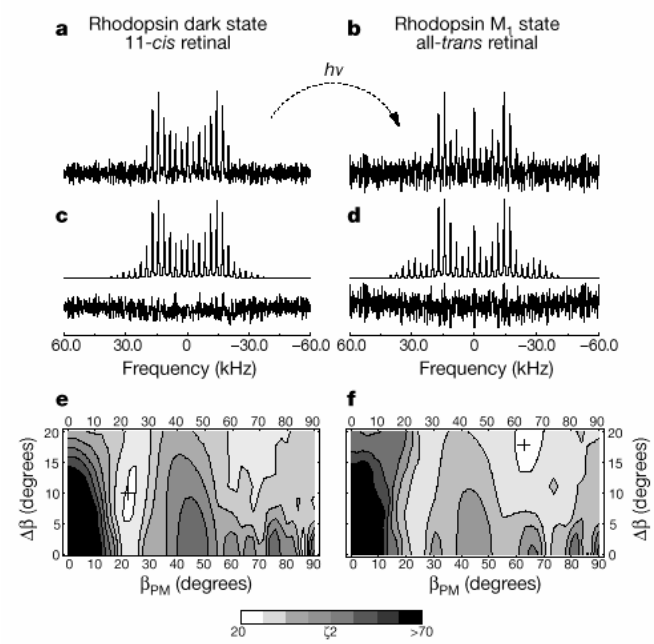

Fig 1.12. Example of MAOSS being used to determine bond angles. Deuterium-MAOSS NMR spectra of [18-C(^{2}H)$_3$]-retinal in dark adapted rhodopsin (a) and upon photo-activation in the M_I state (illuminated below 273 K) (b), at ω_r = 2860Hz and T= 213K. The spectra were analysed by minimizing the r.m.s. deviation of the MAS sideband intensities in the [β_{PM}, $\Delta\beta$]-parameter space, as shown by the z 2 - contour plots (e) and (f). The C–C(^{2}H)$_3$ tilt angle is determined to be β_{PM} = 21 ± 5º in the dark adapted state and 62 ± 7º in the M_I state. It can be seen that $\Delta\beta$ changes slightly from 10º in the ground state to 18º in MI. The difference between best fit and experimental spectra are shown in (c) and (d). Taken from Gröbner *et al*, 2000.

1.5 Distances

Dipole-dipole interactions between two spins can be determined quantitatively; their size is proportional to the gyromagnetic ratios of the two spins and the orientation of the internuclear vector, and inversely proportional to the cube of the through space distances that separates them. These measurements can thus be used to determine distance constraints between nuclear spins, providing an approach to accurate determination of molecular structure. Distances represent relative structural constraints in that they restrict the position of one molecular site relative to another.

In static unoriented powder samples the dipolar interactions allow determination of internuclear distances in a straightforward manner as discussed above. Other interactions, however, such as the chemical shift anisotropy and other dipolar couplings, particularly with abundant protons, also exist. These interactions can obscure some of the homo and heteronuclear dipolar interactions between dilute spins. MAS can be used to produce high resolution like spectra, removing these impinging interactions, however the important dipolar interactions are suppressed by the mechanical spinning. The dipolar

interactions can, however, be selectively reintroduced in a number of ways of which a number will be employed in this thesis.

Whilst many solid state NMR techniques are used to determine peptide or protein structure one variation of the technique involves studying small compounds that bind or interact with large proteins. In conventional NMR the large size of the protein would prevent any useful information being obtained from even a very small compound due to its anisotropic motion. Solution NMR techniques have recently been developed that reduce the impact of the decreased isotropic motion found in larger proteins and complexes and allow the study of relatively small compounds complexed with much larger proteins. Such techniques might have promising applications in the study of small macromolecules interacting with membrane proteins which have a large effective molecular weight due to their lipid environment. Transverse relaxation optimised spectroscopy (TROSY) improves resolution and sensitivity at high magnetic fields and has allowed the structures of two outer membrane proteins, OmpX (Fernandez *et al*, 2001) and OmpA (Arora *et al*, 2001) to be determined in lipid micelles. These proteins have molecular masses of 16 and 19kDa respectively but when in micelles have an effective molecular mass of about 60kDa. TROSY used in conjunction with the transfer NOE experiment, which has been used to study small peptides complexed to large proteins (e.g. Marshall *et al*, 1999), would then allow the study of reasonably large peptides complexed with their protein receptors.

Isotopic labelling coupled with solid state NMR can also overcome this problem and accurate structural information can be determined with almost no restriction on the size of the protein or its ligand. Rotational-echo double resonance (REDOR)

spectroscopy is a powerful method for measuring weak heteronuclear dipolar couplings between unlike spins. For example, it has been used to measure ^{15}N-^{19}F distances of fluorolumazines complexed with the huge 1 MDa β_{60} capsid of lumazine synthase (Goetz *et al*, 1999). The measured distances between the CF_3 groups of the ligands to side and main chain nitrogens in conjunction with coordinates from x-ray crystallography of the wild type synthase were used to produce a model of the lumazine binding site. The combination of these techniques is a potent tool for defining ligand structure and conformation on binding and the use of solid state NMR in this way is becoming increasingly prevalent. Combining heteronuclear distance measurements with oriented samples can improve the quality and usefulness of the data. REDOR has recently been performed on oriented DMPC bilayers containing a specifically labelled (^{15}N-Leu_{37}, ^{13}C-Leu_{39}) phospholamban peptide (Middleton *et al*, 2000). Using this technique, not only was the internuclear distance measured, confirming a proposed α-helical structure for the peptide, but also a tilt angle for the peptide in the phospholipid membrane.

Distances are measured through space and can be either inter or intra-molecular. Hence in the field of biological solid state NMR, distance measurements can be an important complement to orientational constraints and can be used to define even tertiary and quaternary structure. As mentioned before, a high-resolution structure of the channel forming polypeptide, gramicidin A, has been solved with 120 orientational constraints. Using an approach that measures residual dipolar couplings between NMR labelled nuclei that are close in space the precise geometry of the gramicidin dimer interface have been characterised (Fu *et al*, 2000). The technique used, simultaneous frequency and amplitude modulation (SFAM), allowed distances between ^{15}N and ^{13}C nuclei that were

of the order of 4.2 ± 0.2 Å spanning a hydrogen bond. The internuclear distance of 4.3 ± 0.1 Å between specific labels ($^{13}C_1$-Val_1, ^{15}N-Ala_5) on separate monomers confirmed, in lipid bilayers, the model for the monomer-monomer junction derived from solution NMR studies of the peptide in sodium dodecyl sulphate (SDS) micelles.

1.6 Torsion angles

The determination of relative tensor orientations was first described in 1980, however the technique has received only a little attention until recently when the secondary structure determination of *Samia Cynthia ricini* silk was published (van Beek *et al*, 2000). This high profile publication highlights the ability of solid state NMR to identify torsion angle pairs ($\boldsymbol{\varphi}$, $\boldsymbol{\psi}$) in the protein backbone.

Torsion or dihedral angles define the relative orientations of rigid structural elements such as an indole group, a methylene or a peptide plane. In a 2D MAS exchange experiment the spinning side band cross peak intensities are dependent on the relative orientations of the CSA tensors. With the principal tensor values of the CSA tensor already determined, simulations can be performed which can be compared with the experimental cross peaks to find accurate values for the torsion angles. The accuracy of this method is sufficient to distinguish between α helical and 3_{10} helical conformations (Long & Tycko, 1998)

1.7 Future perspectives

The above description of the ability of solid state NMR to resolve structural details in a wide variety of systems irrespective of molecular weight or environment shows the emergence of this technique and its potential whilst at the same time highlighting some of its limitations. The three main types of structural information have their different applications and suitabilities, however in many situations if two or all three types of information could be acquired then a much greater degree of understanding with improved accuracy would be possible. This would move solid state NMR much closer in ability to its solution state counterpart. Linking orientational, torsional and distance information will develop solid state NMR into a more powerful technique. Some of the links are starting to be made (e.g. Ishii & Tycko, 2000) and linking orientational and distance measurements is one of the themes of this thesis.

2. Bacteriorhodopsin and the Purple Membrane

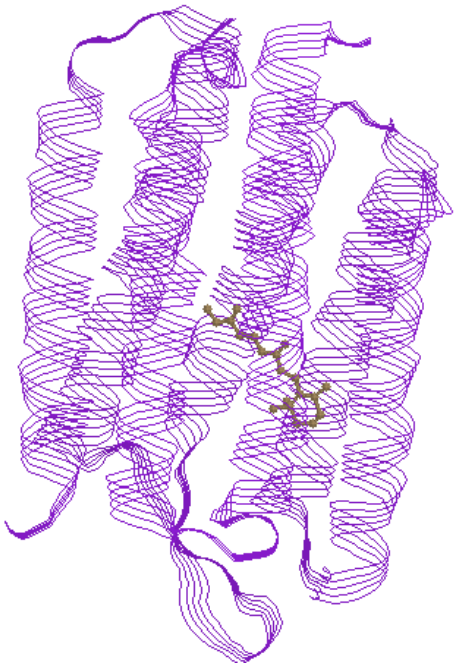

Fig 2.1. The helical disposition of bacteriorhodopsin showing the seven trans-membrane region (derived from 1c3w.pdb Luecke *et al*, 1999[a]). The prosthetic group, retinal is in yellow.

2.1 Structure and function of bacteriorhodopsin

Bacteriorhodopsin (Fig 2.1) is a light driven proton pump, discovered in the early 1970s (Stoeckenius *et al*, 1979), that harnesses energy from light to create a proton gradient across the bacterial membrane to drive energetic processes. Bacteriorhodopsin is derived from the purple membranes of the extremely halophilic bacterium *Halobacteria salinarium*, an obscure organism that is found naturally in hyper-saline lakes found only

in remote and unusual locations, or in salt evaporation beds and salt preserved food. This trimeric membrane spanning protein comes from a family of rhodopsins including halorhodopsin (anion pump), phoborhodopsin (photosensors) and sensory rhodopsins (Mukohata, 1994). Bacteriorhodopsin can be considered an ideal transport protein for study. It is available in large quantities, can be purified relatively simply, is extraordinarily stable and is uncomplicated in its function. Although other trans-membrane pumps such as the cytochrome *c* oxidase and mitochondrial ATPase have been studied, much progress has been made and they may have greater relevance to mammalian systems but have more complicated chemistry driving the pumping and a proton stoichiometry greater than one. The study of bacteriorhodopsin has tested established technologies and has caused new ones to be developed. Extensive mutagenesis has been carried out both in heterologous and later homologous expression systems and the wild type and mutated proteins were subjected to a battery of new physical techniques (Lanyi, 1999) including infrared, Raman and solid-state NMR spectroscopy. Time resolved measurements at visible wavelengths are now possible in the fs time range (Kobayashi *et al*, 2001). The structure of bacteriorhodopsin was solved first by electron diffraction of naturally occurring two-dimensional crystals (Henderson *et al*, 1990) and then improved by studies of three-dimensional crystals that diffract unusually and uniquely well for an integral membrane protein (e.g. Pebay-Peyroula *et al*, 1997; Luecke *et al*, 1998).

Bacteriorhodopsin consists of a single polypeptide chain of 248 amino acid residues, whose sequence is known from both amino acid (Ovchinnikov *et al*, 1977; Khorana *et al*, 1979) and DNA sequencing (Dunn *et al*, 1981) giving the protein a

molecular weight of approximately 26kDa. As a happy consequence of its presence in purple membrane as well ordered two-dimensional crystals, the structure of bacteriorhodopsin was one of the first integral membrane proteins to be solved, initial measurements using image reconstruction from electron microscope images allowed bacteriorhodopsin to be described as having seven rods of density that traverse the lipid bilayer region (Henderson & Unwin, 1975). Knowledge of the sequence of amino acids coupled with the identification of likely helical segments from proteolytic cleavage experiments and hydropathic energy calculations (Engelman *et al*, 1982) allowed a set of structural models to be developed. A current model showing the distribution of residues between trans-membrane helices is shown in Fig 2.2.

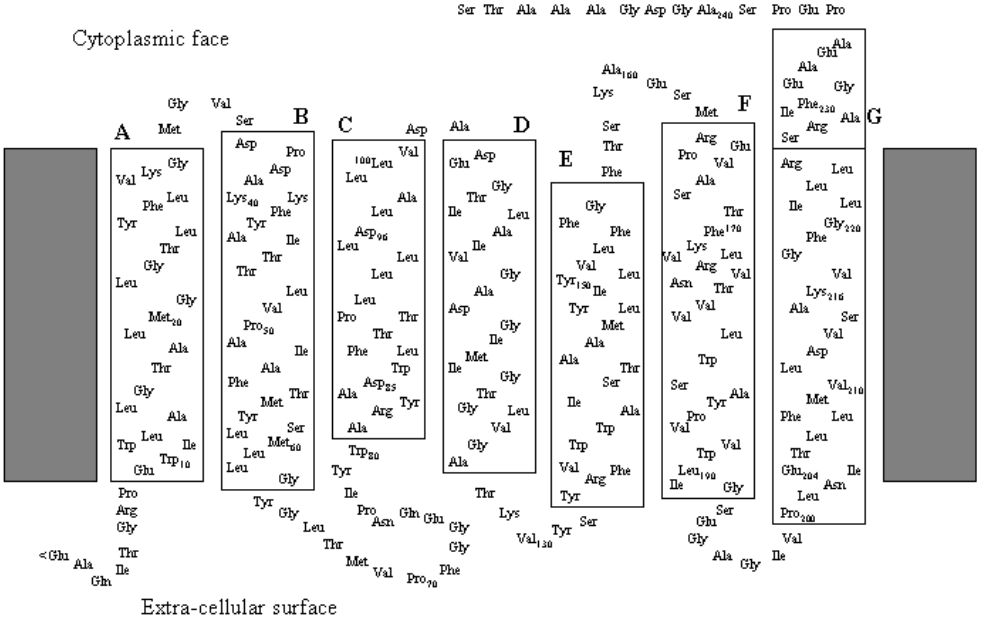

Fig 2.2. Schematic representation of bacteriorhodopsin primary and secondary structure based on sequence analysis (Dunn *et al*, 1981) and a combination of x-ray crystal structures. An extension of helix G extends beyond the bilayer.

The structure was improved by electron diffraction methods and, whilst initially the resolution was not at an atomic level, the resolution has now reached 3.5Å (Henderson *et al*, 1990; Grigorieff *et al*, 1996). Functional understanding of this protein, although well advanced, was to some extent hampered by the lack of resolution around the retinal, other key residues involved in proton pumping (known from mutagenesis studies (Khorana, 1993)) the loop regions and also associated lipids. For this reason, other, complementary approaches were used to demonstrate gross structural changes during the photocycle by neutron diffraction (Seif *et al*, 1985, 1986; Dencher *et al*, 1989; Weik *et al*, 1998) and, more accurately, by solid-state NMR (Watts *et al*, 1995[b]; Glaubitz *et al*, 1999). Electron diffraction techniques were improved such that the loop regions could be more clearly resolved, revealing a β-hairpin in loop B-C (Kimura *et al*, 1997[a,b]) which has been confirmed in later x-ray structures (Luecke *et al*, 1999[a])(Fig 2.1).

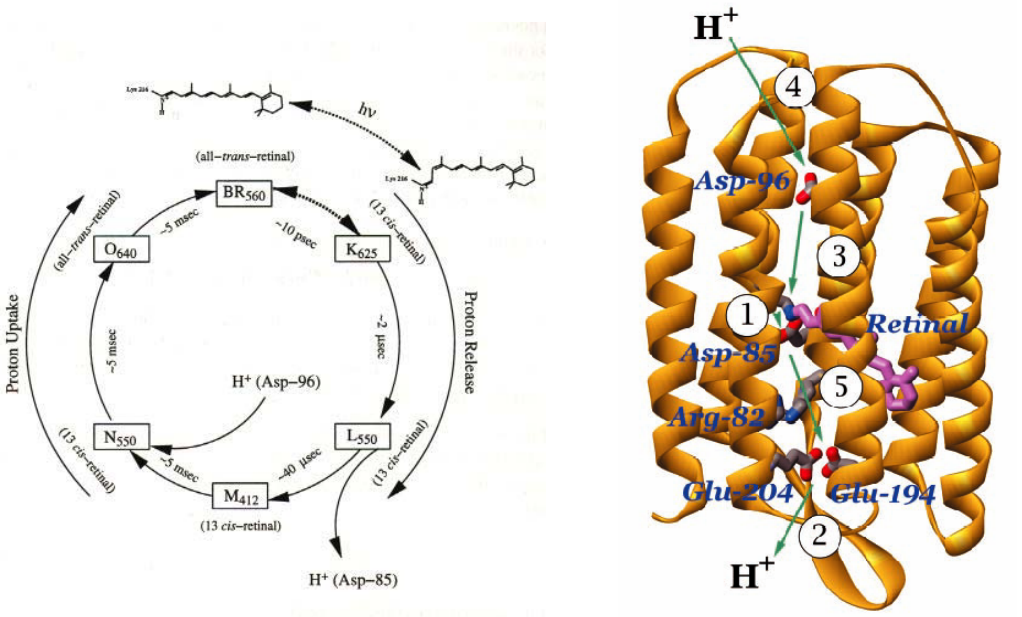

Fig 2.3 Diagram (left) showing the main stages of the bacteriorhodopsin photocycle as determined from FTIR studies (Khorana, 1988) and how these relate (right) to the protein and key amino acids, as discovered by mutagenesis. Top is the cytoplasmic side. Arrows indicate proton transfer stages during the

photocycle: (1) deprotonation of the Schiff base, protonation of Asp-85; (2) proton release to the extra-cellular surface; (3) reprotonation of the Schiff base, deprotonation of Asp-96; (4) reprotonation of Asp-96 from the cytoplasmic surface; and (5) deprotonation of Asp-85, reprotonation of the proton release site (Luecke *et al*, 1999[b]).

The proton pumping ability of this protein is conferred by the prosthetic retinal attached via a Schiff base to lysine 216. The light induced isomerisation (Fig 2.3) from all-*trans* to 13-*cis* causes the release of a proton from the Schiff base, which in turn passes through the protein and across the membrane. What has not been totally understood is the relationship between this event and the actual cycle that leads to the transfer of a proton from one side of the membrane to the other. For this reason there has been much interest and controversy over the locations of the crucial residue side chains, retinal and water molecules at each stage of the photocycle. The production of a family of higher resolution structures (Pebay-Peyroula *et al*, 1997; Luecke *et al*, 1998; Belrhali *et al*, 1999) from x-ray diffraction of 3D crystals produced from lipidic-cubic phases (Landau & Rosenbusch, 1996) has done much to solve some of this controversy.

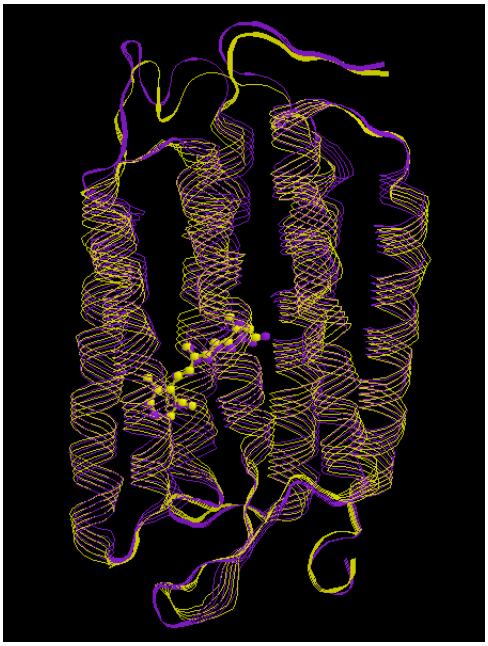

Fig 2.4. Comparison of backbone conformations for bR_{568} (purple) and M_{412} (yellow) states for bacteriorhodopsin in 3D crystals (Figure rendered in Chemscape Chime™ v 2.0.3 using coordinates 1cwq.pdb (Sass *et al*, 2000)).

With a 1.55Å structure recently published (Luecke *et al*, 1999), the structures of the D96N and E204Q mutants (Luecke *et al*, 1999[b]; 2000) and wild type (Sass *et* al, 2000 (Fig 2.4) in the M_{412} state of the photocycle, K and L state intermediates also trapped in crystals (Edman *et al*, 1999; Royant *et al*, 2000) and M (D96G, F171C, F219L triple mutant) and N states trapped in 2D crystals (Subramaniam & Henderson, 2000; Vonck, 2000), a higher level of understanding of the processes that underlie proton pumping is now possible (see Fig 2.5).

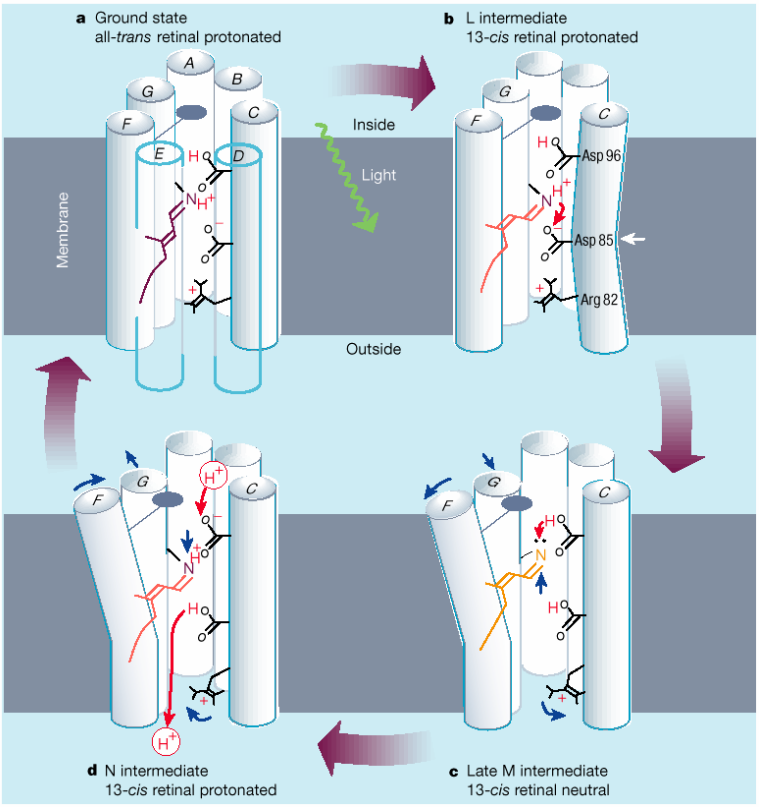

Fig 2.5. Cartoon diagram describing some of the key structural events, as determined from a number of crystallographic experiments, that accompany proton pumping in bacteriorhodopsin. These include the isomerisation of retinal from all-*trans* to 13-*cis*, kinking of helix C during L photointermediate and movement of helices F and G during late M and N to accommodate proton translocation. The "paddle" attached to helix F represents bulky side chains that move to open the cytoplasmic channel. Figure taken from Kühlbrandt, 2000.

The highest resolution structure reveals an extensive three-dimensional hydrogen-bonded network of protein residues and water molecules in the extracellular region, which leads from the buried retinal Schiff base and the Asp85 proton acceptor to the membrane surface. The protonated Schiff base is hydrogen bonded to a water molecule which is itself hydrogen bonded to two anionic aspartates. This water molecule stabilises the separate charges at the active site. The intracellular region contrasts with the

extracellular region in that it contains only a few water molecules and acts as a hydrophobic barrier. A π-bulge that causes a kink, not induced by proline, has been found on helix G near Lys216. The role of this bulge is as yet, unclear, however it is proposed that the resultant redistribution of residues along the helical face may be functionally important. Photoisomerisation of the retinal initiates changes that begin near the Schiff base and then propagate to the rest of the protein during the 10ms photocycle. The local and then large-scale conformational reorientations change the p*K* of acidic residues which alters their proton affinities.

A step-by-step movement of a proton from the cytoplasmic to extracellular side of the protein results, the most important steps being the protonation of Asp-85 on the extracellular side of the Schiff base and a deprotonation of Asp-96 on the cytoplasmic side. These steps provide the unidirectional force for the proton transport, yet are still not completely understood despite the high resolution crystal structures now available. A number of differing models have been proposed that describe this "protonation switch" (Herzfeld & Tounge, 2000; Pebay-Peyroula, 2000; Luecke, 2000; Kataoka & Kamikubo, 2000, Balashov, 2000). Suggestions for the switch mechanism include a strongly distorted retinal that relaxes through a single bond rotation after a proton has passed from Schiff base to Asp-85, removing electrostatic constraints or the movement of a water molecule at the Schiff base carrying a proton across the electrostatic barrier. The unidirectional proton transfer could be due to events immediately around the Schiff base or maybe decided by the varying proton affinities and proton transfer pathways away from the retinal binding site. Some of the protein-lipid contacts have also been identified (Essen *et* al, 1998) and, on the hydrophobic protein surface, grooves are formed by

specific arrangements of the side chains with which the lipid chain are aligned throughout. This discovery, coupled with evidence that specific lipids influence the steps of the photocycle (Joshi *et al*, 1998) leads to the exciting question of how lipids might influence the function of this protein? Whilst the structural changes that accompany proton translocation are being demonstrated there remains debate surrounding the relative merits of some of the techniques being applied. For example, although high-resolution structures of bacteriorhodopsin in its M-state have been produced in 3D crystals (Sass *et al*, 2000; Luecke *et al*, 1999[b]; 2000), slightly conflicting results have been found when studying bacteriorhodopsin in 2D crystals (Subramaniam & Henderson, 2000). The movement of the top of the F helix is restricted in 3D crystals to only about 1Å when compared with the bR_{568} state whilst in the D96G, F171C, F219L mutants (a triple mutant that mimics the full extent of the conformational change) studied in the purple membrane the helix moved by as much as 2-3Å. There remains the question of what differences the differing environments of the protein impose on the structural changes of the protein during the photocycle. These questions and more, considering proton uptake and release at the membrane surfaces which is also poorly understood, remain to be answered. Answering these questions and resolving the contradictions that have arisen from differing approaches and different structures remains an important goal and could lead to a complete understanding of one of the key processes underlying the generation of energy and life in bacteria.

2.2 Contribution of Solid State NMR

Solid-state NMR has been used to probe a number of structural aspects of bacteriorhodopsin including information about conformational changes and dynamics. These studies can be broadly divided into two categories; firstly those concentrated around the retinal chromophore, either directly looking at the chromophore itself or looking at its relationship with the binding pocket, secondly more attention has recently been paid to the rest of the protein in an attempt to follow the conformation of the polypeptide chain and understand how it contributes to the function of the protein.

Prior to a high-resolution structure of bacteriorhodopsin being available, a structural understanding of the retinal chromophore was obtained from a number of solid-state NMR experiments. One approach compared ^{13}C chemical shifts from labelled retinals in bacteriorhodopsin with shifts obtained from retinal model compounds (Smith *et al*, 1989). ^{13}C MAS spectra were obtained for light- and dark-adapted bacteriorhodopsin confirming an all-*trans* conformation of retinal in bR_{568} whilst a predominantly 13-*cis* conformation in bR_{548}. These experiments were followed up by a set of distance measurements on the labelled retinals, performed by Rotational Resonance, which confirmed the 6-s-*trans* conformation of the retinal in bR_{568} (Creuzet *et al*, 1991; Thompson *et al*, 1992). Another approach, performed in this laboratory, used static oriented samples labelled with retinals containing deuterated methyl groups. The angles of three methyl groups' bond vectors with respect to the membrane normal were determined in the bR_{568} ground state and the fate of the CD_3-19 methyl group was

followed into the M_{412} state (Ulrich *et al*, 1994; 1995). This approach was later repeated with one additional bond vector (Moltke *et al*, 1998; 1999). These studies showed that the retinal chain is somewhat distorted and that the retinal chain undergoes only minor re-orientations which suggested that the major conformational change that accompanied the retinal isomerisation took place around the Schiff base, a deduction now observed in the crystal structures.

The Schiff base linkage between the retinal and protein has also been studied by solid-state NMR. ^{15}N MAS spectra of [ζ-^{15}N-Lys] labelled purple membranes have revealed the conformation of the Lys216 Schiff base and its protonation state in bR_{568}, L_{550}, early and late M (M_0 and M_N) and N_{520} photostates (Hu *et al*, 1997; 1998). A similar study followed the fate of guanidyl-^{15}N chemical shifts from arginines during the photocycle. "Wing" peaks were assigned to Arg82 indicating an increase in asymmetry of this side chain which was interpreted as a possible stabilising role for this residue during proton transfer from the Schiff base to Asp85 (Petkova *et al*, 1999).

More recently, studies of the retinal chromophore have been extended to include its relationship with the protein residues that constitute the retinal binding pocket. These studies, requiring more advanced NMR methodology, have employed highly accurate distance measurements to describe the geometries of the retinal-binding pocket. [14-^{13}C] retinal to [4-^{13}C] Asp distances have been measured using the two-dimensional RFDR technique (Griffiths *et al*, 2000). A comparison of relative cross peak intensities between [14-^{13}C] retinal and [4-^{13}C] Asp212 yielded distances of 4.4 ± 0.6 and 4.8 ± 1.0 Å for bR_{568} and M_{412} states respectively (see Fig 2.6). This homonuclear study has recently been complemented by a heteronuclear study applying the new technique of SFAM

REDOR to bacteriorhodopsin (Helmle *et al*, 2000). Accurate distance measurements were obtained between the [14-^{13}C] of retinal and the [*indole*-^{15}N] of Trp86 in dark-adapted bacteriorhodopsin. Two retinal conformers were distinguished on the basis of their isotropic 14-^{13}C chemical shifts and two different distances of 4.2 Å and 3.9 Å were obtained for the 13-*cis*-15-*syn* and all-*trans*-15-*anti* conformers respectively.

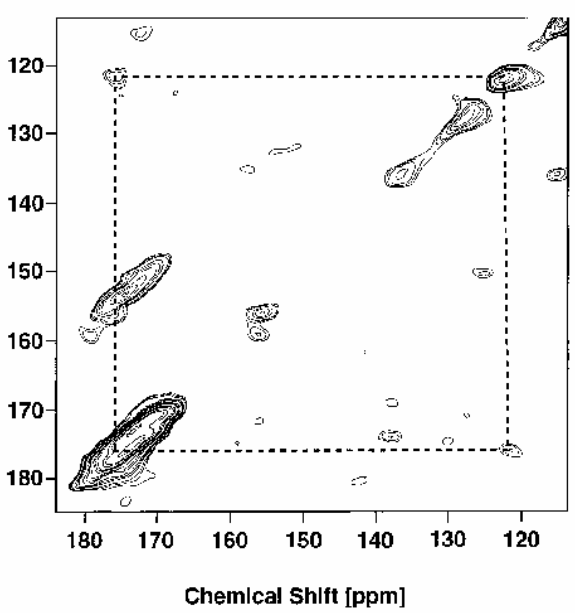

Fig 2.6. An example of a recoupling experiment in bacteriorhodopsin (Griffiths *et al*, 2000). 2D RFDR spectrum of dark-adapted [4-^{13}C]-Asp, [4-^{13}C]-retinal bR recorded with a mixing time of 31 ms at 6.2 kHz spinning speed, utilizing 24 *t*1 slices with 1200 scans/slice. The observed pair of dipolar cross-peaks corresponds to exchange between [4-^{13}C]-Asp-212 and [4-^{13}C]-retinal in bR568.

Although lacking structural details, a further solid-state NMR approach has studied the conformation and dynamics of the protein backbone (reviewed by Saito *et al*, 2000). Following specific labelling, commonly with either [1-^{13}C] alanine or valine or [3-^{13}C] alanine and assignment based on comparison with samples prepared from mutants, with enzymatic cleavages or interaction with Mg^{2+} ions, two separate approaches have

been used. The first of these relies on the conformational dependence of the $^{13}C_O$, $^{13}C_\beta$ (Taki *et al*, 1981; Saito, 1986) and $^{13}C_\alpha$ chemical shifts (Hong, 2000) such that a direct observation of the chemical shift of a labelled protein when compared with chemical shifts from simple polypeptides of known conformation will give an idea of the secondary structure at the labelled site. One such study (Tuzi *et al*, 1993) showed evidence for some small amount of β-sheet in bacteriorhodopsin which had not been seen in structures based on electron diffraction due to poor resolution in the loop regions. This β-sheet element was confirmed in a later electron structure that had specifically improved resolution in the loop regions (Kimura *et al*, 1997[b]) and also in the latter x-ray structures. The second approach involves interpretation of changes in CPMAS spectra and dipolar decoupled MAS (DD-MAS) spectra and relating these changes to increased/decreased motions on the timescale of either cross polarisation or magic angle spinning. This approach was used to study the conformational changes in the D85N mutant of bacteriorhodopsin that mimics the M-state of the wild type protein (Kawase *et al*, 2000). A reduction in peak intensities of three to four labelled and assigned alanine residues in the D85N mutant and D85N/D96N double mutant was interpreted as a development of intermediate time-range motions following a conformational change. These changes were assigned to alanines 39, 51, 53 from helix B and alanine 215 from helix G showing that these helices have an altered conformation in this M-like state. Other similar studies have probed the effects of site-directed mutations (Tanio *et al*, 1999), temperature (Tuzi *et al*, 1996[a]), the retinal (Tuzi *et al*, 1996[b]), and cations (Tuzi *et al*, 1999) on the protein's conformation and dynamics, whilst the C-terminus has also been studied (Yamaguchi *et al*, 1998). The actual nature of the conformational change in the helices is clearer from x-

ray structures of trapped intermediates, however solid-state NMR coupled with specific labelling and strategic assignment has been shown to be a sensitive tool for studying conformational changes and may be particularly helpful in studying areas that are less well resolved in the crystal structures, such as the loops and termini.

These studies are just a few examples of how solid-state NMR has been applied to bacteriorhodopsin. The range and detail of information available from these experiments is great but are they really important when viewed in the context of the numbers of 2D electron and, now, 3D x-ray diffraction structures available? Firstly these NMR experiments are important since, in most cases, they are the first applications of technically demanding experiments, initially developed on simple model compounds, to large proteins in biological membranes. As such these techniques should then be readily applicable to other membrane proteins which have less known about them and are far from being crystallised. Bacteriorhodopsin has become something of a proving ground for solid-state NMR experiments, as with many other biophysical techniques and is a real test of what can be achieved by solid-state NMR. This in itself makes the experiments described in this thesis worthwhile with a new technique, however the impact of these experiments should be felt at different levels since solid-state NMR is capable of revealing details of membrane proteins and their environments at a level beyond that of crystallographic methods (Watts *et al*, 1999). Precise orientations and distances measured by NMR can add fine level detail to a crystal structure as, theoretically, the resolution achievable by solid-state NMR is within 0.1Å over short distances with angles accurate to ±1° whilst the best resolution obtained by 3D crystallography remains 1.55Å. This outstanding potential to obtain detailed structural information is even more impressive

when coupled with the innate advantage of solid-state NMR in that it can be performed on non crystalline materials.

The measurements described in this thesis and in the experiments above were performed on bacteriorhodopsin in the purple membrane. Whilst not exactly *in vivo*, protein in membrane preparations are clearly closer to their natural state than those in 3D crystals, detergents or even reconstituted membranes. It has already been suggested that some crystal structure data may be compromised by motional restrictions imposed by crystal packing and that photostates are not cleanly trapped when helices cannot move freely (Vonck, 2000; Subramaniam & Henderson, 2000).

Development of new solid-state NMR techniques and their application to bacteriorhodopsin increases the range and possibilities of experiments applicable to membrane proteins in general and can, at the same time, yield important details about bacteriorhodopsin unavailable even from x-ray crystallography.

2.3 Aims of the thesis

The introduction given above describes the climate under which the experiments described in this thesis were formulated. In general it is difficult to obtain high-resolution structural information about membrane proteins and whilst a number of advances have been made, progress in this field remains relatively slow. NMR is a powerful technique for structure determination and has been successfully applied to relatively small, soluble proteins. Solid-state NMR aims to circumvent some of the problems that hinder the application of NMR to membranes and has the potential to produce high-resolution

structural information where other methods may not be suited. It may also have its own intrinsic advantages.

Bacteriorhodopsin has been described as a well studied membrane protein and is arguably the most understood of all membrane proteins. Despite its popularity and the high levels of information that have been revealed about this protein, there remains controversy about the finer aspects of its function. The complete understanding of its function is a tantalising prospect.

The work described in this thesis combines the study of the structure and function of bacteriorhodopsin with new solid-state NMR approaches to achieve two main goals. Firstly it will be demonstrated that solid-state NMR has the ability to identify key structural features of bacteriorhodopsin. These experiments can be performed without the need for crystals and can provide information that is not found even with the recent high-resolution crystal structures. Secondly bacteriorhodopsin will be used as a paradigm for 7-TM proteins to develop solid-state NMR methodology with a view to increasing the range and depth of information that can be obtained from large membrane proteins. Purple membrane samples used in this thesis are prepared with relatively simple procedures and consist of functional protein in hydrated biological membranes. The membrane environment of the protein can be a limiting factor to the linewidths observed in the NMR spectrum and hence the resolution, however such preparation procedures can be realistically applied to most if not all proteins that span a lipid bilayer and any structural information obtained may have greater significance in relation to the protein in its natural state. Goals include increasing the number of constraints that can be determined in a single experiment under MAS conditions; improving the efficiency and

applicability of distance measurement techniques and developing the range of questions that can be studied by making use of a variety of NMR active nuclei.

3. The Reorientation of the Retinal Chromophore in Bacteriorhodopsin Revealed by Deuterium MAOSS NMR

3.1 Introduction

As described in chapter 2, the light induced isomerisation of the prosthetic retinal is the trigger for proton pumping by bacteriorhodopsin. Rapid isomerisation about a unique double bond leads to changed configuration and orientation of the chromophore within its binding pocket. Later, slower thermal steps involve the distorted chromophore driving the protein into its active state. To understand the mechanism of action of this pump the first stage of the cycle needs to be characterised. How does this simple conformational change lead to a functioning protein pump? A number of theories have been proposed as to how pumping is initiated and are founded on a structural understanding of how the chromophore responds to its isomerisation from all-*trans* to 13-*cis* retinal.

The first high-resolution structural details of the retinal in bacteriorhodopsin came from solid-state NMR studies performed in this laboratory (Ulrich *et al*, 1994). Using static oriented samples specifically labelled with deuterium carrying retinals, the absolute alignment of the retinal chromophore whilst in the protein binding site has been resolved giving light to the structure and environment of the ligand. Bond vectors for the methyl groups at C_{18}, C_{19} and C_{20} were determined in the ground state (bR_{568}) (Ulrich *et al*, 1994). The measured angles show a distorted retinal structure constrained by the binding pocket, which differs from crystalline retinal. Static deuterium NMR methods

have also been employed on macroscopically oriented purple membrane films to observe the reorientation of the retinal in the M_{412} state using the C_{19} vector as a probe (Watts *et al*, 1995[a]; Ulrich *et al*, 1995). In this way the structural re-alignment of retinal through the photocycle can be probed. The movement of the C_9-C_{19} bond vector from 40° in the bR_{568} state to 44° in the M_{412} state indicates that the polyene chain does not move significantly on photo-isomerisation and that the major movement resulting from the conformational change of retinal must be located towards the Schiff base. These results have been confirmed by the recent crystal structures featuring M-state photointermediates (Luecke *et al*, 1999[b] & 2000, Sass *et al*, 2000).

Lineshapes of deuteron-wideline spectra are highly sensitive to molecular order and the type and time scale of molecular motion. This useful property can, however, in static NMR spectroscopy be compromised by the broad spectra of disordered samples (up to 200kHz wide) resulting in low signal sensitivity. Magic-angle spinning, averaging the rather weak dipole-dipole coupling among deuterons as well as the chemical shift anisotropy such that only the quadrupole interaction remains, refocused in the sidebands, causes much greater sensitivity. This sensitivity enhancement can, in some cases, be as great as a factor of 30. In an ordered system, such as a membrane uniaxially oriented onto a glass disk, side band intensities can be used to determine tilt angle (β_{PR}) orientation distribution functions. The α and γ Euler angles of the tensor do not contribute here as the quadrupolar coupling is symmetric about the CD_3 bond angle.

The intensity of a spinning side band I_N, at the magic angle θ, is calculated by the following equation:

$$I_N(\beta_{PR}) = \left|F_N(\beta_{PR})\right|^2 \qquad (4)$$

where

$$F_N(\beta_{PR}) = \int_0^{2\pi} \frac{d(\omega_r t)}{2\pi} \exp\left[i\left(C_{1\sin}(\omega_r t) + \frac{1}{2} C_{2\sin}(2\omega_r t) - N\omega_r t \right)\right] \qquad (5)$$

and

$$C_1 = -3/4 \sin 2\theta \sin 2\beta_{PR} \qquad (6)$$

$$C_2 = +3/4 \sin^2 \theta \sin^2 \beta_{PR} \qquad (7)$$

As with many direct methods, solid-state deuterium NMR requires relatively large amounts of sample. Static measurements are typically performed on upwards of 80 mgs of bacteriorhodopsin which limits the application of the technique when sample is scarce. MAOSS NMR can, in theory, be performed on far lower amounts (c 20mgs protein) of sample and has the potential to resolve different deuterium species. Whilst an increase in signal to noise is hard to quantify when comparing published spectra, it is clear that when comparing intrinsic linewidths from static deuterium experiments (Ulrich *et al*, 1994; Moltke *et al*, 1998), which can be of the order of 1-2 kHz with those found in MAOSS spectra which are in the range of 50-180 Hz, far sharper lines are produced under the spinning conditions used for MAOSS (Glaubitz & Watts, 1998). The resulting

improvement in sensitivity can therefore be expected to be in a range between 10 and 50 fold. This chapter shows the application of the new solid state NMR technique, MAOSS for a re-evaluation of the C_{20} and C_{18} methyl group bond vectors (previously determined by static ^2H solid state NMR (Ulrich *et al*, 1994)) in light of the first published x-ray structure (Pebay-Peyroula *et al*, 1997) of bacteriorhodopsin in the bR_{568} state which had good agreement for the C_{18} bond angle but some discrepancy around the C_{20}. The angle changes of these vectors during the photocycle following light activation will also be observed.

3.2 Materials and methods

3.2.1 Sample preparation

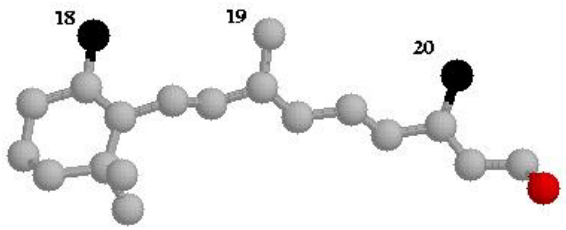

Fig 3.3. Structure of all *trans* retinal showing positions of the C_{18} and C_{20} methyl groups that were deuterated in this experiment. The Lys-216 nitrogen that forms the Schiff base is shown in red.

Retinals, with deuterons incorporated into the methyl groups at either position C_{18} or C_{20} (Fig 3.3), were regenerated into retinal deficient bacteriorhodopsin according to (Oesterhelt, 1982). The retinals had been prepared according to published procedures (I. Burnett, Watts laboratory), synthesis according to Groesbeck (1993) and deuteration according to Pardoen (1986). Retinal deficient strain JW5, *Halobacteria salinarium* was

grown in a complex, peptone based medium (1 litre medium in 2 litre conical flasks at 105rpm and 37°C; Appendix 2.1.1). When growth slowed (O.D checked at 660nm), 6mg all-*trans* retinal, dissolved in 2ml ethanol, was added over two days to each litre of culture. Purple membrane was isolated according to the method of Oesterhelt & Stoeckenius (1974). A final purification stage was performed using a 25-45% sucrose gradient (average RCF 83,000g; 18hrs; 15°C). The density of the purple membrane was monitored and any membranous components not in the main purple membrane band at 33% sucrose were rejected. The purple membranes were washed in double distilled water and then deuterium depleted water. The purity of the membrane preparation was assed by in the UV-VIS spectrum and a characteristic maximum was found at 568nm (Fig 3.4). The ratio of the maximum at 280nm to that at 568nm (approximately 2:1) is typical of a preparation uncontaminated by any significant quantities of unprocessed bacteriorhodopsin precursor proteins which are the only other proteins found in the purple membrane (Kates *et al*, 1982). On average 1 bacteriorhodopsin was obtained at a yield of 12mg per litre of culture.

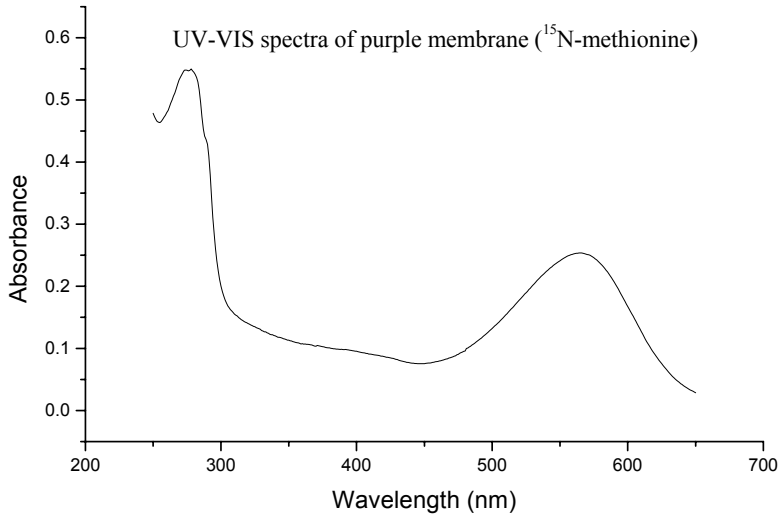

Fig 3.4. UV-VIS spectrum of purple membrane, typical of all preparations made in this work.

Purified purple membrane (24mg bR) was again washed with (average RCF 90000; 30m; 4°C) and resusupended in deuterium depleted water and spread evenly over 60 round, 0.07mm thin glass plates with a diameter of 5.4mm (Marienfeld GmbH, Germany), 0.2mg protein in 25µl water was applied to each plate. Through controlled evaporation (85% humidity, RT; over a period of 2 days) in deuterium-depleted water, these samples produced uniaxial films with good orientation of the purple membrane patches parallel to the sample plane. A second application produced a final concentration of 0.4mg protein per plate. The optimum between maximal protein concentration and best orientation was checked by polarized light microscopy. The glass plates had previously been cleaned in nitric acid and methanol/ethanol and dried under a stream of nitrogen gas. The plates fitted precisely a standard 7mm Bruker MAS rotor (RotoTec GmbH, Germany) with special KelF inserts to keep the plates secure in the spinning rotor. Drying bR pellets on glass plates and scratching the protein film in to the MAS rotor produced an unoriented sample. Sample orientation and stability was monitored by static ^{31}P NMR before and after the MAOSS experiments and showed no change in spectral lineshape.

Bacteriorhodopsin was trapped in the M_{412} state by soaking disks in 0.3M guanidine hydrochloride pH10 for two hours. Guanidine Hydrochloride has been shown to increase dramatically the lifetime of the M intermediate (Yoshida *et al*, 1977). The disks were returned to 85% humidity for a further 12 hrs (hydration is crucial for effective trapping). Disks were then mounted on a pre-cooled stacking tool (-60°C) under strong illumination from a halogen lamp. A purple to yellow/orange colour change was observed almost immediately. The disks were mounted and kept in a 7mm rotor at -60°C.

bR_{568} was maintained during NMR measurements also at -60°C, the sample having been light adapted at room temperature with five minutes of white light.

3.2.2 NMR measurements and data analysis

Experiments were performed at 61.4MHz for ^2H on a BRUKER MSL 400 with double resonance 7mm MAS probes. Simple one pulse experiments without proton decoupling were performed at 210K and at a spinning frequency of 4000Hz. A 6μs π/2 pulse (41kHz) was used with a recycle delay of 300ms. Between 100,000 and 400,000 scans were acquired. Following zerofilling with 16K points, complex Fourier transform and phase correction, an exponential line broadening of 50Hz was applied. Finally, spectra were symmetrised to account for any remaining asymmetry and referenced to D_2O at 0Hz. Lineshape simulations were performed on a Silicon Graphics INDY R4600 workstation using a programme written by C. Glaubitz (Oxford). Spinning sideband patterns of a single spin-½ or spin-1 can be calculated for various distributions, from a single crystal to a full powder. This is achieved by defining explicitly the range of the Euler angles, which define the orientation of the principle axis system with respect to the molecular frame and the orientation of the molecular frame to the rotor fixed system. The Monte Carlo method is used for sampling over these defined intervals. Experimental

spectra were matched to simulated spectra from which an experimental angle could be derived. A χ^2 merit function

$$\chi^2(\beta_{PM}, \Delta\beta) = \sum_N \left(\frac{I_N^{ex} - I_N^{sim}(\beta_{PM}, \Delta\beta)}{\Delta I_N^{ex}} \right)^2 \qquad (8)$$

was minimised for the tilt angle β_{PM} and mosaic spread $\Delta\beta$ with I_N^{ex} and I_N^{sim} being experimental and simulated spectral intensities. The r.m.s noise amplitude is used as an experimental error ΔI_N^{ex} with which a sideband intensity can be measured directly. The derived angles were modelled on existing coordinates from varying experimentally derived structures of bR using Insight II on a Silicon Graphics INDY R4600.

3.3 Results

The spectral resolution obtainable in this MAOSS experiment (Fig 3.5) is a great improvement on previous static experiments since the intrinsic deuterium linewidth has been reduced from 1-2kHz typical for static experiments to 180Hz whilst the line broadening applied to the spectrum can similarly be reduced. The improvement in sensitivity and resolution in this case is tenfold such that it is possible to observe clearly a shift of the central MAS resonance line, corresponding to the chemical shift of CD_3, with respect to the referenced chemical shift of D_2O. The r.m.s noise amplitude is determined to be approximately 10% of the maximum intensity.

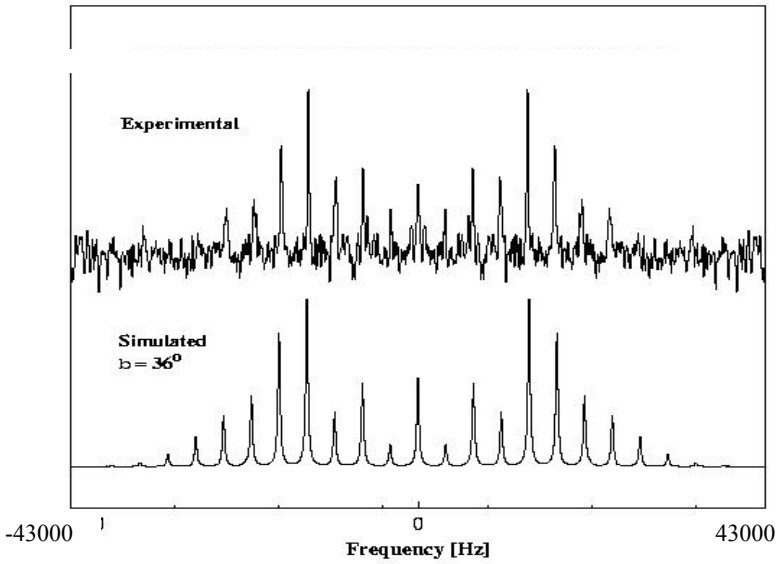

Fig 3.5. Simulated and experimental ^2H NMR spectra acquired for CD_3 group at position 18 on the retinal. Here bacteriorhodopsin is in the bR_{568} state. Measured angle is 36° ±5°. Spectrum was acquired at 210K at a spinning speed of 4000Hz. This figure shows how the acquired spectrum is compared with a simulation. Discrepancies between simulated and experimental data could arise from small populations of other retinal isomers or from dynamic effects not included in the data analysis.

The comparison of ^2H MAOSS spectra for the two differently labelled retinals (Figures 3.6 and 3.8) shows the response of the spectra, reflected in the distribution of sideband intensities, to differing orientations of the C-CD_3 vectors in both the bR_{568} (light adapted) and M_{412} photostates. The corresponding χ^2 plots are shown (Figures 3.7 and 3.9) which demonstrate the differing possible solutions when fitting the simulated spectra with the experimental data. More than one possible solution is present for the ground state samples however the solution with the lowest mosaic spread is chosen.. On trapping the M-state more solutions, where minima have similar low χ^2 values, appear and it is not possible to select the solution with lowest mosaic spread to agree with values found using other methods. Good fits are, however, found when allowing for an increase in the mosaic spread. This anomaly will be discussed below.

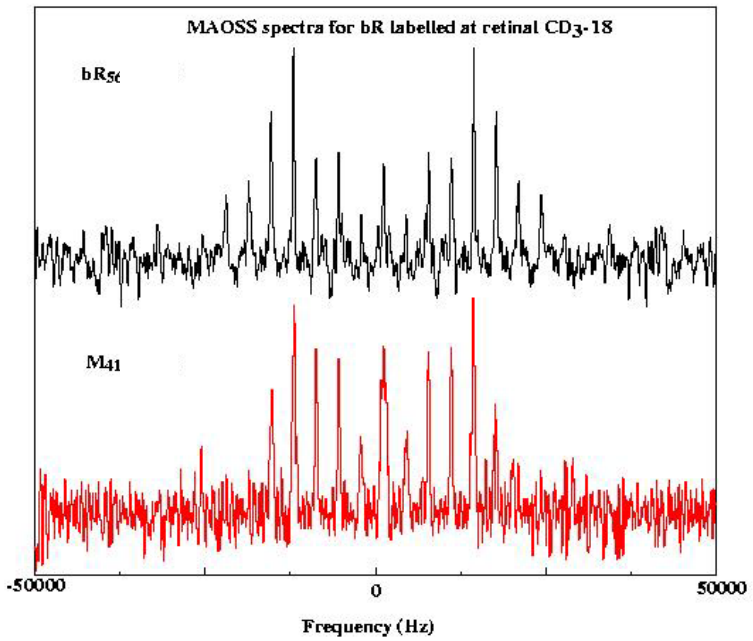

Fig 3.6. MAOSS spectra acquired for bR with retinal labelled at CD_3-18 in the ground state and trapped in M_{412}. Observe the change in distribution of intensity between the side bands caused by a change in orientation of the CD_3 bond vector with respect to the rotor axis. Measured angles are 36°±2° (bR_{568}) (black) and 25°±2° (M_{412}) (red).

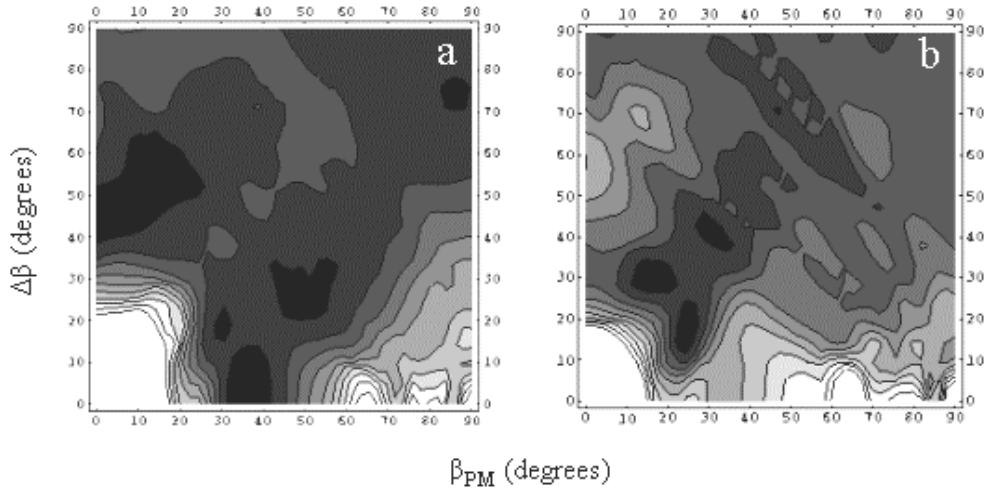

Fig 3.7. χ^2 plots of r.m.s deviation of the MAS sideband intensities from simulated spectra for CD_3-18 in bR_{568} (a) and M_{412} (b). Minima (darker areas showing least r.m.s) with lowest mosaic spread are used for angle determination. For bR_{568} the lowest minimum has an angle of 36° whilst in the M_{412} photostate there are three minima; 25° (with lowest mosaic spread and lowest χ^2), 15° and 34°.

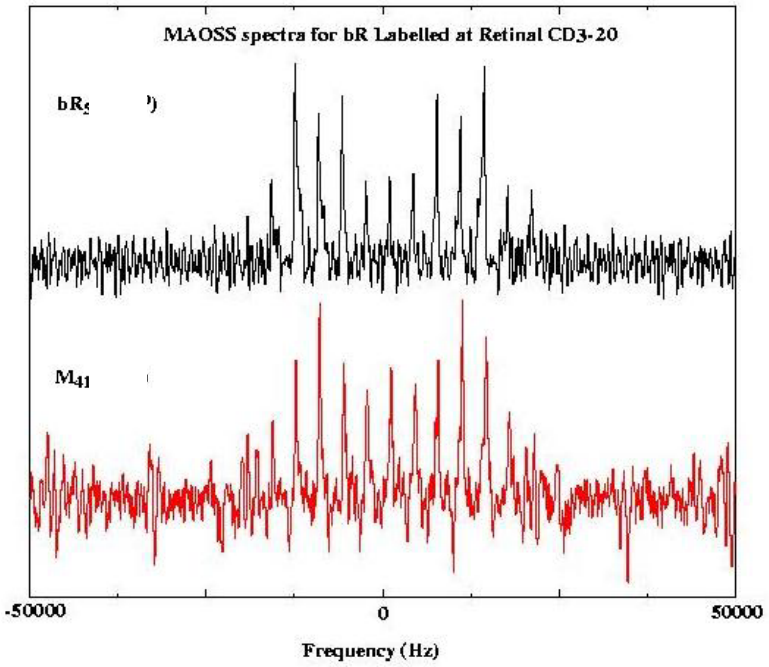

Fig 3.8. MAOSS spectra (as in Fig 3.6) for bR labelled at retinal CD_3-20. Measured angles are 22°±2° (bR_{568}) (black) and 10°±2° (M_{412}) (red).

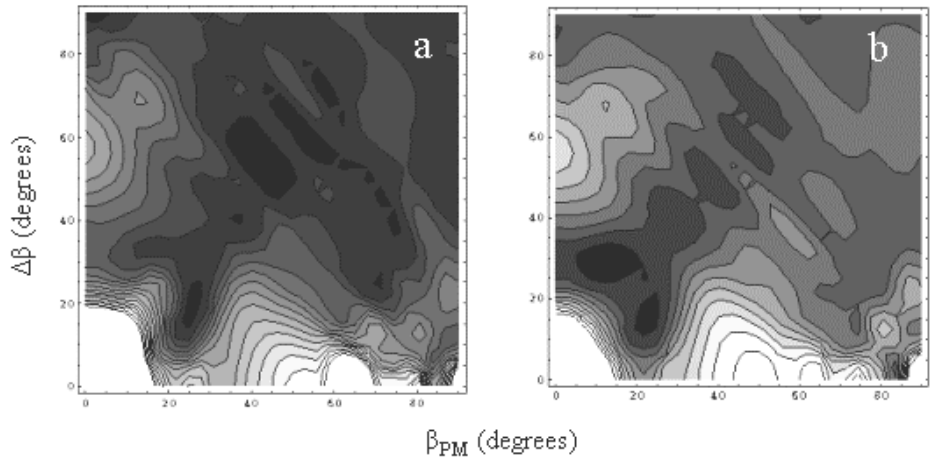

Fig 3.9. χ^2 plots of r.m.s deviation of the MAS sideband intensities from simulated spectra for the CD_3-20 orientation in bR_{568} (a) and M_{412} (b). Minima (darker areas showing least r.m.s) with lowest mosaic spread are used for angle determination. For bR_{568} the lowest minimum has an angle of 22° whilst in the M_{412} state there are two minima; 22° (with lowest mosaic spread) and 10° (with lowest χ^2).

The modelled structure (Figure 3.10) shows the refined structure of retinal in the light adapted state of bacteriorhodopsin. The helix coordinates are after the highest resolution electron diffraction structure (Grigorieff *et al*, 1996). The retinal is based on that included in 2brd.pdb but has been altered to accommodate the angular information from this study. The measured angles are in close agreement with those obtained from the highest resolution x-ray structure of bacteriorhodopsin (Luecke *et al,* 1999[a])

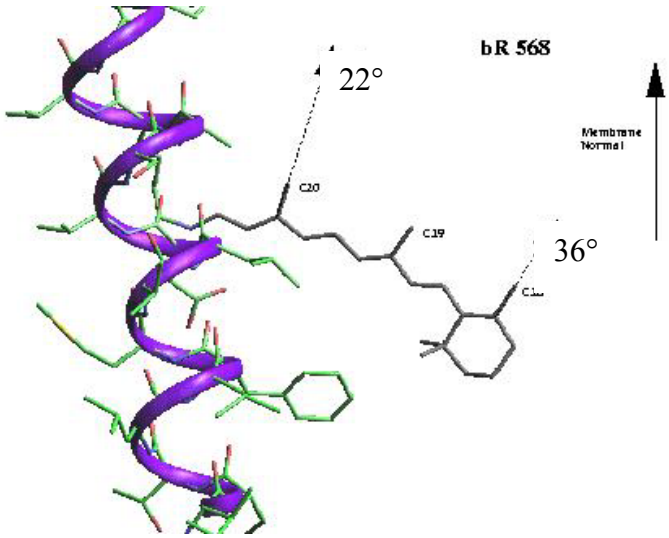

Fig 3.10. Modelled structure of retinal in bR_{568} (light adapted) showing angles determined by ^{2}H MAOSS NMR in this experiment.

3.4 Discussion

3.4.1 Contributions of other biophysical techniques

The orientation and re-orientation of the retinal chromophore has been studied by a range of methods. Time resolved linear dichroism has shown the orientation of the chromophore relative to the membrane plane during the photocycle (Song *et al*, 1996; Borucki *et al*, 1999) and neutron diffraction has been used to measure the positions of two deuterated labels at the Schiff base and β-ionone ends of the chromophore. The neutron diffraction data for light adapted bR gives an angle between the membrane normal and polyene chain of 66° (Hauss *et al*, 1994) which compares well with the linear dichroism value (an average from a number of experiments reviewed in Heyn *et al*, 2000) of 69°. These experiments provide lower-resolution data which is an average angle of the polyene chain and it is difficult to reconcile these measurements with higher resolution

data from solid-state NMR and x-ray crystallography (although see Hudson & Birge, 1999) which can describe individual angles and so are sensitive to bends, kinks or twists of the chain.

Angles measured by MAOSS solid-state NMR are accurate to within 2°. It is difficult to estimate errors associated with angles derived from x-ray crystal structures since only a small variation in the position of an atom fitted to the electron density will cause a significant alteration in the measured angle. An illustration of this can be seen in a comparison of two structures at differing resolution (Figure 3.11).

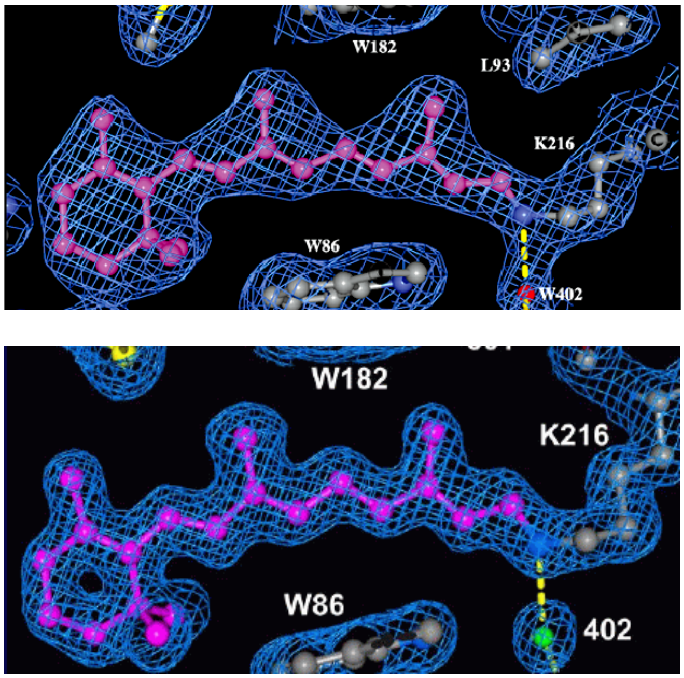

Fig 3.11. Figure showing electron density map of retinal in bacteriorhodopsin (bR_{568} photostate) at 2.3Å resolution (top) (Luecke *et al*, 1998) and 1.55Å (bottom) (Luecke *et al*, 1999[a]). The improvement in data quality and hence accuracy of measured angles at improved resolution is evident.

3.4.2 Comparison of solid-state NMR and x-ray crystallography data

The improved resolution of the x-ray crystal structures over recent years should be considered to provide more accurate angles when measured from the 3D coordinates. This improved accuracy is reflected in the increasing consensus between angles measured by solid-state NMR methods and x-ray crystallography as shown in Table 3.1. To highlight the values derived from MAOSS and the highest resolution x-ray structure (36° compared with 35°and 22° compared with 21° for the C-C_{18} and C-C_{20} vectors respectively) illustrates this point.

Method and *bR state*	**Resolution**	**Angle (°)**		
		C-C_{18}	**C-C_{19}**	**C-C_{20}**
Static ^{2}H NMR (Ulrich *et al*, 1994)	±2°	**37**	**40**	32
Static ^{2}H NMR (Ulrich *et al*, 1995) M_{412}	±2°	nd	44	nd
Static ^{2}H NMR (Moltke *et al*, 1999)	±3°	**36**	**40.5**	nd
Static ^{2}H NMR (Moltke *et al*, 1999) M_{412} (D96A)	±3°	38.8	47.5	nd
MAOSS ^{2}H NMR (this work 1999)	**±2°**	**36**	**nd**	**22**
MAOSS ^{2}H NMR (this work 1999) M_{412}	**±2°**	**25**	**nd**	**10**
X-ray (Pebay-Peyroula *et al*, 1997)*	2.5Å	45	38	10
X-ray (Luecke *et al*, 1998)	2.3Å	**34**	30	**20**
X-ray (Belrahi *et al*, 1999)	1.9Å	**40**	41	**23**
X-ray (Luecke *et al*, 1999)[a]	1.55Å	**35**	34	**21**
X-ray (Luecke *et al*, 1999)[b] M_{412} (D96N)	2.0Å	35	42	37
X-ray (Edman *et al*, 1999) K_{590}	2.1 Å	38	39	40
X-ray (Sass *et al*, 1999)	2.2 Å	**36**	**39**	**19**
X-ray (Sass *et al*, 1999) M_{412}	2.2 Å	42	48	38

Table 3.1. Comparison of measured bond vectors in retinal for bacteriorhodopsin in differing photostates and by differing methods. * This structure was later shown to be compromised by merohedral twinning of the crystals, which was not taken into account in the structure determination. The crystal co-ordinates y axis in these structures is regarded as being coincident with the membrane normal.

When focussing on the data obtained from solid-state NMR methods, there is a good match for the bR_{568} CD_3-18 vector between MAOSS and static methods, which is not unexpected. The disparity in the CD_3-20 vectors between static and MAOSS methods may highlight problems with the static data. Although there is some degree of variation amongst these figures there is a consensus emerging between NMR and x-ray data (highlighted in bold) that the bR_{568} angles are c36°, 40° and 21° for the $C_{18, 19}$ and $_{20}$ methyl groups respectively. Whilst a direct comparison of NMR and x-ray derived vectors may be compromised by variation of the membrane normal from the Y-axis of the PDB file, the agreement suggest that any such variation is limited. The measured angles are quoted with an error of ±2° which is derived from the width of the χ^2 minimum for the best fit value. The width of this minimum is related to the mosaic spread, a measure of the quality of orientation in the sample, and it is found that with increasing mosaic spread the χ^2 minimum also becomes broader. An additional error of ±2° for a mosaic spread of $\Delta\beta$ = ±8° has been derived from Monte Carlo simulations. Knowledge of the quality of the sample orientation and the ability to perform a χ^2 minimisation are particularly valuable when identifying angle solutions amongst mixed population samples as will be discussed below. Further errors would be expected from poor signal to noise spectra, decreased spin concentration (increased contribution from natural abundance background) and increased disorder in the sample.

Whilst there is little change in the angles near the β-ionone ring on formation of the M_{412} intermediate, there is a much more noticeable change at the C_{20} position. The consensus between the M_{412} static NMR data and crystal structures is that whilst there is little change in the angles at the C_{18} position there is a slight increase in the angle with

respect to the membrane normal at the C_{19} position which becomes even more pronounced at the C_{20} position (Fig 3.12). This data shows that the β-ionone ring acts as an anchor whilst the end of the chain attached to the Schiff base moves and initiates proton pumping.

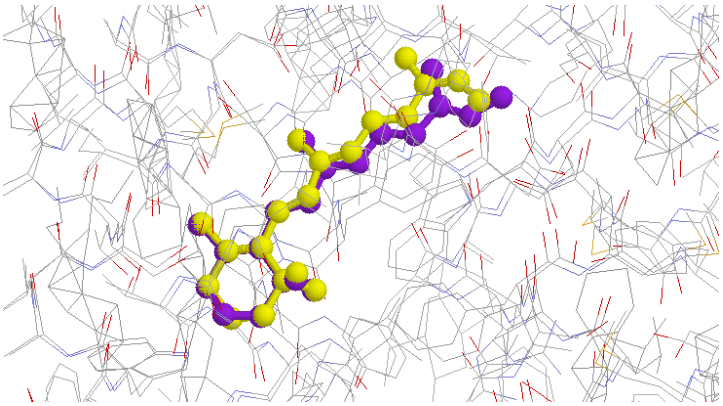

Fig 3.12. Figure showing superimposition of M_{412} (yellow) on bR_{568} (purple) state of retinal (From 1cwq.pdb (Sass *et al*, 1999). Note movement of retinal at C_{20} position whilst the β-ionone ring remains largely unaltered.

3.4.3 Problems with data analysis

The MAOSS data now diverges from the static NMR and crystal data for a number of reasons. In the case of the CD_3-18 vector, in the M_{412} state, it is possible to discern more than one solution for the angle from the NMR data when compared with a simulation. Using the lowest mosaic spread, an angle of 25° has been determined, however if a greater mosaic spread were to be used (as in Moltke *et* al, 1999) then a greater angle would be obtained, coincident with values from the static NMR and crystal structures. How should a mosaic spread be chosen for use in the data analysis? Moltke *et al*, 1999 evaluated the CD_3-18 vector in the D96A mutant and used two mosaic spreads

of Gaussian distribution with widths of σ 9.4° and 42.3° in their simulations. Clearly these two values are quite different and were taken to indicate two populations of purple membrane in their sample. This could well be the case with the data reported here with differing populations arising from either early or late M intermediates or residual ground state conformations which, whilst helping to understand the data, presents a number of issues. The first of these is very positive in that we are able to discern more than one population with this technique which will lead to greater accuracy of measurements as a result will not be an average of two or more solutions. This could be a real advantage when multiple conformations are allowed in a more complex system. Two main problems, however, are evident. Firstly how does one choose the correct solution? The three minima in Fig 3.7 have similar χ^2 values and the minimum with least mosaic spread (25˚) does not agree with static deuterium NMR experiments. In this case the "correct" solution is one with an increased mosaic spread. Mosaic spreads have previously been estimated from ^{31}P lineshapes from the lipids which are related, of course, to the protein environment but are still secondary reporters. Secondly what effect does the trapping have on the sample besides the conformational change? Is there increased mosaic spread due to trapping? Is the purple membrane alignment affected by Guanidine-HCl? These problems mean that the photostate of the sample needs to be more carefully controlled than was possible in these experiments. This will necessitate some technical steps whereby the sample can be cooled and illuminated in the NMR magnet whereas previously this has been done by trapping the sample in M_{412} at low temperatures outside of the magnet followed by as rapid as possible transfer into the pre-cooled magnet. This methodology is clearly a variable in the technique.

3.4.4 Conclusions

Deuterium MAOSS has been proven with these experiments to be able accurately to determine bond vectors in a functional protein. The low relative sensitivity of deuterium has traditionally meant poor signal to noise spectra with long acquisition times even with quite considerable amounts of sample. The MAOSS approach used here required only 25mg of singly CD_3 labelled protein whereas static approaches have required 100mg protein or more. By reducing spectral linewidths MAOSS can improve significantly the signal to noise obtainable, improving sensitivity by as much as 30 times whilst, at the same time, improving resolution such that a chemical shift difference can be observed between D_2O and CD_3. Deuterium has a low chemical shift range and it is not practicable at low fields to use deuterium labelling to discern chemically different sites. The improved resolution from MAOSS coupled with higher fields (800MHz plus) may mean that multiply labelled samples could be investigated. For the present though, the low natural abundance of deuterium and its non-perturbing nature when chemically engineered into a protein mean that deuterium MAOSS should be a valuable tool in the biological solid-state NMR spectroscopist's box.

The data obtained for the protein in the M_{412} state is of great importance for understanding the conformational changes, which underlie proton pumping in this

protein. The high-resolution structure determination from this work shows the events that follow light activation. The retinal chromophore provides the driving step for proton pumping and here the initial movement has been described. The β-ionone ring end of the retinal seems anchored into a tryptophan rich pocket and does not move much during photoexcitation. At the Schiff base end however the isomerisation to 13-*cis*, 15-*anti* causes the polyene chain to move toward the cytoplasmic side causing a larger change in orientation with respect to the membrane normal (see Figure 3.12). This data provides some clues as to how light activation may lead to proton pumping since this first conformational change must have a number of effects. These effects, with relation to the immediate local structure and proton pumping, have been discussed elsewhere (Luecke *et al*, 1999), but the question now arises about what other conformational changes result from the initial conformational change and how are they related to the movement of protons through the protein (in the bR_{568} state there is no channel visible through the entirety of the protein)? Since the major structural change in the retinal structure occurs close to the Schiff base linkage, it is clear that experiments will now focus on that region to determine how the retinal movement is commuted into the protein backbone and what pathways exist for the movement of protons around the protonated Schiff base.

4. Helix-Retinal Relationships in Bacteriorhodopsin using Homonuclear ^{13}C Through Space Interactions

4.1 Introduction

From the MAOSS NMR work in the previous chapter, other solid-state NMR sources (Ulrich *et al*, 1994; Watts *et al*, 1995[a]; Ulrich *et al*, 1995; Moltke *et al*, 1999) and x-ray evidence (Luecke *et* al, 1999[b]; Sass *et al*, 2000) the structure of the retinal chromophore of bacteriorhodopsin in both the bR_{568} and M_{412} states of the photocycle has been described to high resolution. Having ascertained that the major movement in the retinal is located at the Schiff base end of the polyene chain (Fig 3.12), a further, precise determination of the retinal-protein interaction can be attempted. This chapter will develop methods that can describe how the retinal is located with relation to helix G of the protein rather than with respect to the membrane normal as described using ^{2}H MAOSS in the previous chapter. Using recoupling techniques to reintroduce the dipolar couplings between nuclei, usually lost under MAS conditions, the distance between the C_{20} methyl group of retinal and the carbonyl of alanine 215 will be determined in the bR_{568} photostate. The recoupling experiments are being performed with a view to deriving conditions applicable to MAOSS experiments such that the orientation of the internuclear vector can be determined with respect to the membrane normal.

Distance measurements performed under MAS conditions have traditionally been applied only to randomly oriented "powder" dispersions where the orientational aspect of the internuclear dipolar coupling is averaged. By reintroducing macroscopic order to the

sample and comparing observed dipolar couplings between powder and oriented samples on reintroduction of the internuclear dipolar couplings an accurate measurement of the internuclear vector's orientation with respect to the membrane normal is possible. Most homo and heteronuclear recoupling techniques feature a more or less complex orientational dependence on the Euler angles Ω_{PR}. For example the pulse sequence C7 has a $\sin 2\beta_{PR}$ dependence whilst MELODRAMA and REDOR additionally depend on $\cos\gamma_{PR}$. Such angular dependence:

$$d^2_{0\pm1} = \pm\sqrt{3/2}\,\sin 2\beta_{PR} \qquad (9)$$

where the dipolar Hamiltonian terms of spatial elements are $m=\pm1$, leads to angle ambiguities where there may be more than one angular solution for a particular coupling (Glaubitz *et al*, 2001). However, if Hamiltonian terms with $m=\pm2$ are selected then the dependence:

$$d^2_{0\pm2} = \pm\sqrt{3/8}\,\sin^2\beta_{PR} \qquad (10)$$

is followed with unambiguous determination of the orientation of the internuclear coupling tensor (for detailed description see Glaubitz *et al*, 2001).

As an example, such an oriented recoupling experiment has recently been successfully performed in this laboratory, using heteronuclear REDOR recoupling methods on a sample containing [^{15}N-Leu$_{37}$, ^{13}C-Leu$_{39}$] phospholamban incorporated into

DMPC lipid bilayers (Middleton *et al*, 2000). If a REDOR experiment is performed on a well oriented membrane protein system where the internuclear vector for an I-S spin pair has a unique orientation with respect to the membrane normal and hence the rotor axis the observed dephasing (S/S_0) of the signal intensity of a resonance from a nucleus experiencing a single dipolar coupling in a REDOR experiment is given at a spinning frequency (ν_R) as:

$$\frac{S}{S_0}(\alpha_{IP}, \beta_{PM}) = \frac{1}{4\pi}\int_0^{2\pi} \cos\left[\frac{\nu_D}{\nu_R} 2\sqrt{2} \sin 2\beta_{ISM} \sin\alpha_{PM}\right] d\alpha_{PM} \qquad (11)$$

where angle α_{IP} defines the rotational excursion of I from a reference axis perpendicular to the rotation axis, α_{PM} is the azimuthal angle defining the protein distribution about the membrane normal, β_{ISP} is the angle between the I-S internuclear vector and the protein tilt axis and β_{PM} is the tilt angle for the protein away from the membrane normal. These defined angles are depicted in Fig 4.1.

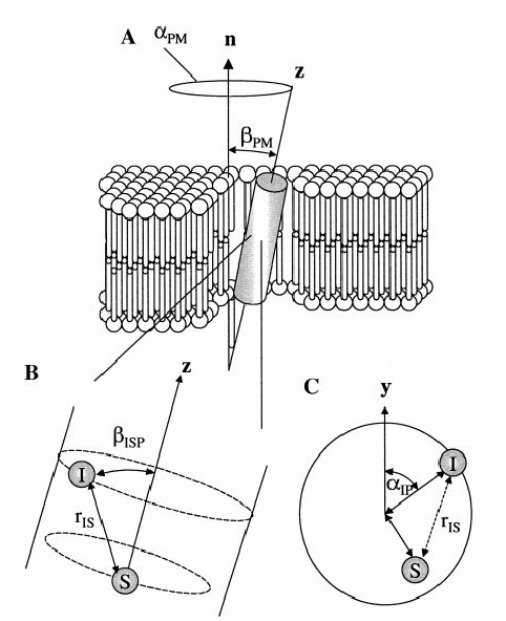

Fig 4.1. Definition of geometric terms for an I–S spin pair in a membrane-spanning peptide distributed within in a perfectly uniaxially oriented lipid bilayer with no mosaic spread. (taken from Middleton *et al*, 2000).

The angle ambiguity expected for an oriented REDOR experiment was observed, but it was noticed that for longer ^{13}C echo times (>15ms), the dephasing curves diverged and it was possible to separate the two solutions. Whilst it was possible to distinguish between the two possible solutions on this occasion it is not clear that this would be possible routinely nor with differing recoupling experiments as performed for homonuclear interactions. To this end rf pulse sequences are being designed using symmetry arguments such that Hamiltonian components with spatial rotational rank of $m=\pm2$ can be selected and a recoupling scheme with a monotonic angle dependence between 0° and 90° (Glaubitz *et al*, 2001). Practically, however, there are many problems associated with performing recoupling experiments on membrane proteins containing multiple spins and hence this chapter serves to analyse the most suitable method of recoupling homonuclear ^{13}C interactions in specifically labelled purple membrane preparations with a view to performing oriented recoupling experiments on large membrane proteins. The challenges incumbent to this approach include a potential lack of resolution between resonances of similar chemical shift, poor sensitivity and interference from natural abundance ^{13}C background. A variety of approaches will be used here to investigate a suitable range of currently practised and new NMR recoupling techniques for direct structural studies in large membrane embedded proteins. The labelling scheme used for this evaluation is shown in Fig 4.2 and highlights the close proximity of the three labelled carbons of Ala215 to the C-20 methyl group of the retinal.

Importantly, the twenty-eight other alanines in the protein (Appendix 1) are also labelled and are also shown in Fig 4.2.

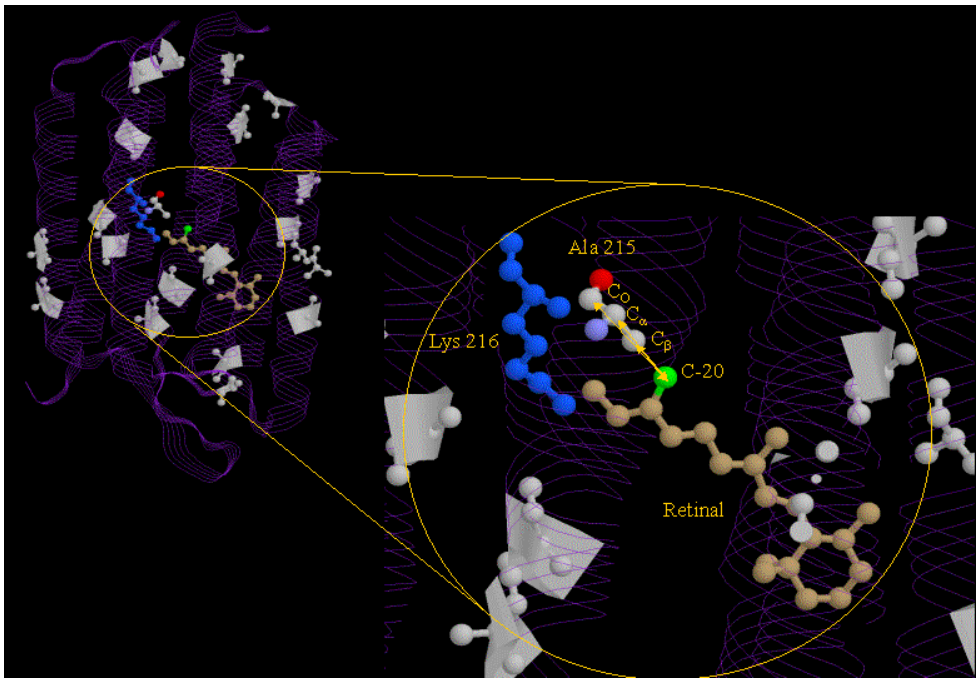

Fig 4.2. Labelling scheme for $^{13}C_{20}$ retinal and 1,2,3$^{13}C_3$-alanine labelled bacteriorhodopsin as a test case for various recoupling methods showing the distances to be measured in the bR_{568} state of the photocycle. The enlarged area shows Ala215 and its relation to the C-20 methyl group. Other alanines in the monomer are marked in white.

4.1.1 Rotational Resonance NMR

In a static solid state NMR experiment there exist dipolar couplings between nuclei in specific sites that may manifest themselves as a dipolar splitting in the powder spectrum in the absence of any decoupling pulses. The dipolar coupling is an important

structural parameter since it displays an r^{-3} distance dependence (equation 12) such that the intensity of the coupling increases as the distance between nuclei decreases. Magic angle spinning, however, reduces or completely removes the dipolar coupling such that this important distance information is lost. At certain spinning speeds however, the resonance lines of abundant nuclei with different chemical shifts have been seen to be dipolar broadened and have an enhanced Zeeman magnetisation exchange (Andrew *et al*, 1963; 1966). This phenomenon is called rotational resonance (RR). The use of rotational resonance for molecular structure determination has been demonstrated for a number of rather complex systems and has led to the generation of a general theory for internuclear recoupling under MAS conditions (Levitt *et al*, 1990).

Briefly, a sample, containing a dipolar-coupled pair of like spin nuclei, is set spinning at a rate $n\omega_r$ (n=1,2,3), which equals the frequency difference between the isotropic chemical shifts of both spins. At these rates the lines are broadened and split into doublets as the dipolar coupling is reintroduced at these spinning speeds and can now be used for distance determination by analysing the lineshape or by measuring Zeeman magnetisation exchange between the two sites.

The recoupling technique employed in this first experiment to measure the C_{20} to Cα-Ala215 is that of rotational resonance (Fig 4.2). The physical basis of R^2 is the measurement of the intensity of the magnetic dipole-dipole interaction which is proportional to r^{-3} where r is the distance between the two nuclei.

$$b_{IS} = -\frac{\mu_0}{4\pi}\left(\frac{\gamma_I \gamma_S \eta}{r_{IS}^3}\right) \qquad (12)$$

Reintroducing the dipole-dipole interaction as described above can lead to accurate internuclear distance measurements in crystalline samples as great as 0.6nm with error of only 0.01nm. This technique has been applied to a number of biological systems from simple α-helical peptides (Peerson *et al*, 1992) and M13 peptide (Glaubitz *et al*, 2000) through bacteriorhodopsin (Creuzet *et al*, 1991; Thompson *et al*, 1992) to the gastric proton pump (Middleton *et al*, 1997).

When the rotational resonance condition is met at spinning speeds which are the same as, or multiples of the isotropic chemical shift difference the dipolar coupling is reintroduced. This leads to two effects; firstly there is a broadening and splitting of the resonance lines that are usually well resolved under MAS conditions, secondly there is an enhancement of Zeeman magnetisation exchange which is the effect most usually employed in studying biological systems.

4.1.2 Radio Frequency driven Dipolar Recoupling (RFDR)

Even though the distances to be measured between the retinal methyl and the Ala215 methyl may be great in space (>3Å), the distances between their respective chemical shifts may be small (<1000Hz). In an instance when the chemical shift difference is of the order of a few hundred Hertz, Rotational Resonance becomes unsuitable for measuring distances since at such low spinning frequencies (which may be difficult to obtain practically) the chemical shift anisotropies and dipolar interactions will not be sufficiently averaged for a well resolved spectrum. RR is also unsuitable when more than one spin is being considered in a single experiment. As it is desired to

determine information from multiple labels, some with chemical shifts separated by only a few Hertz some alternative techniques were required.

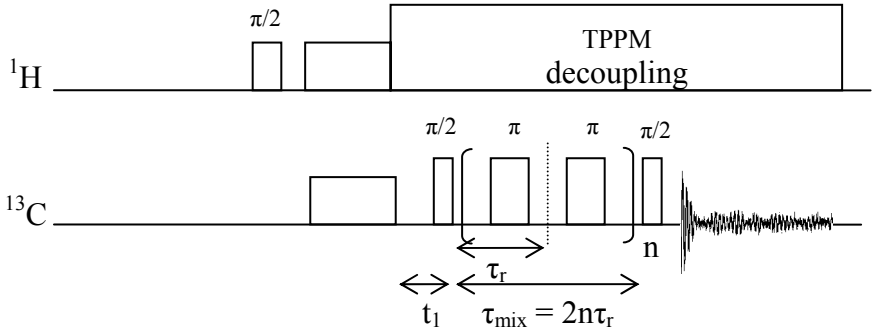

Fig 4.3. Pulse scheme for RFDR experiment with ^{1}H/^{13}C CP step. After a t_1 evolution period a π/2 pulse creates longitudinal magnetisation and rotor synchronised π pulses are applied once per rotor period during the mixing period τ_{mix}. A second π/2 pulse then regenerates observable magnetisation.

RFDR is a solid state NMR longitudinal exchange experiment that uses a series of rotor synchronised π pulses to reintroduce homonuclear dipole-dipole couplings that would normally be removed under MAS conditions (Fig 4.3). For multiply labelled samples RFDR is performed as a single quantum 2D experiment that records cross peaks between coupled spins. The intensity of the cross peaks is related to the size of the dipolar coupling between coupled spins which is itself dependent on the internuclear separation. The cross peak intensities can be compared with simulations to obtain distance information.

RFDR has already been applied to bacteriorhodopsin (Griffiths *et al*, 2000) to measure retinal-protein distances (Fig 2.6). Here the distances between the $^{13}C_4$ of retinal to Asp212 (labelled with 4-^{13}C-Asp) were determined in both bR_{568} and M_{412} states as 4.4±0.6Å and 4.8±1.0Å respectively.

4.1.3 Double Quantum Filtering

Recovering the dipolar couplings in a spinning sample by use of radio frequency pulses is possible using a number of techniques. When the site of molecular interest is labelled with pairs of rare spins, typically ^{13}C, then methods such as rotational resonance or dipolar recovery at the magic angle (DRAMA) allow measurement of internuclear distances. In larger molecules however, it is often difficult to discern the labelled sites from natural abundance signals. Spectral subtractions of experiments repeated with unlabelled samples can help however this obviously requires more sample preparation which can be a limiting factor and resultant subtracted spectra are generally noisy such that subtle interactions may be obscured. One solution to this problem is the excitation and recording of a double quantum coherence (DQC) to produce a double quantum filtered (DQF) spectrum. DQC is a correlation between the polarisations of two or more coupled spins ½ and may be readily distinguished on the basis of its symmetry properties under rf phase shifts. Signals from spin pair labels can be isolated from natural abundance spins by first exciting DQ and then reconverting it into an observable signal. Combining signals with different pulse phases leads to signal from only spin pairs. A number of pulse sequences have been proposed to perform this function in the solid state.

The first of these techniques is MElding of spin LOcking and DRAMA (MELODRAMA) (Sun *et al*, 1995) which is a variation of the DRAMA technique (Tycko & Dabbagh, 1990). This pulse sequence is successful in recoupling dipolar couplings under MAS conditions with a much reduced dependence on isotropic chemical shift differences and CSA which affect standard DRAMA sequences. In DRAMA, two

π/2 pulses of opposite phase for each rotor period recover the dipolar couplings with an efficiency of 27% in practice, or 52% in theory, of the ^{13}C signal when compared with a non-filtered experiment. The theoretical value is an evaluation of the pulse sequence's ability to recouple the dipolar Hamilitonian before being implemented on the spectrometer. The efficiency is low here because the spin dynamics of the coupled pairs is dependent on geometrical parameters, in this case the orientation of the molecule with respect to the rotor axis. Homonuclear rotary resonance (HORROR) has improved efficiency (60% experimental, 73% in theory) due to a reduced dependence on orientational terms (Nielsen *et al*, 1994). HORROR is dependent only on the β Euler angles whilst DRAMA and its variants are dependent on both γ and β. This means that only in samples where β is close to or directly aligned along the rotor axis does the sample experience weak DQ excitation. HORROR is, however, sensitive to rf field inhomogeneities and chemical shift differences. It performs well only for spin pairs with similar chemical shifts. The sevenfold symmetric phase shift scheme known as C7 (Lee *et al*, 1995) (Fig 4.4) is a rather more robust recoupling scheme which is not particularly sensitive to chemical shift and rf amplitude errors. Efficiencies of 54% are possible on systems with large differences in chemical shift. C7 and its modified version, Permutationally Offset Stabilised C7 (POST-C7) (Hohwy *et al*, 1998), are now commonly used as double quantum filters, as here, or for example, as a mixing sequence in a DQF-COSY experiment (Heindrichs *et al*, 2000). C7 is applied to our purple membrane preparations with a view to removing the natural abundance background and measuring dipolar couplings and hence internuclear distances without having to compromise on spinning speed, as in rotational resonance, or on resolution, as in RFDR.

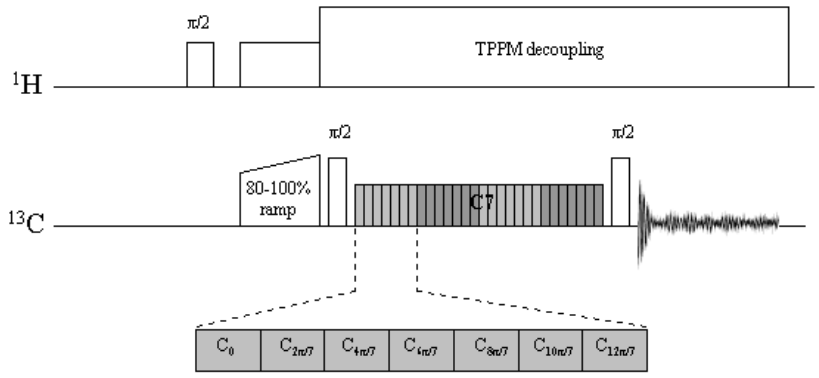

Fig 4.4. Pulse scheme for C7 experiment after Lee *et al*, 1995. In this figure four C7 loops are shown. Each loop occupies two rotor periods and each loop is shifted with respect to its neighbour by 180° to allow DQ excitation and reconversion.

Whilst C7 has been used previously on membrane proteins in measurements of torsion angles in retinal in rhodopsin (Feng *et al*, 1997; Feng *et al*, 2000), it has not yet been extensively applied to labelled membrane proteins, nor has it been extensively used to measure distances. The suitability of this approach for measuring relatively large distances in labelled membrane proteins will be tested here. The sample allows for a comparison of efficiency for establishing double quantum coherences between directly bonded nuclei in amino acid side chains and between nuclei separated by up to 4Å in space. Standard C7 sequences, when applied to membrane proteins can have poor efficiency and are complicated by the presence of more than two coupled spins. Further refinements of the methodology are required to solve these problems.

4.1.4 Selective Inversion and MQ Excitation (SIMQEX)

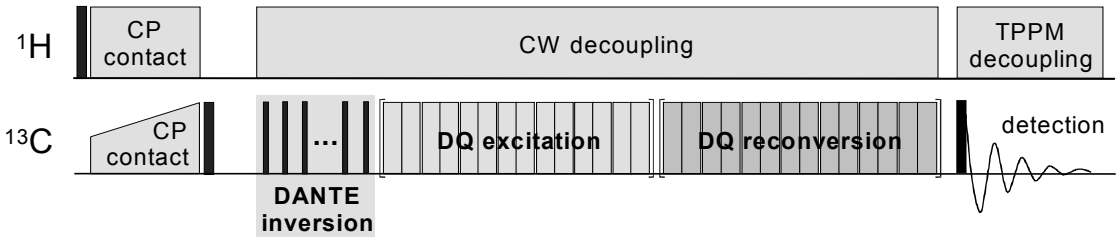

Fig 4.5. SIMQEX pulse sequence for LM and DQ-filtered experiments. A ramped (60 to 100%) CP period is followed by a $\pi/2$ pulse to convert ^{13}C polarisation into longitudinal magnetisation. Spins can be selectively inverted using the DANTE π-pulse prior to excitation of the ^{13}C-^{13}C DQ coherences with a C7 recoupling pulse sequence (Schnell & Watts, 2001). As in the standard C7 sequence each loop of 7 pulses occupies 2 rotor periods.

To compensate for the problems experienced with traditional double quantum recoupling schemes a new approach which allows selective observation of DQ coherences excited during dipolar recoupling was developed in our laboratory (Schnell & Watts, 2001). This approach, SIMQEX (Selective Inversion and MQ Excitation), is a broadband dipolar recoupling scheme (Fig 4.5) which can be tailored for DQ excitation while compensating for chemical shift differences, frequency offsets and other perturbing interactions. Through manipulation of the 64 step phase cycle it is possible to observe both the build up of DQ coherences or the decay of longitudinal magnetisation (LM).

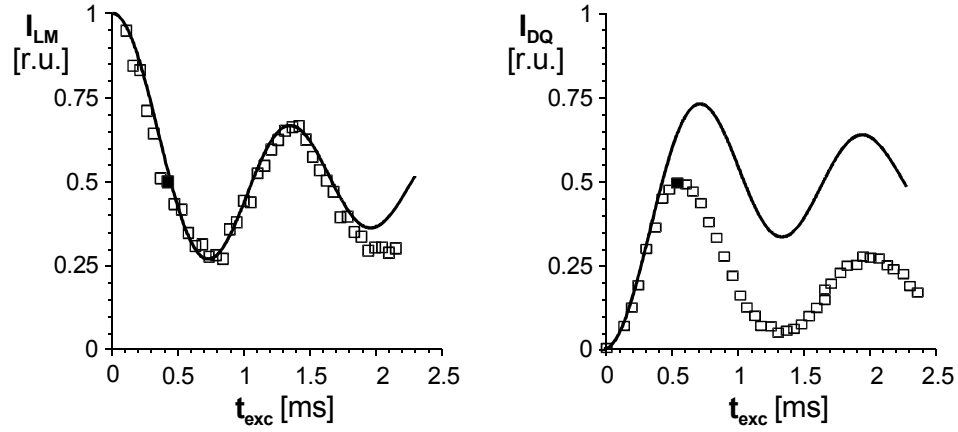

Fig 4.6. LM decay and DQ build up curves recorded on $^{13}C_2$-glycine. For each experiment there is a comparison of experimental (squares) and theoretical curves (solid lines) (Schnell & Watts, 2001).

Comparison of the LM decay and DQ build up curves, for the two ^{13}C spins of glycine experiencing DQC, in Fig 4.6 shows that the experimental LM decay curves agree well with the theoretical line whilst the experimental DQ build up curve is strongly affected by relaxation even at short excitation times. This shows that even in the $^{13}C_2$-glycine model compound the DQ version of this experiment suffers from experimental imperfections such as insufficient heteronuclear decoupling, RF field inhomogeneities and pulse imperfections that the LM decay version is insensitive to. Whilst the build up of DQ coherences has been extensively studied with a variety of recoupling schemes, its application to large compounds has been limited by sensitivity and multiple DQ coherences. Observation of the decay of longitudinal magnetisation allows for the acquisition of good signal to noise spectra in the same number of scans required for a standard CP experiment. This manufactured improvement in sensitivity allows for the study of smaller samples and potentially allows measurement of longer distances in labelled proteins.

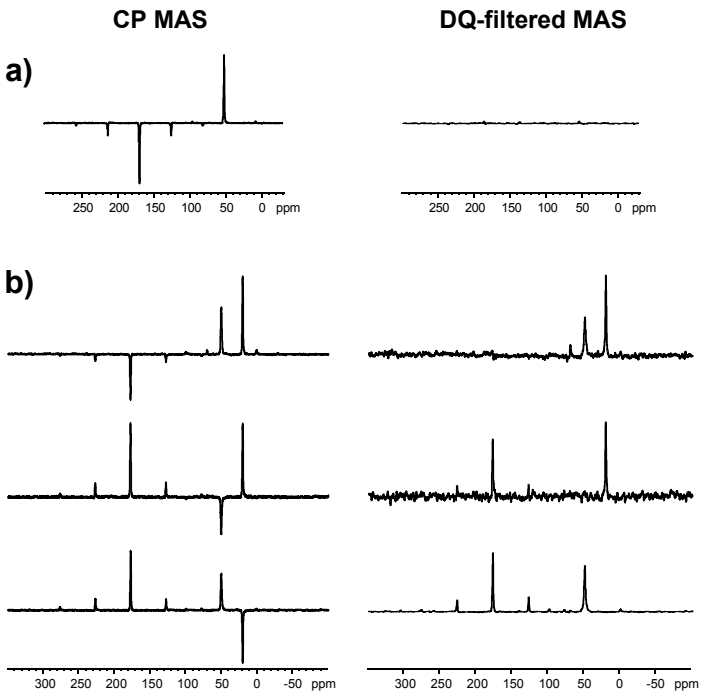

Fig 4.7. ^{13}C CP MAS and DQ-filtered MAS (SIMQEX) spectra of a) $^{13}C_2$-glycine and b) $^{13}C_3$-L-alanine. The CP MAS spectra reflect the initial states of the three spins, where one of the three spins has been inverted by a DANTE pulse, whilst the DQ-filtered spectrum, which can be observed in a SIMQEX experiment, shows the fate of the 3 spins following application of the C7 pulse train. It can be seen that inverted spins do not contribute to the DQ coherence (Schnell & Watts, 2001).

The selectivity of this approach is delivered by preparing an initial state of longitudinal magnetisation in which spins are selectively inverted prior to recoupling. The selective ability of the SIMQEX experiment is shown in Fig 4.7 where inverted signals in the CP MAS experiment are totally absent after application of the C7 pulse train. The selective excitation of the DQ coherence may also improve the range of compounds that can be studied since, in a multiply labelled sample, RR techniques can be impossible when more than one chemical shift difference lies close to a RR condition.

Experimental decay curves performed on the $^{13}C_3$-L-alanine standard are shown in Fig 4.8.

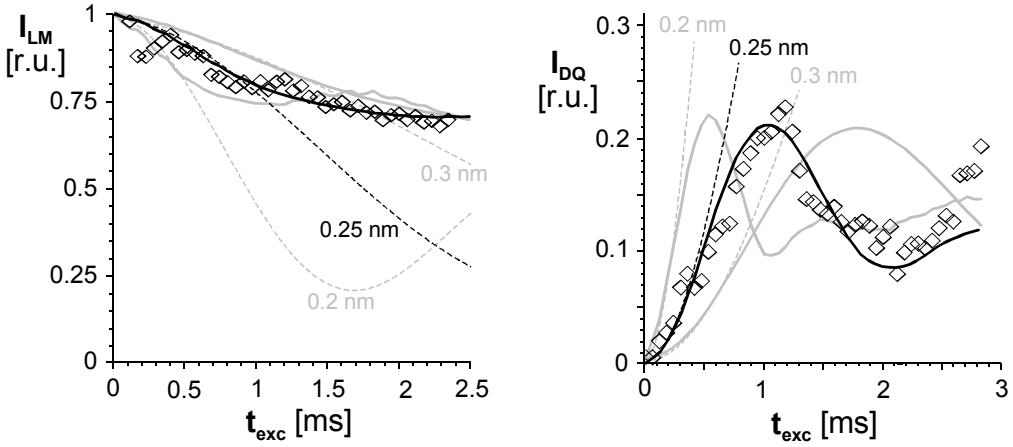

Fig 4.8. Comparison of SIMQEX results for LM and DQ experiments on $^{13}C_3$-L-alanine. Decay curves (LM) and build up curves (DQ) are shown for the ^{13}CO spin after inversion of the ^{13}CH spin. Experimental data points are compared with spin-pair curves (dashed lines) and simulated curves (solid lines) taking into account the three spin geometry in L-alanine. The black curves represent a ^{13}CO to $^{13}CH_3$ distance of 0.25nm (Schnell & Watts, 2001).

4.2 Materials and Methods

4.2.1 Sample preparation

Retinal, with ^{13}C in the C_{20} position (I. Burnett), was regenerated into retinal deficient bacteriorhodopsin according to published procedures (Oesterhelt, 1982).

Retinal deficient strain JW5, *Halobacteria salinarium* was grown in a synthetic medium (see Appendix 2.1.2) containing all nutrients requisite for normal growth (Helgerson *et al*, 1992). For this experiment either [U-^{13}C] or [2,3$^{13}C_2$] L-alanine was added to the synthetic medium in place of the usual unlabelled L-alanine. *H. salinarium* grown on synthetic media plates were used to inoculate 15ml of synthetic media (see Appendix 2.1.2) in a 50ml conical flask. The culture was incubated (105rpm; 37°C; in the dark). The absorbance was followed at 660nm. If growth continued this culture was used to start 1 litre cultures. When growth slowed (O.D checked at 660nm), 6mg all-*trans* retinal, dissolved in 2ml ethanol, was added over two days to each litre of culture. When the OD measurements had peaked the cells were harvested and the purple membrane purified as described previously, the sucrose gradient step was crucial to remove unincorporated retinals. The purity of the prepared membrane was checked through spectrometry as described in Chapter 3. The purple membrane was suspended in distilled H_2O and pelleted (average RCF 100,000g; 1hr; 4˚C) before being loaded into 7mm MAS rotors (Bruker). Approximately 10mg protein was produced from 1 litre of synthetic media.

4.2.2 NMR measurements

^{13}C MAS experiments were performed at 100.63MHz for ^{13}C on a BRUKER AVANCE 400 with double resonance 7mm MAS probes and spectra were referenced to the low field resonance of adamantane at 37.6ppm. Optimised ^{1}H-^{13}C cross polarisation experiments with CW proton decoupling were performed at varying spinning speeds that satisfied rotational resonance conditions to determine whether the sample was suitable for study by rotational resonance. 2D RFDR experiments were performed using a standard pulse program containing a cross polarisation step preceding the ^{13}C-^{13}C mixing period which was itself optimised for a strong (i.e. directly bonded) interaction using doubly ^{13}C labelled glycine as a standard and TPPM proton. The C7 experiment was similarly optimised on doubly ^{13}C labelled alanine such that double quantum build up spectra could be acquired with an efficiency of c40% when compared with equivalent CP spectra. The efficiency of the experiment was strongly dependent on the TPPM proton decoupling field strength which was adjusted to be more than twice the carbon field strength. SIMQEX experiments were optimised on uniformly ^{13}C labelled L-alanine. The experiment has similar characteristics to the C7 approach however the efficiency and selectivity of the inversion of resonances prior to excitation of double quantum coherences is particularly sensitive to the DANTE pulse. The DANTE pulse parameters

are typically optimised on the purple membrane sample using a simple pulse program consisting of a cross polarisation element followed by a π pulse to determine the required pulse length (Fig 4.9). The pulse length for the individual pulses in the DANTE pulse train are then calculated by dividing the π pulse by the number of pulses to be used and then the DANTE pulses are themselves optimised for each of the frequencies to be inverted using a pulse scheme such as that depicted in Fig 4.10. Key parameters for this set up prior to the SIMQEX experiment include the carrier frequencies for the frequency selective DANTE pulses, the DANTE pulse segment delays and the z-filter delay.

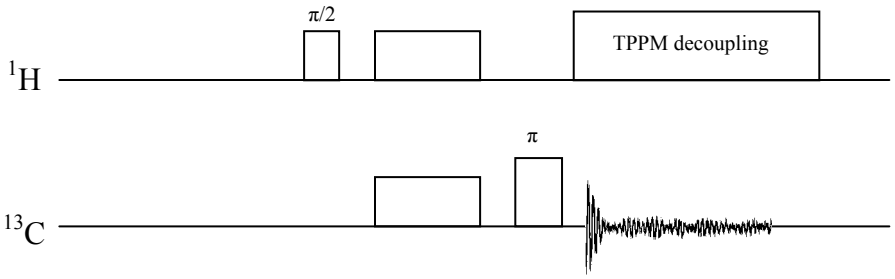

Fig 4.9. Simple pulse program for determining π-pulse length.

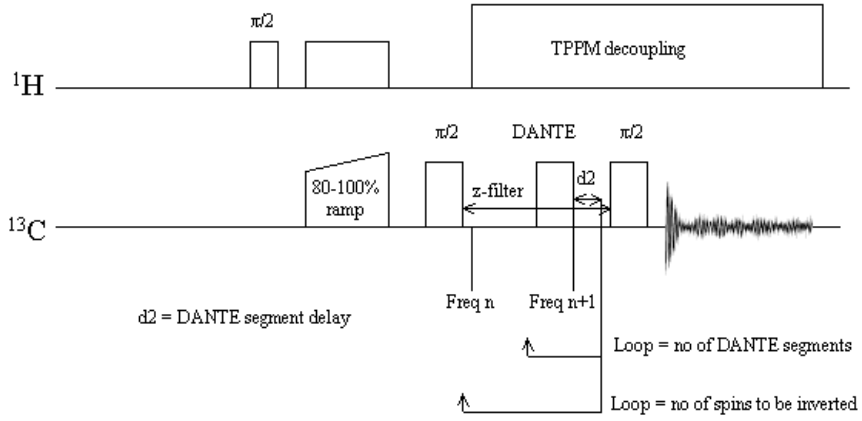

Fig 4.10. Pulse program used for optimising DANTE component of SIMQEX experiment. Following a CP step a π/2 pulse stores magnetisation along the *z* axis until returned to the *xy* plane by a second π/2 pulse. In

the meantime the DANTE pulse train is applied at the frequency of the first spin to be inverted and, after changing the carrier frequency, the program loops and inverts the second spin.

4.3 Results

4.3.1 Rotational Resonance

A comparison of spectra for purple membranes labelled with 2,3$^{13}C_2$-L-alanine and ^{13}C-20 retinal obtained at the RR condition for the C-20 and C_α (Fig 4.11) shows broadening and spitting for the C_α and C-20 as expected. However there is also considerable reduction in intensity of the C_β peaks, which can be more clearly seen in the spectral subtraction (Fig 4.12). At a MAS spinning frequency of 3659Hz (Fig 4.13), which is the rotational resonance condition (n=1) for the coupling between the C_α and C_β of the labelled alanines, a strong broadening and splitting is observed which can be more clearly seen in the spectral subtraction (Fig 4.14). There seems to be little or no contribution here from the C-20 of retinal. The interference observed at the n=1 RR condition was deemed unsuitable for accurate distance measurement and hence a full set of RR experiments at varying mixing times was not performed. In addition the slow spinning frequencies required for maintaining any RR condition may cause incomplete averaging of heteronuclear dipolar couplings to become a factor in spectral line broadening.

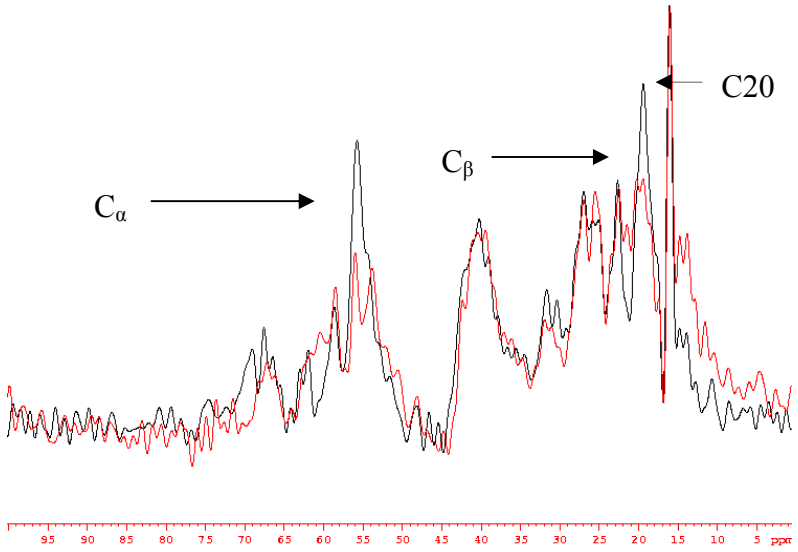

Fig 4.11. Comparison of standard (5000Hz; in black) and RR condition (3989Hz; in red)(between C-20 and C_α) spectra for the ^{13}C-20 retinal, 2,3^{13}CAla labelled bR. ^{13}C CPMAS spectra were acquired at 253K with 8k and 4k scans respectively. A recycle delay of 1.5s was used with a relatively short CP contact time of 500μs. ^{1}H decoupling (CW) field was 80kHz. A reduction in intensity of the C_α and C20 peaks, due to dipolar coupling between these spins, can be seen but also reduction in C_β intensity occurs.

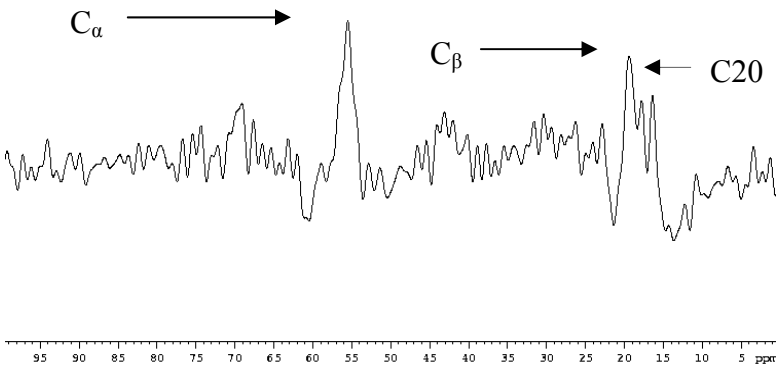

Fig 4.12. Subtraction spectrum from Fig 4.11 showing effect of spinning at RR condition between C-20 and C_α. There is a large reduction of intensity for both C_α (56ppm) and C-20 (16ppm) as well as for the C_β (19ppm). The RR spectrum (red in Fig 4.11) is subtracted from standard spectrum (black spectrum Fig 4.11) and then scaled to reveal less intense contributions.

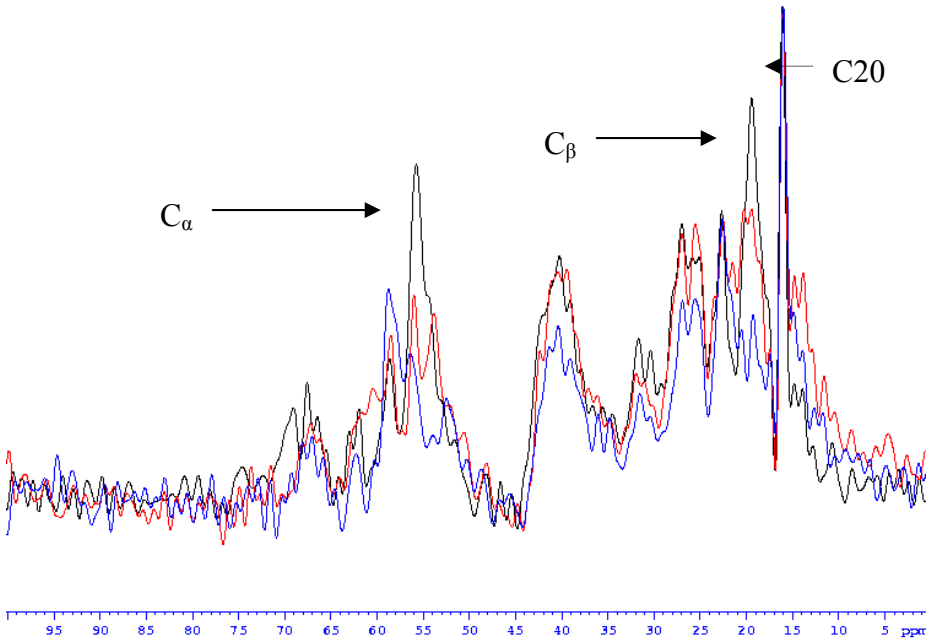

Fig 4.13. Comparison as in Fig 4.11 but also with spectrum at 3659Hz (in blue) (3989Hz spectrum in red) for RR condition between C_α and C_β of 2,3$^{13}C_2$ labelled alanines. ^{13}C CPMAS spectum was acquired as in

Fig 4.11 at 253K with 2k scans. An increased reduction of C_α and C_β peak intensity and increased splitting due to increased size of dipolar coupling is observed as indicated.

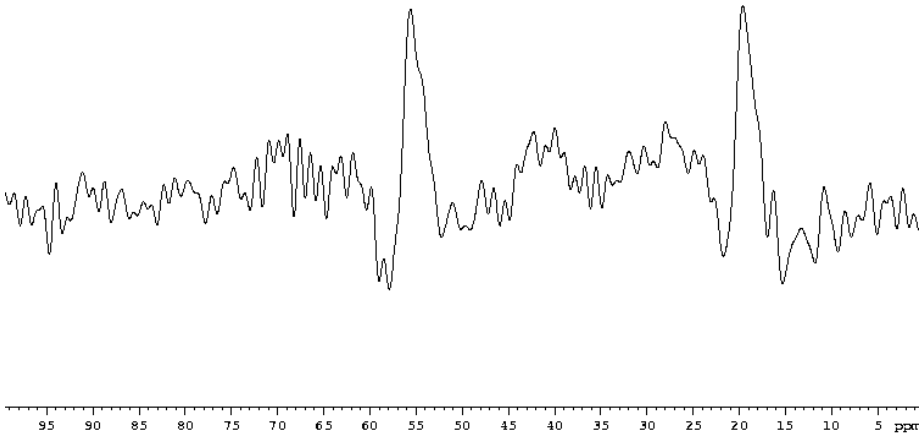

Fig 4.14. Subtraction of spectrum at 3659Hz (RR for C_α and C_β) from standard spectrum at 5000Hz MAS frequency (Fig 4.13 black spectrum), showing much cleaner interaction. There is some reduction in intensity for the C-20 peak however this is likely to due to a reduction of decoupling efficiency at lower MAS frequency. Subtraction performed with second RR condition spectrum (blue spectrum Fig 4.13) subtracted from standard (black spectrum Fig 4.13) and then scaled.

4.3.2 RFDR

The RFDR sequence is less dependent on MAS spinning frequencies and can be used to recouple dipolar couplings between nuclei irrespective of the chemical shift. In Fig 4.15 the RFDR spectrum of the 2,3$^{13}C_2$-Ala labelled sample is shown. In this experiment the usual 1D CPMAS spectrum is located along the diagonal and includes signals from both the labelled residues and, as at 175ppm for the carbonyls, natural abundance signals.

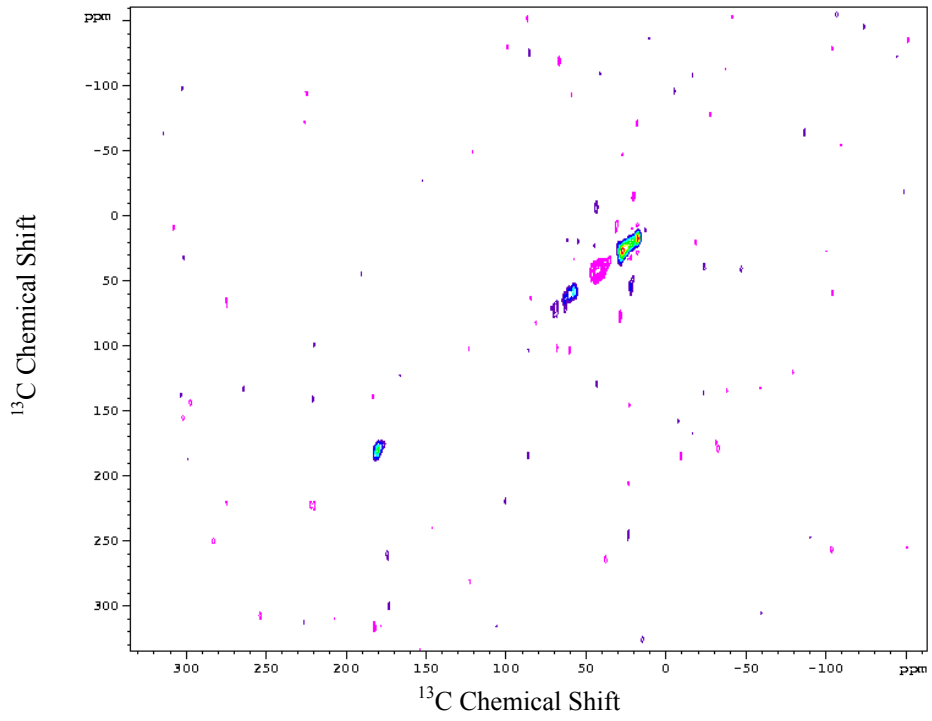

Fig 4.15. ^{13}C RFDR spectrum of ^{13}C-20 retinal, 2,3^{13}C-Ala labelled bR. Spinning speed 5000Hz, 233K, 2k scans with mixing time of 2ms. The CP contact time was 1ms and a 1s recycle delay was used. An 80kHz ^{1}H TPPM decoupling field was maintained over 40kHz used for the ^{13}C π pulses.

The enlarged region containing the labelled residues is shown in Fig 4.16. Cross peaks appear in the spectrum between coupled spins and, although the signal to noise is poor due to a low efficiency of heteronuclear decoupling, a cross peak between the directly bonded C_α and C_β of the 2,3$^{13}C_2$-Ala residues can be seen at 55/21ppm. The poor signal to noise prevents any cross peaks between the retinal and Ala215 being visible. The efficiency of this contact would be less than that of the C_α to C_β since there is only one coupling per bacteriorhodopsin monomer (compared with twenty-nine) and the coupling is over a greater distance. The linewidths in this experiment are poor due to the

relatively low MAS frequencies (5000Hz) and poor decoupling efficiency of the 7mm MAS probe used.

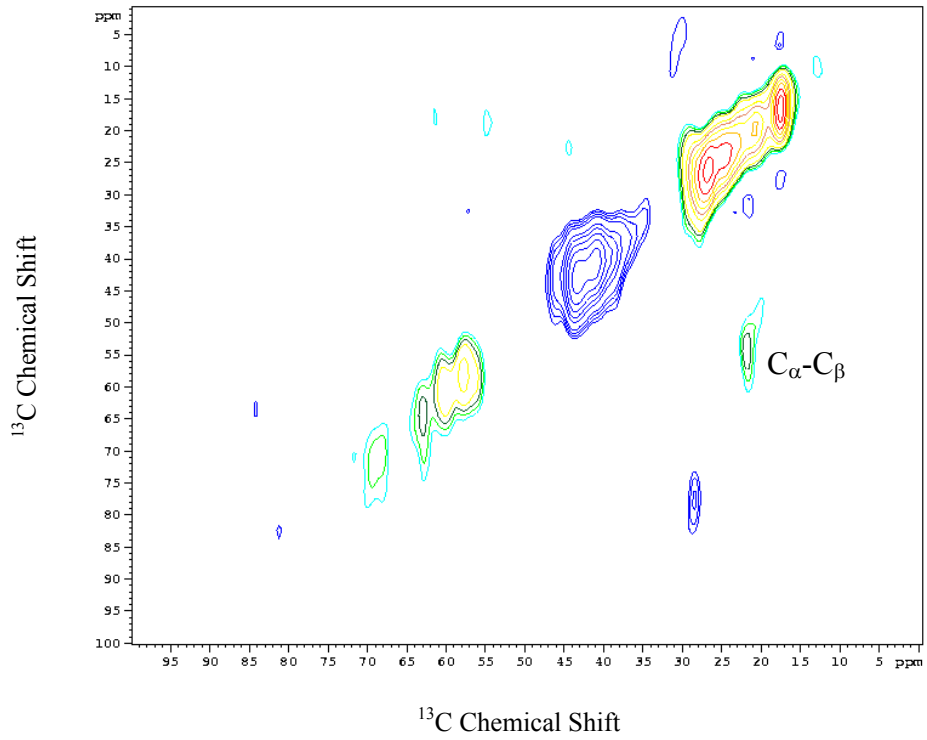

Fig 4.16. Enlargement of previous spectrum, showing cross-peaks for C_α to C_β at c55/21ppm. Blue contours signify negative intensities. C_β/C-20 cross-peaks are not resolvable.

4.3.3 Double Quantum Filtering (C7)

The double quantum filtered spectrum of purple membranes labelled with 2,3$^{13}C_2$-alanine obtained at room temperature shows that DQ coherences can be established between directly bonded labelled atoms in bacteriorhodopsin in the purple membrane. At short mixing times (Fig 4.17), efficient DQ coherence is obtained only between those spins close in space such that the resultant spectrum contains signals only from the C_α and C_β of the twenty-nine alanines in the full bacteriorhodopsin chain. The efficiency (20%) of this C7 experiment is poor considering the relative number of scans required for each spectrum and the poor signal to noise ratio of the DQF spectrum. At longer mixing times, as required to establish DQ coherences between more distant spins such as the C_β of Ala215 and C-20 of retinal, the efficiency will further drop and an accurate assessment of the C-20 resonance would not be possible.

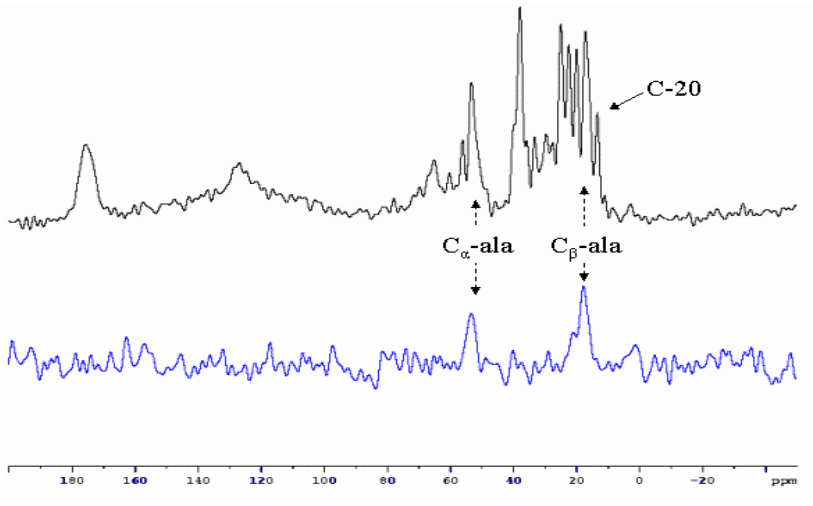

Fig 4.17. Comparison of CPMAS (black) and C7 (blue) spectra for ^{13}C-20 retinal, ^{13}C-2,3 alanine labelled purple membranes. Only the labels (C_α-alanine 56ppm; C_β-alanine 19ppm) that are strongly dipolar coupled appear in the 2QF (C7) spectrum. Spectra acquired with ω=5000Hz and at room temperature. Number of scans: CPMAS 16k; C7, 200k. Contact times of 1ms and recycle delay of 0.75s with 110kHz TPPM ^{1}H decoupling were used.

4.3.4 SIMQEX

The selectivity of the SIMQEX method is based on the ability to select signals for DQ coherence. This is done by inverting selected signals by application of a DANTE sequence which prevents them from contributing to double quantum coherences over short excitation times. The successful inversion of the C_O and C_α signals is shown in Fig 4.18, such that if DQ coherences were now excited, only the C_β resonances can be coupled to the C-20 or retinal. The C_O and C_α remain however coupled to each other so that a DQ coherence is established and, when the degree of dephasing of these resonances is measured, could be used as a calibration of the method in the sample.

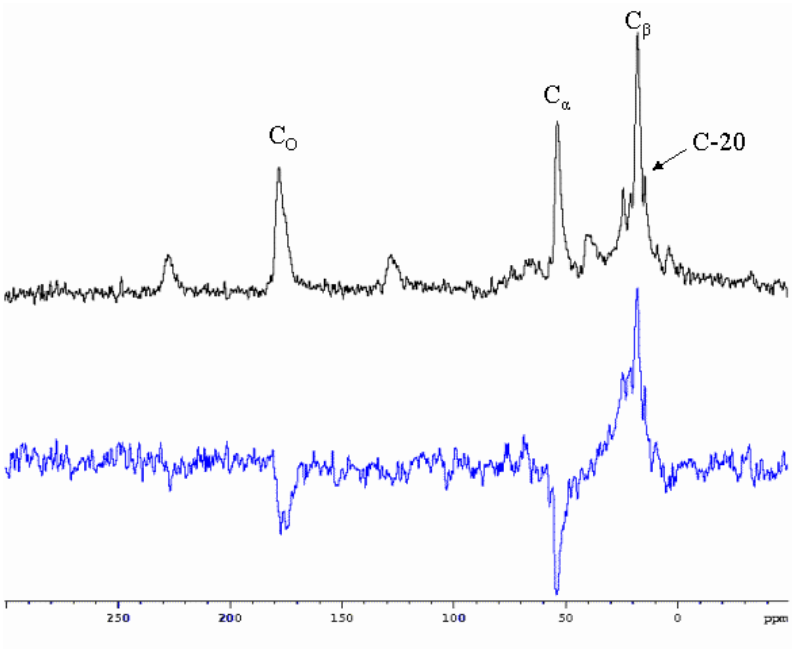

Fig 4.18. Comparison of standard CPMAS spectrum of [U-$^{13}C_3$] alanine, ^{13}C-20 retinal labelled purple membranes and CP spectrum with a double DANTE inversion of the C_O and C_α resonances (blue). Both spectra were acquired at 253K and 5kHz MAS frequency, 16k scans CPMAS, 8k scans DANTE. A ramped CP (60-100%) program was used with 500μs contact time, 2s recycle delay and 80kHz TPPM ^{1}H decoupling. For the DANTE inversion a 10ms Z filter with 12 DANTE segments, each delayed by 20μs, was used to invert the two spins.

The SIMQEX experiment yields a series of 1D spectra with different mixing times for the C7 cycle. Whilst the other NMR experiments used in this chapter suffer from a lack of sensitivity when trying to recouple distant spins or establishing DQ build up for single spin pairs the SIMQEX method reveals a decay of longitudinal magnetization due to DQ coherences between selected spins. In this respect the sensitivity of the SIMQEX method is not affected by the distances being measured and is also less dependent on the number of spins being studied. Preliminary data showed a decay curve for the ^{13}C-20 ($^{13}C_{\alpha}$ and $^{13}C_{O}$ inverted) corresponding to approximately 200Hz however further experimentation is required before an accurate measurement can be made and the data is not presented here.

4.4 Discussion

4.4.1 Rotational Resonance

The CPMAS spectra of the 2,3-^{13}C-alanine labelled purple membranes show that the most straightforward method of homonuclear distance measurement may not be applicable to this sample. The closest labelled nucleus to the C-20 of retinal (from X-ray structures) is the C_{β} methyl of Ala-215. This relatively strong coupling should be easily measurable in a rotational resonance experiment. However it is immediately obvious that this is not possible. This is because the C_{β} and C-20 methyl resonances are separated only by a few hundred Hz in the ^{13}C CPMAS spectrum. It would be physically impossible to spin stably at such low spinning speeds and the chemical shift anisotropies would not be efficiently removed. The more weakly coupled C_{α} has a chemical shift separated from that of the C-20 by 3989Hz which would allow a reasonable MAS rate. Spinning at

3989Hz reintroduces the dipolar coupling the effect of which can be seen in the spectra shown in Fig 4.11. The weak coupling that exists between the C_α and C-20 over a distance of approximately 5Å causes the respective peaks in the CPMAS spectrum to become broadened. At this relatively low spinning speed however a contribution of the very strong coupling between the directly bonded spins in the alanine and weaker heteronuclear decoupling are also able to assert an effect which is characterized by a severe broadening of both the C_α and C_β peaks. It is also not possible to rule out a broadening contribution to the C-20 peak from the C_β. These overlapping effects when trying to measure weak couplings, as in this case, rule out the use of rotational resonance for measuring the retinal-protein distances in this case.

4.4.2 RFDR

RFDR is a more demanding NMR experiment for a number of reasons. Firstly it relies on a series of rotor synchronised π pulses which means that stable spinning of membrane samples is crucial. Secondly it is important that a large mismatch (>2) between the ^1H and ^{13}C fields is maintained otherwise insufficient ^1H decoupling will lead to significant dephasing of the ^{13}C magnetization. In practice this means that very high ^1H power levels are required. Because these experiments are designed with a view to being performed under MAOSS conditions, a 7mm probe (suitable for 5.4mm glass disks) is used. These larger diameter probes are capable of holding more sample but have weaker performance at high ^1H fields. Consequently ^1H decoupling is not ideal which leads to weaker signal and lower resolution. Thirdly digital resolution may be

compromised in this 2D experiment which may prove problematical for spins that are not well resolved. It is possible to improve digital resolution by reducing the spectral width of the experiment, however in this case there are too many resonances from natural abundance ^{13}C widely distributed in the NMR spectrum such that any reduction in spectral width would lead to resonances being cut off and folding back in to obscure peaks. For these reasons RFDR is not suitable, in this case, for the determination of the inter-methyl distances on oriented systems in our 7mm probe however it has been shown that the dipolar couplings can be recoupled using radio frequency pulses. It is possible that the technique could be developed further, for application to bacteriorhodopsin, using different sample preparation techniques or by performing the experiments at much higher spinning frequencies and at higher fields. This could be possible if oriented samples could be prepared to fit in 4mm rotors and the membranes remain oriented stably at higher spinning frequencies. The SH3 domain of α-spectrin has been studied using this NMR technique and well resolved 1D CPMAS and 2D RFDR spectra were obtained (Pauli *et al*, 2000). The resolution obtained at high magnetic fields (18.8 and 17.6T) is impressive and suitable for future backbone and side-chain signal assignments (Pauli *et al*, 2001), however the major improvement in resolution obtained in this experiment occurred when the sample, instead of being lyophilized from solution, was precipitated from an $(NH_4)_2SO_4$-rich solution. What state the protein is in after this procedure is open to question, and this form of sample preparation is not suitable for studying proteins still functional in their natural membrane.

4.4.3 Double Quantum Filtering (C7)

Using a 7mm MAS probe on a Bruker DSX 400 we were enable to obtain C7 spectra for the labelled purple membrane at temperatures below freezing. The LN_2 boil off that we used as a bearing and drive gas at temperature below 253K caused severe arcing in the probe when using high power proton decoupling. This was thought to be due to some moisture in the boil off gas or tube. Consequently we were unable to perform C7 experiments at low temperatures. Experience in our lab has shown that optimum efficiency for C7 applied to fluid membranes can be obtained only at low temperatures since at room temperature the dipolar couplings are to some extent pre-averaged and hence reduced. However a DQ filtered spectrum was obtained at room temperature which, to our knowledge, has not been possible in other membrane systems. This is a reflection of the highly immobilised nature of the purple membrane environment and is possibly a unique property. The sensitivity of the approach for measuring internuclear distances, even for the strong coupling between the twenty-nine directly bonded spin pairs of alanine, was low. 200,000 scans were required to obtain the relatively low signal to noise spectrum shown in Fig 4.17 which is at a DQ excitation time giving the maximum efficiency of coupling for the directly bonded spin pairs. It can be seen that measuring longer distances (3.5Å as opposed to 1.1Å) for only one spin pair per bR monomer would be impracticable. Low temperatures with a new generation Bruker 4mm probe are now obtainable, since only the variable temperature gas and not bearing nor drive need be nitrogen gas. Faster MAS frequencies obtainable on this probe may improve linewidths and hence sensitivity, however the sensitivity might still not be

improved to a level suitable for the measurement of the longer distance. The presence of more than two types of spin cause problems for this approach since it is not possible to guarantee that DQ coherences established between remote spin pairs do not have a contribution from other spins. In this case the Ala215 C_β-C20 coupling could be influenced by the Ala215 C_α. Further development of this technique is required to make it useful in measuring distances in membrane protein containing multiple labels.

4.4.4 SIMQEX

The SIMQEX experiment allows a distance estimate to be determined in a little over a day's acquisition. Previously, it was typical for each data point in a decay curve, needed for a distance measurement, to be obtained in a similar amount of time. The observation of the decay of longitudinal magnetisation reduces the time needed for a single distance measurement from over a week to less than two days. This in itself can be considered a very beneficial advance. It is also possible to measure a single distance in a multiply labelled protein despite the presence of multiple resonances and couplings and irrespective of their relative chemical shifts. Being able to select the resonances to be involved in double quantum coherences allows a number of different couplings to be measured in the same sample.

Preliminary experiments were however deficient in some areas. Due to problems associated with using high proton decoupling fields at low temperatures on our 7mm probe, we were initially unable to perform these experiments on frozen light adapted bR. The CPMAS spectra of frozen purple membrane are much better in terms of signal to noise ratio and natural abundance contribution of lipids when performed at around 243K.

The reduction of signal to noise in spectra acquired at room temperature increases the duration of the experiment and contributes to increased error in the data analysis. Dark adapted bR samples have been shown to possess two populations of retinal. Both the ground state all-*trans* isomer and also the 13-*cis* isomer exist in the dark at room temperature. The chemical shifts for the ^{13}C-20 of these two isomers of retinal in bR are not distinguishable in our spectra. Resonances for carbons further down the polyene chain are reported to give rise to two distinct resonances for each of the two isomers (Griffiths *et al*, 2000; Helme *et al*, 2000). The distance measurement here performed on the dark adapted sample is therefore a demonstration of the technique since the contribution from 13-*cis* retinal, which accounts for up to 60% of retinal in a dark-adapted sample, cannot be controlled for.

The SIMQEX method coupled with specifically ^{13}C labelled protein is suitable for selectively measuring internuclear distances. However with greater separation between the labelled sites the error associated with measuring the dipolar couplings (of only a few hundred Hertz) becomes increasingly significant. With an oriented sample the differences in the measured dipolar couplings are crucial to establishing the orientation of the internuclear vector and the method as it stands would be unable to measure the dipolar couplings with sufficient sensitivity to reliably distinguish differing orientations. The problems associated with comparing peak intensities that change only very slightly over a range of orientations could however be solved by observing the dipolar couplings, refocused in a separate dimension. The observed splitting of these couplings would be more sensitive to the orientation and a more accurate determination of the orientational component of the dipolar couplings could be effected. For this refocusing to be

achievable under experimental conditions a greater level of sensitivity would be required. This may be obtainable by performing the SIMQEX experiments at higher spinning frequencies, lower temperatures and at higher magnetic field strengths. Chemically or dynamically induced polarisation may also serve to increase the sensitivity of this approach and consequently increase the potential to study the magnitude and orientation of dipolar couplings over longer distances that are theoretically measurable between ^{13}C labelled nuclei. The ability to measure accurate distances and orientations between internuclear vectors would be of considerable benefit for the application of distance constraints in solving structural problems.

5. Multiple Angular Constraints from Specifically Labelled Bacteriorhodopsin Identified by ^{15}N-MAOSS NMR

5.1 Introduction

The two main problems from which solid-state NMR suffers when applied to membrane systems, are lack of resolution and sensitivity. Resolution presents a problem in that chemically distinct species cannot be resolved as their resulting lines may be so broad that they merge in the NMR spectrum. One method of improving resolution is to apply two-dimensional PISEMA NMR experiments to static-oriented systems (Fig 1.7). Such experiments use the inherent resolution of the ^{15}N anisotropic chemical shifts and ^{1}H-^{15}N dipolar coupling in combination. These techniques have been used with great success and have lead to the determination of the first three-dimensional structure of a membrane protein for the Protein Data Bank (1mag.pdb; Ketchem *et al*, 1996). The resolution achievable in these experiments is, however, dependent on the spectral linewidths which in turn depend on the magnetic field strength and the quality of the orientation in the membrane sample. For larger membrane proteins, the quality of orientation deteriorates when compared with small peptides, which leads to a reduction in resolution and sensitivity. For large proteins, an alternative method of improving resolution is therefore required.

Greater value will be obtained from MAOSS applied to membrane proteins when more than one NMR active nucleus can be resolved and direct structural information derived. To develop the approach multiply labelled proteins must be studied with a view

to deriving multiple orientational constraints. In this Chapter MAOSS is extended to studying the orientations of labelled sites in selectively ^{15}N-methionine labelled purple membranes. There are nine methionine residues in the sequence of bacteriorhodopsin (Fig 5.1). Six of these residues are located within the helical domains with two in loops, one external, one internal. Methionine 32 appears in the electron diffraction structure (Grigorieff *et al*, 1996) to be at a loop-helix interface.

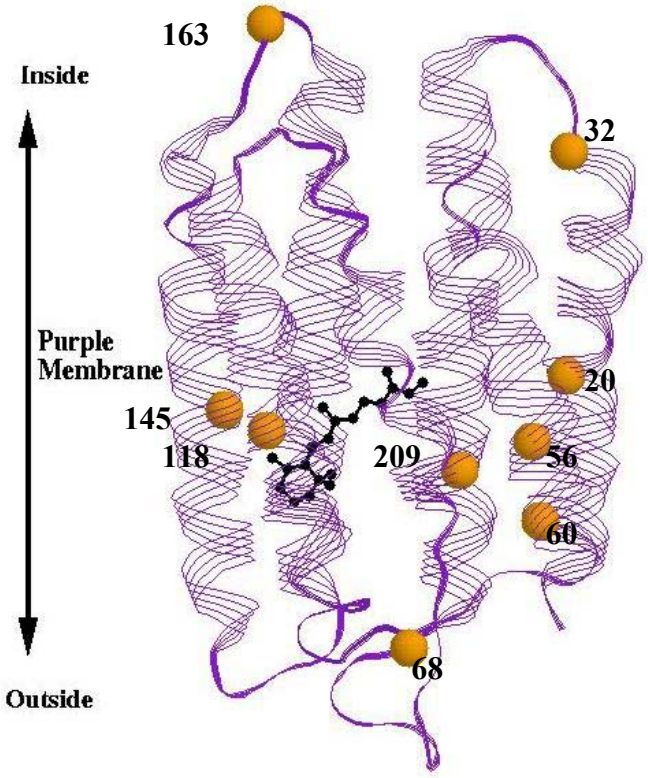

Fig 5.1. Structure of bacteriorhodopsin as obtained from PDB file 2BRD. These coordinates were obtained through electron diffraction of two-dimensional crystals (Grigorieff *et al*, 1996). This structure was one of the earliest high-resolution structures produced and contains information for most of the polypeptide chain. The retinal is shown in black. The methionine residues that were labelled in this experiment are shown as orange spheres. Two methionines are thought to be in the loops whilst the seven remaining residues are in α-helices.

The peptide plane orientations of residues in helices and loops should be radically different from each other and hence it should be possible to differentiate between them. The peptide plane orientations of residues located within helices are also intrinsically related to the helix tilt which can be measured. Methionine has been shown in previous studies to be incorporated into bacteriorhodopsin with an efficiency greater than 95% (e.g. Seigneuret *et al*, 1991). Through enriching bacteriorhodopsin with ^{15}N labelled methionine the aim of this chapter is to resolve the methionine amide peaks under MAS conditions and determine the orientations with respect to the membrane normal of the ^{15}N CSA tensor.

5.1.1 Sensitivity of ^{15}N NMR to the orientation of peptide planes

Magic angle sample spinning (MAS) provides well resolved spectra, even at relatively low magnetic field strengths, by projecting all anisotropic interactions onto the axis of rotation where they collapse at the magic angle (Maricq & Waugh, 1979). The anisotropic interactions that cause line-broadening are removed and, at high spinning frequencies, only the isotropic chemical shift is retained in a solution like spectrum. Under MAS conditions the broad characteristic powder pattern of an inhomogeneous interaction (such as chemical shift or quadrupolar coupling) decays into a set of narrow, well resolved spinning sidebands around the isotropic chemical shift when the spinning frequency does not exceed the anisotropy. The intensity of each of these sidebands depends on the size of the interaction tensor (Herzfeld & Berger, 1980; De Groot *et al*,

1991) and, in an oriented sample, features an additional orientational dependence (Fig 5.2).

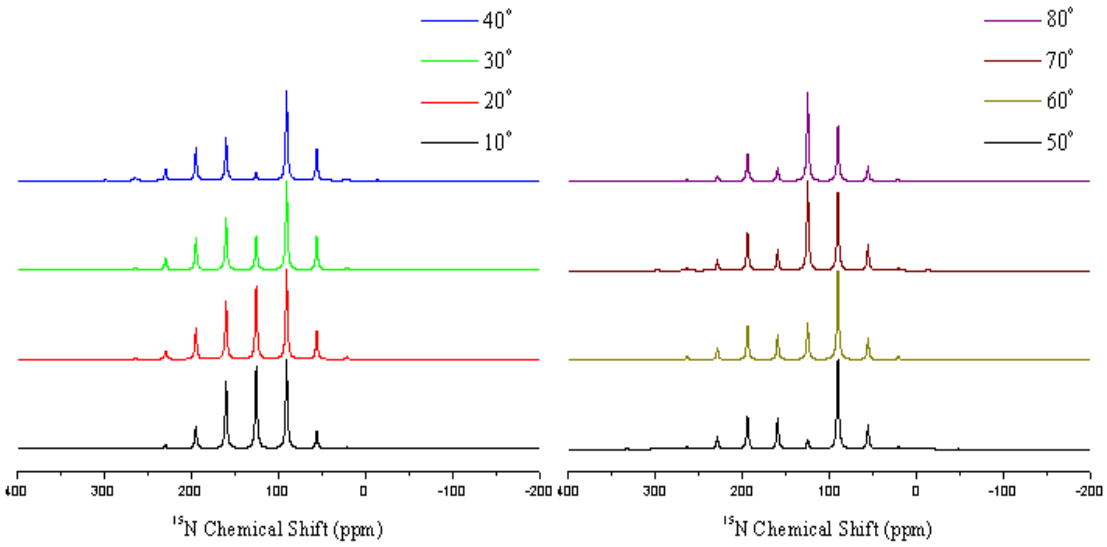

Fig 5.2. Simulated MAOSS spectra for spin = ½ nucleus showing responses to alterations in molecular orientation with respect to the rotating frame (and hence membrane normal). The CSA was set as 4000Hz with a spinning speed of 1400Hz and an asymmetry parameter of 0.25.

This orientational dependence allows the measurement of the tensor vectors with respect to the sample director and led to the introduction of the technique of Magic Angle Oriented Sample Spinning (MAOSS)(Glaubitz & Watts, 1998). As described in the introduction (1.3) the experiment consists of taking a suspension of membrane films and uniformly aligning them on thin glass disks. The disks are then mounted in a MAS rotor which is spun at modest spinning frequencies at the magic angle in a magnetic field. In this case, the principal axes of the ^{15}N chemical shift anisotropy (CSA) tensor will be determined with respect to the membrane normal of the purple membrane. The principal axes of the ^{15}N CSA tensor are related to the molecular frame, in this case the peptide plane, by a set of Euler angles. For this experiment the axes of the peptide plane are

defined as being the same as the ^{1}H-^{15}N dipolar coupling (Fig 5.3). Whilst the y-axis of the dipolar coupling and σ_{22} are collinear the z-axis and σ_{11} (least shielded component) are related to each other by an angle θ which varies slightly from helical to loop residues (Fushman *et al*, 1998).

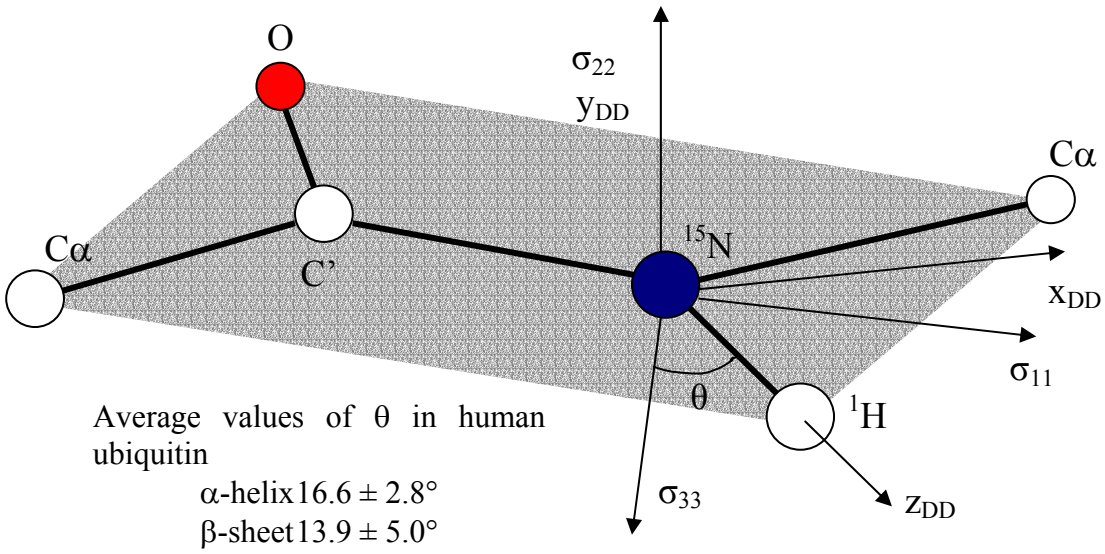

Fig 5.3. Definition of axes for ^{15}N CSA and ^{1}H-^{15}N dipolar coupling relative to the peptide plane in a ^{15}N labelled residue. The y-axis for the dipolar tensor and σ_{22} CSA tensors are assumed to be collinear, therefore the CSA→NH transformation is a rotation about the y_{DD} axis by an angle θ. Average angles for θ in human ubiquitin are given for α-helical and β-sheet residues in solution (Fushman *et al*, 1998).

A hierarchy of Euler angles relates the principal axis system of the ^{15}N CSA tensor to the rotor frame which is equivalent to the membrane normal for membranes oriented on glass plates (Fig 5.4). A simulation of the expected sideband pattern is produced by a computer program that optimises the Euler angles relating the rotor frame to the principal axis system (Glaubitz *et al*, 2000). Hence the best fit spectrum when compared with an experimental spectrum will yield the Euler angles that relate the rotor frame to the principal axis system of the ^{15}N-CSA which can be related in turn either to a

helix tilt angle, the orientation of the peptide plane or, assuming a value for θ (Fushman *et al*, 1998; Heise *et al*, 2000), the orientation of the N-H bond vector.

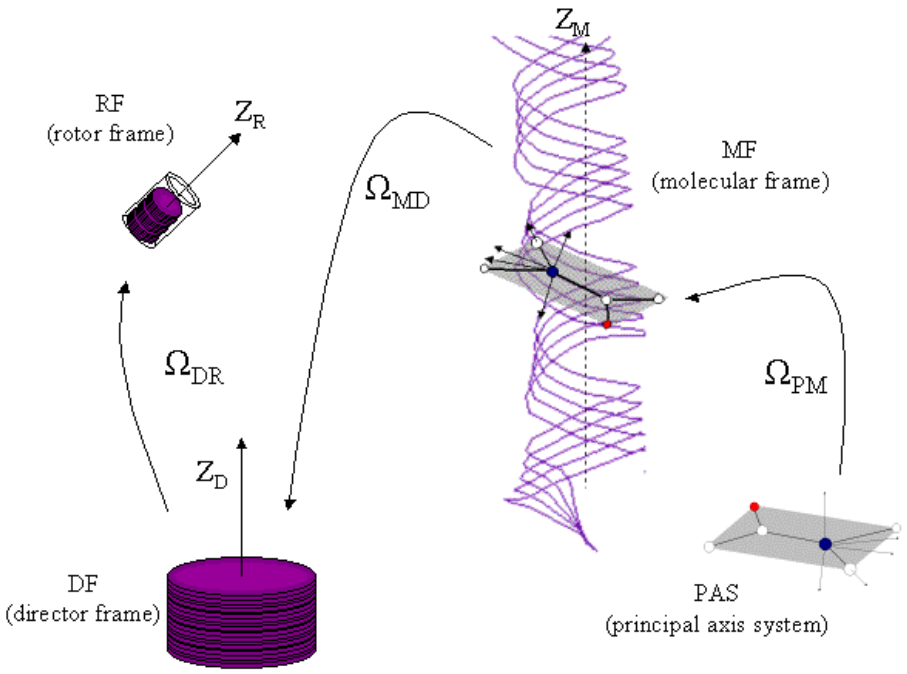

Fig 5.4. The series of Euler angles that relate the membrane normal and the rotor long axis (Z_R) to the principal axis system of the ^{15}N CSA tensor (after Glaubitz *et al*, 2000).

5.1.2 Resolution, assignment and spectral simplification

One potential problem with the MAOSS approach is that the chemical shift differences between these methionine labelled sites may not alone be sufficient to resolve all nine residues. Complete resolution in NMR spectra is a pre-requisite for accurate analysis of data and the resulting production of structural parameters. It may be possible to use other dimensions or faster sample spinning to generate extra resolution or even an

increase in magnetic field strength may be necessary before complete resolution is possible.

One tool for improving spectral simplification might be the application of selective labelling techniques using ^{15}N-enriched amino acids with specific neighbour residues enriched in ^{13}C allowing a HETCOR experiment to be applied (Fig 5.5). In these experiments the ^{13}C amino acids would be used as a selective filter for those ^{15}N labelled amino acids that are adjacent on the primary sequence. This technique would not only simplify the spectrum such that a single site could be analysed but it would also assign the resonance to the particular amino acid. If resolution were not a limiting factor then a standard CP-MAS spectrum could be employed in conjunction with a ^{13}C REDOR dephasing pulse to assign the residue of interest.

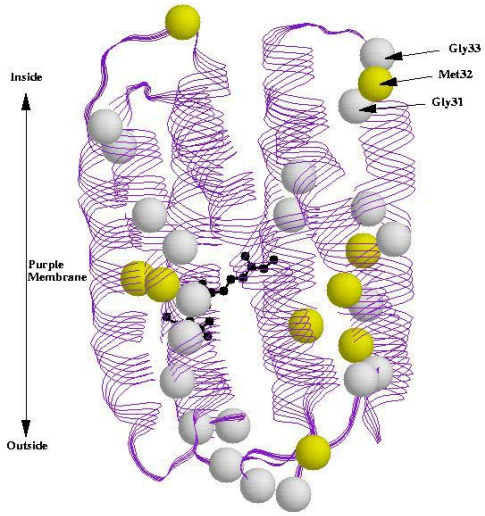

Fig 5.5. Labelling scheme for ^{13}C-^{15}N-correlation spectroscopy or ^{13}C REDOR dephasing of ^{15}N signals, in this case the ^{13}CO of Gly 31 is uniquely directly bonded to the ^{15}N of Met 32. This labelling allows the use of the dipolar coupling to filter out resonances to leave a specific resonance of interest. This will solve the

problem of convoluted spectra and also assignment, in this case of Met 32. Either ^{13}C or ^{15}N can be observed which will allow a range of experiments to be performed.

5.1.3 Anisotropic constraints at high MAS frequencies

At higher spinning speeds there is a dramatic improvement in resolution which would allow nearly all resonances to be resolved. At such high spinning speeds however no spinning sidebands remain and all orientational information is lost from the ^{15}N CP MAOSS spectrum. In addition to the ^{15}N CSA, other useful anisotropic interactions exist in a solid-state sample that can be employed to provide structural constraints. The ^{15}N amide nitrogens, in the ^{15}N L-methionine enriched protein, experience a strong heteronuclear dipolar coupling with the amide protons. The size of the dipolar coupling has a strong distance dependence and is also very sensitive to its orientation with respect to the magnetic field, a property that gives rise to the PISEMA experiment discussed above. The dipolar coupling is a particularly interesting quantity in that it describes the distance and orientation of the ^{15}N-^{1}H bond which is easier to relate to peptide structure than the CSA axes and may be more sensitive to interactions involving the amide proton, such as de-protonation events. Under MAS conditions the ^{15}N-^{1}H dipolar coupling is largely averaged and is usually decoupled with pulses applied to the proton channel since this coupling often contributes considerably to experimental lineshapes of less abundant nuclei. The amide proton also experiences strong homonuclear dipolar couplings with the network of other protons in the sample. These homonuclear couplings serve to hinder the isolation and measurement of discrete ^{15}N-^{1}H couplings. In order to measure the heteronuclear dipolar couplings from resolved resonances in a MAS experiment a

technique that is able to selectively recouple the ^{15}N-^{1}H dipolar coupling without substantial interference from the proton pool is required. One such experiment was recently described (Saalwächter *et al*, 1999) which uses a REDOR (rotational-echo, double resonance) π-pulse train to selectively recouple the heteronuclear dipolar interaction during the excitation and reconversion periods of a heteronuclear multiple quantum correlation experiment. The recoupled polarisation technique (REPT) relies on fast MAS to suppress all homo and heteronuclear dipolar couplings, even between protons. Since such couplings contribute to spectral linewidths when not fully averaged, faster MAS spinning frequencies should be expected to improve resolution and sensitivity in NMR spectra as an extra advantage of this technique. The spinning frequencies initially employed on standard samples were of the order of 35kHz however for biological samples, due to the relatively weak signals, more sample is generally required and larger MAS rotors are needed such that sample spinning frequencies are around 15kHz. The heteronuclear dipolar order rotor encoding (HDOR) variant of the REPT experiment is used (Saalwächter *et al*, 2001). Following the introduction of a t_1 interval, a symmetric sideband pattern emerges, in this case refocused into a second dimension (Fig 5.6), which reflects the size of the dipolar coupling experienced between the ^{15}N-^{1}H spin pairs in the labelled residues. The dipolar coupling can be measured from analysis of the sideband pattern (Fig 5.7) and a bond length determined.

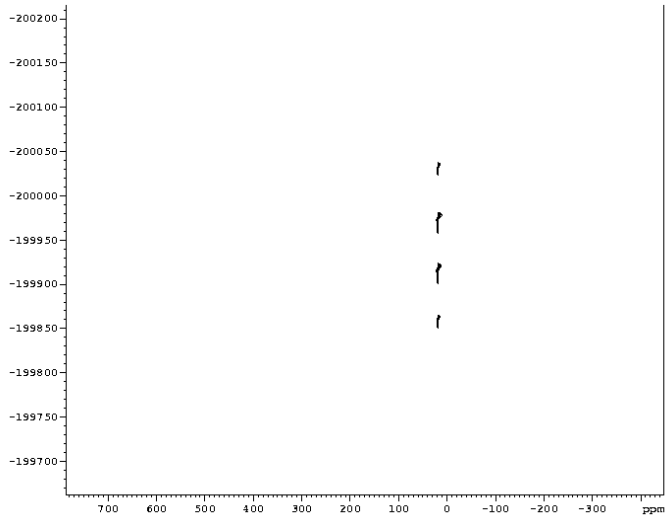

Fig 5.6. 2D ^{15}N chemical shift/^{1}H-^{15}N dipolar coupling REPT-HDOR MAS spectrum of ^{15}N-alanine powder. Experiment performed at 298K with spinning speed of ω=14286Hz and a mixing time equal to 2 rotor periods.

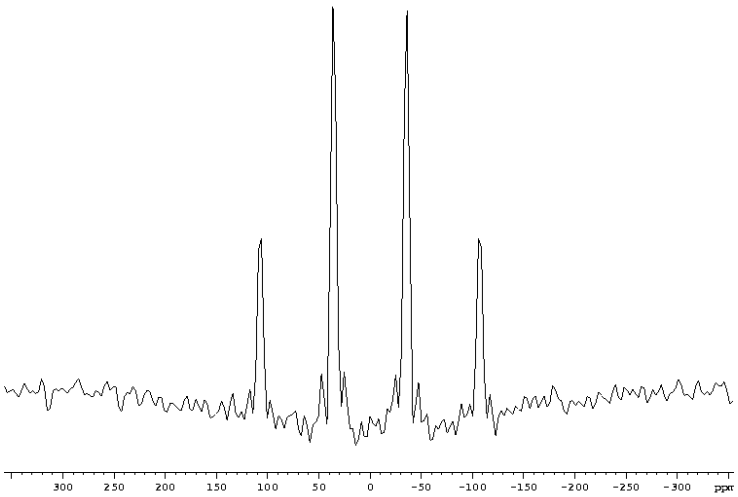

Fig 5.7. 1D slice from 2D (Fig 5.6) spectrum showing ^{1}H-^{15}N dipolar coupling sidebands. The sidebands reflect the size of the dipolar coupling in the powder sample.

The relative intensities of the spinning sidebands have an orientational dependence similar to those of the ^{15}N-CSA and it is also possible to measure the relative

strengths of the dipolar couplings and thence to even get a distance measurement between the amide nitrogen and its proton. The angle measured in an oriented system would then not be the angle of the z-axis of the ^{15}N-CSA but that of the ^{1}H-^{15}N dipolar coupling and hence of the N-H bond. This is an advantage as this measurement is then directly related to the peptide structure whereas in the case of the standard ^{15}N CP MAOSS experiment the measured angle has to be transformed according to an assumed relationship between the geometry of the ^{15}N CSA and the N-H bond. This refinement of the MAOSS technique, providing that samples can be spun stably at high MAS frequencies, allows fast spinning MAS (up to at least 15kHz) which will provide maximum possible resolution in the first, ^{15}N chemical shift, dimension whilst at the same time allowing measurement of angular constraints. The high speed MAS will be particularly advantageous when confronting a sensitivity problem.

5.2 Materials and methods

5.2.1 Sample preparation

Halobacterium salinarium were cultured in a synthetic medium (see Appendix 2.1.2) containing all nutrients required for normal growth (Helgerson *et al*, 1992). For this experiment ^{15}N L-methionine was added to the medium in place of the usual unlabelled L-methionine. *H. salinarium* grown on complex media plates were used to inoculate 15ml of synthetic media (see appendix 2.1.2) in a 50ml conical flask. The culture was incubated (105rpm; 37°C; in the dark). The absorbance was followed at 660nm. When growth continued this culture was used to start 1 litre cultures. When the OD measurements had peaked the cells were harvested and the purple membrane purified

as described previously in Chapter 3. The purity of the prepared membrane was checked through spectrometry as described in Chapter 3. The purple membrane was suspended in distilled H_2O and dried onto 5.4mm round glass plates as described previously. A total of 24mg protein was prepared for the MAOSS experiments in this way. For static NMR experiments, membranes suspended at a concentration of 3mg/ml in 120µl distilled water were also dried onto 25 10×8mm rectangular plates. Two applications gave a final concentration of 0.8mg/plate.

For assignment purposes, bacteriorhodopsin single site mutants were obtained (L.S. Brown, University of California at Irvine) containing the following mutations: M20V, M68K, M145H and M163C. The mutant strains were cultured as above except using only 150ml of ^{15}N-L-methionine labelled complex media.

For the ^{15}N/^{13}C heteronuclear experiments, membranes were prepared as above with both ^{15}N L-methionine and $^{13}C_1$ glycine being added in place of unlabelled L-methionine and glycine.

5.2.2 NMR measurements

Static NMR experiments were performed at 40.54MHz for ^{15}N on a Bruker DSX 400 with a double resonance static probe. Cross polarisation with proton decoupling was performed at room temperature. A recycle delay of 1.5s was used and 100,000 scans were acquired. The FID was zerofilled to 8k points, exponential line broadened with 200Hz prior to Fourier transform and phase correction.

^{15}N MAS and MAOSS experiments were performed at 40.54MHz for ^{15}N on a Bruker DSX 400 with double resonance 7mm MAS probes. Optimised cross polarisation

experiments with CW proton decoupling were performed at room temperature at spinning speeds of 1400Hz. A recycle delay of 1.5s was used with a contact time of 1ms. Up to 200,000 scans were acquired. Spectra were zerofilled to 8k points and referenced to $^{15}NH_4Cl$ at 24.93ppm after Fourier transformation and phase correction. The ^{15}N MAOSS experiment was repeated at low temperature (230K) using compressed air for spinning, cooled through a heat exchanger with dry ice/acetone.

Improved resolution spectra were acquired using two pulse phase modulated (TPPM) decoupling with a 15˚ phase shift on the Bruker DSX 400 with a 4mm MAS probe at spinning speeds up to 14kHz. The FID's were processed with 32k points and no line broadening prior to Fourier transformation. ^{15}N MAS spectra with ^{13}C REDOR (Fig5.8) dephasing pulses were acquired at 253K and 8kHz spinning frequency with differing numbers of ^{13}C REDOR loops. To study the effect of the ^{13}C π pulses, non-dephased spectra were acquired by repeating the REDOR experiments with almost zero power (120dB) for the π pulses (pl3) on the ^{13}C channel.

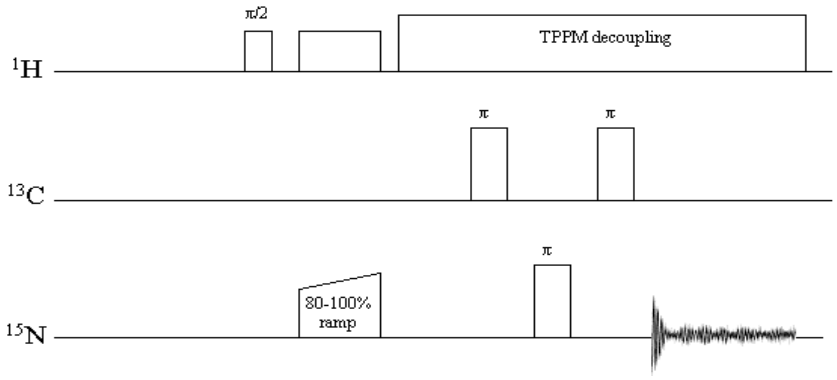

Fig 5.8. Pulse program used for ^{13}C REDOR dephasing of ^{15}N signal. Pulse program adapted from redor1d.98 by Hans Förster (Bruker, Germany).

High resolution spectra were acquired on a Bruker DSX 750 spectrometer (Leiden, The Netherlands) with 4mm MAS probes at spinning speeds up to 14kHz. ^{1}H-^{15}N HETCOR experiments were performed with FSLG decoupling at 233K and at 13kHz spinning frequency. The HETCOR experiments were set up on uniformly ^{13}C, ^{15}N labelled solid tyrosine. The NH proton had a chemical shift of 11.8ppm whilst the $C_{\alpha}H$ and $C_{\beta}H$ protons were found at 4.35ppm and 2.1ppm respectively. The chemical shift separation for protons was seen to be larger for tyrosine in the solid state than is typical for protons in solution state studies of proteins.

Lineshape simulations were performed on a Silicon Graphics INDY R4600 workstation using a programme written by C. Glaubitz (Oxford). Spinning sideband patterns of a single spin-½ can be calculated for various distributions, from a single crystal to a full powder. This is achieved by defining explicitly the range of the Euler angles, which define the orientation of the principle axis system with respect to the molecular frame and the orientation of the molecular frame to the rotor fixed system. The Monte Carlo method is used for sampling over these defined intervals. Analysis of sideband intensities allowed a comparison of deconvoluted spectra with generated spectra to determine a best fit. Powder spectra were optimised in terms of the size of the CSA and the relative sizes of the CSA tensor elements. These parameters are then used in an optimisation of the Euler angles that relate the PAS to the rotor axis which is equivalent to the membrane normal. A comparison of the measured parameters was made with the orientations of N-H bond vectors in the highest resolution crystal structure (Luecke *et al*, 1999; 1c3w.pdb), determined using Insight II also on a Silicon Graphics INDY R4600.

5.3 Results

5.3.1 Static oriented and MAOSS spectra of ^{15}N-methionine labelled purple membranes

In a static-oriented spectrum of a membrane protein the anisotropic chemical shift is dependent on the orientations of the ^{15}N CSA's within the protein, relative to the magnetic field. CSA's from residues located in loop regions are oriented away from an axis parallel to the membrane normal whilst those in helices are to be found close to it. The static NMR spectrum of ^{15}N-methionine labelled purple membranes (Fig 5.9), therefore, shows the distribution of resonance intensity between two domains, one helical and the other loop, which does not necessarily exactly reflect the relative distribution of loop and helical residues due to differences in cross-polarisation efficiency between residues in differing secondary structure. The resolution obtainable in this static NMR experiment is not sufficient to distinguish individual residues however it does have the advantage that the orientational information, which is spun into the sidebands in the MAOSS experiment, contributes here to the chemical shift and leads to a greater separation of the two classes of residues.

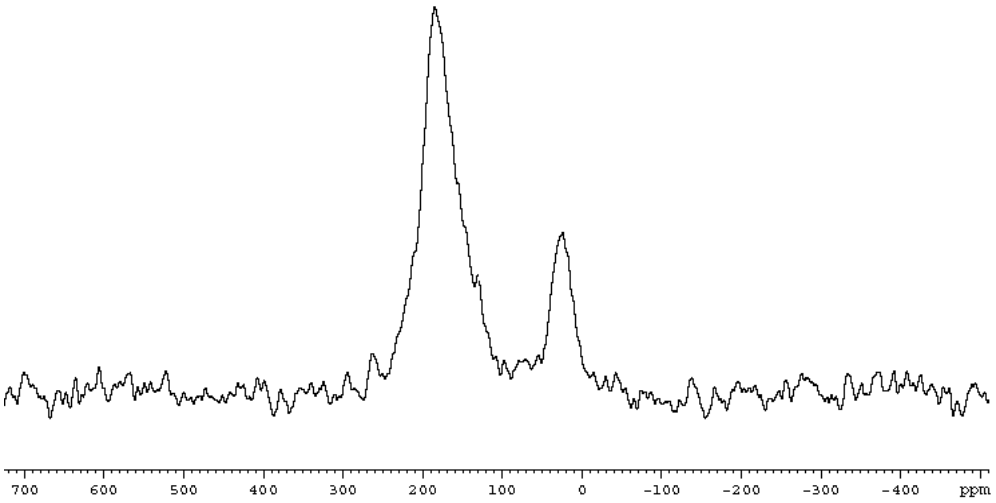

Fig 5.9. Static solid-state ^{15}N CP NMR spectrum of light adapted ^{15}N-methionine bR in purple membranes oriented on glass plates at 0° to B_0. The integral intensities are 7 (180ppm) to 2 (20ppm). The spectrum was acquired using a CP pulse program at 253K with 80kHz CW ^{1}H decoupling on a Bruker DSX 400. 32k scans were recorded.

Under slow MAS conditions (1400Hz) as required for the MAOSS approach, five resonances are resolved in the isotropic central band for ^{15}N-L-methionine labelled purple membrane (Figure 5.10). Resonances from four residues are not resolved in either the MAS or MAOSS spectra. Solution state studies (Orekhov *et al*, 1992; Grabchuk *et al*, 1997) on uniformly and specifically labelled bacteriorhodopsin solubilised in 1:1 chloroform-methanol solvent mixtures also reported the absence of ^{1}H-^{15}N crosspeaks in their HMQC spectrum. Cross peaks that were absent were assigned to helices C, D, E and F (with a few further absences from helix G), the absence being attributed to conformational changes on a millisecond timescale having ruled out line-broadening due to paramagnetic impurities and heterogeneity of chemical shifts through further experimentation. Further MAS experiments carried out on our samples either at decreasing temperatures (≥223K) or at increasing spinning frequencies (≤15kHz) have

been unable to significantly reintroduce missing resonances and the conclusion must be that bacteriorhodopsin must experience similar conformational changes when in the purple membrane. Only with a combination of these methods at high magnetic field strength (Bruker DSX 750, Leiden, Netherlands) (Fig 5.22) or through employing 2D HETCOR experiments (Fig 5.13) have evidence of other resonances been observed. At this higher magnetic field strength, with its intrinsic improvement in resolution and sensitivity, four more small peaks appeared in the spectrum (data not shown) however they were not clearly identifiable and may contribute to the lineshape analysis of the five major peaks.

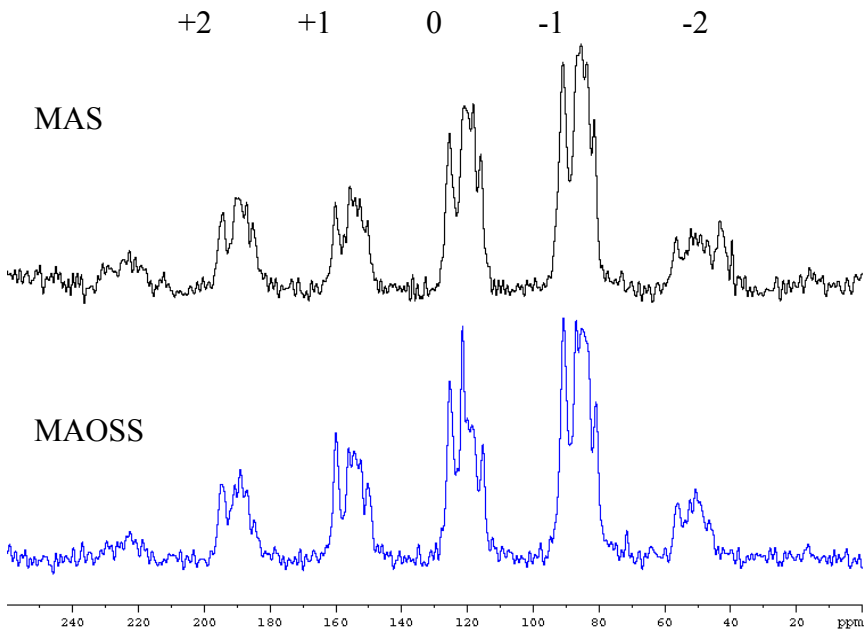

Fig 5.10. CPMAS (random dispersion) and MAOSS spectra for ^{15}N-methionine labelled bacteriorhodopsin in ground state (1400Hz spinning frequency) acquired on a Bruker DSX 400 spectrometer. The isotropic chemical shifts are at around 120ppm with respect to $^{15}NH_4Cl$ (24.93ppm) . Other peaks are side bands whose intensities with respect to each other in the MAOSS spectrum reveal the orientation of the amide nitrogen with respect to the rotor axis. The change in the relative sideband signal intensities, which is

orientation dependent, from random dispersion to oriented system is visible. The MAS spectrum was acquired at room temperature whilst the MAOSS spectrum was acquired at 230K to improve signal to noise and importantly, to maintain sample integrity under MAS conditions. 80kHz CW decoupling was used for both spectra.

Comparison of the two spectra in Fig 5.10 does however show how orienting the membranes affects the relative intensities of the spinning sidebands. These spinning sidebands contain the information about the orientation of the labelled residues' CSA's in the protein. Although at these low spinning speeds complete resolution of all the labelled residues is not possible it is clear that the effect of orienting the membranes is visible in the MAOSS spectrum and, following deconvolution a set of orientational constraints would be obtainable. In an attempt to improve the ^{15}N CP MAOSS experiment, further acquisitions were obtained at temperatures below freezing. No further peaks were resolved however, at temperatures below 253K a marked improvement in the efficiency of the cross polarization was observed which resulted in much improved signal to noise.

5.3.2 Improving resolution at 400MHz

Improved resolution was possible for the isotropic chemical shifts by employing a more sophisticated decoupling scheme during acquisition (TPPM) and faster spinning at the magic angle.

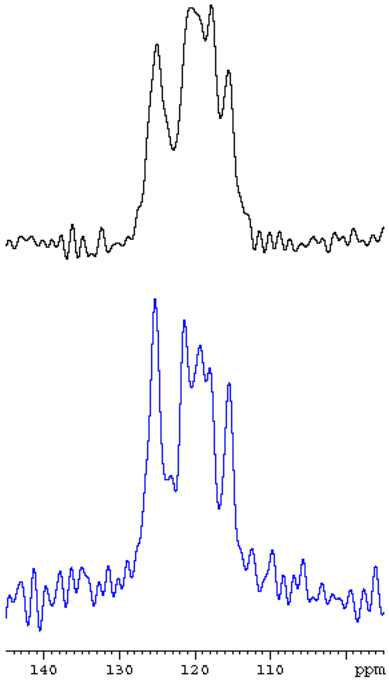

Fig 5.11. Comparison of spectra for ^{15}N-methionine labelled bacteriorhodopsin in purple membrane acquired under standard CW decoupling at a spinning speed of 1400Hz (black) with a 7mm MAS probe and TPPM decoupling spinning at 14kHz (blue) with a 4mm MAS probe during ^{15}N CP-MAS experiments on Bruker DSX 400 spectrometer. Both spectra were recorded at 230K on a Bruker DSX400. Recycle delays of 1.5s and contact times of 1ms were used in both experiments with ^{1}H decoupling fields of 80kHz.

Increasing the MAS spinning speed from 1400Hz to 14kHz and employing TPPM decoupling lead to ^{15}N CP MAS spectra (as shown in Fig 5.11) that are characterised with increased sensitivity and resolution such that six peaks can now be determined.

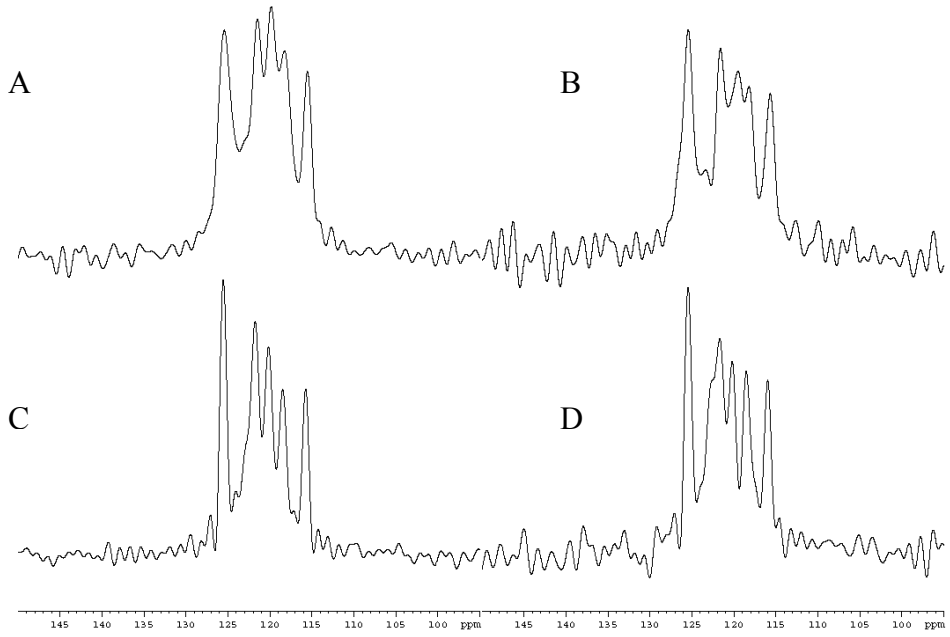

Fig 5.12. Comparison of ^{15}N CPMAS spectra acquired at differing spinning speeds and temperatures on a Bruker DSX 400 spectrometer with 4mm MAS probes: (A) 8kHz MAS, 233K; (B) 14kHz MAS 233K; (C) 8kHz MAS, 253K; (D) 14kHz MAS, 263K. A recycle delay of 1s and contact time of 1ms were used with 80kHz TPPM ^{1}H decoupling.

Whilst decreasing the sample temperature during cross polarisation increases magnetisation transfer leading to improved signal to noise other affects can reduce the resolution obtainable at lower temperatures. The purple membrane samples appear not to be completely immobile even at temperatures as low as 253K although the membranes and associated water is frozen. Residual motion at temperatures down to 253K allow

some increased averaging of heteronuclear dipolar couplings and can lead to narrower lineshapes than at 233K where proton decoupling is not so efficient (Fig 5.12).

At higher spinning frequencies, further experiments can be conducted to improve resolution. Figure 5.13 shows the resolution improvement possible when a second dimension is introduced. The 2D ^{15}N-^{1}H HETCOR spectra are able to further separate the lines seen in the 1D ^{15}N CP spectrum. In Fig 5.13 ^{1}H resonances from aliphatic protons are centered around 0ppm, water protons around 8ppm and amide protons around 11ppm.

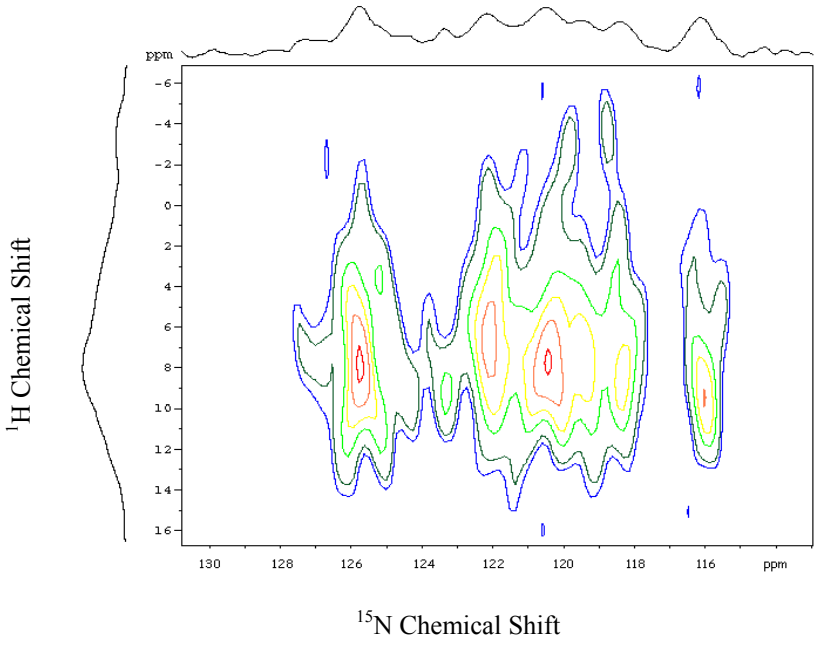

Fig 5.13. 2D ^{15}N-^{1}H HETCOR spectrum of ^{15}N-methionine labelled bR in purple membranes. Experiment performed on Bruker DSX 400 at 233K and 14286Hz MAS frequency with a mixing time of 560μs, recycle delay of 1s and CP contact time of 1ms. The major peak at 117.5ppm (^{15}N-chemical shift) can be seen to be either a peak distinct from, or a product of, two separate peaks at 117 and 118ppm. Four peaks are distinguishable between 110 and 114ppm, whilst two smaller peaks appear at 115.3 and 116.5ppm.

5.3.3 Assignment of resonances by single site mutations

With an improvement in resolution it is important to be able to assign resonances to specific residues. The ^{15}N CPMAS spectra for single site mutants (Figs 5.14-5.17) are able to give an accurate assignment of the specific chemical shift for a given residue. Simple CPMAS experiments are performed on relatively small quantities (2mg protein) of sample. The resultant spectra are expected to have one resonance missing per mutated methionine residue. Some alteration of the relative spectral intensities may be expected due to slight protein conformational changes.

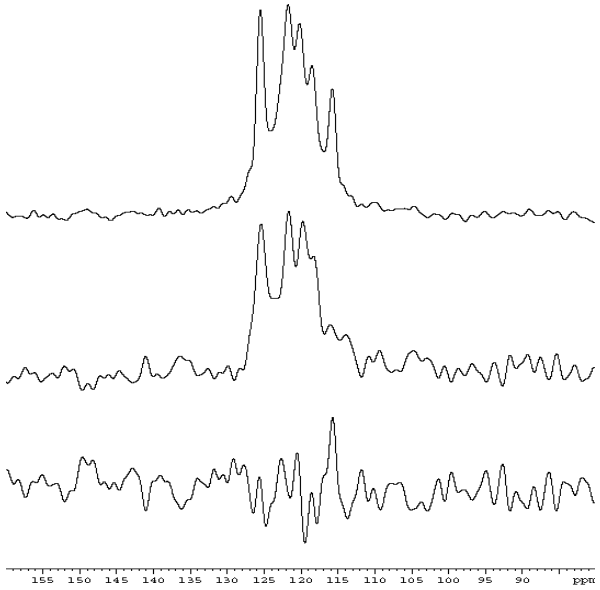

Fig 5.14. Comparison of ^{15}N CPMAS spectra obtained for wild type (S9) (top) single mutant (M20V) (middle) (with subtraction (bottom)) purple membranes labelled with ^{15}N L-methionine. Spectra were obtained as Fig 5.12 C (253K, 8kHz MAS frequency, Bruker DSX 400) with an 80-100% ramped CP program. A major resonance is missing at 115.7ppm in the mutant spectrum and is assigned to Met20.

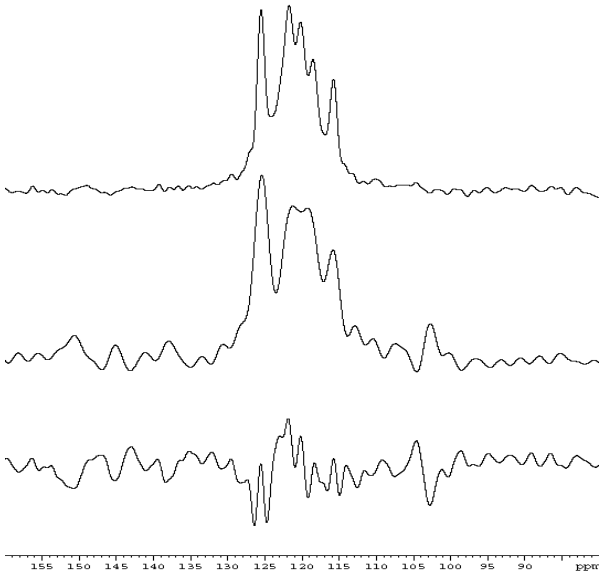

Fig 5.15. Comparison of ^{15}N CPMAS spectra obtained for wild type (S9) (top) and single mutant (M68K) (middle) (subtraction bottom) purple membranes labelled with ^{15}N L-methionine. Spectra were obtained as above. A major resonance is missing at 121.8ppm in the mutant spectrum and is assigned to Met68.

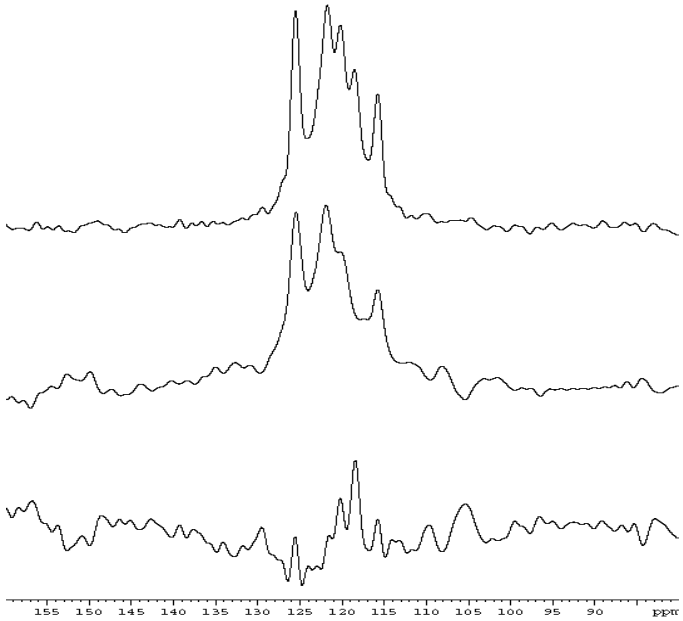

Fig 5.16. Comparison of ^{15}N CPMAS spectra obtained for wild type (S9) (top) and single mutant (M145H) (middle) (subtraction bottom) purple membranes labelled with ^{15}N L-methionine. Spectra were obtained as above. A major resonance is missing at 118.4ppm in the mutant spectrum and is assigned to Met145.

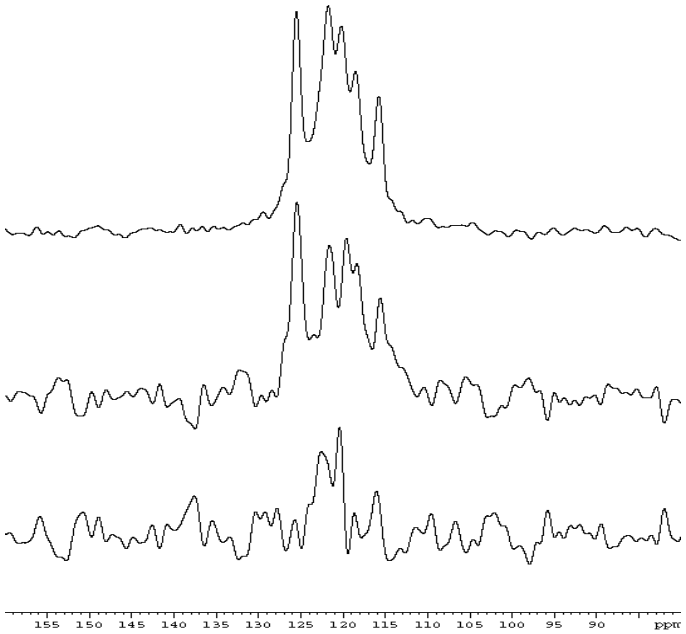

Fig 5.17. Comparison of ^{15}N CPMAS spectra obtained for wild type (S9) (top) and single mutant (M163C) (middle) (subtraction bottom) purple membranes labelled with ^{15}N L-methionine. Spectra were obtained as above. A major resonance is missing at 120.4ppm in the mutant spectrum and is assigned to Met163.

5.3.4 Assignment of resonances by ^{15}N,^{13}C REDOR NMR

Further assignment was performed using ^{13}C REDOR dephasing of ^{15}N CPMAS signal. The experiment was set up on U ^{13}C, ^{15}N L-arginine to determine the optimum dephasing conditions for a directly bonded ^{13}C-^{15}N pair (Fig 5.18). In this case it was found that the terminal amino group (46ppm) had the least efficient dephasing yet was significantly dephased after nine ^{13}C REDOR loops had been applied. This corresponds to a dephasing time of 1.25msec and the level of dephasing for the terminal amino group is in agreement with previously published experiments on 2^{13}C, ^{15}N-L-alanine (Mehta *et al*, 2000). The experiment is largely insensitive to ^{1}H decoupling power levels as 50kHz

CW is sufficient (Mehta *et al*, 2000) whilst experiments described here were performed with 62.5kHz TPPM heteronuclear ^{1}H decoupling.

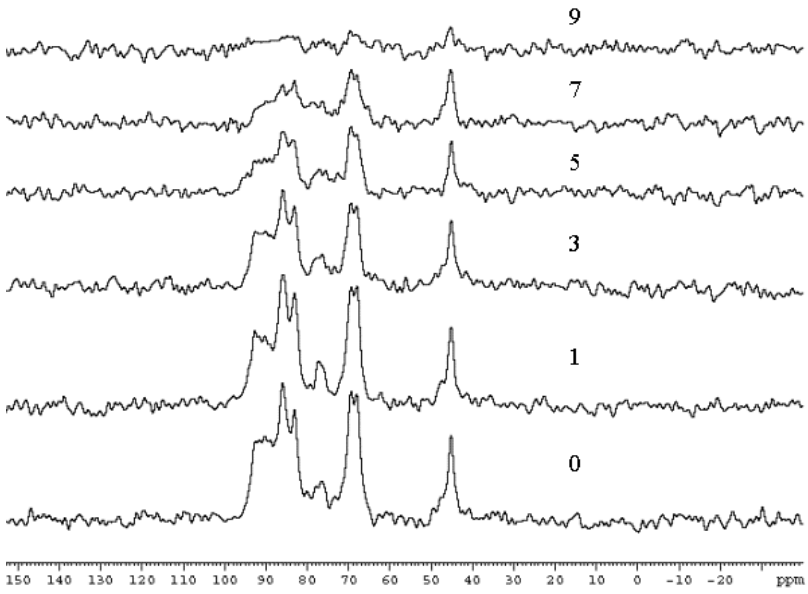

Fig 5.18. Decay of ^{15}N CP signal in uniformly ^{15}N,^{13}C labelled L-arginine following increasing numbers of loops of ^{13}C REDOR pulses. Signal is almost totally dephased after nine REDOR loops. Spectra acquired on a Bruker DSX 400 with 4mm MAS probes with 1s recycle delay and 1ms CP contact time. Fields were 40kHz for ^{13}C, 36kHz for ^{15}N with 62.5kHz TPPM ^{1}H decoupling.

Experiments with seven, nine and eleven loops were performed on the ^{15}N-methionine, $^{13}C_1$-glycine labelled purple membrane samples. Optimal dephasing was expected for a resonance corresponding to Met32 as the ^{13}C carbonyl of Gly31. It was possible to obtain a non-dephased spectrum with nine loops, identical to an experiment performed with no REDOR loops, by turning the power level of the ^{13}C π pulses to their minimum value (120dB) to take into account differences in spectral intensities encountered when increased numbers of REDOR loops are added to the pulse program.

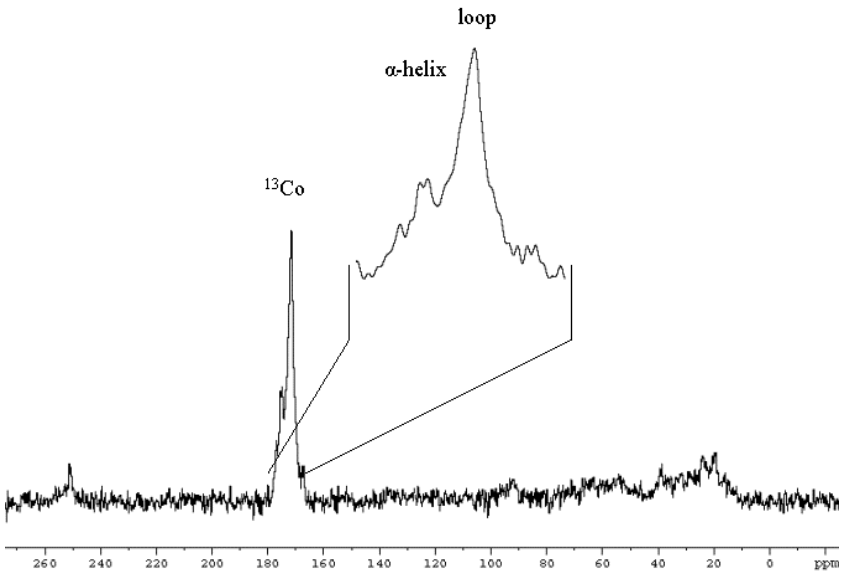

Fig 5.19. ^{13}C CPMAS spectrum of ^{15}N-methionine, $^{13}C_1$-glycine labelled purple membranes (10mg protein) acquired at 8kHz and 253K with 8k scans on a Bruker DSX 400. Enlarged region shows conformational dependence of ^{13}C carbonyl chemical shifts. The carrier frequency for ^{13}C REDOR dephasing of ^{15}N signal was placed on the peak corresponding to the α-helical region at around 176ppm. A recycle delay of 1s was used with a CP (80-100% ramp) contact time of 1.5ms and 62.5kHz TPPM ^{1}H decoupling.

An important element to the REDOR experiment was the setting of the carrier frequency for the ^{13}C π pulses. It is important to set the carrier exactly on top of the coupled resonance in the ^{13}C CPMAS spectrum to avoid offset effects. In this case (Fig 5.19), the carbonyl region of the spectrum consists of resonances from twenty-five glycine residues. The carbonyl chemical shifts are conformation dependent and are separated into regions of α-helical and loop or random coil conformation. The carrier was set in the middle of the α-helical region since Gly31 is known to be α-helical from published crystal structures.

The results of the dephasing experiments are shown in Fig 5.20. Under non-dephasing conditions (pl3 120dB) the shape of the ^{15}N CP MAS spectrum remained

essentially the same with a slight change in intensity for a number of resonances. The resonances at 125.4 and 122.7ppm were noticeably increased with increased numbers of REDOR loops whilst the resonance at 115.7ppm (Met20) was somewhat reduced.

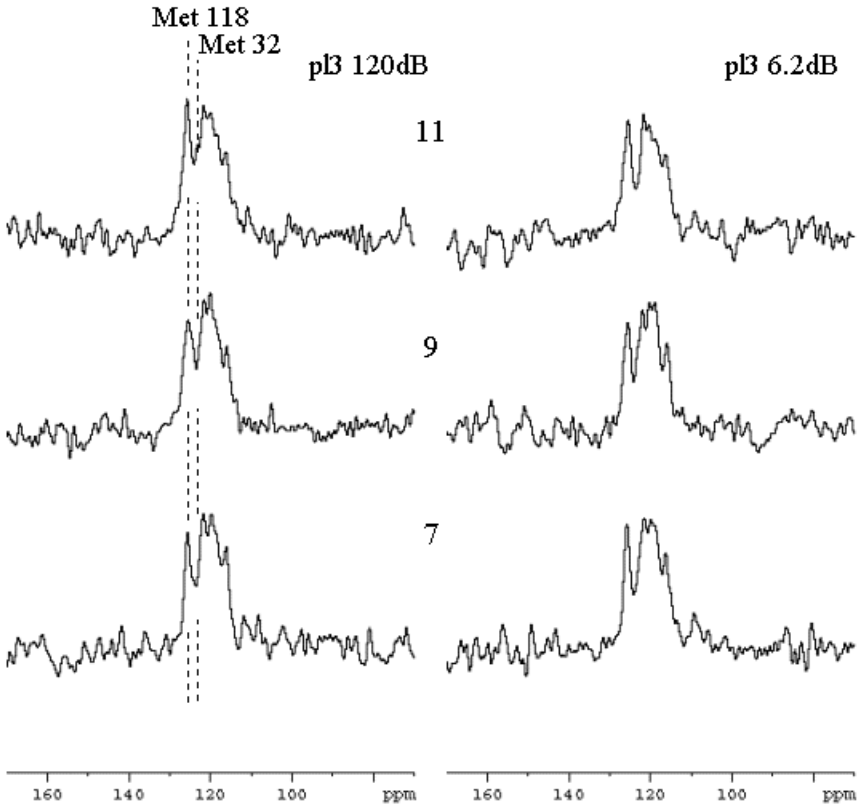

Fig 5.20. ^{15}N CPMAS spectra of ^{15}N methionine, $^{13}C_1$ glycine labelled purple membranes with increasing numbers of ^{13}C REDOR dephasing loops. Methionine 32 is assigned at 122.7ppm on the basis of its high level of dephasing relative to uncoupled residues. Spectra were acquired at 253K and a MAS frequency of 8kHz with 32k scans on a Bruker DSX 400 with parameters as Fig 5.18.

These differences can be attributed to differing rates of relaxation relative to other resonances. Under normal CP conditions the resonance at 122.7ppm is often lost in the envelope for the intense resonance at 121.8ppm (Met68) however it can be seen as a significant shoulder in some sidebands under low spinning frequency MAS. When the ^{13}C π pulses are applied (pl3 6.2dB) the resonance at 122.7ppm becomes severely diminished whilst that at 125.4ppm also has a significant reduction in intensity. Other

resonances are largely unaltered (Fig 5.20) and despite the slightly poor signal to noise it is possible to make a tentative assignment for these two residues based on their known proximities to $^{13}C_1$-glycines.

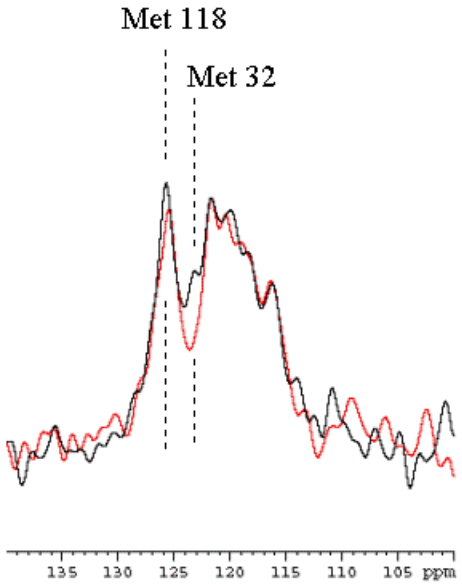

Fig 5.21. Enlarged region of spectra from Fig 5.20 with 11 ^{13}C REDOR loops showing optimised (red) and low power (black).

To determine the expected amount of dephasing expected for each ^{15}N-methionine residue in the REDOR experiment the internuclear distances between ^{15}N labelled methionines and $^{13}C_1$ labelled glycines were measured in the highest resolution crystal structure (Luecke *et al*, 1999). As can be seen from Table 5.1 Methionine 32 which is adjacent to both Glycine 31 and 33 has the shortest distance between labelled sites and hence experiences the strongest dipolar coupling. Methionine 118 experiences the next strongest coupling with Glycine 116. The resultant dephasing of the ^{15}N signal when related to the known distances allows an assignment as described by Fig 5.21.

	Gly 21	Gly 23	Gly 31	Gly 33	Gly 63	Gly 65	Gly 113	Gly 116	Gly 120
Met 20	4.665	6.399	-	-	-	-	-	-	-
Met 32	-	-	1.326	4.926	-	-	-	-	-
Met 60	-	-	-	-	5.586	5.245	-	-	-
Met 118	-	-	-	-	-	-	5.892	3.251	5.487

Table 5.1. Comparison of internuclear distances (Å) between ^{15}N-methionines and $^{13}C_1$-glycines in bacteriorhodopsin. Distances measured in bacteriorhodopsin structure 1c3w.pdb (Luecke *et al*, 1999) using Chemscape Chime™ v 2.0.3. The two closest internuclear distances are highlighted in blue (Met32) and red (Met118).

5.3.5 Improving resolution at 750MHz

An improvement in spectral resolution over that obtained on the Bruker DSX 400 (400MHz proton frequency) can also be obtained by performing experiments at higher magnetic field strengths. The MAS and HETCOR experiments above on wild type protein (S9) were repeated using a Bruker DSX 750 (750MHz proton frequency) in Leiden, The Netherlands equipped with 4mm MAS probes and variable temperature control. The improved resolution and sensitivity can be seen in Figures 5.22 and 5.23. Figure 5.22 shows a comparison of fast spinning ^{1}H-^{15}N CPMAS spectra obtained at 400 and 750MHz proton frequencies. There is a considerable improvement in sensitivity and resolution due to reduced spectral linewidths. More resonances can be resolved although, from this spectrum, the less intense peaks that appear cannot said to be due to labelled residues with 100% certainty as they are still small in comparison with the noise.

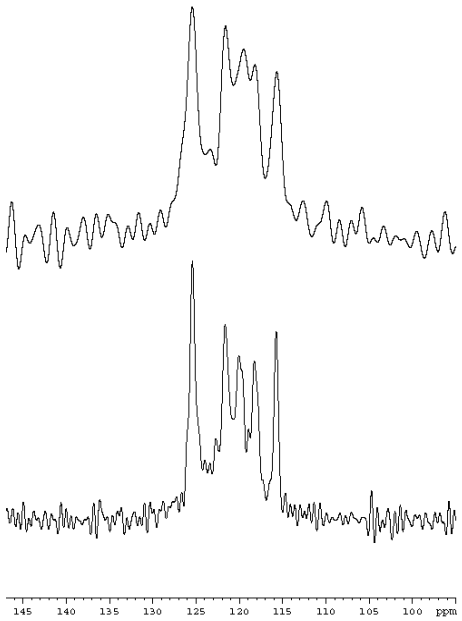

Fig 5.22. Comparison of 1D CPMAS spectra for ^{15}N methionine labelled purple membranes at different field strengths. Top spectrum acquired on a Bruker DSX 400 wide-bore magnet with 4mm MAS probes (233K, spinning speed of 14kHz, 1k scans) as Fig 5.12 B. Bottom spectrum acquired on Bruker DSX 750 (Leiden, Netherlands) also with 4mm MAS probes (243K, spinning speed of 12kHz, 8k scans) with a recycle delay of 1.5s and a CP contact time of 1.6ms with 60kHz TPPM ^{1}H decoupling.

A better picture of how increasing the magnetic field strength can improve the resolution is seen in the 2D ^{1}H-^{15}N HETCOR spectrum (Fig 5.23) which has much improved resolution in the ^{1}H dimension due to the greater relative effect of the higher magnetic field strength and also improved FSLG homonuclear decoupling. This high-resolution spectrum (Fig 5.23) shows the differing couplings between the nine methionine residues and their associated protons. These protons include the amide protons (8-12ppm), the aliphatic protons (2-5ppm) and water (5-8ppm) protons. Assigned loop residues (Met163 at 120.4ppm; Met68 at 121.8ppm) can be seen to have strong cross peaks with water protons, whilst Met20 (115.7ppm) appears sequestered from

water. Met32 appears (122.7ppm) to have a cross peak with its amide proton but other cross peaks have intensities below the threshold for this representation (Fig 5.23).

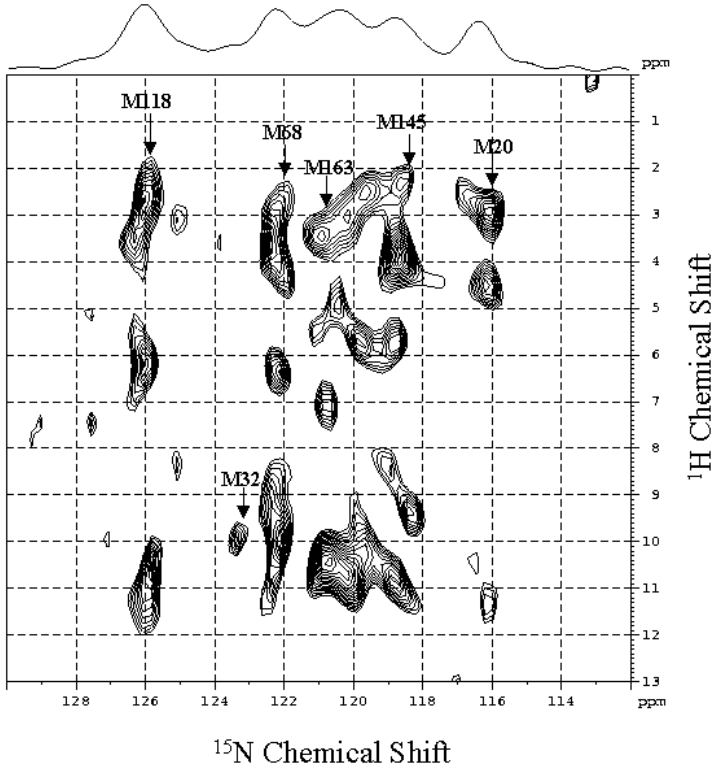

Fig 5.23. 2D ^{1}H-^{15}N HETCOR (FSLG) spectrum for ^{15}N methionine labelled bR in the purple membrane (10mg protein). Spectrum acquired on a Bruker DSX 750 with 4mm MAS probe. (233K, 13kHz spinning frequency, 1k × 80 scans). Homonuclear FSLG decoupling was used during ^{1}H-^{15}N evolution and 60kHZ heteronuclear TPPM ^{1}H decoupling during acquisition. A recycle delay of 1.5s and 1.6ms cP contact time were used.

5.3.6 Determination of orientational constraints from MAOSS data

The isotropic chemical shifts for the nine resolved ^{15}N resonances are given in table 5.2. The known assignments and the method of assignment are also summarised. The determined resonance assignments and the locations of all nine ^{15}N-methionine

resonances and their relative intensities allow a more accurate deconvolution of the MAOSS data and the production of a set of direct structural constraints.

^{15}N Chemical Shift (ppm)	Residue	Method
125.4	Met118	^{13}C REDOR
124.4	?	
122.7	Met32	^{13}C REDOR
121.8	Met68	Resonance Knockout
120.4	Met163	Resonance Knockout
119.7	?	
119.2	?	
118.4	Met145	Resonance Knockout
115.7	Met20	Resonance Knockout

Table 5.2. Summary of resolved ^{15}N-methionine resonances in purple membranes from ^{1}H-^{15}N FSLG HETCOR spectrum (Fig 5.23) (233K) and residue assignments from either resonance knockout mutation of $^{13}C_1$-glycine REDOR dephasing.

The experimental data can now be deconvoluted to determine sideband families for specific assigned residues (Fig 5.24).

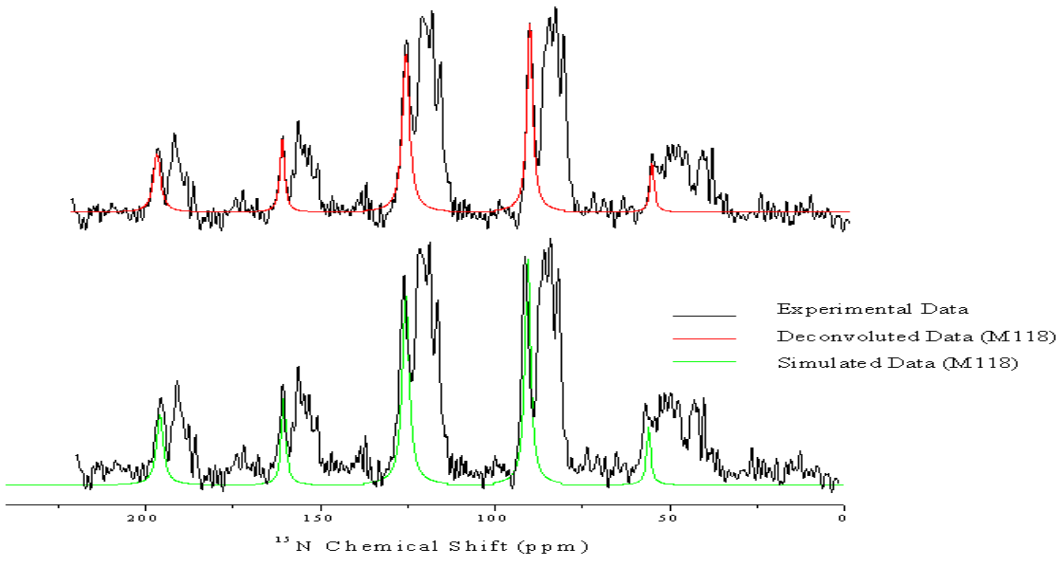

Fig 5.24. Overlay of deconvolution (red) and simulation (green) of experimental (black) MAS spectrum for Met118 sideband family from Fig 5.10.

Using a computer simulation program (C Glaubitz, D.Phil thesis) the MAS powder pattern for each residue is optimised for the size of the CSA and the relative sizes of the σ_{11}, σ_{22} and σ_{33} tensor elements. Using these measured parameters the angles relating the PAS of the ^{15}N CSA to the rotor, and hence membrane normal are optimised with an arbitrary mosaic spread of ±2°. Comparison of sideband intensities for a range of simulated spectra with the deconvoluted spectra lead to a determination of an angle (β) reflecting the orientation of the CSA with respect to the membrane normal. An improved simulation program is being developed that will enable the direct comparison of simulated spectra and experimental data, and will provide a minimisation of χ^2 merit function for the tilt angle and mosaic spread as performed for deuterium studies of methyl bond vectors in Chapter 3 and rhodopsin (Gröbner *et al*, 2000). The error associated with these measurements cannot be accurately assessed here without the χ^2 minimisation however the error associated with the ^{15}N MAOSS method is expected to be similar to that found in Chapter 3 as good signal to noise spectra were obtained on membrane samples prepared in the same manner. Additional error may be introduced through imperfect deconvolution of sideband families and will be discussed below. Deconvoluted spectra for four of the residues assigned by resonance knockout mutations and REDOR NMR are shown in Fig 5.25 and 5.26 where the sideband families for three helical residues (Methionines 20, 118 and 145) and one loop residue (Methionine 68) are compared with simulated spectra under both MAS and MAOSS conditions. The observed differences between loop and helical residues reflects not only the differing orientations

in the MAOSS spectra but may also reflect differences in asymmetry of the CSA in differing environments.

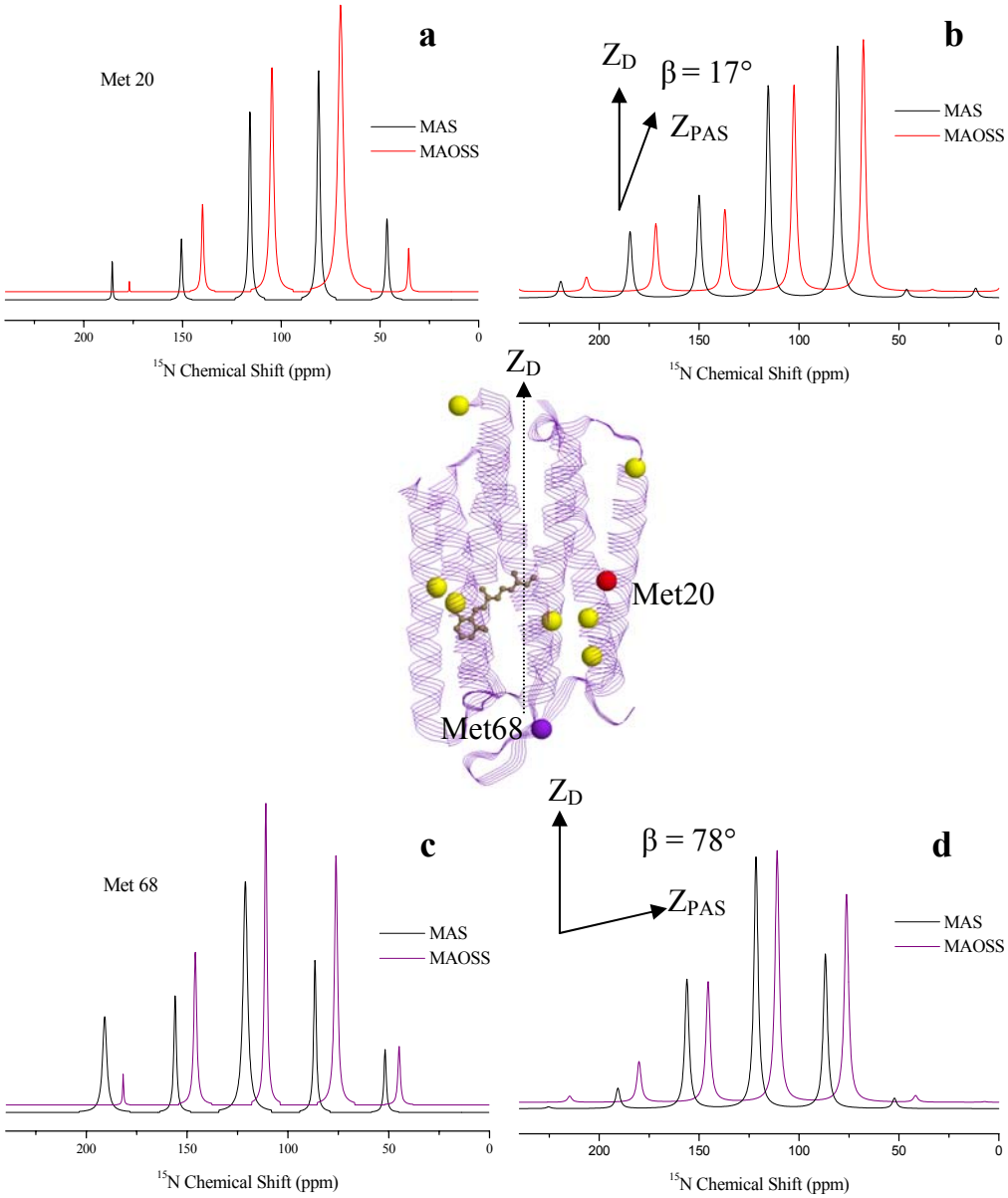

Fig 5.25. Comparison of deconvoluted sideband families with simulated spectra in both MAS and MAOSS experiments on ^{15}N methionine labelled purple membranes for two residues. Simulated spectra are shown normalised whilst deconvoluted spectra are obtained directly from the experimental spectra (Fig 5.10). Deconvoluted spectra are shown for helical residue Met20 (**a**) and compared with simulated spectra (**b**) where the MAOSS spectrum was optimised for an angle (β) between the PAS and the membrane normal of 17±2°. Deconvoluted spectra are also shown for the loop residue Met68 (**c**) and compared with simulated spectra (**d**) where the MAOSS spectrum was optimised for β = 78±2°.

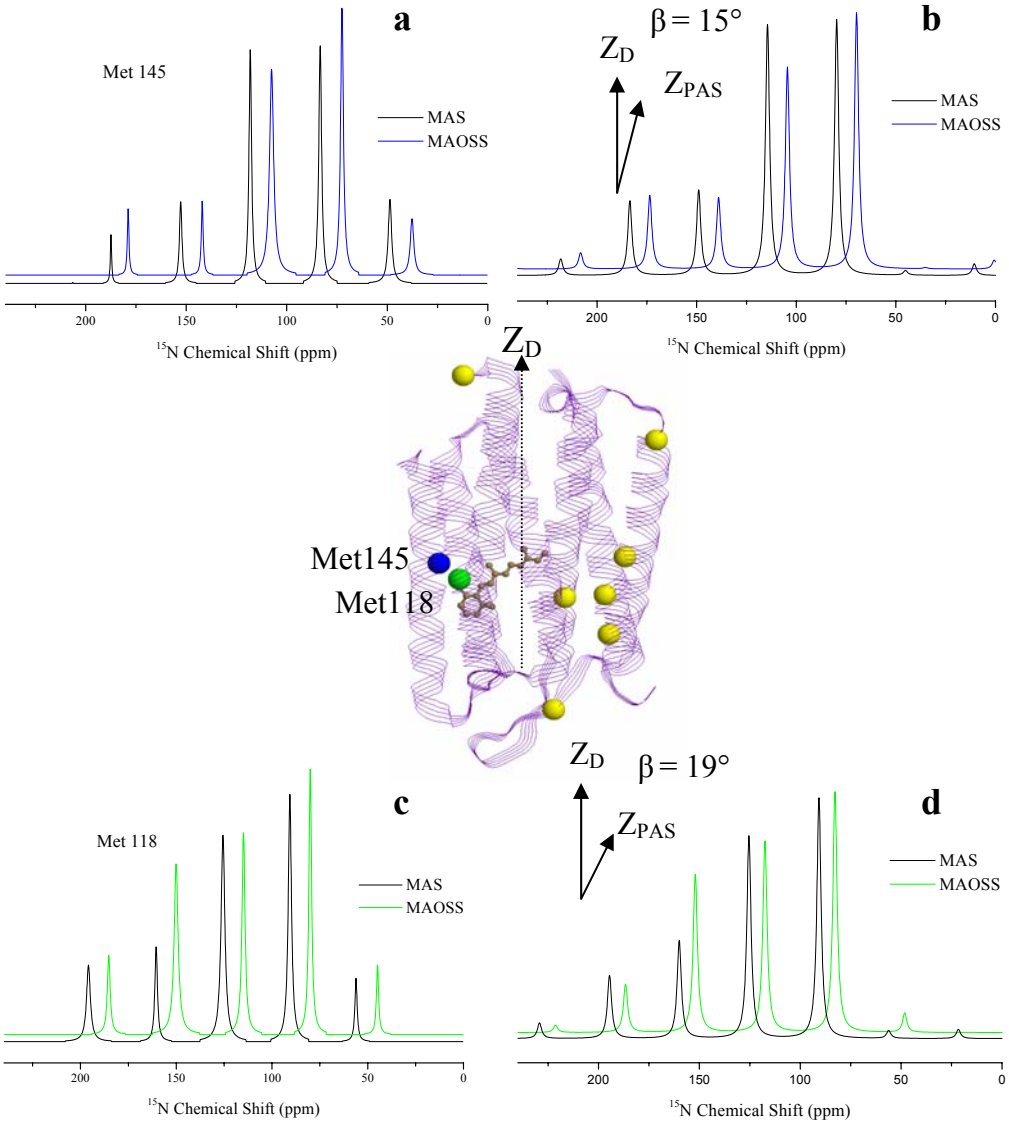

Fig 5.26. Comparison of deconvoluted sideband families with simulated spectra in both MAS and MAOSS experiments on ^{15}N methionine labelled purple membranes for two residues. Simulated spectra are shown normalised whilst deconvoluted spectra are obtained directly from the experimental spectra (Fig 5.10). Deconvoluted spectra are shown for Met145 (**a**) and compared with simulated spectra (**b**) where the MAOSS spectrum was optimised for β = 15±2°. Deconvoluted spectra are also shown for Met118 (**c**) and compared with simulated spectra (**d**) where the MAOSS spectrum was optimised for β = 19±2°.

The derived angles of the PAS (Figs 5.25 and 5.26) cannot be directly compared with current crystal structures since the PAS of the CSA is not directly co-linear with the N-H bond vector. However the two values should be expected to be within a range of 16° and 14° for helical and loop residues respectively (Fushman *et al*, 1998). The derived angles are all within this range and hence the there is good agreement between the MAOSS data and the x-ray crystal data.

Residue	N-H bond orientation (°)	PAS orientation (±2°)
Met20	19	17
Met68	71	78
Met118	9	19
Met145	22	15

Table 5.3. Comparison of determined vector orientations with respect to the membrane normal of the PAS of ^{15}N CSA for four assigned methionine residues compared with N-H bond vectors as measured from 1c3w.pdb (Luecke *et al*, 1999).

5.3.7 Anisotropic constraints at high MAS frequencies

Improvements in resolution, attainable at higher spinning frequencies and with further dimensions, are achieved at the expense of being able to characterise the anisotropy necessary for analysis of orientational constraints. The anisotropy can, however, be reintroduced in the form of ^{1}H-^{15}N dipolar couplings. A demonstration of this is shown in Fig 5.27 and 5.28 where the HDOR-REPT experiment is used to recouple the heteronuclear dipolar couplings under fast spinning conditions. The resulting 2D spectrum is shown in Fig 5.27 where the ^{15}N isotropic chemical shift for the amide

nitrogens, in the first dimension, is correlated with the ^{1}H-^{15}N dipolar coupling in the second.

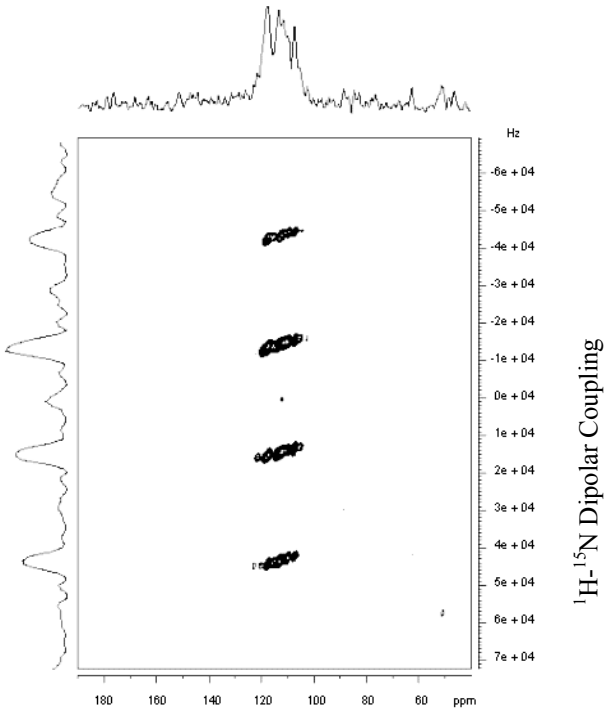

Fig 5.27. 2D ^{15}N chemical shift/^{1}H-^{15}N dipolar coupling HDOR MAS spectrum for the ^{15}N-methionine labelled purple membrane sample. Experiment performed at 223K and at ω = 14286Hz, 10mg protein. Spectra were acquired on Bruker DSX 400 with recycle delay of 0.5s and an increased ^{1}H field strength of 100kHz.

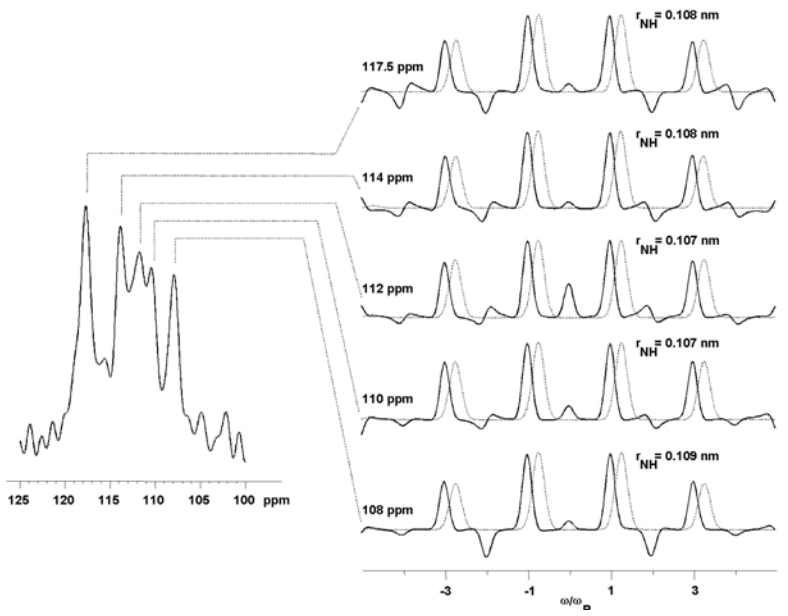

Fig 5.28. Diagram showing selection of 1D dipolar coupling slices from 2D HDOR MAS spectrum (Fig 5.27) for the five resolved resonances. The side bands are evaluated to give coupling strengths and hence an accurate measurement of the amide bonds length (r_{NH}).

The dipolar couplings for the five main resonances that are resolved are shown in Fig 5.28. The resolution is at a level where only five peaks can be clearly discerned in the 2D HDOR MAS spectrum. As would be expected the measured ^{1}H-^{15}N distances are approximately the same for each residue however were this experiment performed on an oriented sample the relative intensities of the sidebands for each ^{15}N resonance would be dependent on the orientation of the heteronuclear dipolar coupling and hence the amide bond. The improved resolution 2D ^{1}H-^{15}N HETCOR (FSLG) spectrum (Fig 5.23) shows where peaks underlying 1D spectra are found and their relative intensities. This information can be used to improve the deconvolution of the MAOSS and HDOR-REPT spectra and allow the analysis of ^{1}H-^{15}N dipolar couplings for all nine resonances.

5.4 Discussion

5.4.1 MAOSS versus static experiments

MAOSS has been shown, for singly labelled membrane proteins, to be an excellent method for obtaining high resolution orientational information. In the case of a deuterated methyl group in the retinal of bacteriorhodopsin the advantages over similar static experiments have been seen in the improved resolution, sensitivity and accuracy of the approach (Chapter 3; Glaubitz *et al*, 1999). The question that is immediately raised is whether this technique can be applied to multiply labelled proteins and whether this technique has real advantages over established techniques, notably standard static experiments and PISEMA.

Spin half nuclei such as ^{15}N and ^{13}C however, display a broad distribution of isotropic chemical shifts determined by the electronic environment of the nuclei. These chemical shifts are characteristic of the type of atom being studied and as such are more interesting to the biologist than say deuterium because of the increased variety of spins that could be studied in one experiment. In a static, oriented experiment this isotropic chemical shift information is largely lost since the spectrum is dominated by the orientation dependence of the chemical shift anisotropy. This can mean that in static and PISEMA spectra, the instant assignment of the nature of the spin is lost. Magic angle spinning has the advantage here in that the anisotropic chemical shift is either removed or refocused into spinning sidebands such that the isotropic chemical shifts are revealed. In theory then, the same number of spins as can be resolved in a MAS experiment can be resolved in a MAOSS experiment. From a comparison of the results obtained with static and spinning oriented ^{15}N methionine labelled purple membrane samples it can be seen

that there is an improvement in resolution under MAOSS conditions. A static one dimensional ^{15}N CP experiment is able to resolve spins on the basis of orientation however the linewidths are not narrow enough to separates spins of similar orientation, it is possible to distinguish only between spins located in either a loop or a helix. The relative intensities of the two peaks in the static oriented CP spectrum (Fig 5.9) confirm the distribution of methionine residues between loop and helical regions expected from study of the crystal structures although some discrepancies might be expected due to differing efficiencies of cross-polarisation between helical and loop regions. This observation (Fig 5.9) indicates that the labelling procedure was successful and that isotopic scrambling was minimal. The lack of high level resolution resulting from broad linewidths would make the standard static technique unsuitable for analysis of small scale conformational changes within a membrane protein upon receptor activation.

There is an inherent improvement in sensitivity under MAOSS conditions (Fig 5.10), from the reduced linewidth, which can allow very high signal to noise spectra to be acquired with little or no line broadening. However the time taken for a spectrum to be acquired is comparable to that required for a static sample because of the requirement to acquire multiple orders of sidebands. The low speeds required (1400Hz), that refocus the ^{15}N chemical shift anisotropy without completely removing it, are also not sufficient to remove completely proton-nitrogen dipolar couplings and resolution is compromised. This lack of resolution makes deconvolution of the spectrum and characterisation of relative sideband intensities nontrivial, and is a considerable source of error. Under the low spinning speed conditions used in this MAOSS approach only five major resonances could be resolved. Using information obtained in improved resolution experiments, nine

resonances were fitted to the spectral intensities. Whilst a good fit was possible, some uncertainty as to the relative contributions of less intense resonances is unavoidable. For this reason a further improvement in resolution is needed before this technique is readily applicable to multiply labelled membrane proteins. This may be achieved by performing the ^{15}N MAOSS experiment at higher magnetic field strengths (750MHz for ^{1}H) where line-widths will narrow and, due to the scaling of the ^{15}N CSA with field strength, faster spinning speeds up to 3kHz are possible whilst still retaining intensities in spinning sidebands.

Polarisation inversion spin exchange at the magic angle (PISEMA) NMR experiments have become established as a technique for measuring structural constraints from multiply labelled membrane peptides. This static technique has more success than a standard CP experiment as it uses the ^{1}H-^{15}N dipolar coupling as a second dimension. The introduction of a second dimension which has a similar orientational dependence to the ^{15}N CSA leads to well resolved spectra from which a set of orientational constraints can be extracted. The resolution obtainable is impressive, however the technique can suffer in comparison with the MAOSS method in a number of ways. The resolution and sensitivity obtainable in a PISEMA experiment are dependent on the linewidths of the cross-peaks in the 2D spectrum. These linewidths are dependent on the sample homogeneity, the quality of orientation of the sample and the strength of the magnetic field. When dealing with larger proteins where good sample orientation is more difficult to achieve and where sample size becomes an issue, sensitivity and resolution will drop off. Because of the dependence of PISEMA on orientational quality for good resolution it

is possible that this technique would not be sensitive enough to detect very slight changes of orientation during a conformational change.

Both the PISEMA experiment and the MAOSS experiment in its current form have differing strengths and weaknesses. MAOSS can provide highly accurate orientational information and, with the sensitivity enhancement of MAS, requires little sample yet suffers from reduced resolution compared with PISEMA. PISEMA provides excellent resolution and does not require spinning probes yet may not be able to provide highly accurate angle information, particularly with larger proteins. An approach combining the most favourable aspects of MAOSS and PISEMA might be extremely powerful.

5.4.2 Assignment of chemical shifts to labelled residues

Both MAOSS and PISEMA methods suffer from assignment difficulties. The MAOSS approach reveals the isotropic chemical shifts that do have characteristic values according to the conformation of the specific residue, but they cannot, unfortunately, be used for assignment purposes in this case. In solution-state NMR, studies have been carried out comparing chemical shifts for residues in proteins with known conformation (Wishart *et al*, 1991). An analysis of amide chemical shifts showed that conformational dependent shifts were evident and that upfield shifts were found for residues in helices and downfield shifts for residues in β-strands. However amide chemical shifts have very broad chemical shift dispersion such that far too much overlap between the two conformational groups is possible to apply this sort of analysis as a rule (Wishart *et al*,

1991). Although no such study has been performed for proteins in a solid-state it is, nonetheless likely to hold for this experiment (a similar study was performed for ^{13}C carbonyl chemical shifts with results in agreement for both states (Taki *et al*, 1981). In this case it has been possible to assign four of the nine methionine resonances under MAS conditions by using single site mutants grown in ^{15}N-methionine enriched media (Figs 5.14-5.17). The single site mutants lack signal from one site and can be used very simply in a comparison of CPMAS spectra obtained for the mutants with a spectrum from wild type protein. Producing mutants is a laborious process and the spectra from them can differ from the wild type spectrum not only at the single site where signal is lacking but also the remainder of the spectrum may be affected by even small alterations in protein conformation effected by the mutation. Mutations that cause the minimal disruption to wild-type function were chosen (L Brown, *pers com*) as it is likely that they have similarly minimal disruption of the protein tertiary structure. The M163C strain is used to provide a site for attachment of spin labels (e.g. Aharoni *et al*, 2000) and as such is unlikely to be involved in any significant level of cross linking that might perturb the protein structure. The mutant strains used were readily available and, due to the high sensitivity of MAS NMR, only a little sample (2mg protein) was necessary to produce spectra of suitable signal to noise.

A further interesting approach developed here involves co-labelling the protein with other labels such that nearby residues are enriched with a separate NMR label. In this case $^{13}C_1$ glycine was used as it is relatively inexpensive and labels with a high level of efficiency (Fig 5.5). Although, by studying bacteriorhodopsin, experimental design is simpler as the structure is well known, knowledge of the primary sequence is alone

sufficient to design a labelling scheme for specific assignment since it is possible to choose the amino acid adjacent to the ^{15}N labelled residue and introduce a ^{13}C label on the carbonyl such that the two labels are directly bonded when in the protein. In this case the distance between ^{15}N-Met 32 and ^{13}CO-Met 31 is 1.3Å (Table 5.1) which will give by far the strongest heteronuclear dipolar coupling which can be manipulated to provide assignment.

The ideal heteronuclear experiment in terms of spectral simplification and assignment would be a double CP from ^{1}H to ^{15}N via ^{13}C such that a normal MAS spectrum would be produced for only the ^{15}N-methionine residue that experiences Hartmann-Hahn magnetisation transfer from the ^{13}C filtering residue. The same experiment could then be performed to provide the glycine ^{13}C carbonyl chemical shift by using the ^{15}N methionine residue as filter. The ^{13}C carbonyl chemical shift is conformational dependent would provide information as to the local secondary structure (Taki *et al*, 1981). A double CP experiment would have interesting complications when applied to the MAOSS experiment as the efficiency of the Hartmann-Hahn transfer is orientation dependent. The resultant ^{15}N MAOSS spectrum would consist of a sideband pattern for the single ^{15}N-^{13}C coupled residue that was dependent on the orientation of the ^{15}N CSA tensor and also modulated by the orientation of the ^{15}N-^{13}C dipolar coupling. At higher spinning frequencies (>c10kHz) the first Hartmann-Hahn condition sideband for the ^{15}N-^{13}C transfer of magnetisation displays a $\sin 2\beta$ in its efficiency of transfer whilst the second sideband displays a $\sin^2\beta$ dependence. A variable contact time experiment with Hartman-Hahn CP set on a sideband would reveal the oscillation of the CP efficiency and hence the orientation of the ^{15}N-^{13}C dipolar coupling. A double CP

experiment was attempted on a ^{15}N-methionine, $^{13}C_1$ glycine powder sample however the efficiency of transfer was found to be quite weak (28% with an increased receiver gain) on a uniformly labelled L-arginine standard sample and, following filtering (nine methionine residues to one) only negligible signal remained. However this experiment may be of use in more concentrated samples.

An alternative to Hartmann-Hahn CP experiments is to use an established heteronuclear recoupling technique to reintroduce the dipolar coupling between coupled ^{15}N-methionines and $^{13}C_1$-glycines. The REDOR approach was used as described above such that ^{13}C π pulses are used to recouple the heteronuclear dipolar coupling (Fig 5.8). The dipolar coupled residues would be revealed in the ^{15}N CPMAS spectrum since the resonances would become dephased, the degree of dephasing being directly related to the distance between the labelled sites.

5.4.3 Improving resolution

As has been shown (Figs 5.12 and 5.13), it is possible to produce much better resolution around the isotropic chemical shifts for ^{15}N-methionone enriched bacteriorhodopsin in purple membranes by increasing the spinning speed. Spinning speeds of up to 5KHz are obtainable with Bruker 7mm MAS probes or even 15KHz using a smaller Bruker 4mm system. The temperature at which these experiments are performed can have a considerable affect on the spectra. Despite an increse in sensitivity below 253K, resolution becomes poorer concomitant with increased spectral linewidths. On freezing the samples slight changes in chemical shifts of some resonances are

observed, once the sample is frozen no further change in chemical shifts are observed at lower temperatures which may reflect different conformational exchange rates in some regions of the protein at differing temperatures. A wide bore 750MHz (for proton frequency) machine is now available in Leiden and a wide bore 800MHz machine is being installed here in Oxford. Experiments performed at higher magnetic field strengths may prove to be able to resolve amide residues, under fast spinning, from ^{15}N chemical shift alone. There was shown to be a considerable improvement in sensitivity and resolution in the 1D CPMAS spectra (Fig 5.12) however the improvement was insufficient for complete resolution. What is more certain is that higher field strength will improve proton resolution in the 2D ^{1}H-^{15}N HETCOR experiments. The reduction in proton linewidth associated with an increase in magnetic field causes a dramatic improvement in resolution and sensitivity when coupled with effective frequency switched Lee-Goldburg (FSLG) homonuclear proton decoupling. The 2D HETCOR spectra obtained at 400MHz (Fig 5.13) for protons is already able to resolve nine peaks and reveal some of their proton connectivities whilst the spectra acquired at 750MHz (Fig 5.23) for protons reveal more clearly the nine ^{15}N labelled amides and the relative strength of their cross peaks with aliphatic, water and amide protons. Assignment of these cross peaks is also not straightforward and cannot be performed with categorical accuracy without further experimentation. Whilst the ^{1}H chemical shifts can be broadly assigned to either aliphatic, water or amide regions, some $C_{\alpha}{}^{1}H$'s might, for example, be downfield shifted and cannot be directly assigned in this experiment alone. The cross peak intensities are not equal and could be evidence for conformational flexibility in some regions of the protein reflected in reduced intensities or multiple populations with slightly

differing chemical shifts. Once assigned, however, the relative strength of the proton-nitrogen couplings for different proton resonances provides some information about the environment surrounding the amide nitrogen and can help with some general assignment.

5.4.4 Anisotropic constraints under fast MAS conditions

Increasing the spinning frequency towards 15kHz has been shown to improve the resolution obtainable under MAS conditions (Fig 5.11). At such high spinning frequencies the chemical shift anisotropy is no longer refocused into spinning sidebands but is completely removed. Since we use the relative intensities of the sidebands to calculate angles of the ^{15}N CSA tensors this is clearly a problem. Reintroducing the ^{1}H-^{15}N dipolar coupling between the amide nitrogens and their respective protons in the HDOR approach can be seen to be an effective way of allowing high speed spinning and improving resolution whilst observing the anisotropy which is necessary for both distance measurements and angle determinations (Fig 5.27). One experimental problem that was encountered was that a relatively long period was required during which the dipolar coupling evolves for a complete sideband pattern to emerge. This time (two rotor periods) has a much lower efficiency of polarisation transfer between protons and nitrogen then shorter time periods such that signal was much reduced and four days were required to obtain the HDOR spectrum (Fig 5.27). This reduction in signal adversely affected the signal to noise ratio and hence the resolution obtainable such that it was not possible to obtain clear sideband families for more than five resonances (Fig 5.28) although two further resonances could be discerned. A higher magnetic field strength may again help

this experiment with improved resolution and sensitivity. If the problems discussed above can be resolved in this way, which is likely, then the oriented HDOR MAS approach would seem to be an excellent method for determining distances and angles in multiply labelled membrane proteins. The complete resolution available through application of the 2D ^{1}H-^{15}N HETCOR techniques discussed above could be the starting point for a method that would combine fast spinning, use of a second dimension to improve resolution and recoupling anisotropic interactions. The ideal method then would require a 3D experiment where the first dimension would be ^{15}N chemical shift, the second dimension ^{1}H chemical shift and the anisotropy (either ^{1}H-^{15}N dipolar coupling or CSA) would be recoupled and displayed in a third dimension. Currently however, sensitivity is likely to be a limiting factor on this approach.

5.4.4 Practical considerations

High speed spinning itself presents some practical problems to the study of oriented systems, which will need to be overcome before this technique can be established. The problems are caused by the smaller diameter of the rotors used to get to higher spinning speeds. The 4mm rotor will, of course, not take the 5.4mm diameter glass disks used thus far in the MAOSS experiments. We have been unable, so far, to obtain glass disks of 3.2mm diameter yet even if available these disks might not be suitable for these experiments. There is a risk that at higher spinning speeds the increased centrifugal force would cause membranes around the edges of the disks to be physically spun out to the rotor walls.

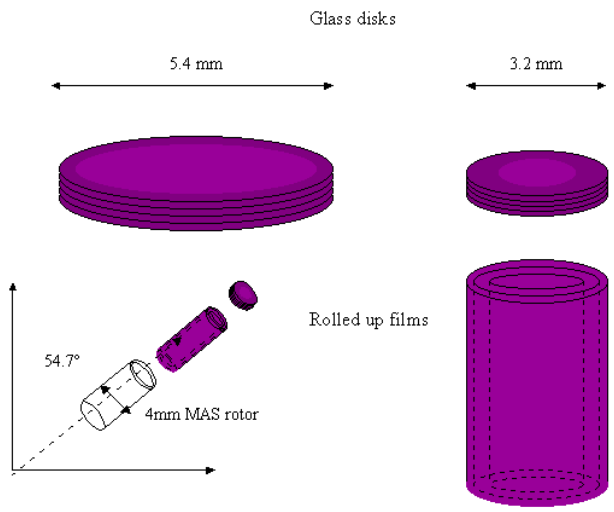

Fig 5.29. Diagram describing technical details of how to produce oriented samples in MAS rotors. 5.4mm diameter glass disks are available to fit 7mm Bruker rotors however 3.2mm disks are not available to fit 4mm MAS rotors. If 3.2mm disks were available then they may suffer from a significant edge effect where the orientation is compromised near to the edge of the disk. One alternative would be to dry membrane films onto a more flexible support that could be rolled up and placed in the 4mm MAS rotor. Centrifugal forces, present under MAS conditions, would help orientation and packing of the films.

One alternative is to use thin plastic films that can be rolled up and placed in practically any diameter rotor (Fig 5.29) after membranes have been dried onto them (Bechinger, 2000). In this case the centrifugal forces would actually help sample packing and would be applied more uniformly across the sample. Experiments employing this technique are currently being developed in our laboratory.

6. Protein-Lipid Interactions in Purple Membrane and Reconstituted Rhodopsin Containing Membranes Studied by ^{31}P NMR

6.1 Introduction

Whilst the three previous chapters have been concerned with determining structural constraints at high resolution for proteins within biological membranes, this last experimental chapter will look at the other major constituent of a biological membrane, the lipids, and the interactions that take place between the lipids and the proteins embedded in them. ^{31}P NMR of phosphate containing lipid headgroups is a useful non-perturbing probe of biological membranes. Here, two applications of ^{31}P NMR are studied. Firstly, experiments are performed to determine the usefulness of ^{31}P NMR as a probe of the lipid environment associated with high concentrations of purified rhodopsin in a mixed lipid bilayer. Secondly, ^{31}P NMR is assessed as a tool for determining structural constraints for lipids in the purple membrane.

6.1.1 Rhodopsin lipid interactions in mixed lipid membranes

In the absence of 3D crystals, 2D arrays of membrane proteins in a lipid bilayer can be used for electron diffraction experiments. This strategy has been successfully applied to c20 different proteins, most successfully for bacteriorhodopsin (Henderson *et al*, 1990). Extending this technique to rhodopsin and other mammalian 7-TM proteins has

been difficult. Rhodopsin, unlike bacteriorhodopsin, does not form 2D arrays *in vivo* so these crystals must be produced *in vitro*. The strategy used for the production of 2D arrays for rhodopsin was to raise the membrane protein content in an attempt to force order through protein density (Unger and Schertler, 1995). In the best samples 10% of vesicles contained 2D arrays. Compared with the structures produced for bacteriorhodopsin the resolution in these studies is low. In electron crystallography, better crystals produce better resolved protein structures. Thus, there is a need for a reproducible method, by which good quality 2D arrays can be produced. Such a method should also be applicable to other membrane proteins.

It has been shown experimentally that one particular lipid, phosphatidylglycerol phosphate methyl ester (PGP-Me) (Fig 6.1) when mixed with another bulk lipid is essential for 2D array formation of bacteriorhodopsin in membranes (Watts *et al*, 1993). A general model has been proposed for 2D array formation, supported by Monte Carlo simulations, proposing that arrays form when a more strongly interacting annular lipid is introduced into lipid bilayers of a less strongly interacting lipid (Sabra *et al*, 1998). If PGP-Me could cause or aid array formation of the structurally related protein, rhodopsin, then a general method for 2D crystallisation of 7TM proteins may be achievable. In this work the effect of PGP-Me on rhodopsin in lipid bilayers will be assessed.

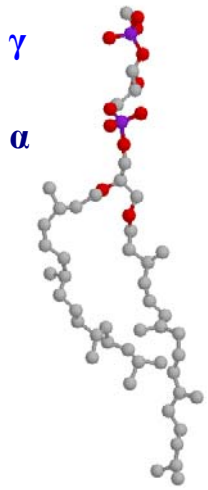

Fig 6.1. PGP-Me the major phospholipid of the purple membrane.

Electron microscopy of reconstituted samples will show, immediately, whether successful reconstitution of rhodopsin in lipid bilayers has been achieved and whether an array has been formed yet it will not help to describe the underlying protein-lipid interactions that produce this effect. Other physical methods employing magnetic resonance will demonstrate the forces existing between the proteins and lipids in these systems.

As an array is being formed it is thought that the rotation of the protein will be slowed down as a result of increasing protein-protein and protein-lipid interactions. Slowing rotational diffusion of rhodopsin in the membrane, can be demonstrated by ESR of spin labelled proteins, whilst the interactions between lipids and their environments can be studied through ^{31}P MAS NMR and spin labelled lipids. Studying the effects of varying the lipid/protein environment on these two constituents of the membrane will allow the observation of some factors thought to promote array formation and protein ordering in the membrane.

ESR can be used to study biological systems that possess a paramagnetic species. The paramagnetism can be introduced as a probe attached to, for example, a lipid or protein.

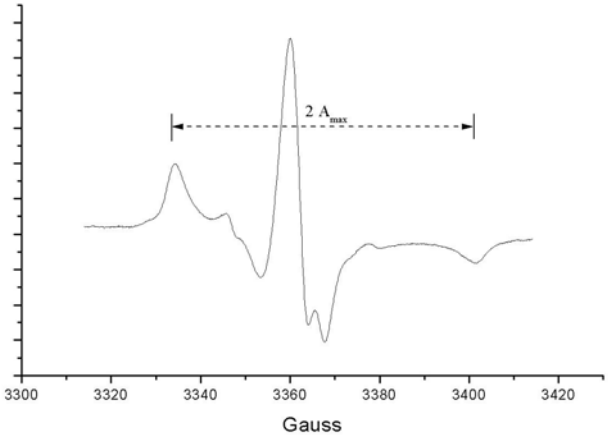

Fig 6.2. Conventional ESR spectra of spin labelled rhodopsin in reconstituted PC vesicles (263K). The spectrum is characteristic of a strongly immobilised spin label.

The ESR lineshape is critically dependent on the orientation and rate of motion of the probe. In a conventional spectrum two components comprising the hyperfine splitting can be observed, the distance between them is defined as 2 A_{max} (Fig 6.2). 2 A_{max} increases in response to a slowing of the rotation of the spin label (and hence the attached protein).

Saturation transfer ESR methods extend by several orders of magnitude the sensitivity of ESR to very slow motion (Thomas *et al*, 1976). Analysis of three different sets of parameters from a saturation transfer spectrum can lead to a calculation of rotational correlation times (τ_c). In this case the parameter L″/L is used, where L is the height of the peak near the low field turning point and L″ is the height of a point intermediate between the two low-field turning points (Fig 6.3). Comparison of this experimentally determined parameter with a calibration curve for proxyl-Hb in defined

water/glycerol mixes, gives correlation times for proteins in a membrane (Kusumi *et al*, 1980).

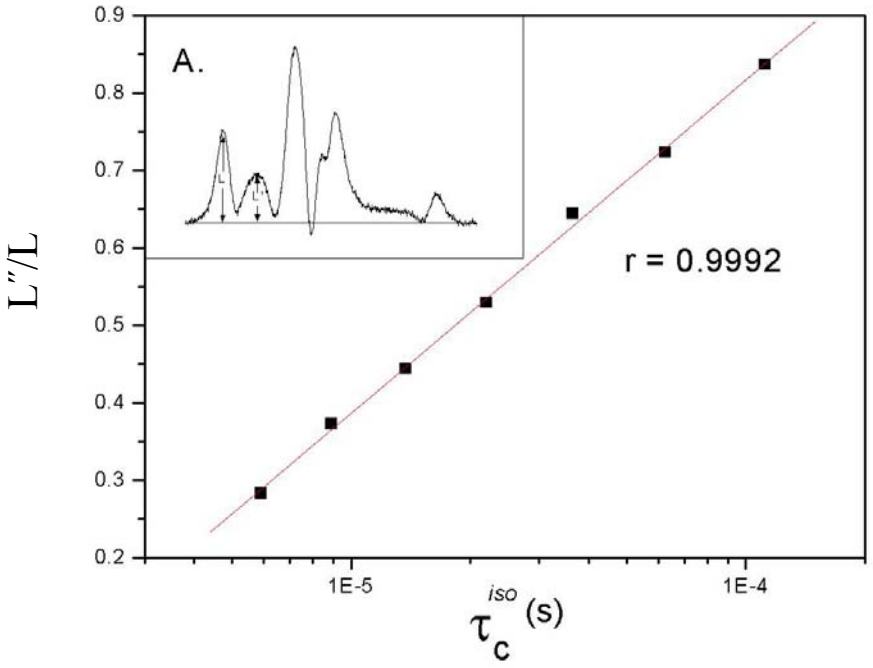

Fig 6.3. Calibration curve for parameter L″/L for different correlation times (P. Spooner)

Rhodopsin does not contain paramagnetic centres, so it is necessary to introduce spin labels. The nitroxide spin label 3-maleimido proxyl $C_{12}H_{17}N_2O_3$ was used to study the rotational correlation time of bovine rhodopsin. The spin label covalently attaches to free cysteine residues in the protein. There are a total of 10 cysteine residues in the sequence of bovine rhodopsin. Two are involved in a disulphide bridge whilst two more are palmitoylated leaving six free cysteines. All remaining accessible cysteines bar one are blocked through brief pre-incubation with N-ethyl-maleimide (NEM) such that only one cysteine is labelled per rhodopsin (Kusumi *et al*, 1980).

Lipid dynamics can also be followed through ESR techniques with the attachment of a spin label to the lipid chains. ESR is particularly sensitive to motions in lipids such

that more than one population of lipid can be discerned. It has already been shown (Watts *et al*, 1979), through ESR, that lipid associated with a protein in the bilayer is motionally restricted. This boundary lipid appears as a second population in the ESR spectrum and consists of lipids within the first and second shells around the protein. The co-reconstitution of the spin labelled lipid 14-PC Spin Label (14-PCSL) with unlabelled PC will show whether PC is present as boundary lipid or not when PGP-Me is present in the system.

^{31}P NMR is used here to observe the lipids involved in the reconstituted system. Natural abundance ^{31}P MAS NMR on the reconstituted sample produces resonances corresponding to the phosphorus atoms in the lipid headgroups (Pinheiro & Watts, 1994). The advantage of this technique is that chemically different lipid species have different NMR chemical shifts and so can be distinguished in the ^{31}P MAS NMR spectrum and so the experiences of the different species can be observed. The NMR lineshapes are indicators of local environments that the lipid may be experiencing.

6.1.2 Lipids of the Purple Membrane

With the arrival of high resolution x-ray and electron diffraction structures of bacteriorhodopsin in multiple photointermediates (Luecke *et al*, 1999[a,b]; 2000; Sass *et* al, 2000; Edman *et* al, 1999; Royant *et al*, 2000; Vonck, 2000) a greater understanding of the processes that drive proton pumping may be sought. The retinal isomerisation that initiates the photocycle and the protein structural changes that result can be combined to describe the events required for a proton to be moved from one side of a membrane to

another. The movements of the chromophore, the protein backbone and even water molecules can be followed by high resolution x-ray and NMR methods. Despite these successes however, there remain gaps in our knowledge. There are other constituents of the purple membrane that contribute to its specified function whose influence is less well characterised. These other components are lipids whose nature and composition in the purple membrane are known (Kates *et al*, 1982). Lipids make up 25% of the weight of purple membrane with bR accounting for the remaining 75%. There are five major classes of lipid present: PGP-Me (phosphatidylglycerol phosphate methyl ester) (49%), GLS (glycolipid sulphate, identified as S-TGA-1) (22%), SQ (squalene) (10%), PG (phosphatidylglycerol) (5%) and PGS (phosphatidylglycerol sulphate) (4%) (Kates *et al*, 1982). This can be simplified by referring to the lipids in relation to the proteins with which they associate. Bacteriorhodopsin is by far the major protein of the purple membrane, the only other proteins present are bR precursors which arise from incomplete processing of an N terminus sequence. Each bacteriorhodopsin monomer can be considered to have approximately 10 lipids associated with it comprising 6-7 phospholipids, 2-3 sulphated glycolipids and 1 squalene (Grigorieff *et al*, 1996).

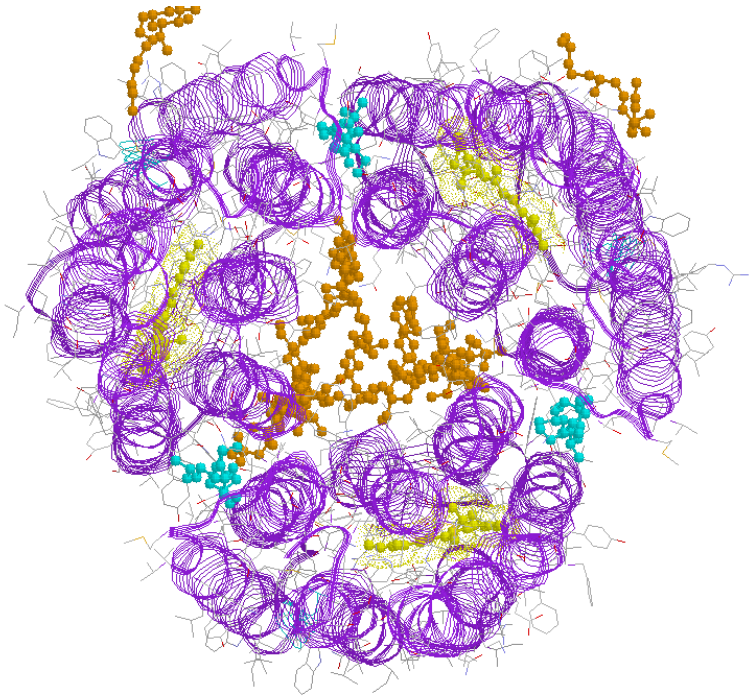

Fig 6.4. Figure showing trimeric arrangement of bacteriorhodopsin with some lipids from the purple membrane co-crystallised (1brr.pdb; Essen *et al*, 1998). The lipid headgroups that can be resolved are from the two glycolipid S-TGA-1's per bR monomer, shown in orange. One of these forms a plug at the extracellular face inside the bR trimer whilst the other is located in the inter-trimer space. Phytanyl chains that may have a PGP-Me headgroup are shown in cyan. Other lipids are unresolved in this structure. This view is from the extracellular face. The retinals are shown in yellow.

Structures derived from two and three-dimensional crystals of purple membrane have revealed some of the detail of the localization of these lipids in the purple membrane and their spatial organization with respect to the bacteriorhodopsin trimer (Belrahi *et al*, 1999; Essen *et al*, 1998; Henderson 1975). Until recently the specific structural relations of the lipids and protein was not known since although the phytanyl chains of the lipids can often be resolved in structures obtained by x-ray diffraction the headgroups have very high temperature factors which prevent their structure from being

modelled. However, both x-ray diffraction of bR crystallised by heterogeneous nucleation on benzamidine (Essen *et al*, 1998), not from cubic phase, and neutron diffraction (Weik *et al*, 1998) methods have shown the localization of glycolipid headgroups within the purple membrane. Neutron diffraction of purple membrane containing S-TGA-1 metabolically labelled with deuterated glucose showed density at two locations per bR monomer, one in the interior of the bR trimer and the other in the intertrimer space (Fig 6.4). The high resolution structure (Essen *et al*, 1998) shows significant structural contacts between S-TGA-1 in the trimer interior and the protein including a number of hydrogen bonds. A "structural complementarity" can be seen between the cavity formed by the bR trimer and the lipids located in it. The specific protein-lipid interactions and high degree of order for S-TGA-1 imply that its tight association with bR is crucial for trimer stabilisation. The S-TGA-1 molecule located in the intertrimer space may have similar protein-lipid interactions and hence be important for the association of bR trimers to form the crystalline lattice. Once the position of the glycolipids has been identified then it is possible, by elimination, to tentatively assign other resolved phytanyl chains as belonging to phospholipids.

The location of one of the PGP-Me lipids has been tentatively assigned in a recent structure; it is bound in a crevice between bR monomers (Sato *et al*, 1999) (Figs 6.4 and 6.5) on the cytoplasmic face of the protein. This structure models the phosphate headgroup however comparison with another structure (Essen *et al*, 1998), where this lipid's chain but not headgroup is resolved, shows some discrepancy in where the phytanyl chain extends. This discrepancy may well be influenced by the relative crystallisation conditions, particularly from detergents used to treat the membranes.

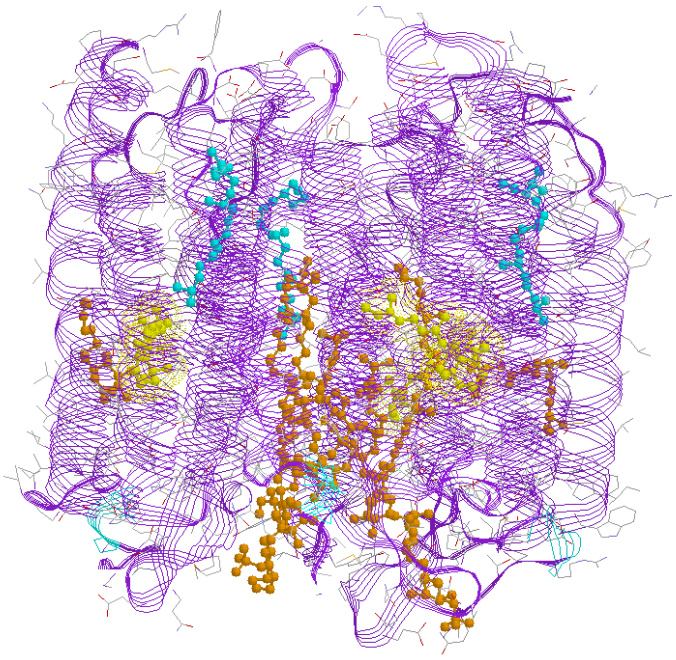

Fig 6.5. Side elevation of same trimer assembly showing distribution of resolved lipids between cytosolic (top) and extracellular (bottom) leaflets. These structures are of bacteriorhodopsin as a trimer in the bR_{568} photostate.

The phytanyl chain attributed to a phospholipid in this crevice is highly ordered and has been seen in a number of high-resolution structures (Luecke *et al*, 1999; Belrhali *et al*, 1999; Mitsuoka *et al*, 1999) suggesting that this phospholipid located at a bR-bR interface may be critical for trimer assembly. The phytanyl chains of four further phospholipids resolved in the intertrimer space contact bR molecules in adjacent trimers (Belrhali *et al*, 1999) and their contacts may contribute significantly to the 2D lattice assembly. The importance of the phospholipid PGP-Me was shown in a biochemical study (Watts, 1995) where the presence of this highly negatively charged lipid was shown

to be essential for 2D array formation of bacteriorhodopsin when co-reconstituted in DMPC liposomes.

Functional studies on bacteriorhodopsin have also shown the importance of the relationships between bR and its associated lipids (Joshi *et al*, 1998). Purple membranes were delipidated with small amount of Triton X-100 and treated with lipid extracts of single lipids or combinations of the classes described above. bR was also successfully reconstituted in membranes containing one or more of the same lipid classes. The photocycle kinetics were followed, with a focus on the M-state decay. The photocycle characteristics were severely compromised following delipidation or reconstitution in the absence of PGP-Me, however normal photocycle could be regenerated by treating delipidated complexes with normal levels of PGP-Me and SQ or with higher levels of PGP-Me alone. This work highlights the important role of PGP-Me not just as a necessary component for 2D array formation (Watts, 1995) but also as a functional mediator of the photocycle. The possible role of a specific amino acid side chain was mentioned, following the observation that in order to obtain reconstitution the charge-charge repulsion must be overcome by either high salt or titration of a group with an apparent pK_a near 5. This specific interaction has not been characterised. Since the roles described above have been demonstrated by a number of separate studies and methods it would be interesting to be able to understand how the purple membrane lipids, in particular the phospholipids, are able to have both structural and functional roles in such an intimate relationship with their associated protein. The experiments in this chapter are designed to show whether solid-state NMR can provide information about the environment of these phospholipids in the purple membrane and whether structural

parameters can be found for the phospholipids to add to the x-ray structures. The behaviour of the phospholipids during the photocycle will also be followed.

Solid state ^{31}P MAS NMR was chosen to probe the environment of the PGP-Me headgroups in the purple membrane and to follow their fate during the photocycle. This would show how strongly the lipids interact with bacteriorhodopsin and might give some clues as to why the lipids may be so important for the proper functioning of the photocycle. ^{31}P NMR is a powerful, non-perturbing probe of membrane structure and dynamics for biological membranes and has been used to describe the interaction of a number of peptides with lipid bilayers (e.g. Bechinger *et al*, 2001; Bonev *et al*, 2000; Harzer & Bechinger, 2000). The 100% natural abundance and relatively high NMR sensitivity of the ^{31}P isotope are beneficial for solid-state NMR experiments. The increased motions of lipids when compared with proteins can often lead to relatively sharp lines in the NMR spectrum especially under MAS conditions. The disadvantages of using ^{31}P include its low level of chemical shift variation, its often slow relaxation times and its susceptibility to pH induced electrostatic effects. The negative charge carried by a phosphorus headgroup can also mean that cations may affect the NMR spectra both in terms of chemical shift but also in the shape of the powder pattern.

The ^{31}P lineshape can be sensitive to motions that the phosphate headgroup might experience. This sensitivity might be reflected in a number of ways. Any decrease in motion of the headgroup, perhaps from an increase in the ordering of the lipid, would cause an enhanced ^{31}P transverse relaxation rate leading to broader lines in the NMR spectrum. Secondly the heteronuclear dipolar coupling between the ^{31}P and protons is, potentially, a considerable source of line broadening. This coupling is removed to an

extent by MAS but is so large that additional pulses are applied on the proton channel to decouple the protons. Motions present in the sample on the timescale of the decoupling pulses can lead to a reduction in decoupling efficiency and hence broader lines in the NMR spectrum.

6.1.2 ^{31}P MAOSS NMR on biomembranes

Structural parameters for the phopholipid headgroups may also be derived from ^{31}P NMR using the MAOSS experiment. ^{31}P has a spin of ½ and as such behaves in a similar fashion to ^{15}N as described previously. Assuming that the ^{31}P CSA tensor displays axial symmetry, a set of simulated MAOSS spectra will clearly show the relative orientations of a set of ^{31}P CSA's provided that the differing phosphorus groups can be resolved and that a well oriented sample can be prepared.

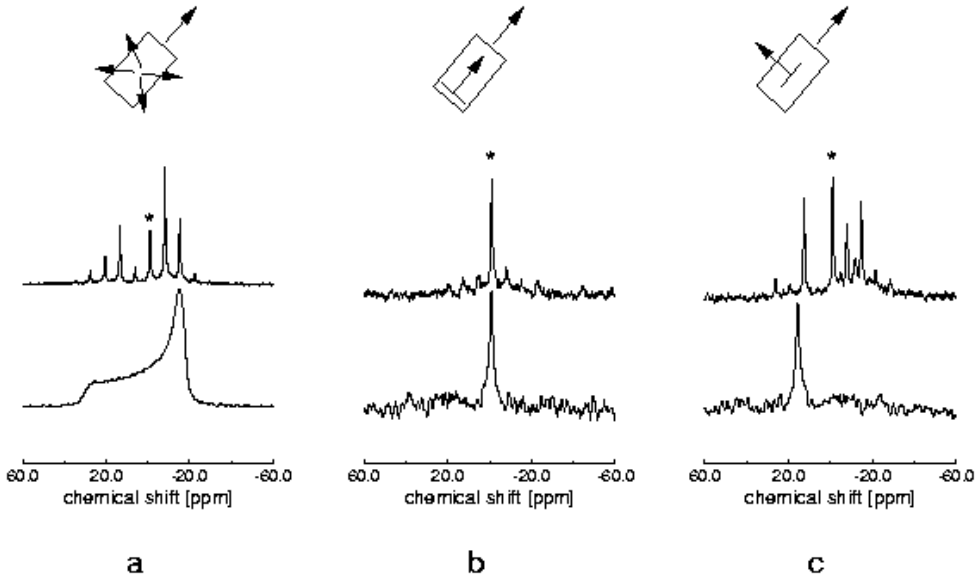

Fig 6.6. Comparison of static and MAS spectra obtained for lipid membranes in "powder" (a), oriented at 0º (b) and 90º (c) to the rotor axis (Glaubitz & Watts, 1998).

Some basic comparisons of MAOSS and static spectra are shown for some DMPC membranes in Fig 6.6. The effect of orienting the membranes at 0 and 90° with respect to the rotor axis is clearly visible with characteristic spectra being produced. The oriented, static spectra are quite narrow due to the rapid rotational diffusion of the lipids. This sample is well oriented and the membranes contain no proteins.

6.2 Materials and methods

6.2.1 Preparation of rod outer segment membranes

All procedures (DeGrip, 1982) were performed in the dark with dim red light (filtered with cut off wavelength at 580 nm) at 4°C unless specified. Briefly, 100 fresh eyes were collected and kept in the dark on ice for 2 hours prior to dissection. Eyes were then dissected and the retina removed, homogenised gently in 50 ml of Buffer I (pH 6.5) (Appendix 2.2.1). 50 ml of 66% (w/w) sucrose containing Buffer I was then mixed with the homogenised solution. The solution was then subjected to centrifugation (average RCF 9000g, 10 m). The pellet was washed once more with 33% (w/w) sucrose containing Buffer I before being discarded and the supernatant from two centrifugations combined and diluted three-fold with Buffer I, centrifuged (average RCF 13,000g; 20 m) to yield the crude ROS in pellet form. For the final purification of ROS, discontinuous sucrose gradient (33%, w/w) centrifugation was used (average RCF 64,000g rpm; 2hr). The purified ROS band was collected and washed with Buffer I in order to remove the

remaining sucrose (DeGrip, 1982). An SDS gel was run of the purified ROS against protein standards (Fig 6.7) (Appendix 2.3).

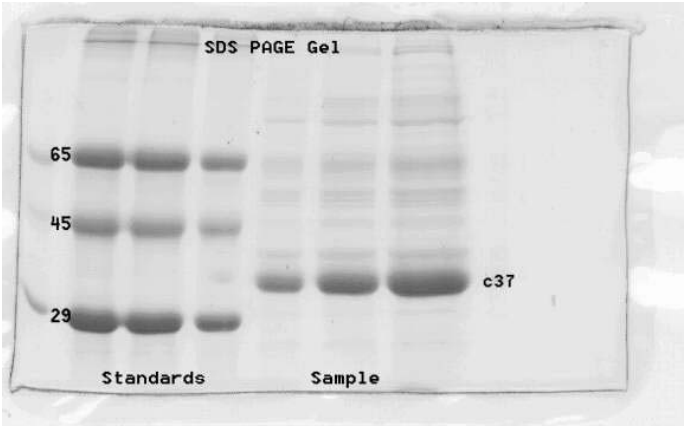

Fig 6.7. SDS Gel of ROS run against protein standards. The gel shows that rhodopsin (M_w 37 k) is the major constituent of the ROS. For gel conditions see Appendix 2.3.

6.2.2 Isolation of Rhodopsin from ROS by Affinity Chromatography

Purification of rhodopsin was performed by Concanavalin A affinity chromatography (DeGrip *et al*, 1982). ROS were suspended in Buffer I (Appendix 2.2.1) and solubilised with 50mM β-octyl glucoside (0.175g/5ml) prior to column separation. The solubilised protein was centrifuged (average RCF 31,000g, 20m). The supernatant was applied to the column, which had been pre-washed with 10 column volumes of column buffer (Appendix 2.2.2). The column was then washed with 4 column volumes of column buffer containing 1% β-octyl glucoside at a flow rate of approx 1ml/min. Eluent was monitored by UV measurements at 214nm showing lipid from the ROS being removed from the column. The rhodopsin was eluted following the addition of buffer containing 0.2M methyl mannoside (1.942g/100ml) in addition to detergent. Eluted

fractions were monitored by UV absorption at 500nm (ε_{500} = 40,000) for the detection of rhodopsin. Concentration of rhodopsin was determined using the Beer-Lambert law and the purified rhodopsin in detergent buffer was concentrated to approximately 2.0 mg/ml by an Amicon Centricon®10 microconcentrator with Diaflo®PM30 Ultrafilter membrane. The rhodopsin was in detergent micelles at this stage in preparation for later lipid-protein reconstitution. A further gel was run to show the purified rhodopsin (Fig 6.8) (Appendix 2.3) and the purity gfurther assessed by UV-VIS spectra (Fig 6.9).

Fig 6.8. SDS gel of purified rhodopsin against protein standards showing elimination of other proteins in ROS. For gel conditions see Appendix 2.3.

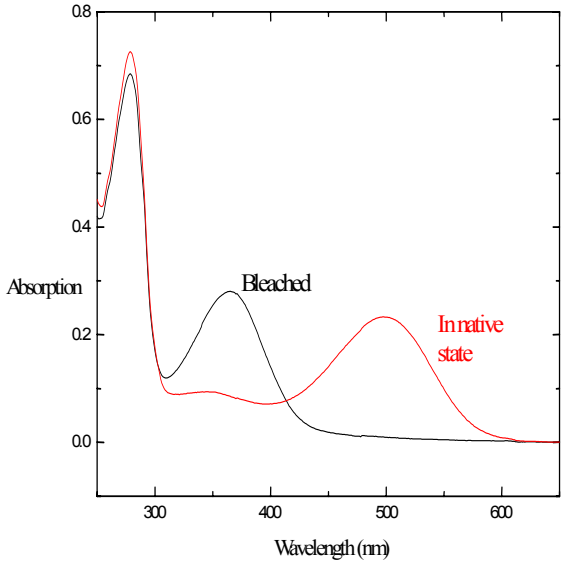

Fig 6.9. Typical absorption spectra for bovine rhodopsin at room temperature in the dark and bleached states.

6.2.3 Extraction and purification of lipids from Halobacterium salinarium

The lipid extraction procedures described here is based on the "Folch wash" method (Kates *et al*, 1982). All procedures were carried out at room temperature unless specified. Purified purple membrane (prepared as described in Chapter 3) was resuspended in 10 ml of distilled water, acidified with a few drops of concentrated HCl and extracted with 100 ml of chloroform/methanol (2:1 v/v). The mixture was then centrifuged (8000g; 10 m) and the organic layer was collected. The aqueous layer was re-extracted once more under the same condition. The two organic extracts were combined and washed with an equal volume of 0.1M KCl and then again with an equal volume of 0.1M KCl/methanol (1:1 v/v). The washed organic layer was dried in a round bottom flask via rotor-evaporation and the lipid extract was redissolved in 5 ml of chloroform.

Column chromatography was performed at room temperature. The silica column was first activated by washing with 500 ml of chloroform/methanol (200:15; v/v) and then with 500 ml of chloroform/methanol/water (200:15:1; v/v). The column was then loaded with 500 ml of chloroform/methanol/saturated NH_4^+ solution (200:15:0.1 v/v) which was used as the first mobile phase solvent. The lipid extract was then applied to the column, and eluted with two litres of chloroform/methanol/saturated NH_4^+ solution (200:15:0.1; v/v). This solvent system eluted the neutral lipid species. After the non-charged species were eluted the mobile phase was changed to chloroform/methanol/saturated NH_4^+ solution (65:35:0.5 v/v). Two litres of the second mobile phase solvent were used to elute the remaining lipid species including PGP-Me. The elutant was collected in 10 ml fractions and the PGP-Me fraction was identified by silica gel thin layer chromatography (TLC). The solvent mobile phase used for TLC was chloroform/methanol/saturated NH_4^+ solution (65:35:5; v/v). R_f value of PGP is 0.26. The isolation of PGP-Me was confirmed by mass spectrometry and ^1H NMR (data not shown).

6.2.4 Lipid-Protein Reconstitution

Phospholipids dissolved in chloroform were dried in a round bottom flask by rotor-evaporation. The lipid was hydrated with 5.0 ml of dialysing buffer (5mM HEPES, 50mM NaCl, 0.5mM EDTA, 0.1mM NaN_3, pH 7.0 (Appendix 2.2.3)) in a bath sonicator to form a uniform suspension, and then drop-wise sodium cholate (5% w/v) was added until the lipid was solubilised. The pre-formed phospholipid vesicles were then

mixed with the rhodopsin-detergent micelles. The mixture was incubated (37°C; 20 m) with constant stirring before being transferred to a dialysis tube. The rhodopsin and lipid vesicles were dialysed against a litre of dialysing buffer at 4°C in the dark, the buffer being replaced every 12 hours. 1 g of thoroughly washed SM2 biobeads (three times with 100 ml methanol, three times with 100 ml distilled water and then equilibrated in dialysing buffer) were applied to the dialysis process after approx. two weeks. The dialysis process was completed within four weeks and a cloudy suspension appeared.

After reconstitution the rhodopsin-lipid vesicles were purified using a 25-45% sucrose density gradient (average RCF 82,000g; 3 hr) the purified band appearing at about 30% sucrose. The vesicles were collected and washed with dialysing buffer to remove the sucrose. Samples were kept at 4°C immediately prior to quenching for electron microscopy. Protein free vesicles were made by drying films of lipid from chloroform and rehydrating with reconstitution buffer with shaking. Vesicles were easily pelleted for NMR in a bench top centrifuge. To assess the success of the reconstitution and to check for 2D protein arrays samples were prepared for freeze-fracture electron microscopy. Under dim red light 2µl of concentrated sample was mounted on a gold-nickel alloy, specimen carrier (Bal-Tec). The mounted sample was rapidly frozen by swift manual immersion into the liquid, chlorodifluoromethane (Freon 22) cooled by liquid nitrogen. The frozen specimens were stored under liquid nitrogen prior to freeze fracturing. The frozen specimens were clamped on a cold table, under liquid nitrogen, which was then rapidly transferred onto the cold stage of the freeze fracture machine. The chamber was evacuated to 10^{-9} bar or less. The frozen specimens were fractured under vacuum using a liquid nitrogen cooled microtome. A replica was produced under vacuum

by oblique deposition (45°) of a fine layer of platinum, followed by a backing layer of carbon deposited from above. The total replica thickness was 15 nm. The specimen was removed from the vacuum chamber and the biological material removed by sodium hypochlorite. The replica was then finally mounted on a copper EM grid for examination in the transmission electron microscope. A typical micrograph is shown in Figure 6.10.

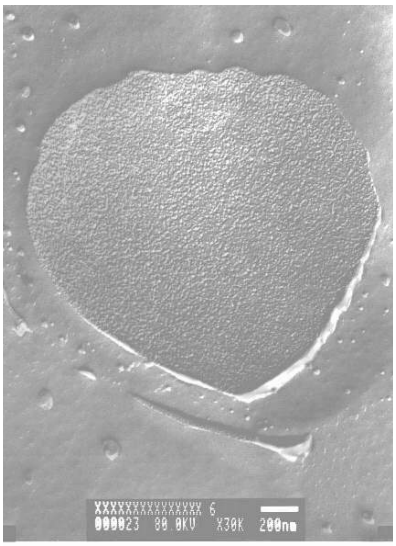

Fig 6.10. Typical electron micrograph of a successfully reconstituted vesicle showing protein densely packed in the membrane. There are no protein arrays present.

6.2.5 Preparation of Samples for ESR

Protein labelling was carried out in the dark under dim red light unless specified. Buffers were subjected to de-oxygenation by presaturation with argon gas. N-ethyl-maleimide (NEM) and 3-malmeido proxyl were dissolved in ethanol at a stock concentration of 1mg/ml. Reconstituted samples (c.a. 80 nmol or 3 mg rhodopsin) were pipetted into a 1ml Eppendorf. The samples were diluted to 1 ml with dialysing buffer followed by the addition of stock solution of NEM (2µl) and incubated (1 hr; room temperature). Excess NEM was then removed by washing the samples with 5% (w/v)

BSA buffer (three times) using centrifugation (10,000rpm; 5m; 4°C). The samples were then resuspended in buffer and incubated with 5µl of 3-maleimido proxyl overnight with constant stirring. Finally the unbound spin label was removed by BSA washes (three times) and buffer washes (five times) (Appendix 2.2.4) as described earlier. Finally the labelled sample was loaded into a glass capillary and centrifuged to form a pellet. The supernatant was removed. Samples were stored at -70°C under argon in an air sealed container before spectrum recording.

For lipid spin labelling, lipid spin labels (14-PCSL) were dissolved in chloroform and added at levels of 1% relative to other lipids prior to lipid-protein reconstitution.

6.2.6 ESR experiments

Saturation transfer ESR spectra were recorded out of phase as a second harmonic signal (Thomas *et al*, 1976). Approximately 25 scans were required for all elements of the spectrum to be resolved. Correlation times were calculated by measuring L″/L ratios on acquired spectra and relating them to values obtained from a haemoglobin standard.

6.2.7 Preparation of purple membrane samples

Wild type (S9) purple membranes were prepared as described in Chapter 3. Both membrane pellets and fully hydrated, oriented samples were prepared as described in Chapter 3. Oriented samples had a protein concentration not exceeding 0.4mg/disk. Wild type bacteriorhodopsin in pellets was trapped in the M_{412} photostate in 0.3M Guan-HCl

pH 10 by strong illumination by a xenon lamp over dry ice for 30 minutes. A purple to yellow colour change was observed.

Static oriented samples were prepared as described in Chapter 5. Initially, for the preparation of well oriented samples the purple membrane was suspended in distilled water and evaporated at a protein concentration of 3.3mg/ml in a volume of 120µl. After two such applications the oriented samples were then treated with 10µl of a buffer containing 50mM NaCl, 50mM Na_2HPO_4 and 50mM Tris-HCl (pH8). The plates (20) were then stacked, wrapped in parafilm and placed horizontally in the coil of the probe.

6.2.8 ^{31}P MAS NMR measurements on reconstituted samples

The reconstituted samples were pelleted and transferred into either a 4 or 6mm MAS rotor. Experiments were performed at 202MHz ^{31}P frequency on a Chemagnetics CMX500 spectrometer with either two channel 4 or 6mm CP MAS probes. Single pulse experiments with 50kHz CW proton decoupling were performed at 298K at spinning speeds of 7000Hz, 65,000 scans were acquired. Following zerofilling with 4K points, complex Fourier transform and phase correction, an exponential line broadening of 50Hz was applied. Spectra were referenced to inorganic phosphate at 0ppm.

6.2.9 ^{31}P MAS NMR measurements on purple membranes

^{31}P CPMAS experiments were performed at 161.92MHz for ^{31}P on a Bruker AVANCE DSX400 with a 7mm MAS (high range) probe. Spectra were referenced to

inorganic phosphate at 0ppm. Room temperature experiments were performed using high power proton decoupling during acquisition with a variety of delay times to check for relaxation effects. Further decoupling schemes, including TPPM were applied to produce as narrow lines as possible. Low temperature (230K) experiments used optimised ^{1}H-^{31}P cross polarisation with proton decoupling. Low temperatures were achieved by cooling compressed air (used for bearing and drive for MAS) in a liquid nitrogen cooled heat exchanger, under pressure to prevent condensation.

6.2.10 Static ^{31}P NMR measurements on purple membrane

^{31}P MAS experiments were performed at 161.92MHz for ^{31}P on a BRUKER AVANCE DSX400 with a Bruker double resonance static probe. Optimised CP experiments were performed at 253K with a recycle delay of 1.5s and a contact time of 1.5ms. Spectra were processed with 100Hz exponential line broadening. For stable trapping of M state intermediates yellow filtered light from a Schott KL 2500 LCD Cold light source was directed through a 5m long (8mm diameter) fibre optic cable (Fig 6.11). Samples were light adapted at room temperature (Appendix 4) and then cooled in the dark. Illumination was initiated five minutes before NMR acquisition and was maintained throughout the experiment. Previously such a procedure was performed outside of the magnet and a purple to yellow colour change was observed throughout the sample.

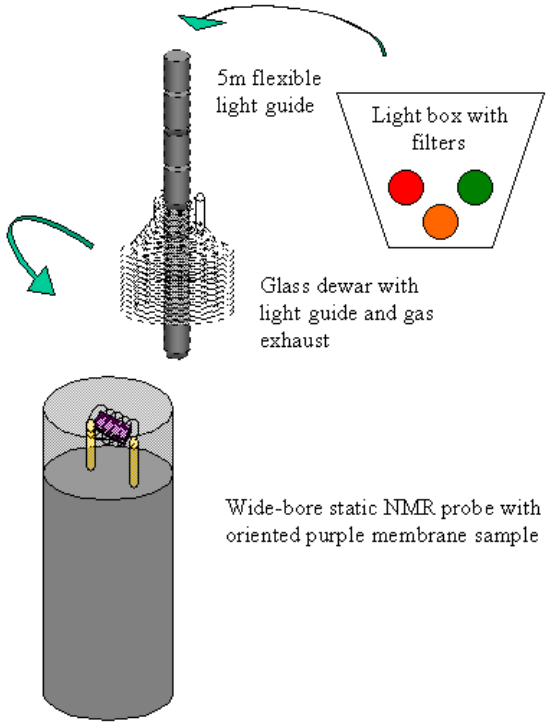

Fig 6.11. Experimental set up for illumination of static oriented films of purple membrane in an NMR probe.

6.3 Results

6.3.1 ESR-spin labelled rhodopsin

ESR was used to investigate whether, following successful reconstitution, rhodopsin was becoming less mobile and hence may begin to associate under controlled conditions or form arrays even if none were observed under EM.

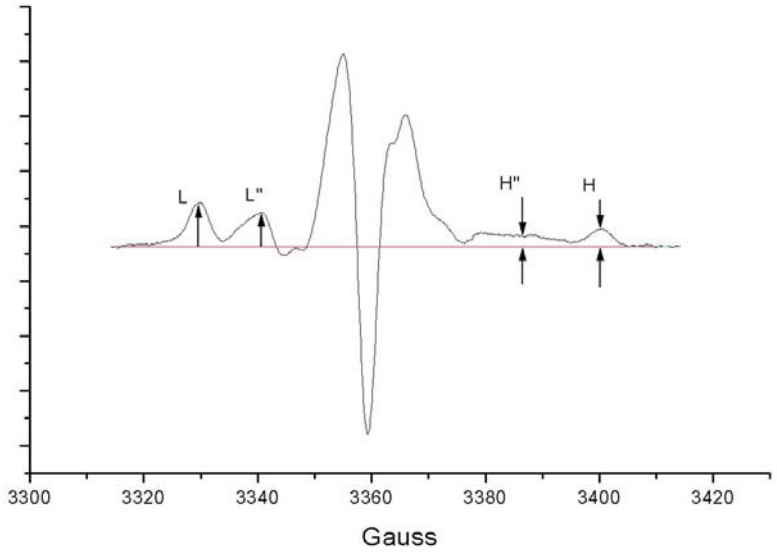

Fig 6.12 Saturation transfer ESR spectrum of proxyl labelled rhodopsin in PC membranes (263K). The points of the spectrum used for calculation of correlation times are marked. H is the height of the peak near the high field turning point and H″ is the height at a point intermediate between the two high-field turning points. L is the height of the peak near the low-field turning point and L″ is the height at a point intermediate between the two low-filed turning points. Both the L″/L and H″/H ratios are sensitive to motions in the range 10^{-6} to 10^{-4}s however some discrepancy between simulated data and experimental results for the H″/H ratio have been observed for spin labelled Haemoglobin (Thomas *et al*, 1976).

Fig 6.12 shows a typical ST-ESR spectrum for proxyl labelled rhodopsin in reconstituted membranes. From the spectra τ_c values were calculated. As good signal to noise spectra were obtained, the error associated with these correlation time measurements is related to the correlation time calibration performed on spin-labelled Haemoglobin in water-glycerol (Fig 6.3). The linear calibration with a correlation coefficient of r = 0.9992 has an error of 5% within the range of measurements.

	T_c ($\times 10^{-5}$ s)		
T (K)	100% EYPC	10%PGP	20%PGP
263	7.47	6.51	3.26
277	6.73	5.20	3.84

Table 6.1. Calculated correlation times for rhodopsin in reconstituted samples at differing temperatures.

The calculated times show that increasing the concentration of PGP in the membrane leads to an increase in rotational diffusion of the protein (Fig 6.13). This observation is contrary to what would be observed if the protein was being ordered into an array. The addition of PGP does clearly cause an effect on the protein, however from this evidence alone the nature of the interaction is unknown.

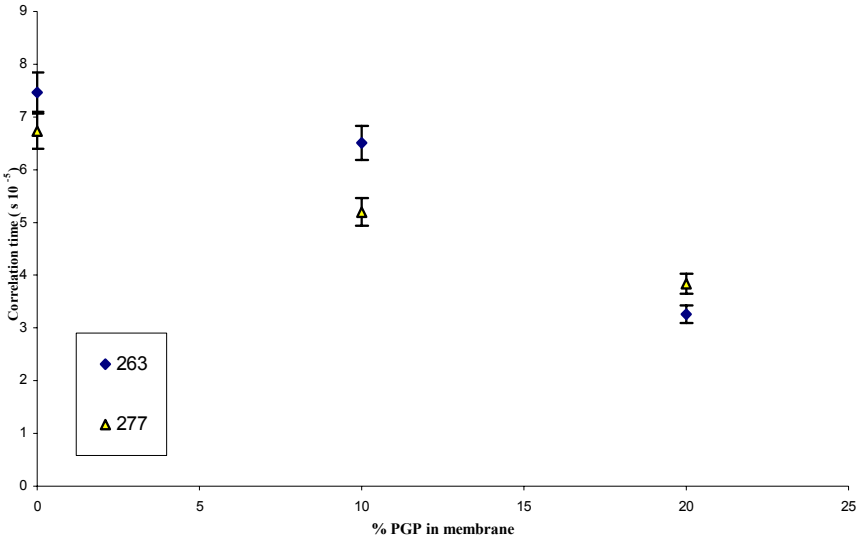

Fig 6.13. Correlation times determined from ST-ESR of reconstituted samples as a function of concentration of PGP in the membrane at differing temperatures (K). Correlation times calculated from L″/L in saturation transfer spectra.

6.3.2 ESR-spin labelled PC

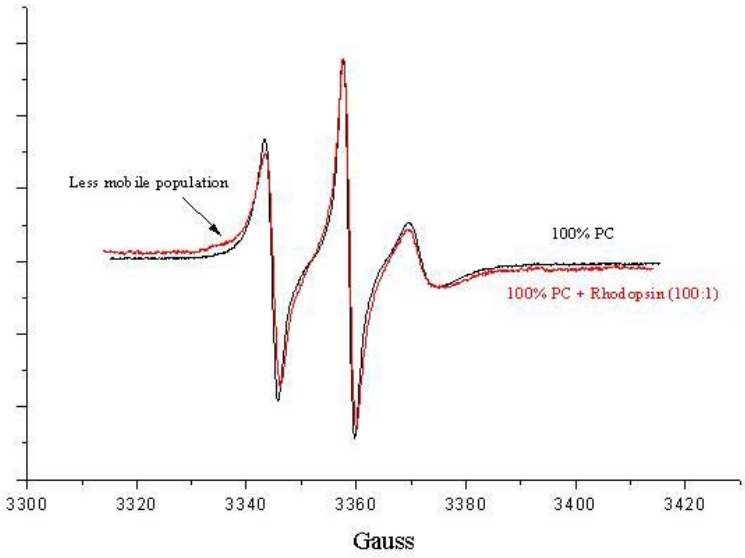

Fig 6.14. Conventional ESR spectra of 14-PCSL in reconstituted membranes with and without rhodopsin (298K).

The presence of rhodopsin in a reconstituted sample containing 14-PCSL causes a second ESR spectral component to appear when compared with protein free bilayers corresponding to lipids which are motionally restricted through contact with the protein. These lipids appear in the ESR spectrum as a shoulder on the resonance corresponding to lipids in the bulk phase (Fig 6.14). Despite the relatively small size of the spectral feature associated with this effect the technique is extremely sensitive and has been used to describe the quantitatively and qualitatively boundary lipids associated with a protein in a lipid bilayer in a number of systems (e.g. Marsh *et al*, 1976; Knowles *et al*, 1979; Watts *et al*, 1979). Any lipid associating preferentially with the protein would displace these boundary lipids and the shoulder would reduce or disappear, in this case PGP would prevent 14-PCSL from coming into contact with rhodopsin. The spectra obtained with and without PGP (Fig 6.15) are identical showing that PC is not excluded from boundary

lipids and hence PGP does not form an annulus with the protein in this case. A number of parallel samples were made in addition to samples containing 20% PGP (molar lipid) (data not shown) and equally no effect on the boundary lipid was seen.

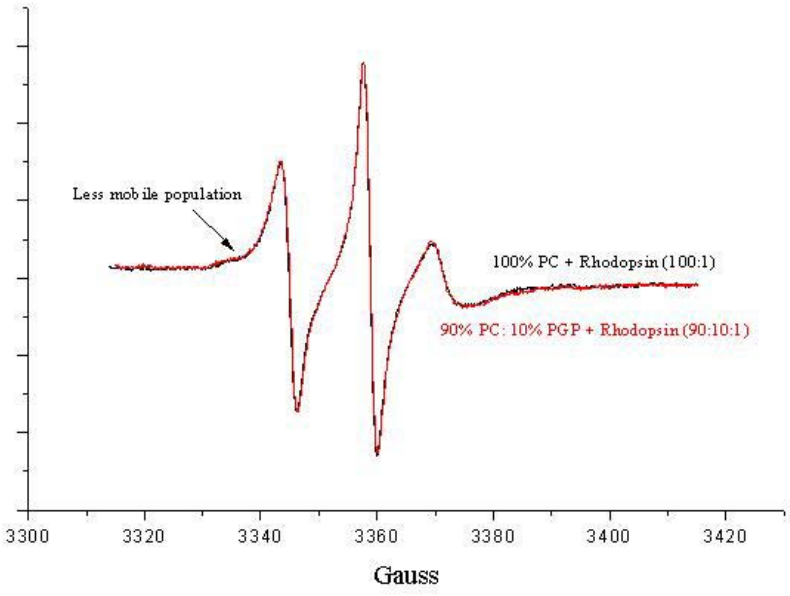

Fig 6.15. Conventional ESR spectra of 14-PCSL in reconstituted membranes (298K) for two different reconstituted samples.

6.3.3 ^{31}P NMR of reconstituted complexes

For complexes containing only PC one significant resonance appears in spectra recorded with and without protein, (Fig 6.16). The small shoulder peak in the lipid only vesicle is attributable to inorganic phosphate, confirmed through its absence in spinning sidebands (data not shown). The addition of rhodopsin to the vesicles causes a significant broadening of the central line from a linewidth of 0.63ppm to 1.04ppm.

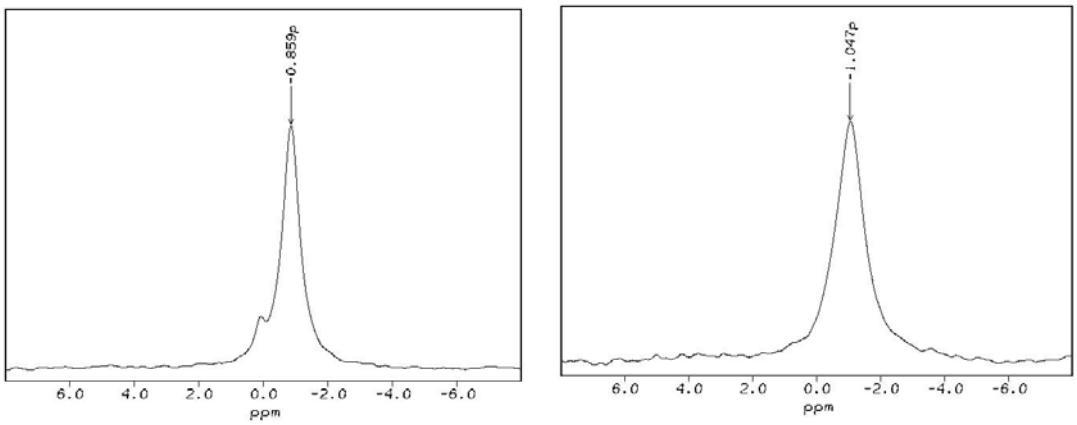

Fig 6.16. ^{31}P MAS NMR spectra of reconstituted vesicles containing EYPC (left) and rhodopsin and EYPC (1:100 molar ratio) (right). Spectra recorded with 6mm MAS probes on a Chemagnetics CMX500 at 298K and 7kHz MAS frequency with recycle delay of 2s and 50kHz ^{1}H CW decoupling.

When 10% PGP-Me is added to the reconstitution (Fig 6.17) the two phosphate groups of PGP-Me appear at approximately 1.6(γ) and 0.4(α)ppm. The PC peak in the lipid only vesicles is slightly broader after the addition of PGP-Me. The PC peak with rhodopsin present is significantly broadened after the addition of PGP-Me with a linewidth of 1.2ppm. The presence of rhodopsin in this sample leads to increased broadening of the PC peak whilst the PGP-Me peaks remain unchanged. A further sample (data not shown) containing 20% PGP-Me molar lipid showed that during reconstitution there is no selective preference in vesicle formation for either lipid as the proportions of lipid added are the same in the spectra.

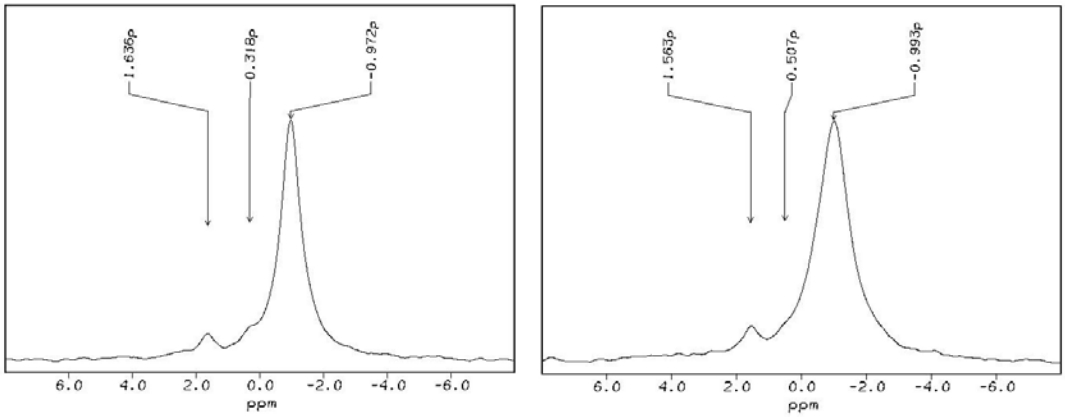

Fig 6.17. ^{31}P MAS NMR spectra of reconstituted vesicles with PGP-Me 10% and PC 90% of total lipid. The spectrum on the right has rhodopsin reconstituted in the membrane (lipid: protein ratio is 100:1). NMR parameters as Fig 6.16.

6.3.4 ^{31}P MAS NMR of purple membrane

First sight analysis of ^{31}P MAS spectra at room temperature (Fig 6.18) shows a very pronounced central line around which can be seen sidebands that have much reduced intensities in comparison with the isotropic peak. The lines in the spectra are broader than might be expected for lipids in a membrane. The intense central line would imply that much of the phosphorus in the sample experiences quite a low level of anisotropy whilst the presence of sidebands (at ω_r = 3000Hz) suggests that some phosphorus does display anisotropic motion. The broadness of the lines confirms the expectation that such a low lipid to protein ratio leads to reduced motion of the phospholipids in this membrane.

Summarising, there are two, or possibly more, populations of phosphorus in the membrane that show differing degrees of anisotropy. Both these populations have considerable line-broadening consistent with them being in contact with the protein

(bacteriorhodopsin) content of the membrane. The two populations are present with the α phosphate having more anisotropic motion than the γ phosphate.

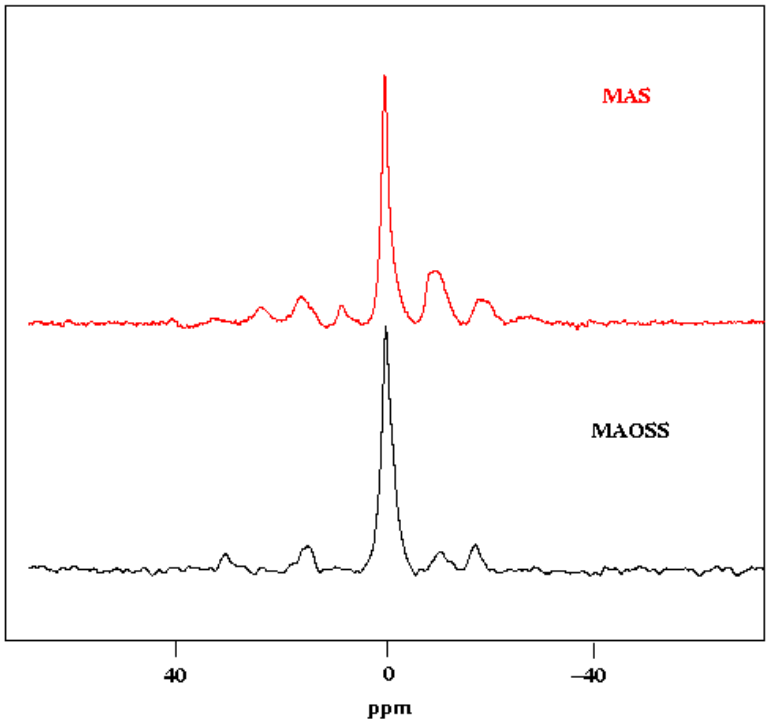

Fig 6.18. Comparison of ^{31}P MAS and MAOSS spectra for purple membrane at room temperature at slow spinning speed. Spectra acquired at MAS frequency of 1400Hz and at 288K with delay of 1.5sec and 60kHz CW ^{1}H decoupling on a Bruker DSX 400 with 7mm MAS probes.

The comparable ^{31}P MAOSS spectrum for purple membrane at room temperature is very interesting as two meaningful features are immediately discernable. Firstly it is clear that the large central line remains and is indeed more intense. Secondly, odd numbered sidebands have much reduced intensities. These two features are characteristic of two "special case" orientations for spin ½ nuclei where, a CSA oriented at 0° to the rotor axis will have all spectral intensity concentrated into the isotropic line and one at 90° will have intensity only in odd numbered sidebands. This result is consistent with two

phosphorus populations, one with CSA oriented at 0° and one at 90° with respect to the rotor axis. An accurate analysis of the spectra in terms of orientational constraints is impossible given that the relationship between the proportions of each phosphate resonance contributing to each line is unknown. The supposed isotropic nature of the γ phosphate means that there is less contribution to the sidebands relative to the α such that its orientation is even harder to accurately measure. One way of increasing the anisotropy of the system is to freeze the sample, reducing the molecular motions. Trapping the M_{412} photostate also requires low temperatures so ^{31}P CP-MAS spectra were acquired for purple membrane samples at 230K in bR_{568} and trapped in M_{412} at pH10 in 0.3M GdnHCl. These spectra are shown in Fig 6.19.

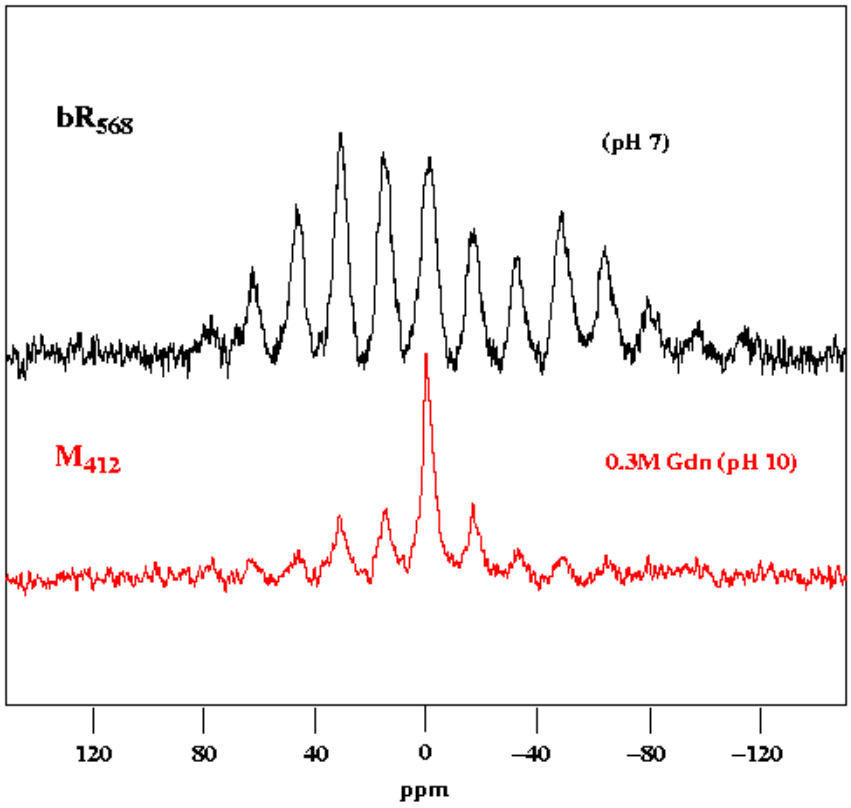

Fig 6.19. Comparison between low temperature (230K) ^{31}P CPMAS spectra for purple membrane pellets in bR_{568} and M_{412} states (trapped in 0.3M Gdn HCl pH10). Spectra acquired at MAS frequency of 2500Hz at

230K with 1.5s recycle delay, 3ms CP contact time, 50kHz CW ^{1}H decoupling on a Bruker DSX 400. 20k scans were accumulated.

What can immediately be seen in the ^{31}P CP-MAS spectrum for the bR_{568} photostate is that the ^{31}P anisotropy has been greatly increased which, even under CP conditions, means that the sensitivity of the experiment has been reduced. Also the axial symmetry of the ^{31}P CSA tensor has been lost which introduces another parameter into the angle simulations when trying to match simulations with results. The increased anisotropy should, however, make angle calculations more accurate, particularly for the γ phosphate. The spectrum for the trapped sample has an unexpected feature (Fig 6.19 red spectrum). In this sample (pH10) there is now again an intense central line although the side bands are now more intense than in the spectrum acquired at room temperature. In the absence of any orientational effects the increase in intensity of the central line must be due to increased motion of the lipid headgroups.

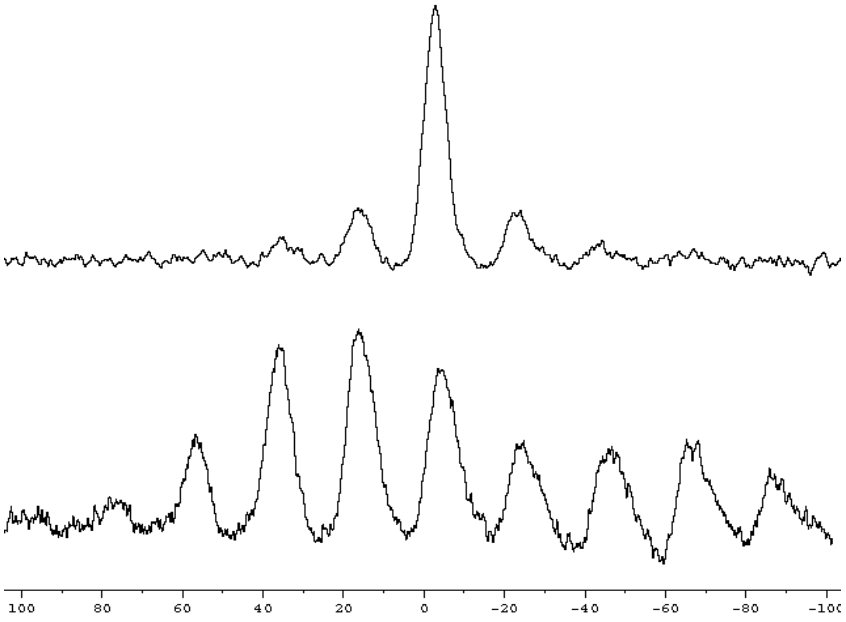

Fig 6.20. Comparison of two low temperature ^{31}P CPMAS spectra of purple membrane acquired at 243K in the bR_{568} state at 3000Hz spinning frequency. Membrane pellets prepared from distilled water (bottom) and pH 8 buffer (top). There is a significant reduction in intensity of the sidebands at higher pH corresponding to a reduction of the ^{31}P CSA. NMR parameters as for Fig 6.19 except CP contact time of 1ms.

CPMAS spectra acquired for untrapped purple membranes at differing pH (Fig 6.20) show how the motion of the ^{31}P CSA is affected by an increase in the electrostatic strength of the surrounding environment. The ^{31}P CSA of both of the two major phosphates are greatly diminished which would correspond to an increase in motion of the lipid headgroups in response to the increase in pH even at low temperature.

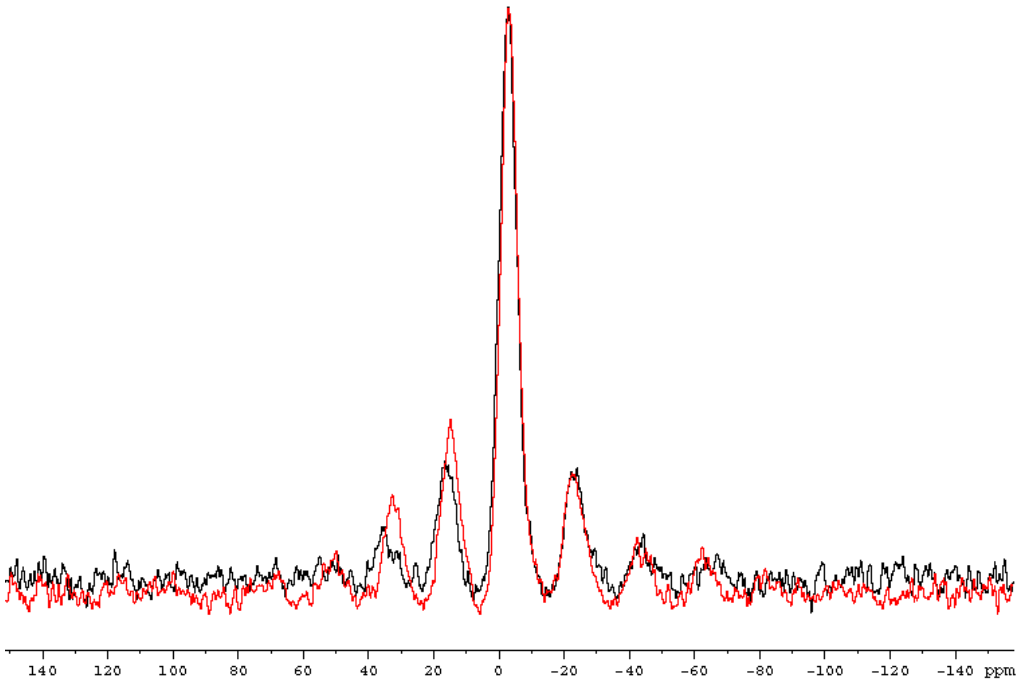

Fig 6.21. Comparison of ^{31}P CPMAS spectra acquired at 243K (black) and 233K (red) and at 3000Hz spinning frequency for purple membranes in bR_{568} state pelleted from pH 8 buffer. NMR parameters as Fig 6.20.

Further CPMAS experiments performed at lower temperatures (Fig 6.21) were unable to fully reintroduce the anisotropy. A slight increase in the intensity of the sidebands was observed relative to the central, isotropic peak.

6.3.5 Static ^{31}P NMR of purple membrane

Since the NMR acquisitions used in this Chapter and indeed this thesis, typically take many hours to acquire; samples that are stable over such periods are required. Generally this is readily achieved by freezing the samples to relatively modest temperatures (253K). At such temperatures an optimum balance is obtained to keep the sample from dehydrating and denaturing, the efficiency of cross polarisation is enhanced whilst some motion is retained in the membrane which aids heteronuclear decoupling and spectral linewidths.

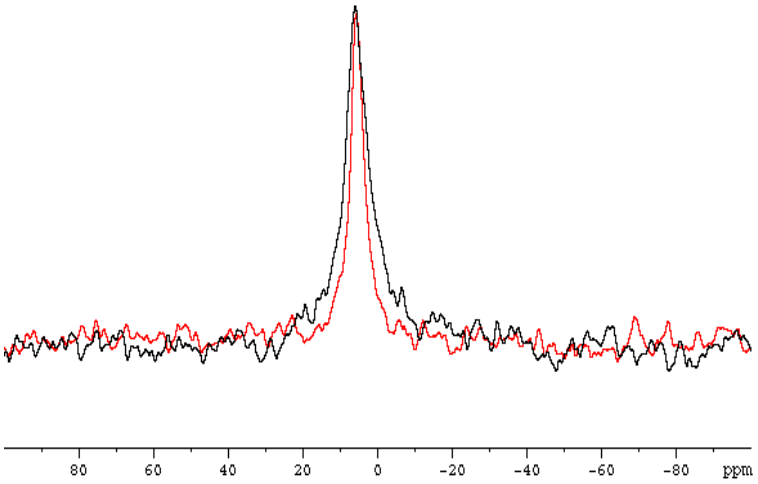

Fig 6.22. Comparison of static oriented ^{31}P CP NMR spectra of purple membranes obtained at 253K in the absence (black) and presence (red) of strong illumination (yellow filtered light). A significant reduction in

linewidth is observed under illumination. Static CP spectra were acquired with 1.5s recycle delay, 1ms CP (80-100% ramped) contact time and 50kHz TPPM ^{1}H decoupling on a Bruker DSX 400 with a static double resonance probe. 32k scans were accumulated.

The bacteriorhodopsin M-state can be trapped and maintained at 253K however some decay does take place (Appendix 4) and over longer periods (24hrs) may decay to less than 50% M_{412}. For this reason continuous illumination was applied (Fig 6.11) when studying oriented membrane film in static experiments at 253K. The resulting spectra (Fig 6.22) show a reduction in linewidth for the lipid resonances when the sample is illuminated. As with the CPMAS experiments on sample prepared from salt containing buffer solutions the differing headgroup resonances cannot be resolved and the orientational dependence of the spectra might be questioned. However tilting the plates at 90˚ caused a large shift of the resonance (data not shown) and the orientation dependence of the sample was confirmed.

6.4 Discussion

6.4.1 ^{31}P NMR of reconstituted membranes

Whilst no array formation has been observed either by direct observation by electron microscopy or indirectly by protein labelled ESR some understanding of protein-lipid interactions in this system has been gained.

One suggestion from this laboratory (Sabra *et al*, 1998) for 2D array formation in mixed lipid bilayers (bacteriorhodopsin) is that PGP-Me forms an annulus around the

protein (Fig 6.23), these annulae associate to increase the entropy of the annular lipids and reduce the overall free energy of the system thus forming protein arrays.

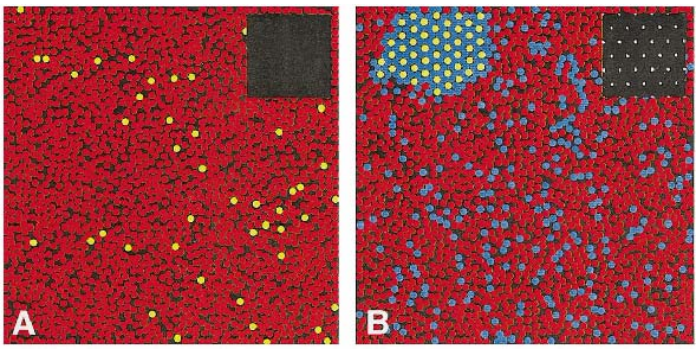

Fig 6.23. Monte-Carlo simulations of array formation. Protein molecules are shown in yellow whilst lipids are in red or blue ("annular"). With no annular lipids (A) no arrays are formed but in the presence of 20 mol% annular lipids (B), array formation can occur (Sabra *et al*, 1998).

In the case of rhodopsin, the evidence from ^{31}P NMR suggests that rather than forming an annulus with the protein the PGP-Me does not come into contact with it. In this case the EYPC is the "annular lipid". Further evidence for this is provided by the ESR spectra of the spin labelled PC (PCSL).

The PC spin label 14-PCSL is a probe of the environment experienced by the PC in the reconstituted system. The presence of rhodopsin in the membrane causes the appearance of a second component in the ESR spectrum attributable to a second population of lipids now in contact with the protein. These lipids in contact with the protein correspond to the first and second shells of lipid around the protein. This phenomenon has been characterised previously (Watts *et al*, 1979). If PGP were to associate with the protein preferentially then the boundary lipids would be composed of PGP-Me and PC would be excluded. If this were the case then this second component comprising 14-PCSL associated with PC should be partially or totally lost on addition of PGP-Me to the bilayer.

The advantages of using ^{31}P NMR in this case are highlighted by the fact that an interaction between rhodopsin and a specific lipid can be discerned due to the chemical shift separation between the PC phosphate and the α and γ phosphates of PGP-Me. Interactions between these resolved lipids and proteins inserted into the bilayer are revealed in the isotropic chemical shift, CSA and resonance half height linewidth. Previously, the interaction between the lantibiotic nisin and mixed lipid bilayers has been studied in this way (Bonev *et al*, 2000) and ^{31}P MAS NMR was able to reveal that the acidic membrane lipid component partitions preferentially into the nisin-associated environment.

The solid state NMR spectra of the lipid protein complexes show that addition of rhodopsin causes broadening to the PC central line and some slight changes in chemical shift. The alterations in chemical shift are very slight and difficult to qualitatively relate to a specific alteration in the lipid environment. However the observed line broadening reflects an enhanced phosphorus transverse relaxation rate, which may result from restrictions imposed on the motional freedom of the lipid headgroups during the interaction between the lipid phosphates and the rhodopsin inserted in the membrane. This broadening effect is increased markedly in the presence of PGP in the bilayer. One possible cause for this could be a low efficiency of incorporation of PGP-Me into the reconstituted membranes leading to smaller vesicles or higher protein to lipid ratios, however no significant variation in vesicles size was observed by electron microscopy (data not shown) and the relative integrals of the lipid resonances in the ^{31}P MAS spectra reveal that the ratio of PC to PGP-Me was maintained in the reconstituted samples. As the broadening effect is greater in the presence of PGP, and the PGP peaks themselves

have no apparent broadening of their own, the protein would seem to be interacting only with the PC and not PGP. This observation is consistent with PC being in contact with protein whilst PGP is sequestered from it. In this case the ^{31}P NMR probe has been successful at describing a very clear effect of a specific lipid protein interaction and would form the basis of a prolonged study of rhodopsin-lipid interactions in the controlled environment of the reconstituted system.

6.4.2 ^{31}P NMR of the purple membrane

^{31}P CPMAS and indeed dipolar decoupled spectra of the purple membrane are unlike spectra typical of many biological membranes. Despite the rather small chemical shift differences found for ^{31}P in phospholipid headgroups it is usually possible to resolve more than one line in a mixed reconstitution. For example in a experiment conducted on mixed membranes (cardiolipin, phosphatidylethanolamine, phospahitdylcholine (1:2:2)) containing cytochrome *c*, despite increased broadening of the isotropic lines when compared with protein free bilayers, three peaks could be resolved within a range of 1ppm (Pinheiro & Watts, 1994). It has not been possible in the case of the purple membrane to resolve clearly more than one resonance in the isotropic central line despite a variety of techniques employed to improve resolution including increased temperatures up to 310K, high proton decoupling fields and temperatures as low as 223K (data not shown). The two major resonances of PGP-Me when either dissolved in organic solvent or reconstituted in a fluid membrane have chemical shifts of ~ 1.6 and 0.4ppm (a separation of 1.2ppm) and should be resolved in a fluid membrane. The inability to

resolve these two species shows that the lipids must have much reduced rotation about their long axis when compared with phospholipids in other membranes. This suggests that the phospholipids in the purple membrane are highly ordered and must interact strongly with the protein in the membrane, a finding totally in agreement with what is known from the high resolution structural studies. This lack of resolution does present a serious problem, however, in that an accurate deconvolution of the spectra is not possible such that information contained in the anisotropic chemical shift, such as orientation, is lost. This means that only a rather simplistic, qualitative analysis of the MAOSS spectra is possible at this time. Further methods of improving resolution in this case are, in theory, possible. One method would use much faster MAS frequencies than the 3000Hz limit imposed by the 7mm MAS probes used here. Faster spinning frequencies coupled with stronger magnetic fields will improve resolution, however as with the ^{15}N experiments already described, the anisotropy would be lost. No specific ^{31}P-^{1}H dipolar coupling exists here so a successful strategy would require the CSA to be reintroduced in a second dimension. An alternative approach might be able to use the rather peculiar nature of the major purple membrane phospholipid. PGP-Me has two ^{31}P nuclei in its headgroup. It may be possible to use the ^{31}P-^{31}P dipolar coupling to excite double quantum coherence between the γ and α phosphates. This would have two benefits: firstly in an oriented system at high spinning speeds with presumed improved resolution, a coupling may be able to be measured which might be used to describe a vector in the PGP-Me headgroup; secondly a double quantum filtered spectrum is often characterised by reduced linewidths. Double quantum filtration tends to select out particular

orientational components, reducing the inhomogeneous broadening of the normal spectrum induced by off resonance homonuclear dipolar couplings (Lee *et al*, 1995).

These experiments were designed to assess whether it is possible to gain any functional information about the lipids during the photocycle. Firstly then the expected effects for a lipid involved in regulating the function of a membrane protein are discussed: Cholesterol as a moderator of photoreceptor function has been studied in some depth since the relative proportions of cholesterol in a membrane controls the ability of rhodopsin in that membrane to function as a light receptor. It has been shown that rod cells contain far less cholesterol (8 mol %) than plasma membranes (28 mol %), rod cell membranes are photoactive yet both rod cell membranes and plasma cell membranes contain rhodopsin. Oxidation of cholesterol in plasma membranes causes the plasma membranes to behave as photoreceptive membranes (Boesze-Battaglia & Albert, 1990). Cholesterol is proposed to act by ordering bilayer lipids, reducing molecular motion in the bilayer and thus inhibiting the meta I to meta II transition of rhodopsin. Cholesterol modulates the packing properties of the lipid bilayer rather than participating in a specific protein-lipid interaction (Mitchell *et al*, 1990). If the same were true of the purple membrane (although more likely in reverse) then PGP-Me might act by increasing disorder in the membrane and hence promoting the bR to M_{412} transition. If this were the case then an increase in motion of the lipids would be expected. If, however, a specific protein-lipid interaction does occur then the electronic environment of the PGP-Me headgroup would be affected with a resultant change in the properties of the CSA.

For stable trapping of the M_{412} intermediate, purple membrane samples are generally kept at 223K whilst being illuminated with yellow light (Appendix 4). If kept at

this temperature then decay of the intermediate is negligible, however it is possible to trap M_{412} at temperatures up to 253K although decay from here is more rapid and mixed M-states (i.e Mo and Mn) may exist. For this reason, ^{31}P CPMAS spectra of purple membranes were acquired at decreasing temperatures. The spectra acquired at 243K for a sample prepared from distilled water (Fig 6.8 top) shows how the anisotropy of the ^{31}P increases as the membrane becomes frozen such that the full anisotropy of the ^{31}P nuclei for both phosphates is revealed. Spectra acquired below 243K show no further increase in anisotropy. The axial symmetry of the ^{31}P CSA tensor is also lost at this temperature, introducing another parameter when simulating spectra for comparison. Trapping the purple membrane in the M_{412} state also requires some salt in the sample and a pH above 7. When samples are prepared from distilled water the final pH may be as low as 5, however when prepared from a buffered solution at pH 8 the final pH is kept above 7. The presence of salt in the buffer has also been shown to be necessary for optimal trapping of M_{412} (Appendix 4) and keeps oriented samples hydrated when the samples are being transferred from a controlled atmosphere to MAS rotors. The higher pH and increased salt affect the NMR spectra acquired even at low temperature (Fig 6.20) since an electrostatic effect appears to increase the motion of the lipid headgroups such that most of the anisotropy is lost. This means that the spectra acquired for purple membrane samples trapped in Guanidine-HCl at pH 10 (Fig 6.19 bottom) are likely to owe more to this effect than a specific interaction with the protein. Samples prepared from pH 8 buffer also demonstrate this electrostatic effect yet it is possible to increase sideband intensities slightly by further freezing (Fig 6.21). Under these conditions then it is possible that the technique remains sensitive to motions in the lipid headgroups.

^{31}P CP MAS has been used as a tool for determining structural constraints in the binding of tetraphenylphosphonium to EmrE, a membrane bound multidrug transport protein of *E. coli* (Glaubitz *et al*, 2000[a]). In this chapter the ability of ^{31}P to be used as a structural tool was limited by the nature of the molecule that was studied. The major phospholipid of the purple membrane, PGP-Me, was shown to be tightly associated with the protein component of the purple membrane and the spectra obtained were characterised by broad lines and poor resolution. When attempting to study the response of the lipid headgroups to induced protein conformational changes in bacteriorhodopsin the conditions required for effective trapping of the sample in photointermediates, increased pH and salt concentration, caused the loss of much of the ^{31}P chemical shift anisotropy in frozen samples without improving resolution. In this case the sensitivity of the ^{31}P probe to the motion and environment of the lipid prevented its use as a structural tool to the same extent as the nuclei used in the previous chapters. However the sensitivity of the nucleus to its environment was reflected in the static oriented experiment and showed some indication of an increased mobility of the lipids in response to the protein conformational change induced in the bR_{568} to M_{412} transition. This result indicates promise in the technique and a more detailed investigation may reveal greater insights into the relationship between bacteriorhodopsin and its associated lipids and how affects the protein function. By studying the lipid component of membrane in addition to the protein a more complete understanding of the functioning of the system can be obtained.

7. Future Perspective

7.1 Benefits of solid-state NMR

When trying to answer a relatively simple structural question, solid-state NMR can be perceived as being a valuable tool for the structural biologist. It is capable of revealing accurate and specific information about a site of interest and does not depend on many other sources of information to get its answer. When single methyl groups containing deuterium are introduced to bacteriorhodopsin an accurate angle measurement for the C-CD_3 bond vector can be made. The value as determined in the MAOSS technique described in this thesis, when compared with angles now measured from crystal structures and previous values from static samples, is in good agreement. The MAOSS method improves the sensitivity of the solid-state NMR approach such that we were able to use between a third and a quarter of the amount of sample necessary for a static experiment. The development of this technique has lead to its application to rhodopsin. The structure of the retinal in rhodopsin in both ground and light activated states was determined using a combination of static and MAOSS methods (Gröbner *et al*, 2000). This structure of the retinal in rhodopsin represented the first high resolution structural model of the key retinal co-factor and was produced without the need for expression or crystallisation of the protein.

One of the major problems affecting solid-state NMR is the production of suitable amounts of labelled sample, the MAOSS approach helps to reduce the amount of sample required for a given experiment and may mean that more experiments on membrane

proteins become viable. Despite its low natural abundance, deuterium is relatively rarely used when compared with other biological NMR nuclei, mainly due to its low sensitivity. MAOSS will allow more experiments to be contemplated using deuterium as a probe.

The experiments in this thesis were designed to probe the limits of solid-state NMR in determining structural constraints for biological membranes. Two approaches to studying multiple labels are pursued, one using distance measurements between specifically ^{13}C labelled sites, the other identifying anisotropic information from multiply labelled ^{15}N residues. An approach has been developed that is able to reduce some of the limitations commonly found in solid-state NMR of membrane proteins. The SIMQEX approach is able to measure accurate internuclear distances between nuclei whose resonances may not be greatly separated in the NMR spectrum and is also able to do this on relatively small samples in a short amount of time. Distance measurements are able to add fine detail to structural problems that have already been solved to some extent by other means. In this last respect the approach is significantly limited by relying on other sources of information before an experiment can be designed. Progress is being made in coupling such distance measurement techniques with orientational restraints to yield greater detail from the NMR experiment (Glaubitz *et al*, 2001). Happily one of the lessons that was learnt from this ^{13}C study was that, using CP methods and reasonable MAS rates some high quality spectra could be obtained. Also the specifically labelled retinal could be resolved and the relative decay of the longitudinal magnetisation could be followed when experiencing couplings with its neighbours in space. The same, however, could not be said about the ^{13}C labelled amino acids and any approach that

hoped to observe changes in their resonances would need further development to improve resolution amongst resonances of the same residue type.

7.2 Problems and solutions in NMR of multiply labelled membrane proteins

The deuterium MAOSS approach, as discussed, above gives an accurate answer when determining the orientation of one group with respect to the membrane. NMR though is capable of answering much more taxing and complex questions as had been shown time and again in solution NMR and in some outstanding examples of solid-state NMR. What happens if we want to know about the structure of a whole protein, peptide or even part of a protein? There is rather a lot of debate within the field of structural biology and outside as well as to whether solid-state NMR can perform this task. Some notable successes have been achieved, particularly in the case of gramicidin (Ketchem *et al*, 1996), however much progress is required before whole structure determination is an everyday reality. One promising approach, PISEMA, uses the high resolution of the ^{1}H-^{15}N dipolar coupling and the ^{15}N chemical shift to separate resonances from multiply labelled samples. The oriented proteins reveal the orientations of their amide bonds in the PISEMA spectrum and their structure can then be modelled. Uniformly labelled peptides as large as twenty-five residues have been studied in this way (Opella *et al*, 1999). The size limit for proteins used in these experiments is dependent on a number of factors. Firstly, and most obviously the more resonances involved then the more overlap is likely in the 2D PISEMA spectrum. Secondly the larger a protein is then the more difficult it

becomes to get well oriented samples. The resolution in the static PISEMA case is heavily dependent on the spectral linewidths that reflect the quality of orientation. This also means that even for a large protein that has reduced or specific labelling the quality of the data will still suffer from poor linewidths and hence accuracy. The approach used in this thesis to determine multiple angle constraints from ^{15}N labelled proteins looks to solve this problem. Initially it was proposed that ^{15}N amides, with their large chemical shift dispersion, would be resolved under relatively slow spinning MAS conditions. Such an approach was very similar to the deuterium MAOSS technique; only the number of labels and the vectors being measured had changed. The approach was hindered by the low sensitivity of the ^{15}N nucleus despite application of CPMAS and resolution that was not high enough for a clear observation of all the labels. The development of the approach here, using faster MAS frequencies and ideally higher magnetic fields allows high-resolution spectra to be acquired with shorter experiment times, due to some increase in sensitivity concomitant with improved resolution, yet still allowing anisotropic information to be obtained.

The MAS experiment also has the advantage that the isotropic chemical shift is revealed. Although the assignment of resonances was aided by the high sensitivity of CPMAS when applied to mutant proteins there is no intrinsic assignment possible in this ^{15}N case as discussed but resolution of isotropic chemical shifts may be very useful for assignment in the case of an analogous ^{13}C experiment particularly when looking at side-chain orientations. Coupled with the increased sensitivity of the ^{13}C nucleus, the oriented REPT-MAS method may become a particularly powerful tool. In summary, the MAOSS experiments performed in this thesis show that currently available labelling techniques,

when applied to membrane proteins can lead to the identification of direct structural information. The potential of the MAOSS approach has been demonstrated and shows considerable promise when allied with recent developments in recoupling techniques and magnet technology.

REFERENCES

Aharoni, A., Weiner, L., Ottolenghi, M. & Sheves, M. (2000) Bacteriorhodopsin Experiences Light Induced Conformational Alterations in Nonisomerizable C_{13}=C_{14} Pigments. *J. Biol. Chem.* **275** (28), 21010-21016

Andrew, E.R. (1996) Magic Angle Spinning. *Encyclopaedia of Nuclear Magnetic Resonance*, 2891-2900. Wiley

Andrew, E. R., Bradbury, A., & Eades, R.G. (1958) NMR spectra from crystals rotated at high speed. *Nature* **182**, 1659

Appleyard, A.N., Herbert, R.B., Henderson, P.J.F., Watts, A. and Spooner, P.J.R. (2000) Selective NMR observation of inhibitor and sugar binding to the galactose-H+ symport protein GalP. *BBA* **1509**, 55-64

Arora, A., Abildgaard, F., Bushweller, J.H. & Tamm, L.K. (2001) Structure of Outer Membrane Protein A Transmembrane Domain by NMR Spectroscopy. *Nature Struct. Biol.* **8**(4), 334-338

Assfalg, M., Banci, L., Bertini, I., Bruschi, M. & Turano, P. (1998) 800 MHz 1H NMR solution structure refinement of oxidized cytochrome c7 from Desulfuromonas acetoxidans. *Eur. J. Biochem*. **256** (2) 261-270

Balashov, S.P (2000) Protonation Reactions and their Coupling in Bacteriorhodopsin. *BBA* **1460**, 75-94

Bechinger, B. (2000) Biophysical Investigations of Membrane Perturbations by Polypeptides using Solid-State NMR Spectroscopy. *Mol. Membr. Biol.* **17**, 135-142

Bechinger, B., Skladnev, D.A., Ogrel, A., Li, X., Rogozhkina, E.V., Ovchinnikova, T.V., O'Neil, J.D.J. & Raap, J. (2000) ^{15}N and ^{31}P Solid-State NMR Investigations on the Orientation of Zervamicin II and Alamethicin in Phosphatidylcholine Membranes. *Biochemistry* **40**(31), 9428-9437

van Beek, J.D., Beaulieu, L., Schäfer, H., Demura, M., Asakura, T. & Meier, B.H. (2000) Solid-state NMR Determination of the Secondary Structure of *Samia cynthia ricini* silk. *Nature* **405**, 1077-1079

Belrahi, H., Nollert, P., Royant, A., Menzel, C., Rosenbusch, J.P., Landau, E.M & Pebay-Peyroula, E. (1999) Protein, Lipid and Water Organisation in Bacteriorhodopsin Crystals: a Molecular View of the Purple Membrane at 1.9Å resolution. *Structure* **7**, 909-917

Betancourt, F.M.H. & Glaeser, R.M. (2000) Chemical and physical evidence for multiple functional steps comprising the M state of the bacteriorhodopsin photocycle. *BBA* **1460**, 106-118

Boesze-Battaglia, K. & Albert, A.D. (1990) Cholesterol Modulation of Photoreceptor Function in Bovine Retinal Rod Outer Segments. *Biol. Chem.* **265**, 20727-20730

Bonev, B.B., Chan, W.C, Bycroft, B.W., Roberts, G.C.K & Watts, A. (2000) Interaction of the Lantibiotic Nisin with Mixed Lipid Bilayers: A ^{31}P and ^{2}H NMR Study. *Biochemistry* **39**, 11425-11433

Borucki, B., Otto, H., & Heyn, M.P. (1999) Reorientation of the Retinylidene Chromophore in the K, L, and M Intermediates of Bacteriorhodopsin from Time-Resolved Linear Dichroism: Resolving Kinetically and Spectrally Overlapping Intermediates of Chromoproteins. *J. Phys. Chem. B* **103**(30), 6371-6383

Bowers, J.L. & Oldfield, E. (1988) Quantative carbon-13 Nuclear Magnetic Resonance Spectroscopic Study of Mobile Residues in Bacteriorhodopsin. *Biochemistry* **27**, 5156-5161

Brown, L.S. (2000) Reconciling Crystallography and Mutagenesis: a Synthetic Approach to the Creation of a Comprehensive Model for Proton Pumping by Bacteriorhodopsin. *BBA* **1460**, 49-59

Colmenares, L.U., Mead, D., Yoshida, W., Alam, M. & Liu, R.S.H. (1996) A ^{19}F NMR Study of Bis(trifluoromethyl)phenyl Bacteriorhodopsin Analogs. *J. Phys. Chem.* **100**(21); 9172-9174

Corcelli, A., Colella, M., Mascolo, G., Fanizzi F.P. & Kates M. (2000) A Novel Glycolipid and Phospholipid in the Purple Membrane. *Biochemistry* **28**; 39(12), 3318-26.

Creuzet, F., McDermott, A., Gebhard, R., Vanderhoef, K., Spijkerassink, M.B., Herzfeld, J., Lugtenburg, J., Levitt, M.H. & Griffin, R.G. (1991) Determination of Membrane Protein Structure by Rotational Resonance NMR- Bacteriorhodopsin. *Science* **251**(4995), 783-786, 1991

DeGrip, W.J. (1982) Purification of Bovine Rhodopsin over Concanavalin A Sepharose, *Methods Enzymol.* **81**, 197-207

DeGroot, H.J.M., Smith, S.O., Kolbert, A.C., Courtin, J.M.L., Winkel, C., Lugtenburg, J., Herzfeld, J. & Griffin, R.G. (1991) Iterative Fitting of Magic Angle Spinning NMR Spectra. *J. Magn. Reson.* 91, 30-38

Delaglio, F., Kontaxis, G. & Bax, A. (2000) Protein Structure Determination Using Molecular Fragment Replacement and NMR Dipolar Couplings. *J. Am. Chem. Soc.* **122**(9), 2142-2143

Demura, M., Minami, M., Asakura, T. & Cross, T.A (1998) Structure of *Bombyx mori* Silk Fibroin Based on Solid State NMR Orientational Constraints and Fiber Diffraction Unit Cell Parameters. *J. Am. Chem. Soc.* **129**, 1300-1308

Dencher, N.A., Dresselhaus, D., Zaccai, G. & Büldt, G (1989) Structural changes in bacteriorhodopsin during proton translocation revealed by neutron diffraction. *PNAS* **86**, 7876-7879

Dunn, R., McCoy, J., Simsek, M., Majumdat, A., Chang, S.H., Rhajbandary, U.L. & Khorana, H.G. (1981) The Bacteriorhodopsin Gene. *PNAS* **78** (11): 6744-6748 1981

Edman, K., Nollert, P., Royant, A., Belrhali, H., Pebay-Peyroula, E., Hajdu, J., Neutze, R. & Landau, E.M. (1999) High-resolution X-ray Structure of an Early Intermediate in the Bacteriorhodopsin Photocycle. *Nature* **401**, 822-826

Egorova-Zachernyuk, T.A., Hollander, J., Fraser, N., Gast, P., Hoff, A.J., Cogdell, R., de Groot, H.J.M. & Baldus, M (2001) Heteronuclear 2D Correlations in a Uniformly [^{13}C, ^{15}N] Labelled Membrane-Protein Complex at Ultra-High Magnetic Fields. *J. Biomol. NMR.* **19**, 243-253

Engelman, D. M., Goldman, A. & Staitz, T. A. (1982) The Identification of Helical Segments in the Polypeptide Chain of Bacteriorhodopsin. *Methods Enzymol.* **88**, 81-88

Essen, L.O., Siegert, R., Lehmann, W.D. & Oesterhelt, D. (1998) Lipid Patches in Membrane Protein Oligomers: Crystal Structure of the Bacteriorhodopsin Lipid Complex. *PNAS* **95**, 11673-11678

Feng, X., Verdegen, P.J.E., Lee, Y.K., Sandstrom, D., Edén, M., Bovee-Guerts, P.H.M., de Grip, W.J., Lugtenburg, J., de Groot, H.J.M., & Levitt, M.H. (1997) Direct Determination of a Molecular Torsional Angle in the Membrane Protein Rhodopsin by Solid-State NMR. *J. Am. Chem. Soc.* **119**(29); 6853-6857

Feng, X., Verdegen, P.J.E., Edén, M., Sandstrom, D., Lee, Y.K., Bovee-Guerts, P.H.M., de Grip, W.J., Lugtenburg, J., de Groot, H.J.M., & Levitt, M.H. (2000) Determination of a Molecular Torsion Angle in the Metarhodopsin-I Photointermediate of Rhodopsin by Double-Quantum Solid State NMR. *J. Biomol. NMR.* **16**, 1-8

Fernandez, C., Adeishvilli, K., Wüthrich, K. (2001) Transverse Relaxation-Optimised NMR Spectroscopy with the Outer Membrane Protein OmpX in Dihexanoyl Phosphatidylcholine micelles. *PNAS* **98**(5), 2358-2363

Fu, R & Cross, T.A. (1999) Solid State Nuclear Magnetic Resonance Investigation of Protein and Polypeptide Structure. *Annu. Rev. Biophys. Biomol. Struct.* **28**, 235-68

Fu, R., Cotton, M. & Cross, T.A. (2000) Inter- and Intramolecular Distance measurements by Solid-State MAS NMR: Determination of Gramicidin A Channel Dimer Structure in Hydrated Phospholipid Bilayers. *J. Biomol. NMR.* **16**, 261-268

Fushman, D., Tjandra, N. & Cowburn, D. (1998) Direct Measurement of ^{15}N Chemical Shift Anisotropy in Solution. *J. Am. Chem. Soc.* **120**, 10947-10952

Glaubitz, C. (2000) An introduction to MAS NMR Spectroscopy on Oriented Membrane Proteins. *Concepts in Magnetic Resonance* **12**(3), 137-151

Glaubitz, C., Carravetta, M., Edén, M. & Levitt, M.H. (2001) Toward Dipolar Recoupling in Macroscopically Ordered Samples of Membrane Proteins Rotating at the Magic Angle. *Perspectives on Solid State NMR in Biology*, 71-82, Kluwer, Dordrecht

Glaubitz, C., Gröbner, G. & Watts, A. (2000) Structural and orientational information of the membrane embedded M13 coat protein by 13 C-MAS NMR spectroscopy. *BBA* **1463**, 151-161

Glaubitz, C., Gröger, A., Gottschalk, K., Spooner, P., Watts, A. Schuldiner, S. & Kessler, H. (2000)[a] ^{31}P-CP-MAS NMR studies on TPP^{+} bound to the ion-coupled multidrug transport protein EmrE. *FEBS Letts.* **480** 127-131

Glaubitz, C., Burnett, I.J., Gröbner, G., **Mason**, **A.J.,** & Watts, A. (1999) Deuterium-MAS NMR Spectroscopy on Oriented Membrane Proteins: Applications to Photointermediates of Bacteriorhodopsin. *J. Am. Chem. Soc.* **121**, 24, 5787-5794

Glaubitz, C. & Watts, A. (1998) Magic Angle-Oriented Sample Spinning (MAOSS): A New Approach toward Biomembrane Studies. *J. Magn. Reson.* **130**, 000-012

Goetz, J.M., Poliks, B., Studelska, D.R., Fischer, M., Kugelbrey, K., Bacher, A., Cushman, M. & Schaefer, J. (1999) Investigation of the Binding of Fluorolumazines to the 1-MDa Capsid of Lumazine Synthase by 15N{19F} REDOR NMR. *J. Am. Chem. Soc.* **121**(33), 7500-7508

Grabchuk, I.A., Orekhov, V.Y., Musina, L.Y. & Arseniev, A.S (1997) ^{1}H-^{15}N Signal Assignment and the Secondary Structure of Bacteriorhodopsin (1-231) in Solution. *Russian Journal of Bioorganic Chemistry* **23**. 8, 560-572

Griffiths, J.A., El-Sayed, M.A. & Capel, M. (1996) Effect of Binding of Lanthanide Ions on the Bacteriorhodopsin Hexagonal Structure: An X-ray Study. *J. Phys. Chem.* **100**(29), 12002-12007

Griffiths, J.M., Bennett, A.E., Engelhard, M., Siebert, F., Raap, J., Lugtenburg, J., Herzfeld, J. & Griffin, R.G (2000) Structural Investigation of the Active Site in Bacteriorhodopsin: Geometric Constraints on the Roles of Asp-85 and Asp-212 in the Proton Pumping Mechanism from Solid State NMR. *Biochemistry* **39**(2), 362-371

Grigorieff, N., Ceska, T.A., Downing, K.H., Baldwin, J.M. & Henderson, R. (1996) Electron-crystallographic Refinement of the Structure of Bacteriorhodopsin. *J. Mol. Biol.* **259**, 393-421

Gröbner, G., Taylor, A., Williamson, P.T.F., Choi, G., Glaubitz, C., Watts, J., de Grip, W.J. & Watts, A. (1997) Macroscopic orientation of natural and model membranes for structural studies. *Anaytical Biochemistry* **254**, 132-136

Gröbner, G., Choi, G., Burnett, I.J., Glaubitz, C., Verdegen, P.J.E., Lugtenburg, J. & Watts, A. (1998) Photoreceptor rhodopsin: structural and conformational study of its chromophore 11-*cis* retinal in oriented membranes by deuterium solid state NMR. *FEBS Letters* **422**, 201-204

Gröbner, G., Glaubitz, C. & Watts, A. (1999) Probing membrane surfaces and the location of membrane compounds by 13C MAS NMR using Lanthanide ions. *J. Magn. Reson*. **141**(2), 336-339

Gröbner, G., Burnett, I.J., Glaubitz, C., Choi, G., **Mason, A.J**. & Watts, A. (2000) Observations of Light-Induced Structural Changes of Retinal within Rhodopsin. *Nature* **405**, 810-813

Gu, Z.T. & Opella, S.J. (1999) Two- and Three- Dimensional $^{1}H/^{13}C$ PISEMA Experiments and Their Application to Backbone and Side Chain Sites of Amino Acids and Peptides. *J. Magn. Reson.* **140**, 340-346

Hauer, J.A., Struppe, J., Taylor, S.S. & Vold, R.R. (1997) The NMR Structure of Myristoylated PKA peptides bound to bicelles. *FASEB J.* **11**(9), 1358

Harzer, U. & Bechinger, B. (2000) Alignment of Lysine-Anchored Membrane Peptides under Conditions of Hydrophobic Mismatch: A CD, 15N and 31P Solid-State NMR Spectroscopy Investigation *Biochemistry* **39**(43), 13106-13114

Hauss, T., Buldt, G., Heyn, M.P., & Dencher, N.A. (1994) Light-induced isomerization causes an increase in the chromophore tilt in the M intermediate of bacteriorhodopsin: a neutron diffraction study. *PNAS* **91**(25), 11854-11858

Heindrichs, A.S.D., Geen, H. & Titman, J.J. (2000) MAS Double-Quantum Filtered Dipolar Shift Correlation Spectroscopy. *J. Magn. Reson.* **147**, 68-77

Heise, B., Leppert, J. & Ramachandran, R. (2000) Characterisation of ^{15}N Chemical Shift tensors via ^{15}N-^{13}C REDOR and ^{15}N-^{1}H Dipolar-Shift CPMAS NMR Spectroscopy. *Solid State Nucl. Magn. Reson.* **16**(3), 177-87

Helgerson, S.L., Siemen, S.L. & Dratz, E.A. (1992) Enrichment of Bacteriorhodopsin with Isotopically Labelled Amino Acids by Biosynthetic Incorporation in *Halobacterium halobium. Can. J. Microbiol*. **38**, 1181-1185

Helmle, M., Patzelt, H., Ockenfels, A., Gärtner, W., Oesterhelt, D. & Bechinger, B. (2000) Refinement of the Geometry of the Retinal Binding Pocket in Dark-Adapted Bacteriorhodopsin by Heteronuclear Solid-State NMR Distance Measurements. *Biochemistry* **39***,* 10066-10071

Henderson, R., & Unwin, P.N.T (1975) Three-dimensional Model of Purple Membrane Obtained by Electron Microscopy. *Nature* **257**, 28-32

Henderson, R., Baldwin, J.M., Ceska, T.A., Zemlin, F., Beckmann, E. & Downing, K.H. (1990) Model for the Structure of Bacteriorhodopsin Based on High Resolution Electron Cryo-Microscopy. *J. Mol. Biol.* **213**, 899-929

Herzfeld, J. & Tounge, B. (2000) NMR Probes of Vectoriality in the Proton-Motive Photocycle of Bacteriorhodopsin: Evidence for an "Electostatic Steering" Mechanism. *BBA* **1460**, 95-105

Herzfeld, J. and Berger, A.E. (1980) Sideband Intensities in NMR Spectra of Samples Spinning at the Magic Angle. *J. Chem. Phys.* **73**, 6021-6040

Heyn, M.P., Borucki, B. & Otto, H. (2000) Chromophore Reorientation During the Photocycle of Bacteriorhodopsin: Experimental Methods and Functional Significance. *BBA* **1460**, 60-74

Hohwy, M., Jakobsen, H.J., Edén, M., Levitt, M.H. & Nielsen, N.C. (1998) Broadband Dipolar Recoupling in the Nuclear Magnetic Resonance of Rotating Solids: A Compensated C7 Pulse Sequence. *J. Chem. Phys.* **108**, 2686-2694

Hong, M (2000) Solid-State NMR Determination of $^{13}C\alpha$ Chemical Shift Anisotropies for the Identification of Protein Secondary Structure. *J. Am. Chem. Soc.* **122**, 3762-3770

Hong, M., Gross, J.D., Hu, W. & Griffin, R.G. (1998) Determination of the Peptide Torsion Angle ϕ by ^{15}N Chemical Shift and $^{13}C^{\alpha}$-$^{1}H^{\alpha}$ Dipolar Tensor Correlation in Solid-State MAS NMR. *J. Magn. Reson.* **135**, 169-177

Hu, J.G., Sun, B.Q., Petkova, A.T., Griffin, R.G. & Herzfeld, J. (1997) The Predischarge Chromophore in Bacteriorhodopsin: A ^{15}N Solid-State NMR Study of the L Photointermediate. *Biochemistry* **36**, 9316-9322

Hu, J.G., Sun, B.Q., Bizounouk, M., Hatcher, M.E., Lansing, J.C., Raap, J., Verdegem, P.J.E., Lugtenburg, J., Griffin, R.G. & Herzfeld, J. (1998) Early and Late M Intermediates in the bacteriorhodopsin Photocycle: A Solid-State NMR Study. *Biochemistry* **37**, 8088-8096

Hudson, B.S. & Birge, R.R. (1999) Angular Orientation of the Retinyl Chromophore of Bacteriorhodopsin: Reconciliation of ^{2}H NMR and Optical Measurements. *J. Phys. Chem. A* **103**, 2274-2281

Ishii, Y. & Tycko, R. (2000) Mutidimensional Heteronuclear Correlation Spectroscopy of a Uniformly ^{15}N- and ^{13}C-Labelled Peptide Crystal: Toward Spectral Resolution, Assignment, and Structure Determination of Oriented Molecules in Solid-State NMR. *J. Am. Chem. Soc.* **122**, 1443-1455

Joshi, M.K., Dracheva, S., Mukhopadhyay, A.K., Bose, S. & Hendler, R.W. (1998) Importance of Specific Lipids in Controlling the Photocycle of Bacteriorhodopsin. *Biochemistry* **37**, 14463-14470

Jost, P.C & Griffith, O.H. (1982) *Lipid-Protein Interactions*. Wiley Interscience

Kataoka, M. & Kamikubo, H. (2000) Structures of Photointermediates and their Implications for the Proton Pump Mechanism. *BBA* **1460**, 166-176

Kates, M. (1988) Structure, Physical Properties, and Function of Archaebacterial Lipids. *Prog. Clin. Biol. Res.* **282**, 357-84

Kates, M., Kushwaha, S.C. & Sprott, G.D. (1982) Lipids of the PM from Extreme Halophiles and Methanogenic Bacteria. *Methods Enzymol*. **88**, 98-105

Kaulen, A.D (2000) Electrogenic processes and Protein Conformational Changes Accompanying the Bacteriorhodopsin Photocycle. *BBA* **1460**, 204-219

Kawase, Y., Tanio, M., Kira, A., Yamaguchi, S., Tuzi, S., Naito, A., Kataoka, M., Lanyi, J.K., Needleman, R. & Saito, H. (2000) Alteration of Conformation and Dynamics of Bacteriorhodopsin Induced by Protonation of Asp 85 and Deprotonation of Schiff Base as Studied by ^{13}C NMR. *Biochemistry* **39***,* 14472-14480

Kelly, M.J.S., Ball, L.J., Krieger, C., Yu, Y., Fischer, M., Schiffmann, S., Schmieder, P., Kühne, R., Bermel, W., Bacher, A., Richter, G. & Oschkinat, H. (2001) The NMR Structure of the 47kDa Dimeric Enzyme 3,4Dihydroxy-2-Butanone-4-Phosphate Synthase and Ligand Binding Studies Reveal the Location of the Active Site. *PNAS* **98** (23), 13025-13030

Ketchem, R.R., Lee, K.C., Huo, S. & Cross, T,A (1996) Macromolecular structural elucidation with solid-state NMR-derived orientational constraints. *Journal of Biomolecular NMR* **8** (1), 1-14

Khorana, H.G., Gerber, G.E, Herlihy, W.C., Gray, C.P., Anderegg, R.J., Nihei, K., & Biemann, K. (1979) Amino acid sequence of bacteriorhodopsin. *PNAS* **76**(10): 5046-5050

Khorana, H.G. (1988) Bacteriorhodopsin, a Membrane Protein that uses Light to Translocate Protons. *J. Biol. Chem*. **263**, (16) 7439-7442

Khorana, H.G. (1993) Two Light-inducing Membrane proteins: bacteriorhodopsin and the mammalian Rhodopsin. *PNAS* **90**, 1166-1171

Kim, Y., Valantine, K., Opella, S.J., Schendel, S.L. & Cramer, W.A. (1998) Solid-State NMR Studies of the Membrane-Bound Closed State of the Colicin E1 Channel Domain in Lipid Bilayers. *Protein Sci* **7**, 342-348

Kimura, Y., Vassyiyev, D.G., Miyazawa, A., Kidera, A., Matsushima, M., Mitsuoka, K., Murata, K., Terushisa, H. & Fujiyoshi, Y. (1997)[a] High Resolution Structure of Bacteriorhodopsin Determined by Electron Crystallography. *Photochemistry and Photobiology* **66**(6), 764-767

Kimura, Y., Vassyiyev, D.G., Miyazawa, A., Kidera, A., Matsushima, M., Mitsuoka, K., Murata, K., Terushisa, H. & Fujiyoshi, Y. (1997)[b] Surface of Bacteriorhodopsin Revealed by High Resolution Electron Crystallography. *Nature* **389**, 206-211

Knowles, P.F., Watts, A. and Marsh, D. (1979) Spin-label studies of lipid immobilization in DMPC-substituted cytochrome oxidase. *Biochemistry* **18**, 4480-4487

Kobayashi, T., Saito, T. & Ohtani, H. (2001) Real-time Spectroscopy of Transitions States in Bacteriorhodopsin during Retinal Isomerisation. *Nature* **414**, 531-534

Koenig, B.W., Mitchell, D.C., König, S., Grzesiek, S., Litman, B.J. & Bax, A. (2000) Measurement of Dipolar Couplings in a Transducin Peptide Fragment Weakly Bound to Oriented Photo-activated Rhodopsin. *J. Biomol. NMR.* **16**, 121-125

Kolbe, M., Besir, H., Essen, L.-O. & Oesterhelt, D. (2000) Structure of Light-Driven Chloride Pump Halorhodopsin at 1.8 A Resolution. *Science* **288**, 1390

Kovari, L.C., Momany, C. & Rossman, M.C. (1995). The Use of Antibody Fragments for Crystallisation and Structure Determinations. *Structure* **3**, 521-525

Koyama, K. (1997) Direct Measurements for Isomer Ratio of Retinal in Bacteriorhodopsin by an Electrochemical Method. *Photochemistry and Photobiology* **66** (6), 784-787

Krebs, A., Villa, C., Edwards, P.C. & Schertler, G.F.X. (1998) Characterisation of an Improved Two-dimensional p22121 Crystal from Bovine Rhodopsin. *J. Mol. Biol.* **282**, 991-1003

Kühlbrant, W. (2000) Bacteriorhodopsin – the movie. *Nature* **406**, 569-570

Kusumi, A., Sakaki, T., Yoshizawa, T. & Ohnishi, S. (1980) Protein-Lipid Interaction in Rhodopsin Recombinant Menbranes as Studied by Protein Rotational Mobility and Lipid Alkyl Chain Flexibility Measurements. *J. Biochem.* **88**, 1103-1111

Landau, E.M. & Rosenbusch, J.P. (1996) Lipidic Cubic Phases: A Novel Concept for the Crystallisation of Membrane Proteins. *PNAS* **93**, 14532-14535

Lanyi, J.K. (1999) Progress Toward an Expicit Mechanistic Model for the Light-Driven Pump, Bacteriorhodopsin. *FEBS Letters* **464**, 103-107

Lanyi, J.K (2000) Bacteriorhodopsin. *BBA* **1460**, 1-3

Lee, Y.K., Kurur, N.D., Helmle, M., Johannessen, O.G., Nielsen, N.C, & Levitt, M.H. (1995) Efficient Dipolar Recoupling in the NMR of Rotating Solids. A Sevenfold Symmetric Radiofrequency Pulse Sequence.*Chem. Phys. Lett.* **242**, 304-309

Levitt, M.H., Raleigh, D.P., Creuzet, F. & Griffin, R.G. (1990) Theory and Simulations of Homonuclear Spin Pair Systems in Rotating Solids. *J. Chem. Phys.* **92**(11), 6347-6364

Long, H.W. & Tycko, R. (1998) Biopolymer Conformational Distributions from Solid-State NMR: α-Helix and 3_{10}-Helix Contents of a Helical Peptide. *J. Am. Chem. Soc.* **120**, 7039-7048

Lowe, I.J. (1959) Free Induction Decays in Rotating Solids. *Phys. Rev. Lett.* **2**, 285

Luecke, H., Schobert, B., Cartailler, J-P., Richter, H-T, Rosengarth, A., Needleman, R. & Lanyi, J.K. (2000) Coupling Photoisomerisation of Retinal to Directional Transport in Bacteriorhodopsin. *J. Mol. Biol.* **300**(5), 1237-1255

Luecke, H., Schobert, B., Richter, H-T., Cartailler, J-P. & Lanyi J.K (1999)[a] Structure of Bacteriorhodopsin at 1.55 Angstrom Resolution. *J. Mol. Biol*. **291**(4), 899-911

Luecke, H., Schobert, B., Richter, H-T., Cartailler, J.P. & Lanyi, J.K (1999)[b] Structural Changes in Bacteriorhodopsin During Ion Transport, at 2 Angstrom Resolution. *Science* **286**, 255-260

Luecke, H., Richter, H-T. & Lanyi, J.T. (1998) Proton Transfer Pathways in Bacteriorhodopsin at 2.3 Angstrom Resolution. *Science* **280**, 1934-1937

Luecke, H. (2000) Atomic Resolution Structures of Bacteriorhodopsin Photocycle Intermediates: the Role of Discrete Water Molecules in the Function of this Light-Driven Ion Pump. *BBA* **1460**, 133-156

Maricq, M.M. & Waugh, J.S. (1979) NMR in Rotating Solids. *J. Chem. Phys.* **70**, 3300-3316

Marsh, D., Watts, A. & Knowles, P.F. (1976) Evidence for Phase Boundary Lipid. Permeability of Tempocholine into Dimyrostoyl-Phosphatidylcholine Vesicles at the Phase Transition, *Biochemistry* **15**, 3570-3578

Marshall, G.R., Ragno, R., Makara, G.M., Arimoto, R. & Kisselev, O. (2001) Bound Conformations for Ligands for G-Protein Coupled Receptors. *Letters in Peptide Science* **6**(5-6), 283-288

Matthews, C.K. & van Holde, K.E, (1990) *Biochemistry. 1st ed.* Benjamin/Cummings Publishing Company Inc.

Mehta, A.K., Hirsh, D.J., Oyler, N., Drobny, G.P. & Schaefer, J. (2000) Carbon-Proton Dipolar Decoupling in REDOR. *J. Magn. Reson.* **145,** 156–158

Middleton, D.A., Robins, R., Feng, X., Levitt, M.H., Spiers, I.D., Schwalbe, C., Reid, D.G. & Watts, A. (1997) The conformation of an inhibitor bound to gastric proton pump. *FEBS Letts*. **410**, 269-274

Middleton, D.A., Ahmed, Z., Glaubitz, C. & Watts, A. (2000) REDOR NMR on a Hydrophobic Peptide in Oriented Membranes. *J.Magn. Reson.* **147**, 366-370

Mitchell, D.C., Straume, M., Miller, J.L. & Litman, B.J. (1990) Modulation of Metarhodopsin Formation by Cholesterol-Induced Ordering of Bilayer Lipids. *Biochemistry* **29**, 9143-9149

Mitsuoka, K., Hirai, T., Murata, K., Miyazawa, A., Kidera, A., Kimura, Y. & Fujiyoshi, Y. (1999) The Structure of Bacteriorhodopsin at 3.0 A Resolution Based on Electron Crystallography: Implication of the Charge Distribution. *J. Mol. Biol.* **286**, 861-882

Miyazawa, A., Fujiyoshi, Y., Stowell, M. & Unwin, N. (1999) Nicotinic Acetylcholine Receptor at 4.6Å Resolution: Transverse Tunnels in the Channel Wall. *J. Mol. Biol*. **288**, 765-786

Moltke, S., Nevzorov, A.A., Sakai, N., Wallat, I., Job, C., Nakanishi, K., Heyn, M.P. & Brown, M.F. (1998) Chromophore Orientation in Bacteriorhodopsin Determined from the Angular Dependence of Deuterium Nuclear Magnetic Resonance Spectra of Oriented Purple Membranes. *Biochemistry* **37**(34), 11821-11835

Moltke, S., Wallat, I., Sakai, N., Nakanishi, K., Brown, M.F., & Heyn, M.P. (1999) The Angles between the C1-, C5-, and C9-Methyl Bonds of the Retinylidene Chromophore and the Membrane Normal Increase in the M Intermediate of Bacteriorhodopsin: Direct Determination with Solid-State ^{2}H NMR. *Biochemistry* **38**(36), 11762-11772

Mukohata, Y. (1994) Comparative studies on ion pumps of the bacterial rhodopsin family. *Biophysical Chemistry* **50**, 191-201

Nielsen, N.C., Bildsøe, H., Jakobsen, H.J. & Levitt, M.H. (1994) Double-Quantum Homonuclear Rotary Resonance: Efficient Dipolar Recovery in Magic-Angle Spinning Nuclear Magnetic Resonance. *J. Chem.Phys.* **101**, 1805-1812

Oesterhelt, D. (1982) Reconstitution of the retinal Proteins Bacteriorhodopsin and Halorhodopsin. *Methods Enzymol.* **88**, 11-17

Oesterhelt, D. & Stoeckenius, W. (1974) Isolation of the Cell Membrane of *Halobacterium halobium* and its Fractionation into Red and Purple Membranes. *Methods Enzymol.* **31**, 667-678

Ogawa, H., Stokes, D.L., Sasabe, H & Toyoshima, C. (1998) Structure of the Ca^{2+} pump of sarcoplasmic reticulum: A view along the lipid bilayer at 9-A resolution. *Biophys. J.* **75** (1) 41-52

Oka, T., Kamikubo, H., Tokunaga, F., Lanyi, J.K., Needleman, R. & Kataoka, M. (1999) Conformational Change of Helix G in the Bacteriorhodopsin Photocycle: Investigation with Heavy Atom Labelling and X-ray Diffraction. *Biophysical J.* **76**, 1018-1023

Opella, S.J. (1997) NMR and Membrane Proteins. *Nature. Struct. Biol.* **4**, 845-848

Opella, S.J., Marassi, F.M., Gesell, J.J., Valente, A.P., Kim, K., Oblatt-Montal, M. & Montal, M. (1999) Structures of the M2 channel-lining segments from nicotinic acetylcholine and NMDA receptors by NMR spectroscopy. *Nature Struct. Biol.* **6** (4), 374-379

Orekhov, V.Y., Abdulaeva, C.V., Musina, L.Y. & Arseniev, A.S. (1992) ^{1}H-^{15}N-NMR Studies of Bacteriorhodopsin *Halobacterium halobium*: Conformational Dynamics of the four-helical bundle. *Eur. J. Biochem.* **210**, 223-229

Ottiger, M. & Bax, A. (1999). Bicelle-Based Liquid Crystals for NMR-Measurement of Dipolar Couplings at Acidic and Basic pH Values. *J. Biomol. NMR.* **13**, 187-191

Ovchinnikov, Y.A., Abdulaey, N.G., Feigina, M.Y., Kiselev, A.V. & Lobanov, N.A. (1977) Recent findings in the structure-functional characteristics of bacteriorhodopsin. *FEBS Lett*. **84**, 1-4

Palczewski, K., Kumasaka, T., Hori, T., Behnke, C.A., Motoshima, H., Fox, B.A., Le Trong, I., Teller, D.C., Okada, T., Stenkamp, R.E., Yamamoto, M. & Miyano, M. (2000) Crystal Structure of Rhodopsin: A G Protein-Coupled Receptor. *Science* 289, 739-745

Pauli, J., van Rossum, B., Förster, H., de Groot, H.J.M. & Oschkinat, H. (2000) Sample Optimisation and Identification of Signal patterns of Amino Acid Side Chains in 2D RFDR Spectra of the α-Spectrin SH3 Domain. *J. Magn. Reson.* **143**, 411-416

Pauli, J., Baldus, M., van Rossum, B., de Groot, H. & Oschkinat, H. (2001) Backbone and Side-Chain ^{13}C and ^{15}N Signal Assignments of the α-Spectrin SH3 Domain by Magic Angle Spinning Solid-State NMR at 17.6 Tesla. *Chembiochem* **2**, 272-281

Pebay-Peyroula, E., Rummel, G., Rosenbusch, J.P. & Landau, E.M. (1997) X-ray Structure of Bacteriorhodopsin at 2.5 Angstroms from Microcrystals Grown in Lipidic Cubic Phases. *Science* **277**, 1676-1681

Pebay-Peyroula, E., Neutze, R. & Landau, E.M. (2000) Lipidic Cubic Phase Crystallisation of Bacteriorhodopsin and Cryotrapping of Intermediates: Towards resolving a Revolving Photocycle. *BBA* **1460**, 119-132

Peerson, O.B., Yoshimura, S., Hojo, H., Aimoto, S. & Smith, S.O. (1992) Rotational Resonance NMR Measurements of Internuclear Distances in an Alpha-Helical Peptide. *J. Am. Chem. Soc.* **114**(11), 4332-4335

Pervushin, K., Riek, R., Wider, G. & Wüthrich, K. (1997) Attenuated T_2 Relaxarion by Mutual Cancellation of Dipole-Dipole Coupling and Chemical Shift Anisotropy Indicates an Avenue to NMR Structures of Very Large Biological Macromolecules in Solution. *PNAS* **94**, 12366-12371

Petkova, A.T., Hu, J.G., Bizounok, M., Simpson, M., Griffin, R.G., & Herzfeld, J. (1999) Arginine Activity in the Proton-Motive Photocycle of Bacteriorhodopsin: Solid-State NMR Studies of the Wild-Type and D85N Proteins. *Biochemistry* **38**(5), 1562-1572

Pinheiro, T.J.T. & Watts, A. (1994) Resolution of individual lipids in mixed phospholipid membranes and specific lipid-cytochrome c interactions by magic angle spinning solid-state phosphorus-31 NMR. *Biochemistry* **33**, 2459-2467

Prestegard, J.H. (1998) New Techniques in Structural NMR- Anisotropic Interactions *Nature Struct. Biol.* **5**, 517-522

Prosser, R.S., Bryant, H., Bryant, R.G. & Vold, R.R. (1999) Lanthanide Chelates as Bilayer Alignment Tools in NMR Studies of Membrane-Associated Peptides. *J. Magn. Reson.* **141**(2) 256-260

Radionov, A.N. & Kaulen, A.D (1999) Two Forms of N Intermediate (N-open and N-closed) in the Bacteriorhodopsin Photocycle. *FEBS Letters* **451**, 147-151

Rothschild, K.J., Yi-Wu, H., Gray, D., Roepe, P.D., Pelletier, S.L., Brown, R.S. & Herzfeld, J. (1989) Fourier Transform Infrared Evidence for Proline Structural Changes During the Bacteriorhodopsin Photocycle. *PNAS* **86**, 9832-9835

Royant, A., Edman, K., Ursby, T., Pebay-Peyroula, E., Landau, E.M & Neutze, R. (2000) Helix Deformation is Coupled to Vectorial Transport in the Photocycle of Bacteriorhodopsin. *Nature* **406**, 645-648

Saalwächter, K., Graf, R. & Spiess, H.W. (1999) Recoupled Polarization Transfer Heteronuclear ^{1}H–^{13}C Multiple-Quantum Correlation in Solids under Ultra-fast MAS *J. Magn. Reson.* **140**, 471-476

Saalwächter, K., Graf, R. & Spiess, H.W. (2001) Recoupled Polarization-Transfer Methods for Solid-State $^{1}H–^{13}C$ Heteronuclear Correlation in the Limit of Fast MAS. *J. Magn. Reson.* **148**, 398-418

Sabra, M.C., Uitdehaag, J.C.M. & Watts, A. (1998) General Model for Lipid-Mediated Two-Dimensional Array Formation of Membrane Proteins: Application to Bacteriorhodopsin. *Biophys. J.* **75**, 1180-1188

Saito, H. (1986) Conformation-Dependent ^{13}C Chemical Shifts: A New means of Conformational Characterisation as Obtained by High-Resolution Solid-State ^{13}C NMR. *Magnetic Resonance in Chemistry* **24**, 835-852

Saito, H., Tuzi, S., Yamaguchi, S., Tanio, M. & Naito, A. (2000) Conformation and Backbone Dynamics of Bacteriorhodopsin Revealed by ^{13}C-NMR. *BBA* **1460**, 39-48

Sasaki, J & Spudich, J.L. (2000) Proton Transport by Sensory Rhodopsins and its Modulation by Transducer-Binding. *BBA* **1460**, 230-239

Sass, H.J., Schachowa, I.W., Rapp, G., Koch, M.H.J., Oesterhelt, D., Dencher, N.A & Büldt, G. (1997) The Tertiary Structural Changes in Bacteriorhodopsin Occur Between M States: X-Ray Diffraction and Fourier Transform Infrared Spectroscopy. *EMBO. J.* **16**, 1484-1491

Sass, H.J., Büldt, G., Gessenisch, R., Hehn, D., Neff, D., Schlesinger, R., Berendzen, J. & Ormos, P. (2000) Structural Alterations for Proton Translocation in the M State of Wild-Type Bacteriorhodopsin. *Nature* **406**, 649-653

Sato, H., Takeda, K., Tani, K., Hino, T., Okada, T., Nakasako, M., Kamiya, N. & Kouyama, T. (1999) Specific lipid-protein interactions in a novel honeycomb lattice structure of bacteriorhodopsin. *Acta Crystallographica D* **55,** 1251-1256

Schertler, G.F.X., Villa, C. & Henderson, R. (1993) Projection Structure of Rhodopsin. *Nature* **362**, 770-772

Schertler, G.F.X (1998) Structure of rhodopsin. *Eye* **12** (3B) 504-510

Schnell, I. & Watts, A. (2001) Towards Selective Recoupling and Mutual Decoupling of Dipolar-Coupled Spin Pairs in Double-Quantum Magic-Angle Spinning NMR Experiments on Multiply Labelled Solid-State Samples. *Chem .Phys. Lett.* **335**, 111-122

Seiff, F., Westerhausen, J., Wallat, I., & Heyn, M.P. (1985) A neutron diffraction study on the location of the polyene chain of retinal in bacteriorhodopsin. *PNAS* **82**, 3227-3231

Seiff, F., Westerhausen, J., Wallat, I., & Heyn, M.P. (1986) Location of the Cyclohexene Ring of the Chromophore of Bacteriorhodopsin by Neutron Diffraction with Selectively Deuterated Retinal. *PNAS* **83**, 7746-7750

Seigneuret, M., Neumann, J-M., Levy, D. & Rigaud, J-L. (1991) High-Resolution ^{13}C NMR Study of the Topography and Dynamics of Methionine Residues in detergent Solubilised Bacteriorhodopsin. *Biochemistry* **30**, 3885-3892

Shon, K-J., Kim, Y., Colnago, L.A. & Opella, S.J. (1991) NMR Studies of the Structure and Dynamics of Membrane-Bound Bacteriophage Pf1 Coat Protein. *Science* **252**, 1303-8

Singer, S.J. & Nicolson, G.L. (1972) The Fluid Mosaic Model of the Structure of Cell Membranes. *Science* **175**, 720-731

Smith, S.O., de Groot, H.J.M., Gebhard, R., Courtin, J.M.L., Lugtenburg, J., Herzfeld, J. & Griffin, R.G. (1989) Structure and Protein Environment of the Retinal Chromophore in Light- and Dark-Adapted Bacteriorhodopsin Studied by Solid-State NMR. *Biochemistry* **28**, 8897-8904

Song, Q., Harms, G. S. & Johnson, C. K. (1996) Chromophore Reorientation Relative to the Membrane Plane Detected by Time-Resolved Linear Dichroism during the Bacteriorhodopsin Photocycle in Oriented Purple Membrane. *J. Phys. Chem.* **100**(38), 15605-15613

Spooner, P.J.R., Veenhoff, L., Watts, A**.** & Poolman, B. (1999) Structural information on a membrane transport protein from NMR using sequence-selective nitroxide labelling. *Biochemistry* **38**, 9634-9639

Stoeckenius, W., Lozier, R.H. & Bogomolni, R.A. (1979) Bacteriorhodopsin and the Purple Membrane of Halobacteria. *Biochim. Biophys. Acta* **505**, 215-278

Stokes, D.L. & Green, N.M. (1990) Structure of CaATPase: Electron Microscopy of Frozen-hydrated Crystals at 6 Å Resolution in Projection. *J. Mol. Biol.* **213**, 529-538

Struppe, J. & Vold, R.R. (1998). Dilute Bicellar Solutions for Structural NMR Work. *J. Magn. Reson.* **135**(2), 541-546

Subramaniam, S. & Henderson, R. (2000) Molecular Mechanism of Vectorial Proton Translocation by Bacteriorhodopsin. *Nature* **406**, 653-657

Subramaniam, S & Henderson, R. (2000)[a] Crystallographic Analysis of Protein Conformational Changes in the Bacteriorhodopsin Photocycle. *BBA* **1460** 157-165

Subramaniam, S., Lindahl, M., Bullough, P., Faruqi, A.R., Tittor, J., Oesterhelt, D., Brown, L., Lanyi, J. & Henderson, R. (1999) Protein Conformational Changes in the Bacteriorhodopsin Photocycle. *J. Mol. Biol.* **287**, 145-161

Sun, B.-Q., Costa, P.R., Kosicko, D., Lansbury, Jr, P.T. & Griffin, R.G. (1995) Internuclear Distance measurements in Solid State Nuclear magnetic Resonance: Dipolar Recoupling via Rotor Synchronised Spin Locking. *J. Chem. Phys.* **102**, 702-707

Taki, T., Yamashita, S., Satoh, M., Shibata, A., Yamashita, T., Tabeta, R. & Saito, H. (1981) ^{13}C Chemical Shifts of Solid Polypeptides by Cross Polarization/Magic Angle Spinning (CP/MAS) NMR Spectroscopy: Conformation-Dependent ^{13}C Shifts Characteristic of α-Helix and β-Sheet Forms. *Chem. Lett.* 1803-1806

Tanio, M., Inoue, S., Yokota, K., Seki, T., Yuzi, S., Needleman, R., Lanyi, J.K., Naito, A. & Saito, H. (1999) Long-Distance Effects of Site-Directed Mutations on Backbone Conformation in Bacteriorhodopsin from Solid-State NMR of [^{13}C] Val-Labelled Proteins. *Biophys. J.* **77**, 431-442

Teng, Q., & Cross, T.A. (1989) The *in situ* Determination of the ^{15}N Chemical-Shift Tensor Orientation in a Polypeptide. *J. Magn. Reson.* **85**, 439-447

Teng, Q., Iqbal, M. & Cross, T.A (1992) Determination of the ^{13}C Chemical Shift and ^{14}N Electric Field Gradient Tensor Orientations with respect to the Molecular Frame in a Polypeptide. *J. Am. Chem. Soc.* **114***,* 5312-5321

Thomas, D.D., Dalton, L.R. & Hyde, J.S. (1976) Rotational Diffusion Studied by Passage Saturation Transfer Electron paramagnetic Resonance. *J. Chem. Phys.* **65**:8, 3006-3021

Thompson, J.K., McDermott, A.E., Raap, J., Vanderwielen, C.M., Lugtenburg, J. Herzfeld, J., & Griffin, R.G. (1992) Rotational Resonance NMR Study of the Active Site Structure in Bacteriorhodopsin- Conformation of the Schiff Base Linkage. *Biochemistry* **31**(34), 7931-7938

Tjandra, N (1999) Establishing a Degree of Order: Obtaining High Resolution NMR Structures from Molecular Alignment. *Structure* **7**, R205-211

Tjandra, N. & Bax, A. (1997) Direct Measurement of Distances and Angles in Biomolecules by NMR in a Dilute Liquid Crystalline Medium. *Science* **278**, 1111-1114

Toyoshima, C., Sasabe, H. & Stokes, D.L. (1993) Three Dimensional Cryo Electron Microscopy of the Calcium Ion Pump in the Sarcoplasmic reticulum Membrane. *Nature* **362**, 469-471

Toyoshima, C., Nakasako, M., Nomura, H. & Ogawa, H. (2000) Crystal Structure of the calcium Pump of Sarcoplasmic Reticulum at 2.6Å Resolution. *Nature* **405**, 647-655

Turner, G.J., Miercke, L.W., Mitra, A., Stroud, R.S., Betlach, M.B., & Winter-Vann A.M. (1999) Expression, Purification, and Structural Characterization of the Bacteriorhodopsin-Aspartyl Transcarbamylase Fusion Protein. *Protein Expression and Purification* **17** (2), 324-338

Tuzi, S., Naito, A. & Saito, H. (1993) A High Resolution Solid-State ^{13}C-NMR Study on [1-^{13}C]Ala and [3-^{13}C]Ala and [1-^{13}C]Leu and Val-Labelled Bacteriorhodopsin. *Eur. J. Biochem.* **218**, 837-844

Tuzi, S., Naito, A. & Saito, H. (1996) Temperature-dependent Conformational Change of Bacteriorhodopsin as Studied by Solid State ^{13}C NMR. *Eur. J. Biochem.* **239**, 294-301

Tuzi, S., Yamaguchi, S., Naito, A., Needleman, R., Lanyi, J.K., & Saito, H. (1996)[b] Conformation and Dynamics of [3-^{13}C] Ala-Labelled Bacteriorhodopsin and Bacterioopsin, Induced by Interaction with Retinal and Its Analogs, As Studied by ^{13}C Nuclear Magnetic Resonance. *Biochemistry* **35**(23), 7520-7527

Tuzi, S., Yamaguchi, S., Tanio, M., Konishi, H., Inoue, S., Naito, A., Needleman, R., Lanyi, J.K. & Saito, H. (1999) Location of a Cation Binding Site in the Loop Between Helices F and G of Bacteriorhodopsin as Studied by ^{13}C NMR. *Biophys. J.* **76**, 1523-31

Tycko, R. & Dabbagh, G. (1990) Measurement of Dipole-Dipole Couplings in Magic Angle Spinning NMR. *Chem, Phys. Lett.* **173**, 461

Ulrich, A.S., Watts, A., Wallat, A., & Heyn, M. P. (1994) Distorted Structure of the Retinal Chromophore in Bacteriorhodopsin Resolved by ^{2}H-NMR. *Biochemistry* **33**, 5370-5375

Ulrich, A.S., Wallat, I., Heyn, M.P. & Watts, A. (1995) Re-orientation of retinal in the M-photointermediate of bacteriorhodopsin. *Nature Structural Biology* **2** (3), 190-192

Unger, V.M. & Schertler, G.F.X. (1995) Low Resolution Structure of Bovine Rhodopsin Determined by Electron Cryo-Microscopy. *Biophysical Journal* **68**, 1776-1781

Unger, V.M., Hargrave, P.A., Baldwin, J.M. & Schertler, G.F.X (1997) Arrangement of rhodopsin transmembrane alpha-helices. *Nature* **389**, (6647) 203-206

Unwin, N. (1993) Nicotinic Acetylcholine receptor at 9Å Resolution. *J. Mol. Biol.* **229**, 1101-1124

Unwin, N. (1995) Acetylcholine Receptor Imaged in the Open State. *Nature* **373**, 37-43

Varo, G. & Lanyi, J.K. (1990) Pathways of the rise and decay of the M photointermediate(s) of bacteriorhodopsin. *Biochemistry* **29**, 2241-2250

Varo, G. (2000) Analogies between Halorhodopsin and Bacteriorhodopsin. *BBA* **1460**, 220-229

Verdegem, P.J.E., Bovee-Geurts, P.H.M., de Grip, W.J., Lugtenburg, J. & de Groot, H.J. (1999) Retinylidene Ligand Structure in Bovine Rhodopsin, Metarhodopsin-I, and 10-Methylrhodopsin from Internuclear Distance Measurements Using 13 C-Labeling and 1-D Rotational Resonance MAS NMR. *Biochemistry* **38**, 11316-11324

Vold, R.R. & Prosser, R.S (1996) Magnetically Oriented Phospholipid Bilayered Micelles for Structural Studies of Polypeptides. Does the Ideal Bicelle Exist? *J. Magn. Reson. Series B* **113**(2), 267-271

Vonck, J.A. (1996) Three-Dimensional Difference Map of the N Intermediate in the Bacteriorhodopsin Photocycle: Part of the F Helix Tilts in the M to N Transition. *Biochemistry* **18**, 5870-5878

Vonck, J.A. (2000) Structure of the Bacteriorhodopsin Mutant F219L N Intermediate Revealed by Electron Crystallography. *EMBO J.* **19**, 2152-2160

Watts, A. *Protein-Lipid Interactions (New Comprehensive Biochemistry Vol 25).* Elsevier

Watts, A., Ulrich, A.S. & Middleton, D.A. (1995) Membrane Protein Structure: the Contribution and Potential of Novel Solid State NMR Approaches. *Molecular Membrane Biology* **12**, 233-246

Watts, A., Venien-Bryan, C., Sami, M., Whiteway, C.A., Boulter, J. & Sternberg, B. (1993) Lipid-Protein Interactions in Controlled Membrane Protein Array and Crystal Formation. *New Comprehensive Biochemistry* Vol. 25 "Protein-Lipid Interactions"

Watts, A., Volotovski, I.G. & Marsh, D. (1979) Rhodopsin-Lipid Associations in Bovine Rod Outer Segment membranes: Identification of Immobilised Lipid by Spin Labels. *Biochemistry* **18**, 5006-5013

Watts, A. (1995) Bacteriorhodopsin: the Mechanism of 2D Array Formation and the Structure of Retinal in the Protein. *Biophysical Chemistry* **55**, 137-151

Watts, A. (1998) Solid state NMR approaches for studying the interaction of peptides and proteins with membranes. *BBA* **1376**, 297-318

Watts, A., Burnett, I.J., Glaubitz, C.,Gröbner, G., Middleton, D.A., Spooner, P.J.R., Watts, J.A. & Williamson, P.T.F. (1999) Membrane protein structure determination by solid state NMR. *Natural Product Reports* **16**, 419-423

Weik, M., Patzelt, H., Zaccai, G. & Oesterhelt, D. (1998) Localisation of Glycolipids in Membranes by In Vivo Labelling and Neutron Diffraction. *Molecular Cell* **1**, 411-419

Whiles, J.A., Struppe, J.O., Komives, E.A. & Vold, R.R. (1998) NMR Studies of the Structure and Orientation of Mastoporan X in Bicelles. *Biophys. J.* **74**(2), 302

Williamson, P.T.F., Gröbner, G., Spooner, P.J.R., Miller, K.W. & Watts, A. (1998) Probing the agonist binding pocket on the nicotinic acetylcholine receptor: a high resolution solid state NMR approach. *Biochemistry* **37**, 10854-10859.

Williamson, P.T.F., Watts, J.A., Addona, G.H., Miller, K.W. & Watts, A. (2001) Dynamics and orientation of N+(CD3)3-bromoacetylcholine bound to its binding site on the nicotinic acetylcholine receptor. *PNAS* **98**, 2346-2351

Wishart, D.S., Sykes, B.D. & Richards, F.M (1991) Relationship between Nuclear magnetic Resonance Chemical Shift and Protein Secondary Structure. *J. Mol. Biol.* **222**, 311-333

Yamaguchi, S., Tuzi, S., Seki T., Tanio, M., Needleman, R., Lanyi, J.K., Naito, A. & Saito, H. (1998) Stability of the C-Terminal α-Helical Domain of Bacteriorhodopsin that Protrudes from the Membrane Surface, as Studied by High Resolution Solid State ^{13}C NMR. *J. Biochem.* **123**, 78-86

Yeagle, P.L (1996) Membranes: Phosphorus-31 NMR. *Encyclopaedia of Nuclear Magnetic Resonance*, 3015-3022. Wiley

Yoshida, M., Ohno, K., Takeuchi, Y. & Kagawa, Y. (1977) Prolonged Lifetime of the 410-nm Intermediate of Bacteriorhodopsin in the Presence of Guanidine Hydrochloride. *Biochem Biophys Res Comm* **74**(4), 1111-1116

Zhang, P., Toyoshima, C., Yonekura, K., Green, N. M. & Stokes, D. L. (1998) Structure of the Calcium Pump from Sarcoplasmic Reticulum at 8Å resolution. *Nature* **392**, 835-839

Zweckstetter, M., & Bax, A. (2000) Prediction of Sterically Induced Alignment in a Dilute Liquid Crystalline Phase: Aid to Protein Structure Determinations by NMR. *J. Am. Chem. Soc.* **122**(15), 3791-3792

APPENDICES

Appendix 1. Amino acids and their number in bacteriorhodopsin

The numbers of each amino acid type are given based on the published sequence (Dunn *et al*, 1981). The relative numbers of amino acids are considered when designing experiments using biosynthetically enriched amino acids.

Amino acid	Number of residues in bR (248)
Alanine	29
Arginine	7
Asparagine	3
Aspartate	9
Cysteine	0
Glutamate	10
Glutamine	3
Glycine	25
Histidine	0
Isoleucine	15
Leucine	36
Lysine	7
Methionine	9
Phenylalanine	13
Proline	11
Serine	13
Threonine	18
Tryptophan	8
Tyrosine	11
Valine	21

Appendix 2. Media, buffers and gel conditions

2.1 Culture media

2.1.1 Standard Culture medium.

Standard medium used for culturing *Halobacterium salinarium* in the production of protein with unlabelled protein backbone (Oesterhelt & Stoeckenius, 1974). This medium is used in Chapter 3 for the culture of JW5 cells for incorporation of deuterium labelled retinals (Oesterhelt, 1982) and in Chapter 6 for the production of unlabelled purple membranes. Typically no pH adjustment is made however improved yield may be obtained with culture buffered close to pH 6.2.

In 1litre distilled water:

NaCl	250g
Oxoid Bacteriological Peptone	10g
$MgSO_4.7H_2O$	20g
Na_3Citrate	3g
KCl	2g

2.1.2 Selective labelling medium

Composition of medium used for selective labelling of bacteriorhodopsin (Helgerson *et al*, 1992).

For 1litre of culture make up:

1) In 500ml distilled H_2O

L-alanine	0.22g
Glycine	0.08g
L-proline	0.10g
L-threonine	0.25g
L-arginine	0.40g
L-lysine	0.85g
L-phenylalanine	0.13g
L-serine	0.30g
L-valine	0.50g
L-asparagine	0.40g
L-leucine	0.80g
L-methionine	0.19g
Adenine	1.4mg

2) In 100ml distilled H_2O

L-glutamic acid	1.3g
L-tyrosine	0.20g
L-isoleucine	0.22g
Guanine	1.5mg
Hypoxanthine	1.4mg
Xanthine	1.5mg

Add ammonia until all components dissolve.

Combine 1) and 2) then add:

NaCl	250g
NH_4Cl	5g
$MgSO_4.7H_2O$	20g
KCl	2g
$CaCl_2.2H_2O$	0.03g
KNO_3	0.1g
Na_3Citrate	0.5g
KH_2PO_4 (3%)	10ml
Na_2HPO_4 (2%)	10ml
Malic Acid	15g
Glycerol (10%)	10ml

Adjust volume to 850ml by adding distilled water. Adjust pH to 6.2 using 4M NaOH then increase volume to 1000ml. Then add 1ml of the following stock solutions:

A) 100ml 0.01M HCl containing:

$MnSO_4$	0.03g
$FeCl_2.4H_2O$	0.36g
$ZnSO_4.7H_2O$	0.044g
$CuSO_4.5H_2O$	0.005g

B) 100ml distilled H_2O containing:

Thiamine	0.1g
Biotin	0.1g

2.2 Buffers

Composition of buffers used in isolation of Rod Outer Segments, purification of rhodopsin (DeGrip, 1982), reconstitution and spin labelling for ESR.

2.2.1 Buffer I

In 1 litre distilled H_2O add:

NaCl	7.013g	120mM
HEPES pH 7.5	3.575g	15mM
KCl	0.373g	5mM
$MgCl_2$	0.407g	2mM
$CaCl_2$	0.147g	1mM
EDTA	0.292g	1mM
NaN_3	0.065g	1mM

Then add freshly:

Glucose	0.901g	5mM
Dithiothreitol	0.154g	1mM
PMSF	0.010g	10µg/ml

2.2.2 Column Buffer

To two litres distilled water add:

Tris-HCl	12.110g	50mM
Na Acetate	8.204g	50mM
$CaCl_2$	0.294g	1mM
Adjust pH to 7.0		
$MnCl_2$	0.324g	1mM
NaN_3	0.130g	1mM

2.2.3 Dialysing Buffer

To ten litres of distilled water add:

NaCl	29.225g	50mM
HEPES	11.925g	5mM
EDTA	1.45g	0.5mM
NaN_3	0.065g	0.1mM

Adjust pH to 7.

2.2.4 ESR buffer

To 100ml distilled water:

HEPES	0.36g
NaCl	0.7g
KCl	0.04g
EDTA	0.03g
NaN_3	6.5mg

Adjust pH to 7.

2.3 Gel conditions

To generate 10ml of 10% Acrylamide Separating Gel the following components were combined:

H_2O	4.02ml
1.5M Tris-HCl solution pH 8.8	2.50ml
10% (w/v) SDS	100µl
Acrylamide	3.33ml
10% APS	50µl
TEMED	5µl

The stacking gel was generated by combining the following elements:

H_2O	1.22ml
0.5M Tris-HCl solution pH 6.8	0.5ml
10% (w/v) SDS	20µl
Acrylamide	0.26ml
10% APS	10µl
TEMED	10µl

When the gel was set 5µl of sample was applied followed by 15µl of 4x concentrate dye. The gels were run at 125v for between 45 and 90 mins.

Appendix 3. Table showing characteristics of NMR active nuclei

	^{1}H	^{2}H	^{13}C	^{15}N	^{19}F	^{31}P
Nuclear Spin, I	1/2	1	1/2	1/2	1/2	1/2
Nuclear magnetic Moment, μ	2.793	0.857	0.702	-0.283	2.689	1.131
Gyromagnetic ratio, γ (rad T^{-1} s^{-1})	26.75×10^{7}	4.11×10^{7}	6.73×10^{7}	-2.71×10^{7}	25.16×10^{7}	10.83×10^{7}
Quadrupole moment		2.73×10^{-31}				
Relative sensitivity	1.00	9.65×10^{-3}	1.59×10^{-2}	1.04×10^{-3}	0.83	6.63×10^{-2}
Natural abundance	99.985	0.015	1.10	0.37	100	100
Frequency (MHz) @ 4.70 T	200	30.70	50.29	20.27	188.15	80.96
Frequency (MHz) @ 9.40 T	400	61.40	100.58	40.55	376.31	161.92
Frequency (MHz) @ 11.74 T	500	76.75	125.72	50.68	470.38	202.40
Frequency (MHz) @ 18.79 T	800	122.80	201.15	81.09	752.61	323.84

Appendix 4. Trapping of bacteriorhodopsin photointermediates in hydrated films.

4.1 Introduction

To achieve a greater understanding of the photochemistry of bacteriorhodopsin in membrane films, as used in the MAOSS approach, a detailed characterisation of the UV-VIS absorption spectra was performed under differing conditions, replicating those found in an NMR experiment. The experiments were designed to show the effects of hydration and the differing wavelengths and temperatures used for trapping the various bacteriorhodopsin photointermediates.

4.2 Materials and Methods

Absorption spectra were recorded on a Shimadzu UV-1602 spectrophotometer whose sample chamber was modified to accommodate a liquid nitrogen cryostat (Oxford Instruments DN1714), controlled by a homebuilt digital temperature control unit. Illumination was carried out with a 200W lamp, through a 50cm long fibre optic providing effective heat filtration and an appropriate colour filter. ASCII files were transferred to and rendered using the programme Microcal Origin 5.0. Membrane films were prepared on quartz plates to a concentration equal to that on one glass plate as prepared for MAOSS experiments. “Dry” samples were prepared (as described in Chapter 3) from distilled water and were hydrated as much as possible in a controlled humidity atmosphere whilst “wet” samples were prepared from pH 8 and

100mM NaCl, 100mM Na_2PO_4, 100mM Tris-HCl buffer in the same atmosphere and were observed to retain their hydration more effectively. Both wild type (WT) and D96N mutant samples were used for these studies.

4.3 Results and Conclusions

4.3.1 bR_{568}-state (Light adapted (LA)) (WT)

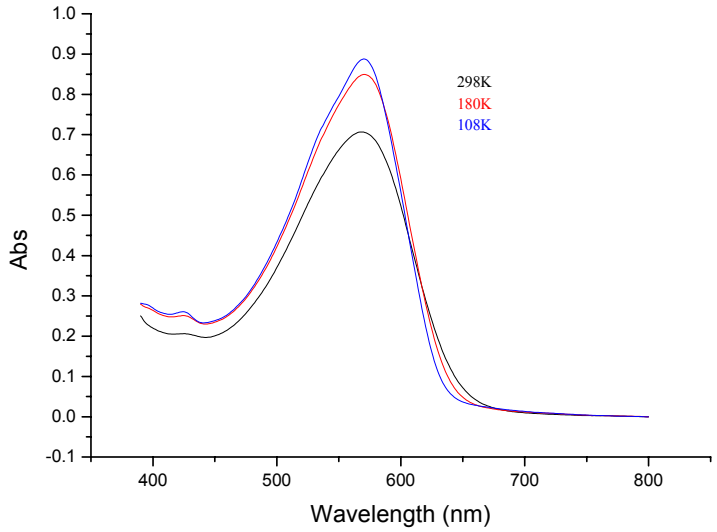

Fig I. UV-VIS spectra of LA bR at three temperatures. Light adapting conditions are 298K, 5mins of illumination with green light.

Purple membrane films were studied to see if they possessed differing abilities to light adapt under the above conditions. It was discovered that the ability to light adapt was related to the degree of hydration. Membrane films prepared from distilled water were observed to be more ready to dehydrate than those prepared from low salt buffer. It is thought that low amounts of salt in the films can help to maintain hydration through a hydroscopic effect. Membrane films prepared from distilled water are termed “dry” whilst those from salt containing buffer are termed “wet”, although both types of sample were prepared under conditions thought to produce

hydrated membrane films. Absorption maxima for bacteriorhodopsin at 568nm are greater at low temperature (Fig I).

4.3.2 K_{590}-state (WT)

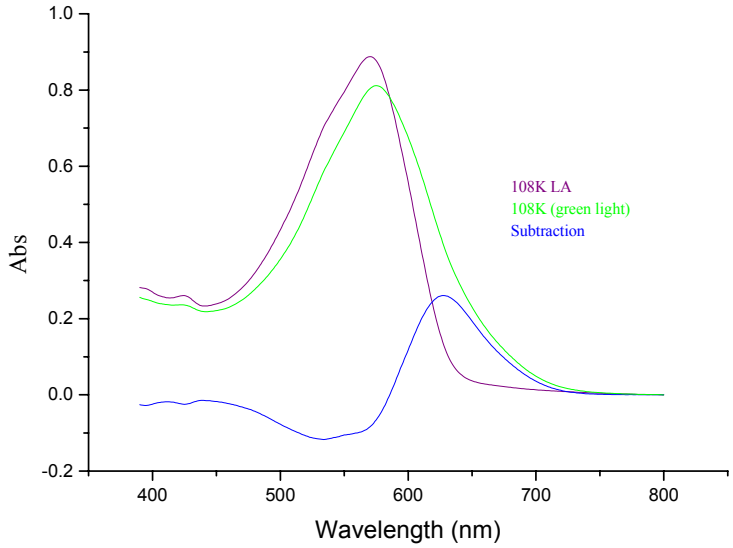

Fig II. Comparison of UV-VIS spectra for LA bR and bR in K-state at 108K. Trapping conditions are 108K, 5-10mins of illumination with 500-550nm (green light) giving c50% K-state in a "dry" sample. "Wet" sample not measured.

Hydration appeared to be less crucial in trapping the first photointermediate, K as the spectrum (Fig II) is typical of K-state spectra. The above spectra show the changes due to trapping of this photointermediate. The shift in absorption maximum is due to production of a species, revealed in the spectral subtraction, with maximum at 630nm. Trapping was performed at 108K. These low temperatures may be difficult to achieve in even a static NMR probe.

4.3.3 L_{550}-state (WT)

Initially a sample was used prepared from distilled water ("dry"). L_{550} state was trapped using conditions of 170K, and 5-10mins illumination with >610nm (red light) giving c 50% L-state (Fig III).

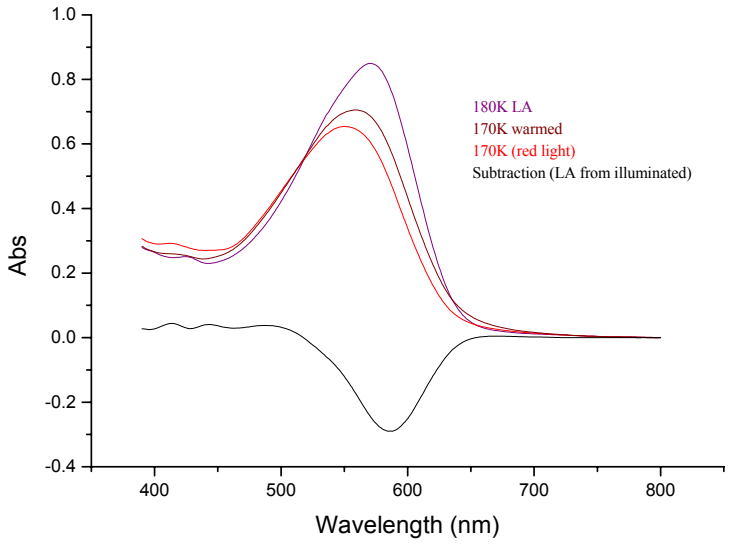

Fig III. UV-VIS spectra of "dry" purple membrane films showing comparison of LA bR and bR in L-state at 170K.

L-state (Fig III) can be trapped in the sample prepared from distilled water, however in the drier sample a considerable amount of M-state has been accumulated. The study of the L-state in the purple membrane films shows that hydration is very important for effective accumulation of this intermediate. It is possible to accumulate more L-state in the films by allowing them to warm slightly to 180K (Fig III brown trace), however the proportion of M increases also. Much improved spectra were obtained using the "wet" films (Fig IV). When illuminating the "wet" films" (Fig IV) the optimum temperature seems to be around 160K where most L is present, all of K

has decayed and only a little M has accumulated. This is most clearly seen in the subtracted spectra (Fig V). 160K is achievable in a static NMR probe however this would not be achievable in an MAS probe where the bearing and drive gases used for sample spinning would warm the sample.

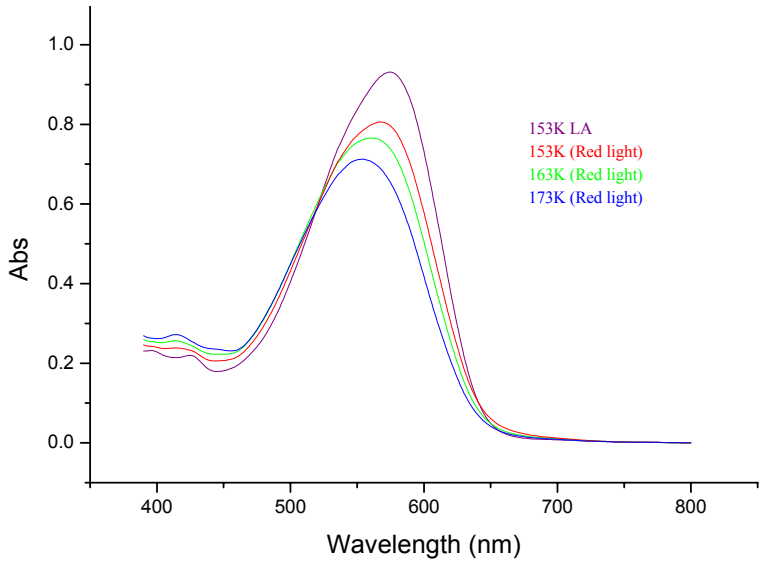

Fig IV. UV-VIS spectra of "wet" purple membrane films trapped in L-state at three temperatures.

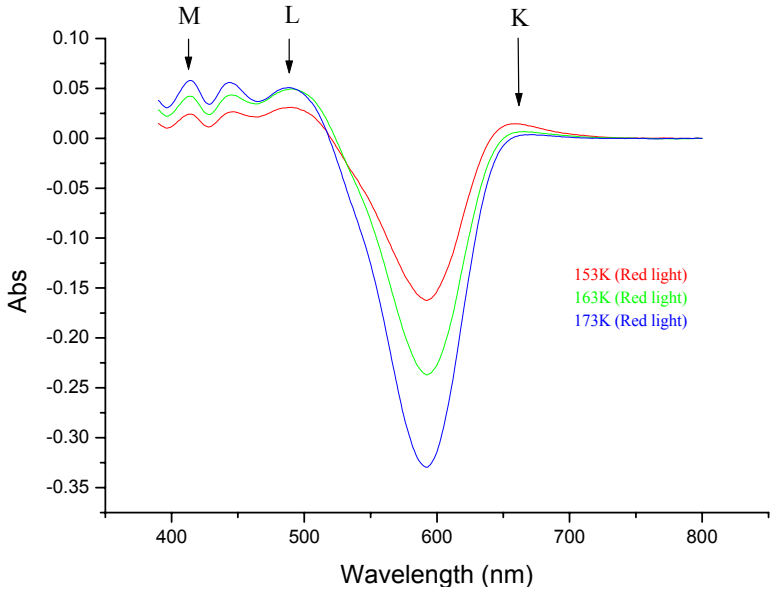

Fig V. Spectral subtractions from spectra in Fig IV showing relative amounts of K, L and M states trapped at three temperatures.

4.3.4 M_{412}-state (D96N)

In an attempt to accumulate the M intermediate in "dry" films, two approaches were used. Firstly the sample was cooled to 230K and a variety of different colour filtered lights were used during illumination. Secondly, continuous illumination with yellow light was applied whilst the sample was cooled from 283 to 173K. In this drier sample only about 40-50% of the LA bR was converted to the M-state (Fig VI).

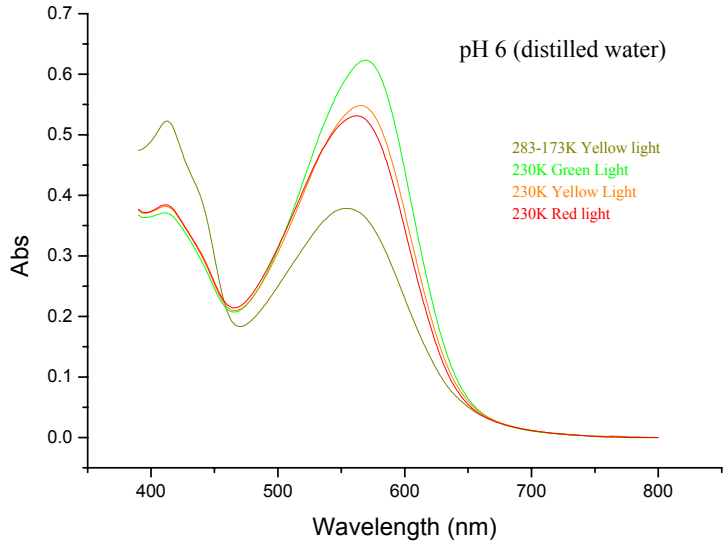

Fig VI. Comparison of UV-VIS spectra for a "dry" sample trapped in M-state at 230K and whilst cooling from 283-173K, pH 6 (approx).

Ideal trapping conditions for M-state were obtained with pH 8 and 100mM NaCl, 100mM Na_2PO_4, 100mM Tris-HCl buffer. M-state could be trapped at approximately 100% at temperatures between 220 and 230K (Fig VII). A temperature of 220K should be readily attainable in a solid state MAS probe using liquid nitrogen to cool the VT gas.

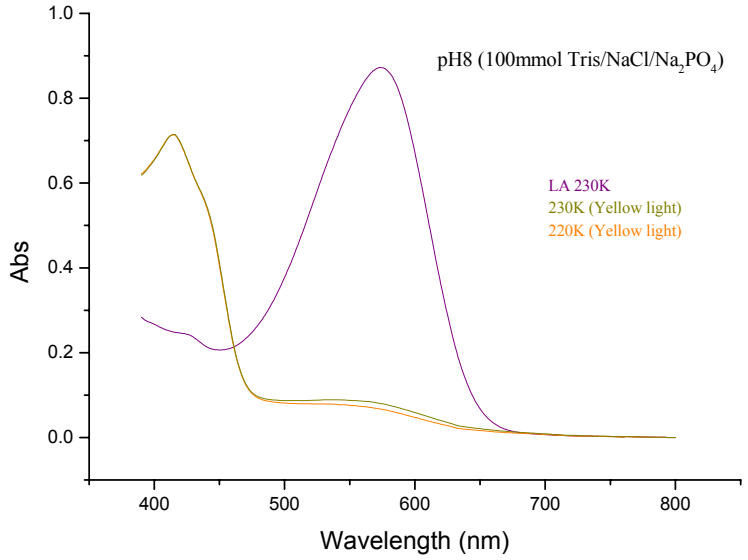

Fig VII. Comparison of spectra for "wet" sample in M-state at two temperatures

As the sample was warmed up the M-state was shown to be stable only at low temperatures (220-230K) without constant illumination whether in the presence of a salt buffer (Fig IX) or not (Fig VIII). Thermal relaxation of the M-state must be considered an important factor at temperatures above 243K. The buffer probably does not need NaCl or phosphate but the presence of some ions helps to maintain the sample in a hydrated state. Two different M states are just distinguishable by the movement of the M maximum during thermal relaxation (Fig IX). M_1 is trapped at 223K whilst at temperatures above 253K M_2 is trapped.

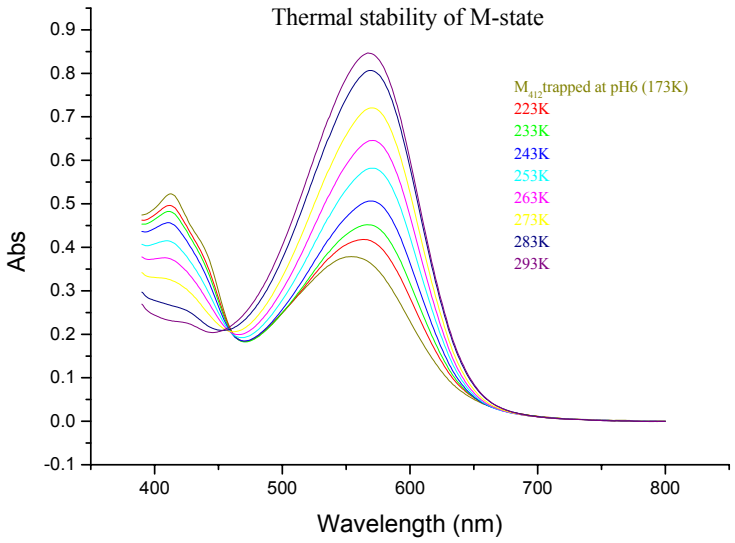

Fig VIII. Thermal decay of "dry" sample trapped as in Fig VI.

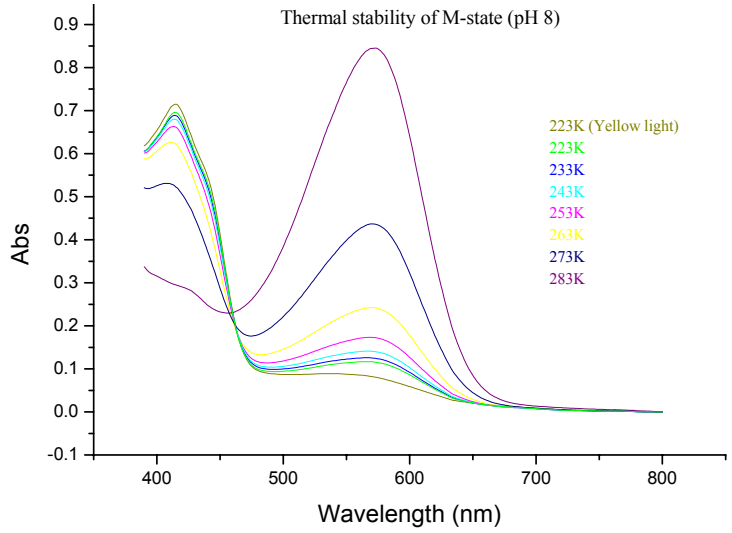

Fig IX. Thermal decay of M-state in "wet" sample, trapped as in Fig VII.